University of Southampton

Main Group Complexes of Group 15 and Group 16 Ligands

Nicholas James Hill

A Thesis Submitted for the Degree of Doctor of Philosophy

Department of Chemistry

September 2002

UNIVERSITY OF SOUTHAMPTON

ABSTRACT

FACULTY OF SCIENCE
CHEMISTRY

Doctor of Philosophy

Main Group Complexes of Group 15 and Group 16 Ligands

by Nicholas James Hill

Complexes of MX_3 (M = As, Sb or Bi; X = Cl, Br or I) with the phosphine and arsine ligands o-$C_6H_4(ER_2)_2$, EMe_3 and $MeC(CH_2AsMe_2)_3$ (E = P or As, R = Me or Ph) were synthesised and characterised by ^{1}H- and $^{31}P\{^1H\}$-NMR and IR spectroscopy, microanalysis and X-ray crystallography. Most of the structurally characterized [MX_3{o-$C_6H_4(ER_2)_2$}] complexes adopt a μ^2-halide bridged M_2X_6 dimer structure, with the bridge comprised of primary and secondary M-X bonds and the ligand bound *cis*. The [$AsCl_3(PMe_3)$] complex forms a weakly associated chain polymer in the solid state, comprised of planar As_2Cl_6 dimer units with axial, mutually *anti* PMe_3 ligands.

Complexes of SbX_3 (X = Cl, Br or I) with the chalcogenoethers $MeE(CH_2)_nEMe$ (E = S or Se, n = 2 or 3) were prepared and characterised by ^{1}H-NMR, IR and microanalysis. X-ray diffraction studies upon a number of examples revealed a diverse array of extended structures. The [SbX_3{$MeS(CH_2)_nSMe$}] (X = Cl, n = 2; X = Br, n = 3) adducts exist as three-dimensional networks and display an unusual mixed bridging/terminal thioether bonding mode. The [$SbCl_3${$MeSe(CH_2)_3SeMe$] complex adopts a one-dimensional chain comprised of Sb_2Cl_6 dimers linked by bridging $MeSe(CH_2)_3SeMe$ ligands. Complexes of SbX_3 with the thiacrowns [N]aneS_4 (X = Cl, Br; N = 12, 14 or 16) were characterised as above. All were of 1:1 stoichiometry except for the structurally characterised [$(SbBr_3)_2$([14]aneS_4}] species which displayed a two-dimensional sheet structure comprised of Sb_2Br_6 units linked by the macrocycle.

Complexes of AsX_3 (X = Cl, Br or I) with $MeE(CH_2)_nEMe$ (E = S or Se, n = 2 or 3, [9]aneS_3, [14]aneS_4 (X = Cl only), [8]aneSe_2 (X = Cl, Br), [16]aneSe_4 (X = Cl, Br) and [24]aneSe_6 (X = Cl, Br) were synthesised and characterised as above. [AsX_3{$MeS(CH_2)_2SMe$}] (X = Br, I) exist as discrete dimeric molecules similar to the [MX_3{o-$C_6H_4(ER_2)_2$}] complexes, while [$AsCl_3$([9]aneS_3)] consists of an $AsCl_3$ unit face-capped by the ligand. The [$AsCl_3$([14]aneS_4)] complex exists as a two-dimensional sheet. [$AsCl_3$([8]aneSe_2)] displays a one-dimensional ladder motif with planar As_2Cl_6 units linked by mutually *trans* Se-ligands, while the [$(AsX_3)_2$ ([16]aneSe_4)] (X = Cl, Br) adducts are structurally very similar to [$(SbBr_3)_2$([14]aneS_4}]. A novel mixed endo/exo coordination mode was observed in the [$(AsCl_3)_4$([24]aneSe_6)] complex, with an As_2Cl_6 dimer bound within the crown cavity and two $AsCl_3$ units bound exodentate.

The reaction of $TlPF_6$ with $MeSe(CH_2)_nSeMe$ (n = 2 or 3) gave the complexes [Tl{$MeSe(CH_2)_nSeMe$}][PF_6] in very low yield, with the bulk of the isolated solid being unreacted $TlPF_6$. X-ray crystallography revealed that both of the adducts exist as extended coordination networks, with the [Tl{$MeSe(CH_2)_2SeMe$}][PF_6] species adopting a sheet structure displaying a mixed bridging/terminal selenoether bonding mode and [Tl{$MeSe(CH_2)_3SeMe$}][PF_6] forming a one-dimensional chain. In both examples, weak Tl---F interactions supplement the Tl-Se bonding.

The telluroethers PhTeMe and o-$C_6H_4(CH_2TeMe)_2$ react with MeI to give the telluronium species [$PhTeMe_2I$] and [o-$C_6H_4(CH_2TeMe_2I)_2$]. The structure of [$PhTeMe_2I$] shows iodo-bridged dimers linked into a sheet by weak Te---I interactions such that each iodine is μ^3-bridging, while similar contacts in the [o-$C_6H_4(CH_2TeMe_2I)_2$] species produce a pseduo-cubane Te_4I_4 unit. Reaction of $PhTe(CH_2)_3TePh$ with I_2 gave the [$Ph(I)_2Te(CH_2)_3Te(I)_2Ph$] adduct, characterised as above, which displays an extended cradle motif. Complexes of MX_3 with PhTeMe, $MeTe(CH_2)_3TeMe$ and $MeC(CH_2TeMe)_3$ (M = Bi, X = Br for PhTeMe; X = Br and I where M = Sb, X = Cl where M = Bi for $MeTe(CH_2)_3TeMe$; M = Bi, X = Cl and Br for $MeC(CH_2TeMe)_3$) were characterised by IR spectroscopy and microanalysis, all of which were of 1:1 stoichiometry. The [$BiBr_3$(PhTeMe)] adduct forms a planar, bromo-bridged Bi_2Br_6 unit with axial, mutually anti PhTeMe ligands. These units are linked by weak Bi---Br contacts to give a stacked arrangement.

CONTENTS

Acknowledgements

I am indebted to my supervisors, Professor Bill Levason and Dr. Gill Reid, for their guidance, support and encouragement during the three very enjoyable years I have spent in their research group. In addition, I am grateful for the collection of multinuclear NMR data and proof reading of this thesis.

The majority of the discussion in this thesis is based upon single crystal X-ray diffraction data, and a number of people deserve special mention in this regard. Firstly, I must extend my thanks to Dr. Mike Webster for his superb advice and guidance in all aspects of X-ray crystallography, and his eagerness to tackle all of my crystallographic problems. Similarly, thanks go to Drs. Tony Genge and Bhavesh Patel for their coaching in the use of both the Rigaku four-circle diffractometer and TeXsan program, and Professor Mike Hursthouse and the staff of the EPSRC National Crystallography Service for providing me with regular access to the Kappa CCD diffractometer.

In terms of the chemistry, I owe particular thanks to Dr. Andy Barton for his involvement in much of the antimony(III) halide work, and also for guiding me along the rocky road of chalcogenoether ligand synthesis. The awful stench generated by these preps has offended most members of the second floor at one time or another, and I thank them all for not taking my declaration of war upon their sense of smell as a personal matter. On the social side, "cheers" go to Drs. Andy Barton, Tony Genge, Arran Tulloch, Sven Kleinhenz, Bhavesh Patel, Mike Popham and Pete Bolton, the latter three all being amusing lab partners and great house-mates (among a cast of many).

I wish to thank EPSRC for a research studentship and University of Southampton for provision of facilities. Finally, I thank my parents for their constant encouragement, belief and trust.

Abbreviations

Techniques

NMR	Nuclear Magnetic Resonance	ppm	Parts per million
$\{^1H\}$	Proton decoupled	δ	Chemical shift
D_p	Relative receptivity to ^1H	Hz	Hertz
J	Coupling constant	s	Singlet
d	Doublet	t	Triplet
q	Quartet	m	Multiplet
IR	Infrared	υ	Vibrational frequency
br	Broad	UV	Ultraviolet
λ	Wavelength	Å	Ångstrom (10^{-10} m)

Solvents

THF	Tetrahydrofuran	MeCN	Acetonitrile
DMF	N,N-Dimethylformamide	DMSO	Dimethylsulfoxide
Et_2O	Diethyl Ether	EtOH	Ethanol

Ligands

Me_3[9]aneN_3	1,4,7-trimethyl-1,4,7-triazacyclononane
cyclen	1,4,7,10-tetraazacyclododecane
cyclam	1,4,8,11-tetraazacyclotetradecane
dmpe	1,2-bis(dimethylphosphino)ethane
dppm	bis(diphenylphosphino)methane
dppe	1,2-bis(diphenylphosphino)ethane
diphos	1,2-bis(dimethylphosphino)benzene
diars	1,2-bis(dimethylarsino)benzene
dpae	1,2-bis(diphenylarsino)ethane
triars	1,1,1-tris(dimethylarsino)ethane

[12-crown-4]	1,4,7,10-tetraoxacyclododecane
[15-crown-5]	1,4,7,10,13-pentaoxacyclopentadecane
[18-crown-6]	1,4,7,10,13,16-hexaoxacyclooctadecane
[9]aneS_3	1,4,7-trithiacyclononane
[12]aneS_4	1,4,7,10-tetrathiacyclododecane
[14]aneS_4	1,4,8,11-tetrathiacyclotetradecane
[16]aneS_4	1,5,9,13-tetrathiacyclohexadecane
[18]aneS_6	1,4,7,10,13,16-hexathiacyclooctadecane
[18]aneN_2S_4	1,4,10,13-tetrathia-7,16-diazacyclooctadecane
[8]aneSe_2	1,5-diselenacyclooctane
[16]aneSe_4	1,5,9,13-tetraselenacyclohexadecane
[24]aneSe_6	1,5,9,13,17,21-hexaselenacyclotetracosane
dmit	1,3-dimethyl-2(3*H*)-imidazolethione

Miscellaneous

Me	Methyl	Et	Ethyl
^{i}Pr	iso-Propyl	^{n}Pr	n-Propyl
^{n}Bu	n-Butyl	Ph	Phenyl
R	Alkyl or aryl	mesityl	2,4,6-$Me_3C_6H_2$
o	Ortho	m	Meta
p	Para	mmol	Millimoles
K	Kelvin		
MO	Molecular Orbital		
HOMO	Highest Occupied Molecular Orbital		
LUMO	Lowest Unoccupied Molecular Orbital		
σ^*	Anti-bonding		
HSAB	Hard-Soft Acid-Base concept		

Chapter 1

Introduction

1.1 The Elements of Group 15

Group 15, the third column of the p-block of the Periodic Table, is comprised of the elements nitrogen, phosphorus, arsenic, antimony and bismuth (collectively termed the pnictogens). As for most p-block groups, there is a marked variation in both the chemical and physical properties of the group 15 elements as the group is descended. Phosphorus and arsenic are non-metals, antimony a metalloid (or semi-metal) and bismuth is considered metallic. Nitrogen, the lightest element of the group, is not included in this survey since its characteristics and chemistry bear little resemblance to those shown by the heavier congeners. Table 1.1 shows a selection of physical properties of the elements phosphorus through bismuth.[1]

Element	**Electronic Configuration**	**Electronegativity (Allred-Rochow)**	**Covalent radius[a] (Å)**	**van der Waals radius (Å)**
P	$[Ne]3s^2 3p^3$	2.06	1.10	1.90
As	$[Ar]3d^{10}4s^2 4p^3$	2.20	1.21	2.00
Sb	$[Kr]4d^{10}5s^2 5p^3$	1.82	1.41	2.20
Bi	$[Xe]4f^{14}5d^{10}6s^2 6p^3$	1.67	1.52	2.40

[a] For trivalent state

Table 1.1 Physical properties of the group 15 elements.

The group 15 elements form two series of halides, MX_3 and MX_5 (M = P, As, Sb or Bi; X = F, Cl, Br or I), although not all are known. Oxidation states +3 and +5 are possible, although the +3 oxidation state is the most common for arsenic, antimony and bismuth.

In the +3 oxidation state the group 15 elements possess a lone pair of electrons, a feature which usually confers Lewis basicity upon a system. As the group is descended, however, the basicity decreases markedly, exemplified by the vast literature on metal-phosphine complexes compared to that for metal-stibine or bismuthine complexes. Experimental evidence for this reduction in basicity comes from ligand exchange studies upon $[(C_5H_5)Fe(CO)_2]^+$ complexes containing monodentate group 15 ligands MR_3 (M = N, P, As, Sb or Bi), where the σ-donor ability was found to decrease in the order P > As > Sb > N > Bi.[2]

It is often assumed that this reduction in basicity (and hence σ-donor ability) is due to the lowering in energy of the lone pair as the group is descended. An alternative approach considers the increasingly poor hybridisation of valence s and p orbitals down the group. In this model, bonding occurs mainly *via* p orbitals with the lone pair residing in an orbital of predominantly s character. The poorer directional properties of s orbitals (compared to s - p hybrids) accounts for poorer orbital overlap, weakening of bonds down the group, and concomitant reduction in basicity. The decrease in basicity is such that the predominant reactivity of SbX_3 and BiX_3, in particular, is as Lewis acids. Consequently, the coordination chemistry of species such as MX_3 and $PhMX_2$ (M = Sb or Bi) with phosphines (PR_3), ethers (OR_2) and sulfur-containing ligands is now well documented, and discussed later in this chapter.

The lone pair is also an important consideration in the structural chemistry of group 15 halides and their complexes. Although pyramidal in the gas phase, the MX_3 molecules form weak, secondary M---X interactions to adjacent units in the crystalline state. Sawyer and Gillespie propose that these interactions form in the direction of maximum electron density of the lone pair, but not directly over it.[3] Structural aspects of MX_3 molecules have been examined extensively by Galy and Enjalbert,[4] who concluded that these species adopt one of three coordination polyhedra: a trigonal antiprism a bicapped trigonal prism or a tricapped trigonal prism (Figure 1.1). The following general trends are apparent: the stereochemical activity of the lone pair decreases in the order As > Sb > Bi, with increasing coordination number, and with increasing atomic number of the halogen.

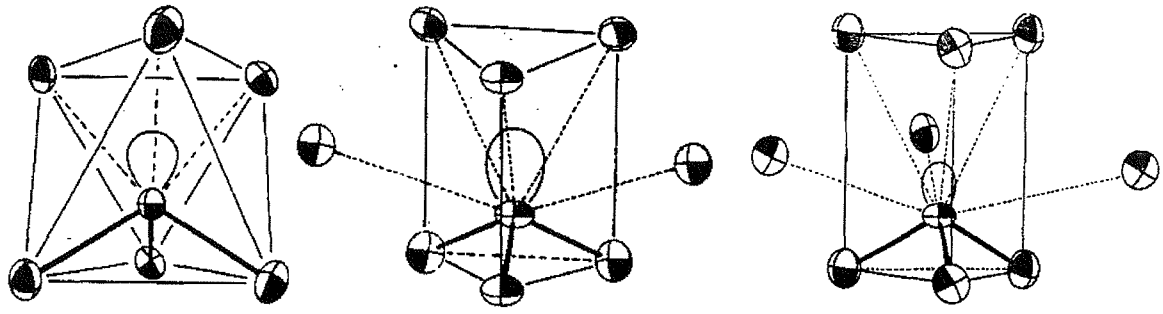

Figure 1.1 The three coordination polyhedra observed for MX_3 species.[4]

In MX_3 adducts, the stereochemical activity of the lone pair varies from compound to compound and it is difficult to predict the extent to which the coordination geometry of a particular complex will be distorted. However, from the above observations, a six-coordinate $[BiI_3(L)_3]$ species would be expected to show the least lone-pair distortion of all the MX_3 species considered.

1.1.1 The Hard/Soft Acid/Base principle

The hard/soft-acid/base (HSAB) principle, proposed by Pearson,[5] is an extension of the Lewis and Chatt-Ahrland classifications of metal-ligand interactions.[6] Based upon the Lewis definition of acids and bases as electron pair acceptors and donors respectively, metal ions are classified as hard or soft acids and ligands as hard or soft bases. The definition of each class of acid and base is as follows:

1) Hard acid: the acceptor atom is of high positive charge, small size and has no easily polarisable valence electrons.
2) Soft acid: the acceptor atom is of low positive charge, large size and possesses polarisable valence electrons.
3) Hard base: the donor atom is of high electronegativity, difficult to oxidise, not easily polarisable and has vacant orbitals of high energy.
4) Soft base: the donor is of low electronegativity, easy to oxidise, readily polarisable and has low-lying vacant orbitals.

A useful generalisation is that hard acids preferentially bond to hard bases and soft acids to soft bases, although there are many cases where the distinction between hard and soft is not clear. Some examples of hard, soft and so-called "borderline" acids and bases are shown in Table 1.2.

	Hard	Borderline	Soft
Acids	H^+, Li^+, Na^+, Ca^{2+}, Ti^{4+}, Fe^{3+}, As^{3+}, Ga^{3+}, BF_3	NO^+, Fe^{2+}, Cu^{2+}, Pb^{2+}, Zn^{2+}, Ru^{3+}, Sb^{3+}, Bi^{3+},	Tl^+, Cu^+, Au^+, Ag^+, Pd^{2+}, Pt^{2+}, Pt^{4+}, Cd^{2+}, Hg^{2+}, Tl^{3+}, Te^{4+}
Bases	F^-, Cl^-, HO^-, NO_3^-, H_2O, OR_2, NR_3, ClO_4^-, SO_4^{2-}	Br^-, NO_2^-, N_2, N_3^-, SO_3^{2-}	ER_2 (E = S, Se, Te), $E'R_3$ (E′ = P, As, Sb), CO, CN^-

Table 1.2 A selection of hard, soft and borderline acids and bases.[1]

From the above definitions, it is evident that hard-hard interactions result in mainly ionic bonding, and soft-soft combinations lead to covalent bonding. However, a hard-soft combination clearly leads to a mismatch in electronic properties of the acid and base, and so these interactions are less stable than hard-hard and soft-soft interactions.

The HSAB principle has a number of implications for the systems considered in this study. For example, since the Sb(III) and Bi(III) species are considered to be borderline cases, the relative hardness of the ligand donor atom will be a major factor in determining whether a stable donor-acceptor interaction occurs. Furthermore, once the ligand is coordinated, the hardness of the central main group atom will be moderated by the hardness of the donor ligand. This is a synergic effect, with hard ligands making the central atom harder and soft ligands making it softer. Clearly such an alteration will influence the subsequent reactivity of the complex. The formation of secondary interactions, for example, may be affected by a change in hardness of the group 15 atom.

1.1.2 Bonding in MX_3 species

The bonding within hypervalent main group species was first explained in terms of valence bond theory, implying hybridisation of low-lying d-orbitals.[7] This approach was accepted until the mid-1950's, when an alternative scheme, which used only p-orbitals, was proposed (independently) by Rundle and Pimental.[8, 9] The Rundle-Pimental (RP) model was initially applied to rationalise the geometry and bonding within the I_3^- species (formed from $I_2 + I^-$), and subsequently used to explain or predict structural aspects of various other systems. The RP scheme invokes delocalised three-centre σ bonding (Figure 1.2); three p-orbitals combine to give one bonding (ψ_1), one non-bonding (ψ_2) and one anti-bonding (ψ_3) molecular orbital, with the lower two orbitals occupied.

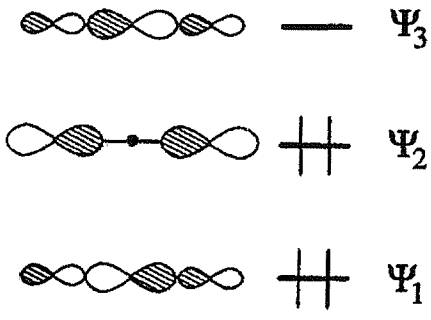

Figure 1.2 Schematic diagram of the p-orbital overlaps in the RP bonding model.

The basis of the model is still sound, and recent calculations have revealed that the d-orbitals used in valence bond theory are too high in energy to play any (significant) role in the bonding.[10]

Another model has also gained currency in explaining the structure and bonding within main group compounds. The Donor-Acceptor (DA) model considers σ^* anti-bonding orbitals to function as acceptors toward ligand donor atoms. This broad approach was employed by Norman to explain the observed structural trends in a series of MX_3 species.[11] The M-X σ^* anti-bonding orbitals, situated *trans* to the primary M-X bonds, are considered as acceptors for ligand donation and the donor-acceptor interaction can be represented by a simple molecular orbital diagram (Figure 1.3).

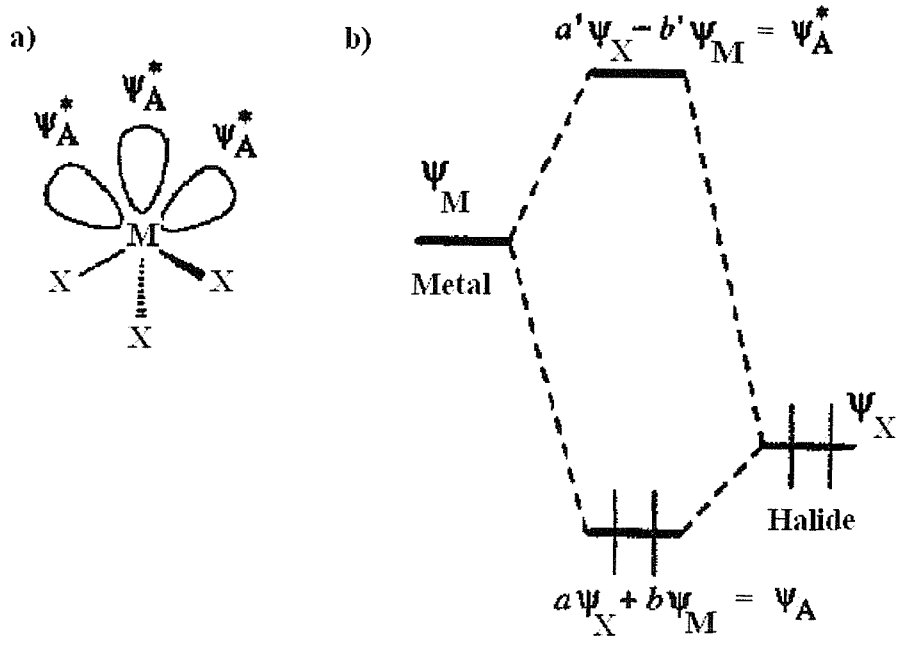

Figure 1.3 a) Schematic diagram of the M-X σ^* anti-bonding orbitals. b) MO diagram showing the derivation of the M-X σ^* anti-bonding orbitals.

Hoffmann *et al* have shown that the RP and DA models are, in fact, variations upon the same basic model (Figure 1.4).[12, 13] The concept connecting the two models is orbital interaction between occupied levels on one fragment and unoccupied levels on another. In this scheme, one fragment possessing only a donor function (ψ_D) interacts with a fragment containing both donor (ψ_A) and acceptor (ψ_A^*) functions. The net result of this donor-acceptor interaction is the generation of three molecular orbitals (ψ_1, ψ_2 and ψ_3) and the occupation of the previously empty ψ_A^* level. The resultant orbitals are equivalent to those shown in Figure 1.2 for the simple RP model. The extent of the contribution of ψ_A and ψ_A^* to the HOMO of the complex (ψ_2) determines the net bonding character of the donor-acceptor interaction.

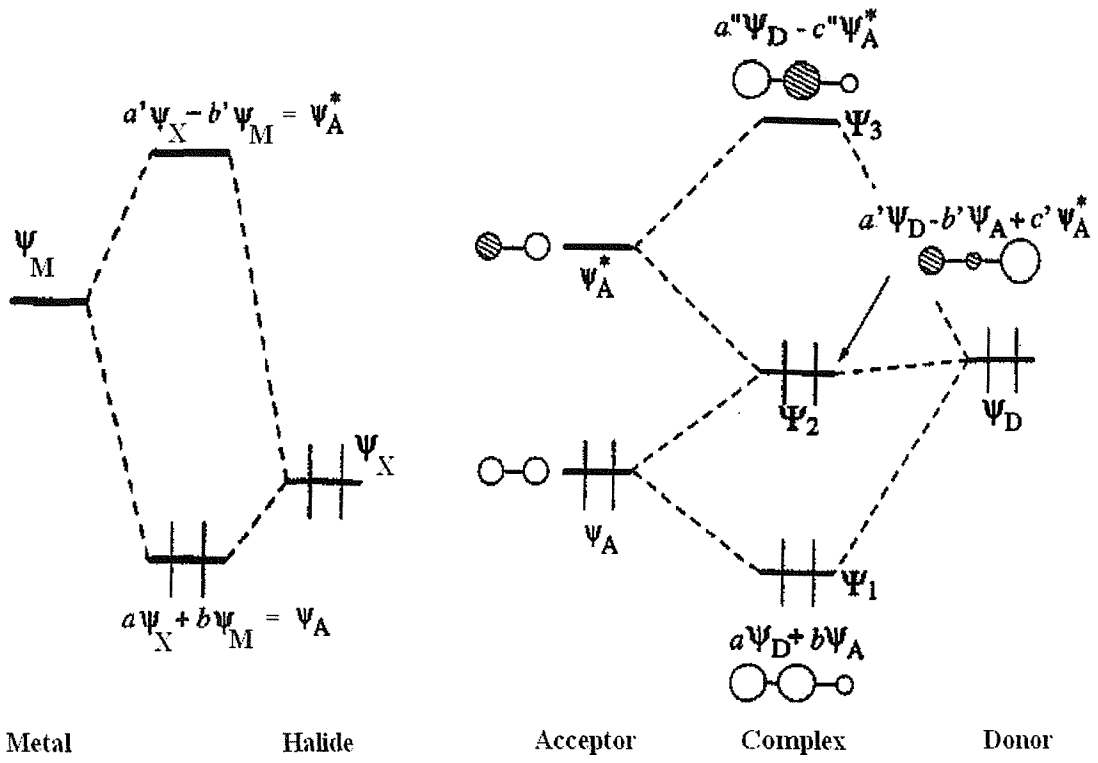

Figure 1.4 MO diagrams showing the equivalence of the DA and RP bonding models.

This bonding scheme accounts for a number of structural details, such as coordination geometry, bond distances and the role of secondary M-X bonding within the MX_3 species themselves. The concept of secondary bonding was developed by Alcock, and involves intermolecular hypervalent interactions between a p-block element and an electron pair donor (such as X, O, N or S).[14] The secondary bond is weak compared to a "normal" equivalent covalent bond, but measures less than the sum of the van der Waals radii of the two atoms and can have significant effects upon the structure of molecules. Such bonding has been observed in the crystal structures of various Pb-, Sb-, Bi-, Te- and I-containing complexes.[15]

There are two variables to account for when considering the nature of M-X interactions; altering the group 15 atom for a fixed halogen, and *vice versa*. The isomorphous iodide structures of arsenic, antimony and bismuth illustrate the effect of descending group 15. For AsI_3, there are three mutually *cis* primary As-I bonds with three longer, secondary As-I interactions *trans* to these bonds. The difference between primary and secondary bond distances, Δ, is 0.876 Å. In SbI_3, the basic structure is the

same, but the difference between primary and secondary bonds lengths is smaller (Δ = 0.450 Å). In BiI_3 there is no difference between primary and secondary bonding (Δ = 0). The isomorphous $SbCl_3$ and α-$SbBr_3$ structures show the effect of altering the halide. For $SbCl_3$, the difference between the three primary bonds and the three *trans* secondary bonds is 1.25 Å while for $SbBr_3$ Δ = 1.10 Å.

Two important trends become evident. First, the heavier group members show a greater tendency toward secondary bonding and, second, the propensity for such bonding increases with increasing mass of the halide; the extreme case is seen for BiI_3, where the distinction between primary and secondary bonds is lost (indeed, it is probably more accurate to state that only primary bonding occurs in BiI_3).

The DA bonding model relies upon X being more electronegative than M (since X = Cl, Br or I in this discussion, this is always the case), thus the σ-bonding orbital (ψ_A) will be polarised toward the X atom, i.e. the lower energy atomic orbital (Figure 1.3). The σ^* anti-bonding orbital (ψ_A^*) will be localised about the M atom so that, if this orbital is of sufficiently low energy, it can function as an acceptor orbital toward a donor. Hence the stronger the M-L interaction becomes (where L = ligand donor atom) the more the anti-bonding orbital is populated, and the primary M-X bond becomes weaker and longer (thus accounting for Δ = 0 in BiI_3).

Clearly, the extent to which the M and X atomic orbitals overlap is an important factor. The effects of changing both the group 15 and halide species, outlined above, can be rationalised in terms of overlap efficiency. The outcome of altering the M(III) species for a given X atom is considered first.

On descending the group the electronegativity of M(III) decreases (Table 1.1). The energy of the M valence orbitals is increased and thus, for a particular X atom, the extent of M-X atomic orbital overlap is reduced. The increasing size of M(III) orbitals down the group also results in poorer overlap. As a consequence, the σ bonding orbital (ψ_A) is raised and the σ^* anti-bonding orbital (ψ_A^*) is lowered in energy. Since ψ_A^* is considered as the acceptor orbital, a lowering in energy (and thus an increase in availability) will lead to stronger secondary bonding.

In accounting for the effect of changing X for a given M(III) atom, both the acceptor properties of M(III) and the donor capability of X must be considered. The heavier halides are better electron donors (since electronegativity decreases down a

group) and thus have a greater tendency toward bridging. In addition, as halide orbitals become larger and more diffuse down group 17, overlap with the M(III) orbitals is reduced and thus the σ^* orbital is lowered in energy. Crucial, however, is the raising in energy of the halide atomic orbitals relative to those of the M(III) atom. This reduces the energy separation between M and X, increasing the σ^* anti-bonding orbital energy (thus decreasing its availability for interaction with a Lewis base) and reducing the polarisation of this orbital toward the M atom. Overall, the availability of the σ^* anti-bonding orbital is tempered by the reduced M-X orbital energy separation.

Very recent work by Hoffmann has considered the implications of s-p mixing at the central atom in the non-bonding orbital.[16] The most important effect of this was found to be destabilization of the non-bonding orbital, determined by the extent of overlap between the s orbital of the central atom and the p orbital of the terminal atom. However, this development does not necessarily alter the overall implications of the "classical" model (i.e. s-p mixing not considered) and it is this combined RP-DA approach, outlined above, that will be used in this work.

1.2 Phosphine, Arsine and Chalcogeno-ether Ligands

1.2.1 Tertiary Phosphines and Arsines

In contrast to the elements of the d-block, the coordination chemistry of the heavier p-block elements with phosphine and arsine ligands is poorly developed. Such ligands are soft bases in terms of the HSAB principle (Table 1.2), and thus favour complex formation with softer acid centres. In this respect, the low-oxidation state d-block elements are ideally suited to metal-ligand coordination, with the metal-ligand bonding adequately described by the Chatt and, more recently, Orpen-Connolly models.[17, 18] However, p-block elements are also regarded as displaying soft to borderline acidity and, even though the bonding lacks the stabilising effect of π-back-donation associated with d-block complexes, the relatively few reported examples of heavy p-block complexes containing phosphine or arsine ligands is surprising.

Tertiary phosphines have been the most extensively studied since they are the strongest σ-donors / π-acceptors (other things being equal) as defined by the above

bonding models. In addition, since the nuclear spin quantum number of the ^{31}P nucleus is non-zero (I = ½ , 100% abundant, D_p = 0.066), the availability of ^{31}P NMR greatly aids the study of phosphine complexes. Trialkyl phosphines and arsines are malodorous, air-sensitive and highly toxic. Many advances in coordination chemistry can be traced to studies of metal-phosphine and metal-arsine complexes, although such work has invariably involved d-block compounds.[19] This progress continues, with recent highlights being the development of synthetic routes to chiral and macrocyclic phosphine ligands for catalytic applications.[20]

In addition to the electronic considerations mentioned above, steric effects also influence the M-P and M-As interaction. Tertiary phosphines and arsines possess three organyl substituents, and the steric properties of the ligand are greatly influenced by the size and shape of these groups. The Tolman cone angle concept attempts to establish a quantitative basis for these steric effects.[21] The space occupied by the ligand is estimated by an imaginary cone, which extends from the metal to the hydrogen atoms of the ligand. The metal-phosphorus distance is fixed at 2.28 Å, and so the cone angle is defined as the angle subtended at the metal centre (Figure 1.5). A different donor atom would require a different metal-ligand distance. Listings of cone angles for many tertiary phosphines have been published, with typical values ranging from 118° for PMe_3 to 212° for $P(mesityl)_3$. The treatment of the ligands as solid cones tends to overestimate the steric effects, and a number of more sophisticated models have been developed.

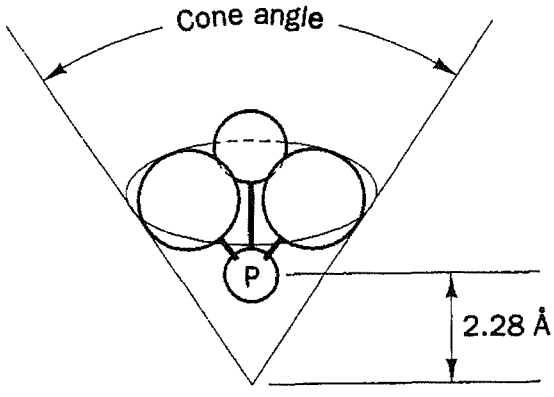

Figure 1.5 Definition of the cone angle for a symmetrical phosphine, PR_3.

Examples of d-block complexes containing antimony and bismuth donor ligands are comparatively sparse, although a review of the area has been published.[22] There are few reports of arsine complexes of p-block species, and even fewer examples of stibine and bismuthine complexes. The inherent instability of the Sb-C and Bi-C bond, coupled with poorer σ-donor capability and often non-trivial synthetic procedures appears to have forestalled work in this area.

1.2.1.1 Synthesis of Tertiary Phosphines and Arsines

Procedures for the synthesis of mono-, bi- and poly-dentate phosphines and arsines can be broadly classified into three general types: reaction of halogenophosphine/arsine with organometallic reagents (RLi, RMgBr), reaction of alkali metal phosphide/arsenides R_2EM (M = Li, Na, K) with organic halides or reduction of phosphine/arsine oxides.[23, 24, 25] The ease of oxidation of M(III) to M(V) is a complicating factor, and thus most phosphine and arsine syntheses are performed under anaerobic conditions. The synthetic procedures for a number of the phosphine and arsine ligands used in this study are discussed below.

- **o-$C_6H_4(PPh_2)_2$** [26]

The route shown is adapted from that reported by McFarlane and McFarlane, who obtained o-$C_6H_4(PPh_2)_2$ by reaction of o-$C_6H_4F_2$ with Ph_2PNa in liquid ammonia.[26] The air-stable ligand is isolated as a white solid in good yield, whereas reaction of the metal phosphide with o-$C_6H_4X_2$ (X = Cl , Br) reportedly gives yields of < 1 %.[27] Other procedures are either multi-stage or similarly low yielding.[28]

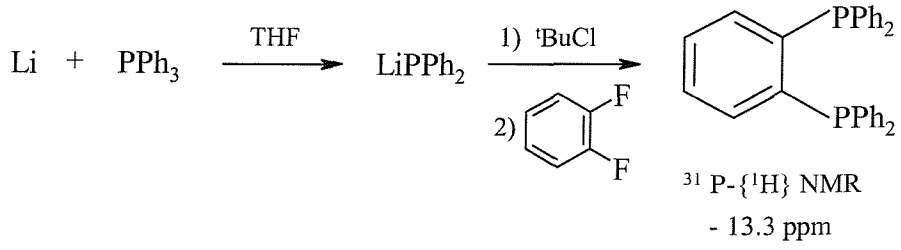

^{31}P-{^{1}H} NMR
- 13.3 ppm

- **o-$C_6H_4(PMe_2)_2$** [29]

Kyba reported the photolytic synthesis of the diphosphonate ester, which on reduction with a 1:1 mixture of $LiAlH_4/Me_3SiCl$ yields 1,2-bis(phosphino)benzene. Treatment of the diprimary phosphine with two equivalents of ^nBuLi at – 78° C followed by addition of two equivalents of methyl iodide affords the secondary phosphine 1,2-bis(methylphosphino)benzene, which is subsequently transformed into 1,2-bis(dimethylphosphino)benzene by a similar deprotonation-methylation sequence. In contrast to the phenyl substituted analogue, o-$C_6H_4(PMe_2)_2$ is isolated by vacuum distillation as a very air-sensitive liquid. This ligand has also been prepared by a similar route to that used for o-$C_6H_4(PPh_2)_2$.[30]

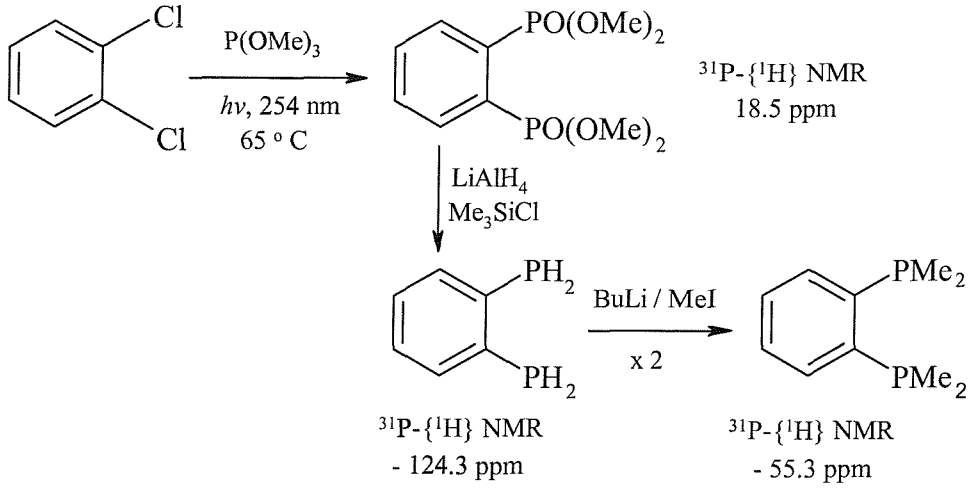

- **o-$C_6H_4(AsMe_2)_2$** [31]

Chatt and Mann first prepared o-$C_6H_4(AsMe_2)_2$ by a six-stage process starting from o-nitroaniline,[32] however a more direct route was described by Nyholm *et al.*[31] This involves formation of iododimethylarsine by rapid addition of $HCl_{(aq)}$ and SO_2 to an aqueous solution of sodium cacodylate, followed by reaction of Me_2AsNa with o-dichlorobenzene (*cf.* routes to o-$C_6H_4(PPh_2)_2$ described above). The ligand is isolated as a pale yellow, air-sensitive liquid by *in vacuo* fractionation.

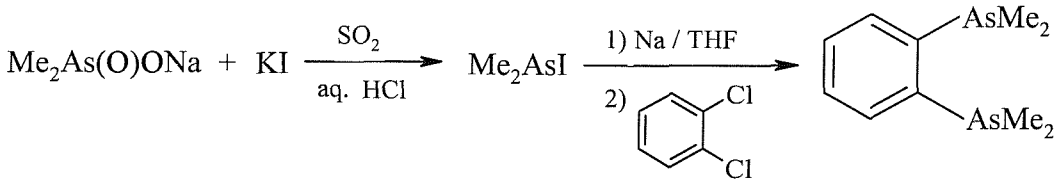

The coordination chemistry of o-$C_6H_4(AsMe_2)_2$ was developed by Nyholm, and the ligand was thought to be unique among phosphines and arsines in its ability to stabilize unusual coordination numbers and oxidation states. However the analogous phosphine o-$C_6H_4(PMe_2)_2$ has been shown to be as least as versatile in this regard.

1.2.2 Chalcogenoethers

In contrast to the rapid growth of phosphine and arsine coordination chemistry during the 20th Century, the development of chalcogenoether ligands (R_2E, E= S, Se or Te) has been slow. Indeed only in the past two decades have the first reviews concerning these species appeared.[33, 34] The major reason for this imbalance is the generally accepted opinion that chalcogenoether ligands are poorer donors than phosphines and arsines. In addition, the toxicity, malodorous nature and commercial unavailability of these species have not enhanced their appeal. Recent progress in synthetic procedures and FT-NMR techniques, however, has provided impetus to this field. In particular, developments in the area of macrocyclic thio-ether ligands have prompted new synthetic efforts into seleno- and telluro-ether ligands, and improvements in ^{77}Se- and ^{125}Te-NMR methods have complemented this work.

1.2.2.1 Synthesis of Chalcogenoethers

The acyclic dithio- and diseleno-ethers used in this study are air-stable liquids, and the thia-macrocycles are air-stable white (often crystalline) powders. The telluroethers are moderately air-sensitive oils. The synthesis, bonding and coordination chemistry of acyclic and macrocyclic thioethers has been reviewed,[35] and Levason and co-workers have surveyed recent developments in selenoether and telluroether chemistry.[34, 36] Synthetic routes to the chalcogenoethers used in this study are discussed below.

- **$MeS(CH_2)_nSMe$ (n = 2 or 3)**[37]

$$HS(CH_2)_nSH \xrightarrow[2)\ MeI]{1)\ Na\ /\ EtOH} MeS(CH_2)_nSMe$$

The acyclic dithioethers used in this work were readily prepared by reaction of the appropriate dithiol with sodium in ethanol, followed by treatment of the disodium salt with methyl iodide. Fractionation *in vacuo* affords the ligands as colourless (n = 2) or pale yellow (n = 3) liquids in > 70 % yield.[37]

- **$MeSe(CH_2)_nSeMe$ (n = 2 or 3)**[38]

$$Se \xrightarrow[MeLi]{THF} MeLiSe \xrightarrow{Cl(CH_2)_nCl} MeSe(CH_2)_nSeMe$$

n = 2, ^{77}Se NMR = 121 ppm
n = 3, ^{77}Se NMR = 74 ppm

A number of routes to acyclic diselenoethers exist, with early examples being reported by Greenwood[39] and Westland.[40] The diselenoethers used in this study were obtained by reaction of the appropriate α, ω-dichloroalkane with a frozen THF solution of MeSeLi (prepared from MeLi and Se powder).[38] The pale yellow liquid ligands are isolated in > 70 % yield by fractionation *in vacuo*.

The mono- and ditelluroethers were prepared by an analogous procedure, using elemental tellurium and RLi (R = Me or Ph), but their synthesis is complicated by their moderate air-sensitivity and ready cleavage of the Te-C bond (for example, the attempted synthesis of $RTe(CH_2)_2TeR$ leads to formation of the di-telluride R_2Te_2 and the elimination of ethene).[41] They are stable if handled under a nitrogen atmosphere.

- **Macrocyclic Thioethers**[35, 42]

The macrocyclic thioethers used in this study were obtained commercially. However, it is worth outlining the major synthetic procedures devised for these ligands since prior to these developments they were obtainable only *via* low yielding reactions.

In contrast to the high yield synthesis of crown ethers by use of an alkali metal template, the lower affinity of sulfur for the alkali metals limits the use of this route for the preparation of sulfur macrocycles. As such, the competition between cyclisation and polymerization is more acute in thiacrown synthesis as witnessed by the very low yields reported in early work. For example, one of the first thiacrowns to be prepared was [18]aneS_6, isolated in less than 2 % yield (this was later improved to *ca.* 30 % although the route required the use of mustard gas).[43] Initial routes to [9]aneS_3 gave a yield of less than 1 %, which was subsequently improved by performing the reaction under high dilution conditions. This process typically involves the very slow addition of the reactants to a large volume of solvent, and favors cyclisation over polymerization.[44] A major synthetic improvement was made by the development of Cs_2CO_3/DMF-promoted cyclisation, which allowed these once precious ligands to be isolated in *ca.* 70 % yields (shown below for [12]aneS_4).[45, 46]

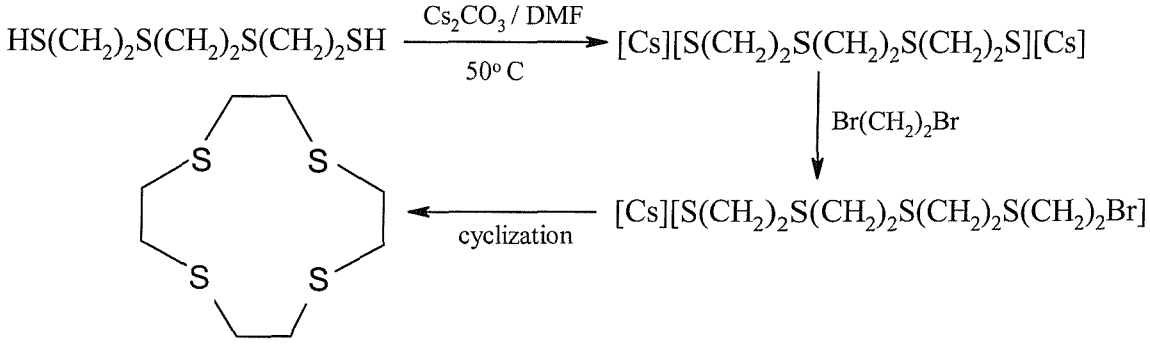

[12]aneS_4

The major effect of the Cs^+ ion is to render the thiolate ion highly nucleophillic and hence promote intra- over inter-molecular reaction of the acyclic [$X(CH_2)_nS^-$][Cs^+] intermediate (X = Cl, Br). Smaller alkali metal cations do not promote cyclisation to the same extent.

A template-based high yield synthesis of [9]aneS$_3$ has also been reported, using the Mo(CO)$_3$ fragment as a template around which cyclisation of HS(CH$_2$)$_2$SH and Br(CH$_2$)$_2$Br occurs to give [Mo(CO)$_3$([9]aneS$_3$)]. Free [9]aneS$_3$ was obtained in *ca.* 60 % yield by treatment of the complex with an equivalent of the acyclic thiolate.[47] The synthesis of unsaturated thiacrowns has recently been reported,[48] albeit in very low yield (18 % for 7 products) despite the use of Cs_2CO_3. This was increased to 40 % by use of [15-crown-5] as a phase transfer catalyst.

- **Macrocylic Selenoethers** [49]

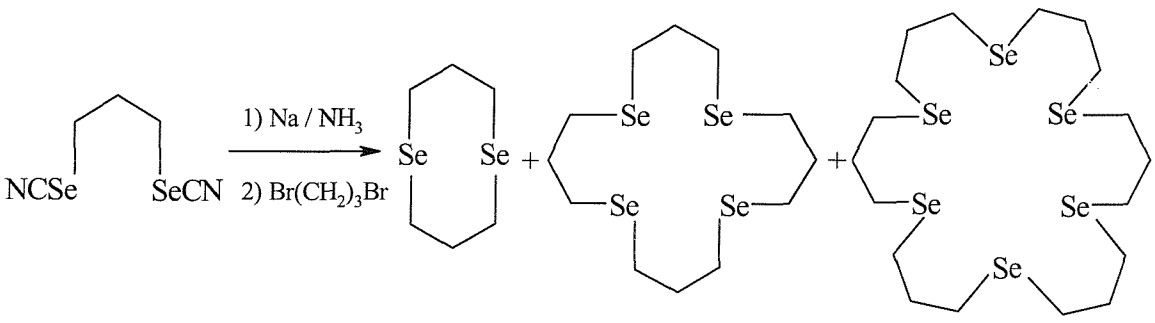

[8]aneSe$_2$	[16]aneSe$_4$	[24]aneSe$_6$
18 %	40 %	15 %
^{77}Se NMR = 137 ppm	157 ppm	153 ppm

There have been only a small number of reports concerned with the synthesis of macrocyclic selenoethers, and thus the cyclisation mechanisms remain uncertain. The selenacrowns employed in this study, [8]aneSe$_2$, [16]aneSe$_4$ and [24]aneSe$_6$, were obtained following the method described by Pinto *et al.*[49] This involves Na/NH$_{3(liq)}$ reduction of NCSe(CH$_2$)$_3$SeCN (prepared by reaction of KSeCN with Br(CH$_2$)$_3$Br in anhydrous DMF), and treatment of the resulting disodium salt with Br(CH$_2$)$_3$Br at *ca.* – 45° C over 3-5 hours. The crude mixture is purified by silica-gel flash chromatography to yield the ligands as pale yellow oils or waxy solids. The hydroxy-functionalised macrocycles [8]aneSe$_2$(OH), [16]aneSe$_4$(OH) and [16]aneSe$_4$(OH)$_2$ have recently been synthesised by the above method, using the appropriate HO-functionalised bis-selenocyanate precursor.[50]

1.2.2.2 Bonding in Chalcogenoether Complexes

The valence electronic configuration of the donor atoms in ER_2 species (E = S, Se, Te) is $ns^2\ np^4\ nd^0$. Two of these electrons are employed in the two E-R bonds, leaving four electrons to occupy non-bonding orbitals on the chalcogen atom. The nature of these orbitals varies with the chalcogen. Thioethers are considered to possess sp^3 hybrids, with the extent of hybridisation decreasing down the group. Hence, two hybrid lone pair orbitals are available for bonding. One of these is donated into the acceptor orbital of a metal atom upon E-M σ-bond formation. The remaining lone pair has a number of consequences for the structure and bonding within the complex, the most intriguing being σ-donation to a second metal centre to give a bridging ER_2 unit. Otherwise the lone pair can act as a source of stereoelectronic repulsion if uncoordinated or, *via* hybridisation to sp^2, as a π-base toward vacant d-orbitals of suitable symmetry on a σ-bonded metal centre (although there is little evidence that π-donation is significant). A further aspect of M-ER_2 bonding is the possibility of the chalcogeno-ether functioning as a π-acid. Such bonding can be described in terms of donation into E-C σ^*-anti-bonding orbitals, analogous to the Orpen-Connolly model for PR_3 species, although the extent of π-acceptance by ER_2 ligands is very much less than in phosphines.[33] The π-acid/base characteristics of chalcogenoethers are unimportant in p-block complexes and, in general, this effect is regarded as being of marginal importance in d-block complexes.[33-35]

With regard to σ-bond strength, Schumann and co-workers reported X-ray structural data and extended Hückel molecular orbital calculations on the series $[(C_5H_5Fe(CO)_2EMe_2]^+$ (E = S, Se, Te), and revealed that the strength of the Fe-E interaction increases in the order Fe-Te >> Fe-Se > Fe-S.[51] A similar trend has been shown to operate in other low valent transition metal systems such as the $[Mn(CO)_3X(L\text{-}L)]$ series (X = Cl, Br; L-L = dichalcogenoether).[52] This increasing σ-donor capacity is due to the decreasing electronegativity down the group and generally applies to low oxidation state metals, where the d-orbital extension is greatest and allows maximum overlap with the large, diffuse Te σ-bonding orbital. Studies using higher oxidation state metals (where the d-orbitals are more contracted) show the donor ability to be in the order S < Se > Te.[34] This is illustrated by the lack of telluroether

complexes of high oxidation state platinum group metals, while thio- and selenoethers form stable adducts with these metals.

In the absence of d-electrons, the main contributions to M-E bond stability within the p-block complexes described in this work will be the extent of orbital overlap, electronegativity differences, HSAB and donor-acceptor interactions; however, at the outset, it is unclear as to the relative contribution of each of these factors.

Although the presence of only two organyl substituents reduces steric considerations (in comparison to tertiary phosphines and arsines), the hybridisation of the chalcogen atom does have stereochemical consequences. Upon coordination to a metal the chalcogen adopts a pseudo-tetrahedral geometry and, assuming that the two substituents are different and the second lone pair remains non-bonded, becomes chiral. For an RER' ligand, chirality leads to the possibility of *meso* and DL stereoisomers. Rotation about the M-E bond is a low energy process for monodentate ligands and so the stereoisomers are indistinguishable by NMR in these systems. However, rotation is more difficult for chelating ligands and so the magnetically nonequivalent invertomers may be observed by NMR provided they do not rapidly convert by pyramidal inversion. The most common mechanism for this process involves the interchange of two degenerate configurations *via* a planar transition state (i.e. without bond cleavage, Figure 1.6). Alternative mechanisms, involving dissociation and recombination of one or more of the substituents, have been proposed however the strength of the metal-chalcogen bond suggests that cleavage is not a favoured mechanism for inversion.

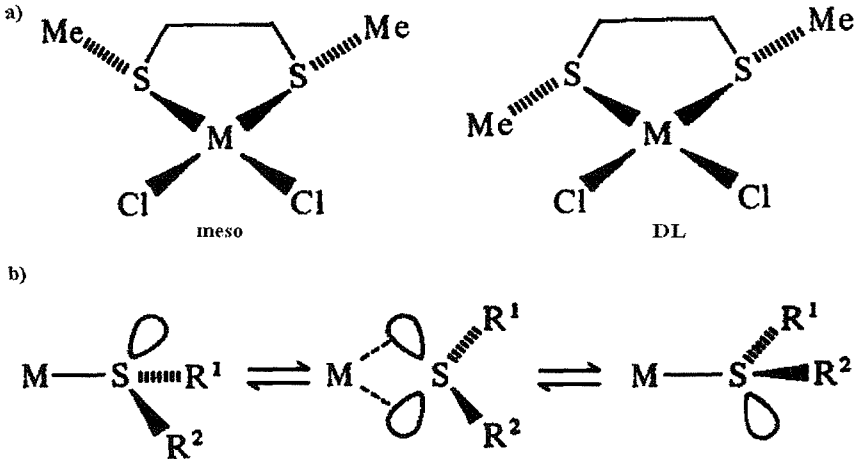

Figure 1.6 a) View of the meso and DL invertomers and b) proposed mechanism for pyramidal inversion of coordinated chalcogenoethers.

Abel and co-workers were the first to observe inversion of a coordinated chalcogenoether (in the low temperature ^{1}H-NMR spectrum of the chelate complex [$PtCl_2${$MeS(CH_2)_2SMe$}]),[53] and there have since been various studies into the factors influencing this process.[54]

1.3 Coordination Chemistry of Arsenic, Antimony and Bismuth(III) Halides

This section aims to provide a general (rather than comprehensive) overview of the coordination chemistry of MX_3 species (M = As, Sb, Bi; X = F, Cl, Br, I). Using selected examples, the discussion will focus chiefly upon neutral, structurally characterised complexes containing ligands related to the tertiary phosphines, arsines and chalcogenoethers used in this work (e.g. aza- and oxa-crown ethers, phosphine and arsine oxides etc.). A detailed review of the literature regarding MX_3 complexes of such ligands is made in the relevant chapter.

1.3.1 Complexes of Nitrogen Donor Ligands

What appears to be the only structurally characterised example of an amine complex of AsX_3 is the discrete molecular species [$AsCl_3(NMe_3)$], reported by Webster.[55] The arsenic(III) atom adopts a pseudo-trigonal bipyramidal structure, with the amine ligand and one chlorine atom bound axially, with two chlorine atoms and the lone pair in the equatorial plane. The structure of [$SbCl_3(PhNH_2)$] is similar.[56] The [SbF_3(terpy)] (terpy = 2,2':6',2''-terpyridine) complex is also discrete, adopting a six-coordinate pseudo-pentagonal pyramidal structure with the lone pair occupying one of the coordination sites.[57] The [$SbCl_3$(bipy)] complex (bipy = 2,2'-bipyridine), in contrast, adopts a dimeric structure through weak Sb---Cl interactions (3.34(2) Å) to give a distorted octahedral geometry at the antimony(III) atom.[58]

The [As(cyclenH)] and [As(cyclamH)] species were prepared by treatment of the azamacrocycle with $As(NHMe_2)_3$.[59] Each arsenic atom has a distorted pseudo-trigonal bipyramidal geometry with two of the ring nitrogens and a lone pair in the equatorial position and the two remaining ring nitrogen atoms in the axial positions. One of the axial nitrogens in each species is protonated, leading to a longer As---N interaction (e.g. 2.400(7) *vs. ca.* 1.85 Å for [As(cyclenH)]).

Willey and co-workers prepared and structurally characterised the yellow complex *fac*-[$BiCl_3(Me_3[9]aneN_3)$], in which the pyramidal $BiCl_3$ unit is bound to the three nitrogen atoms of the aza-macrocycle, resulting in an octahedral coordination environment at bismuth and a half-sandwich structure (Bi-N 2.44(3) – 2.47(2) Å).[60] The [$Bi(cyclen)(H_2O)(ClO_4)_3$] complex displays a square-antiprismatic geometry at the bismuth atom, the upper square defined by coordination to the four nitrogen-donors of cyclen (Bi-N 2.375(10) – 2.412(9) Å) and the lower described by one oxygen from each of the three perchlorates and a water molecule [Bi-O 2.690(10) – 2.810(14) Å].[61]

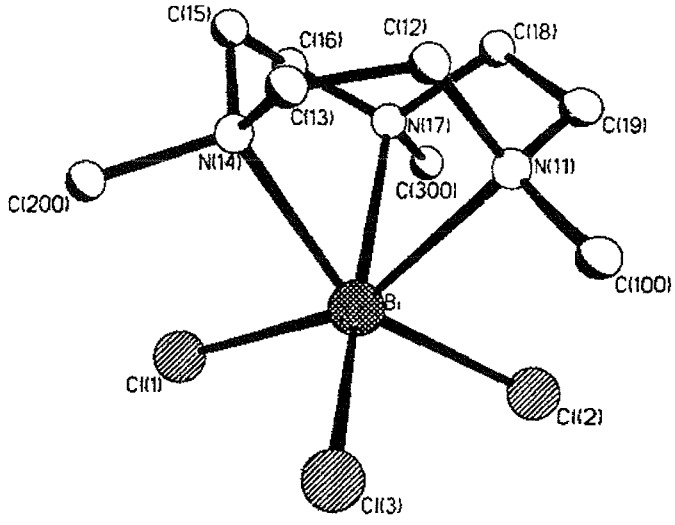

Figure 1.7 View of the [$BiCl_3\{Me_3[9]aneN_3\}$] complex.[60]

Norman *et al* recently examined a range of BiX_3, BiX_2Ph and $BiXPh_2$ complexes of substituted pyridine ligands (py = pyridine, 4-Mepy = 4-methylpyridine, 4-^{t}Bupy = 4-*tert*-butylpyridine).[62] The complexes [$BiI_3(py)_3$] and [$BiCl_3(py)_4$] are discrete six- and seven-coordinate species respectively, while examples such as [$BiBr_2Ph(4\text{-Mepy})_2$] and [$BiI_2Ph(4\text{-Bu}^t\text{py})_2$] show weak intermolecular Bi---X interactions, leading to dimers or oligomers (Figure 1.8). Subsequent work employed a combination of primary (Bi-bipy) and secondary (Bi---X) bonding to control the structure of the complexes *trans*-[$BiX_2Ph(bipy)]_n$, leading to linear chain coordination polymers.[63]

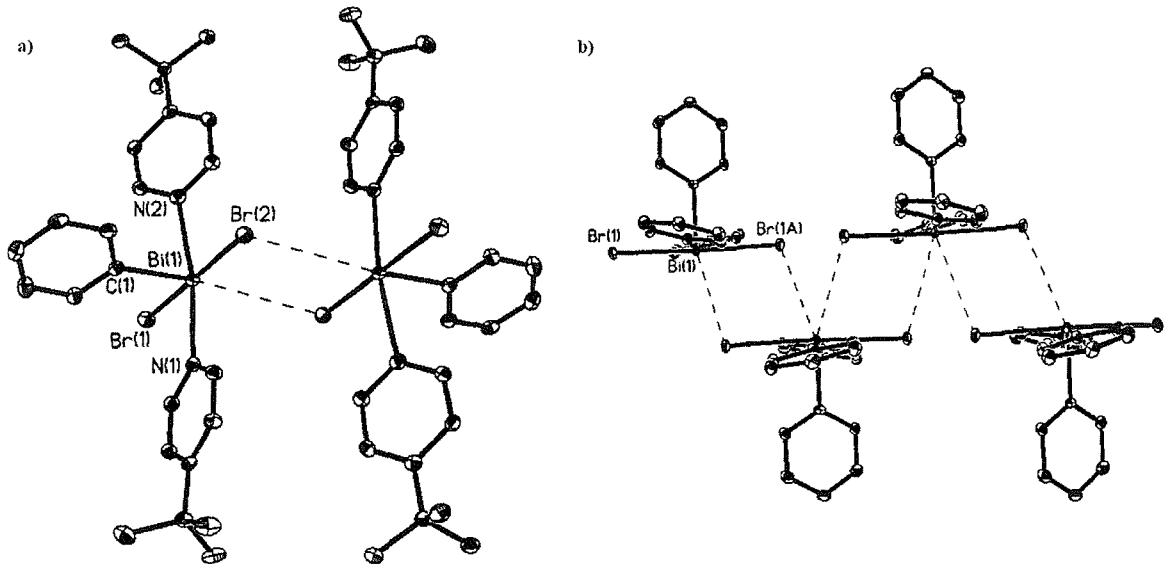

Figure 1.8 View of the $[BiBr_2Ph(4\text{-}Mepy)_2]$ and $[BiI_2Ph(4\text{-}Bu^tpy)_2]$ complexes.[62]

1.3.2 Complexes of Oxygen Donor Ligands

A number of MX_3 (M = Sb, Bi) adducts of ethers such as THF, DMSO and diglyme (diglyme = $MeO(CH_2)_2O(CH_2)_2OMe$) have been reported. The structure of $[SbI_3(THF)]$ comprises an extended chain arrangement of $SbI_3(THF)$ units, the antimony centres being bridged alternately by pairs of iodine atoms and thf ligands such that each antimony atom has an octahedral geometry.[64] The $[BiX_3(THF)_3]$[65, 66] and $[BiX_3(DMSO)_3]$ species[67] are monomeric octahedral (X = Cl, Br) and the $[BiCl_3(THF)]$ and $[BiI_3(DMSO)_2]$ adducts dimeric, displaying a pentagonal pyramidal and octahedral bismuth(III) geometry respectively. The $[BiCl_3(THF)_2]$ adduct adopts a polymeric motif, comprising square-pyramidal monomer $BiCl_3(THF)_2$ units (two *cis* THF and two *cis* chlorines in the basal plane, one apical chorine) linked by very asymmetric chlorine bridges to give an overall seven-coordinate pentagonal pyramidal coordination geometry.[66]

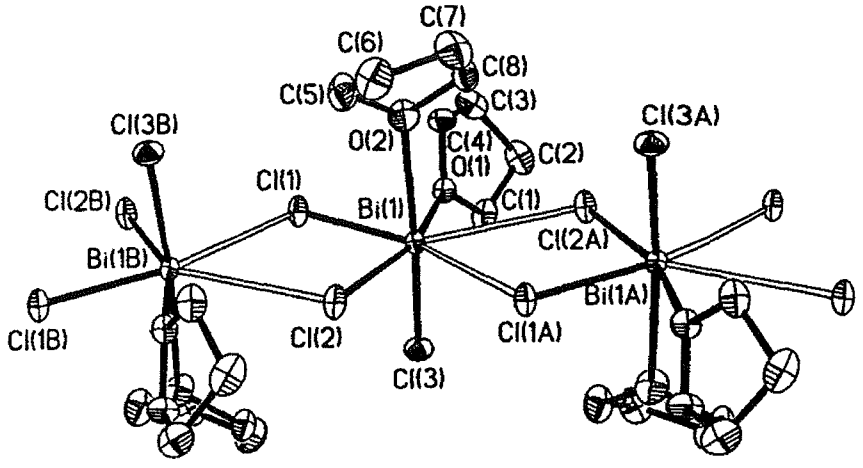

Figure 1.9 View of the chain structure of the $[BiCl_3(THF)_2]$ complex.[66]

The triphenylphosphine and arsine oxide complexes $[SbCl_3(OEPh_3)_2]$ (E = P, As) and $[SbCl_3(C_7H_4N)_2ClP(O)]$ have been described. The former species adopt square pyramidal structures with $OEPh_3$ ligands bound *cis*, while the latter shows a distorted trigonal bipyramidal geometry with the lone pair occupying an equatorial position.[68, 69] Similar complexes of BiI_3 have also been reported, including the dimeric *cis*-$[BiI_3(OPPh_3)_3]_2$ and $[Bi_2I_6(OAsPh_3)_2]$ species,[70, 71] and the polymeric $[Bi_2I_6(OP(NMe_2)_3]_n$.[72]

Willey and co-workers reported structures of two ditertiary phosphine and arsine oxide adducts, apparently obtained by adventitious oxidation of the parent diphosphine and diarsine complexes $[BiCl_3\{Ph_2PCH_2PPh_2\}_2]$ and $[BiCl_3(Ph_2AsCH_2CH_2AsPh_2)]$ during recrystallisation from boiling MeCN.[73] The $[BiCl_3(Ph_2P(O)CH_2P(O)Ph_2)_2]$ species exists as an edge-shared bioctahedral dimer with the bidentate phosphine oxide chelated to the bismuth atom (2.31(3) – 2.42(2) Å).

The structure of $[BiCl_3\{As(O)MePh_2\}\{Ph_2As(O)CH_2CH_2As(O)Ph_2\}]_n$ consists of a polymeric chain with each bismuth atom bound to three chlorine and three ligand oxygen atoms (one from a $As(O)MePh_2$ molecule and one each from two separate $Ph_2As(O)CH_2CH_2As(O)Ph_2$ ligands) in an approximately *mer*-octahedral geometry, with the $Ph_2As(O)CH_2CH_2As(O)Ph_2$ ligands bridging adjacent bismuth(III) centres. Both complexes are only slightly distorted from regular octahedral geometry, indicating no appreciable steric influence of the bismuth-based lone pair.[73]

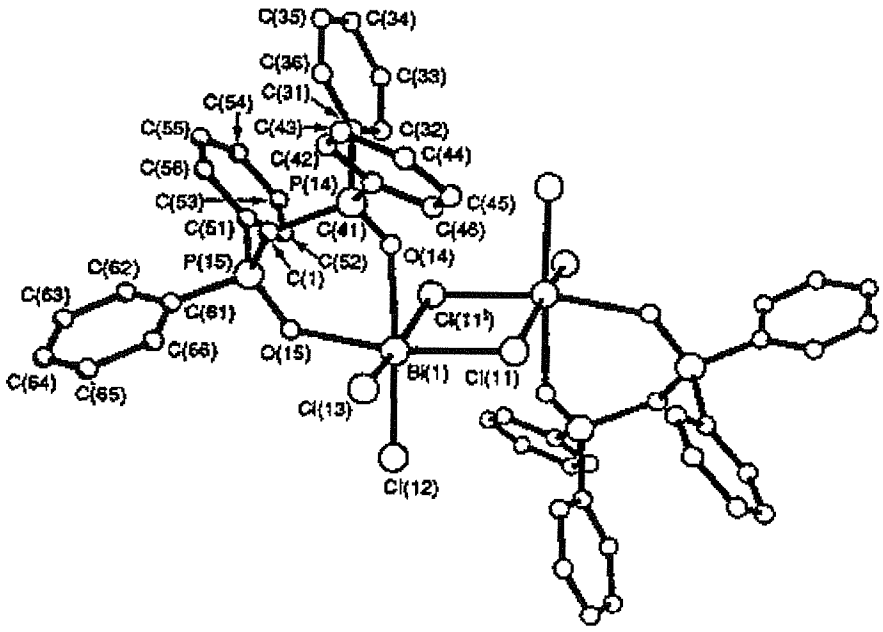

Figure 1.10 View of the $[BiCl_3\{Ph_2P(O)CH_2P(O)Ph_2\}_2]$ complex.[73]

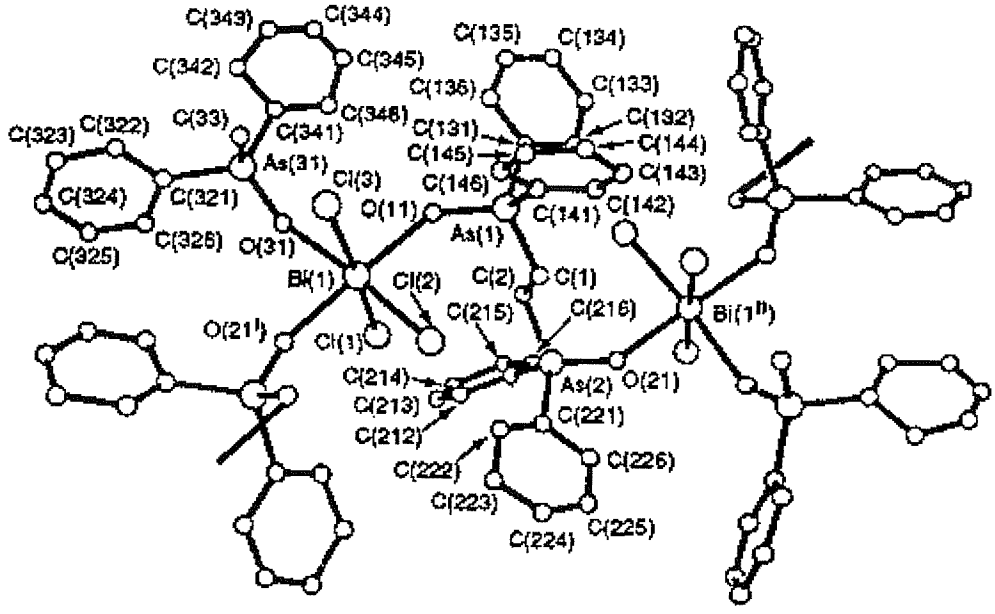

Figure1.11 View of a portion of the polymeric structure adopted by the $[BiCl_3\{As(O)MePh_2\}\{Ph_2As(O)CH_2CH_2As(O)Ph_2\}]_n$ complex.[73]

Adducts of MX_3 (M = As, Sb, Bi; X= F, Cl, Br, I) with crown ethers have received much study, with most of the structurally characterised examples incorporating [12-crown-4], [15-crown-5] or [18-crown-6]. In the large majority of examples, the coordinated MX_3 retains the pyramidal structure of the parent unit and is bound below the plane of the crown ether oxygen atoms to give a half-sandwich arrangement (analogous to the *fac*-[$BiCl_3(Me_3[9]aneN_3)$] complex shown in Figure 1.7).[74, 75, 76] For the MCl_3 adducts of the above stated ligands, Alcock has observed that the M-O interactions are much weaker than M-Cl.[74] For example, in the $SbCl_3$ complexes the Sb-O distances range from 2.71 – 3.40 Å (indicative of secondary interactions), while the Sb-Cl range is 2.38 – 2.42 Å. The strength of the M-O interactions increase in the order Bi > Sb > As and [12-crown-4] > [15-crown-5] > [18-crown-6].

A series of cationic complexes have been reported by Dehnicke *et al*, obtained by reaction of MCl_3 with [12-crown-4] or [18-crown-6] in MeCN solution in the presence of $SbCl_5$ (M= Sb, Bi).[77, 78] The $[M([12\text{-crown-4}])_2(MeCN)][SbCl_6]$ species consist of the M atom sandwiched between two tetradentate crown units, with an MeCN molecule completing the nine-coordinate environment. The M-O distances are typical of primary bonds (2.325(4) – 2.529(5) and 2.436(5) – 2.545(5) Å for M = Sb and Bi respectively, in contrast to the MX_3 complexes), with the lone pair apparently having no steric effect.[77] The $[SbCl_2([18\text{-crown-6}]][SbCl_6]$ species adopts an entirely different structure, with the antimony atom adopting a pseudo-trigonal pyramidal geometry comprised of two crown oxygen atoms bound axially (2.467(1) – 2.485(1) Å) and the two chlorine atoms and the antimony-based lone pair in equatorial positions. Four significantly weaker Sb-O interactions (2.68(1) – 2.75(1) Å). lead to eight-coordination about the antimony atom.[78]

The $[(MCl_3)_2([\text{dibenzo-24-crown-8}])]$ (M = Sb, Bi) and $[(SbBr_3)_2([\text{dibenzo-24-crown-8}])]$ adducts have recently been described ([dibenzo-24-crown-8]= 6,7,9,10,12,13,20,21,23,24,26,27-dodecahydrodibenzo[*b*,*n*][1,4,7,10,13,16,19,22]octa-oxycyclotetracosine).[79] The pyramidal MCl_3 species are bound to opposite sides of the crown ether, which adopts a sigmoidal conformation. Each metal is coordinated to five crown oxygen atoms (2.852(2) –3.1221(4) and 2.733(3) – 3.221(4) Å for M = Sb and Bi respectively), two of which adopt a bridging mode. The $SbBr_3$ units in

$[(SbBr_3)_2$(dibenzo-24-crown-8] again reside on opposite sides of the crown, each one bound to four crown oxygens (2.893(7) – 3.183(8) Å) (Figure 1.12). The M-O distances in these compounds are very similar to those in the $[MX_3$([18-crown-6])] complexes discussed above, indicating that the M-O interactions are essentially secondary in nature.

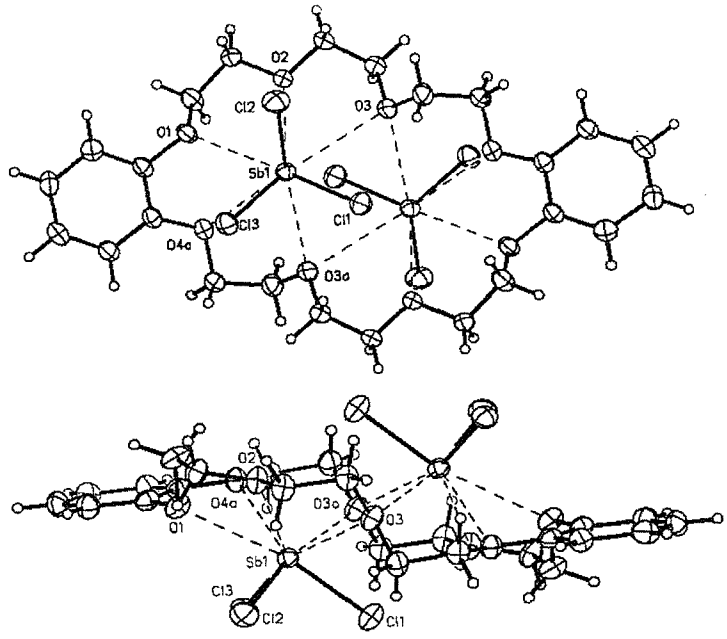

Figure 1.12 Views of the $[(SbCl_3)_2$(dibenzo-24-crown-8)] complex.[79]

In terms of acyclic polyether ligands, Rogers *et al* reported the synthesis and structural characterisation of tetraethylene glycol and pentaethylene glycol (EO_4 and EO_5 respectively) complexes of $BiCl_3$.[76] Both species are structurally very similar to the $[BiCl_3$([15-crown-5)] complex, containing an eight-coordinate, distorted bicapped trigonal prismatic bismuth atom, bound to five oxygen donors and three chlorine atoms. The $[BiCl_3(EO_4)]$ complex exists as a hydrogen-bonded (O-Cl) tetramer, while the uncoordinated oxygen donor in the two forms of the $[BiCl_3(EO_5)]$ complex is also involved in either O-Cl or O-H hydrogen bonding. The Bi-O interactions are quite long, in the range 2.672(8) – 2.828(8) Å for $[BiCl_3(EO_4)]$ and 2.73(1) – 2.91(1) Å for $[BiCl_3(EO_5)]$ (very similar to the distances reported by Alcock *et al* for crown ether complexes).[74]

1.3.3 Complexes of Sulfur, Selenium and Tellurium Donor Ligands

Reports of antimony(III) and bismuth(III) complexes of S-donor ligands (e.g. dithiocarbamates, thiolates, thiocyanates) are much more common than those containing nitrogen and oxygen atoms. However, the structure and bonding of many of these species are not directly related to the chalcogenoether species under study and thus, for brevity, only selected examples are discussed. In view of the lack of examples of AsX_3 complexes containing chalcogen-donor ligands, a general discussion of these adducts is made in the literature review in chapter 4.

A number of N,N-dithiocarbamate and xanthate complexes have been reported, and the majority contain a six-coordinate M atom bound to three chelating R_2NCS_2 or $ROCS_2$ ligands in a distorted octahedral geometry.[80] Two unusual bismuth(III) complexes, containing both thiourea and thiocyanate ligands, were reported recently.[81] The $[Bi(S)NCS(dmit)_3(H_2O)].H_2O$ adduct exists as an irregular octahedral molecule containing dmit ligands bound in a *mer* configuration (Bi-S 2.649(6) – 2.891(9) Å) and a terminal (rather than bridging) N-bonded thiocyanate ligand (Figure 1.13), while the *mer*-$[Bi(SCN)(NCS)_2(dmit)_3]$ complex contains two N-bound and one S-bound terminal thiocyanate ligands (Bi-S 2.789(3) – 2.870(4) Å).[81]

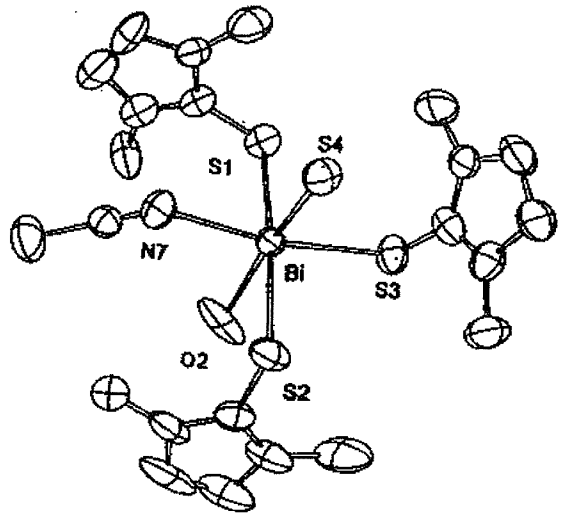

Figure 1.13 View of the $[Bi(S)NCS(dmit)_3(H_2O)].H_2O$ complex.[81]

The antimony(III) thiolate complexes $[Sb\{S(4\text{-}MeC_6H_4)\}_3]$ and $[Sb\{S(o\text{-}C_6H_3(Me)_2)\}_3]$ were prepared by reaction of $SbCl_3$ with the appropriate thiol.[82] Both adducts contain a trigonal-pyramidal antimony atom bound to three arenethiolate groups in a propeller motif (Sb-S ranges 2.4284(8) – 2.4393(7) Å and 2.436(2) – 2.437(2) Å respectively). The former species adopts an extended one-dimensional arrangement due to intermolecular Sb---S contacts (3.7732(8) Å), while the latter shows evidence of intermolecular antimony---arene interactions.

The reaction of $BiCl_3$ with $Pr^n_2P(S)P(S)Pr^n_2$ gave the 1:1 adduct, which adopts a halide-bridged dimer structure where each bismuth is surrounded by four chlorine and two sulfur atoms, the latter chelating to give a five-membered ring.[83] Pohl reported the crystal structures of the dimeric $[SbBr_3(SPPh_3)]_2$ species (Sb-S 2.964(2) Å) (Figure 1.14), where an octahedral antimony geometry was completed by Sb-Ph interactions, and the tetrameric $[SbBr_3(SPMe_2Ph)]_4$ (Sb-S 3.087(4) – 3.182(3) Å).[84]

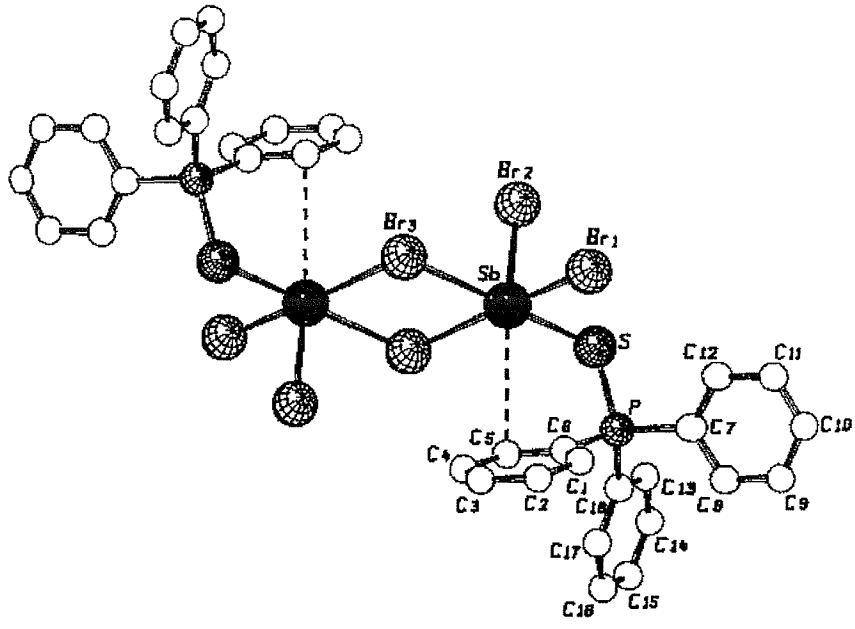

Figure 1.14 View of the $[SbBr_3(SPPh_3)]_2$ complex.[84]

In contrast to the sulfur-containing ligands, examples of MX_3 complexes containing selenium and tellurium ligands are rare. The $[SbI_3(SePPh_3)]_2$ complex was reported by Pohl and is isostructural with the sulfide complex discussed above.[84] Attempts to synthesis a $BiCl_3$ complex of the phosphine selenide $SeP(NMe_2)_3$ produced only the ionic species $[(Me_2N)_3PSeSeP(NMe_2)_3][(BiCl_4)_2]$.[85] IR and Raman data for

N,N-dialkyldiselenocarbamate complexes of arsenic(III), antimony(III) and bismuth(III) has been reported,[86] and Bochmann *et al* described a range of selenolate and tellurolate complexes of MX_3, although no structural data were obtained.[87] The tellurolate complexes were stable only at low temperature, decomposing to diaryl tellurides and elemental tellurium on warming to room temperature.

Although not strictly a coordination complex, the $[Sb(SeMe)_3]$ species is worth highlighting.[88] This substituted stibine compound was obtained by reaction of elemental antimony with Me_2Se_2, with the crystal structure revealing discrete trigonal-pyramidal $SbSe_3$ units (Sb-Se 2.568(1) – 2.588(1) Å). Intermolecular Sb---Se contacts complete a distorted octahedral geometry (Sb---Se 3.546(1) – 3.658(1) Å). The reaction of di-(p-tolyl)telluride with tetra-(*n*-propyl)dibismuthine produced the tellurobismuthine $[(^nPr)_2BiTe(p\text{-}C_6H_4Me)]$ which was characterised by ^{125}Te-NMR (-385 ppm).[89] Aside from solid-state materials and minerals this appears to be the sole example of a compound containing an M-Te bond.

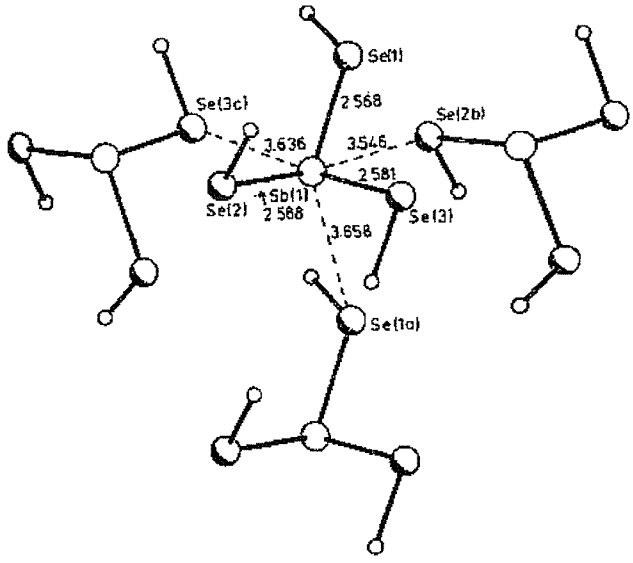

Figure 1.15 View of the $[Sb(SeMe)_3]$ species showing secondary Sb---Se interactions.[88]

1.4 Aims of this study

The work described within this thesis is broadly concerned with the coordination and structural chemistry of a range of heavy p-block complexes containing group 15 and group 16 donor ligands. The aims of the study can be divided into three general themes.

The preparation and structural characterisation of a series of MX_3 complexes (M = Sb, Bi; X = Cl, Br, I) of di-tertiary phosphine and arsine ligands is described in chapter 2. The main focus of this work was to examine the effect of using ligands containing rigid carbon backbones upon the structure of the complex so formed, and to compare these structures to those adopted by complexes with more flexible ligands. A further aim of this work was to examine the coordination chemistry of AsX_3 toward mono- and di-tertiary phosphine and arsine ligands, allowing comparison to the analogous SbX_3 and BiX_3 complexes.

Building upon the examples of bismuth(III)-chalcogenoether complexes recently described by the Southampton research group,[90, 91] the main part of the work aimed to synthesise and structurally characterise a range of MX_3 and $TlPF_6$ complexes of multidentate and macrocyclic chalcogenoether ligands (M = As, Sb; X = Cl, Br, I). Chapter 3 details a study of antimony(III) halide adducts of some bidentate and macrocyclic thio- and seleno-ether ligands, and highlights the range of motifs observed in these complexes. The synthesis and structural diversity of a series of arsenic(III) halide complexes with similar ligands is explored in chapter 4 , while chapter 5 focuses upon the preparation and characterisation of some $TlPF_6$ adducts of selenoethers. The structures of all examples are rationalised in terms of a combination of primary and secondary bonding with respect to the bonding models outlined in section 1.1.2.

Synthetic routes to telluroether species have been a strong interest within the Southampton research group for some time.[92] Chapter 6 describes the synthesis and structures of a range of telluroether-based complexes, from telluronium species to the first structurally characterised bismuth(III)-telluroether complex. Again, the aim was to assess the structures of these species in terms of primary and secondary bonding.

1.5 References

[1] N. C. Norman, *Periodicity and the p-block Elements*, (Ed. J. Evans), Oxford University Press, Oxford, 1995.

[2] H. Schumann and L. Eguran, *J. Organomet. Chem.*, 1991, **403**, 183.

[3] J. F. Sawyer and R. J. Gillespie, *Prog. Inorg. Chem.*, 1986, **34**, 65.

[4] J. Galy and R. Enjalbert, *J. Solid State Chem.*, 1982, **44**, 1.

[5] R. G. Pearson, *Coord. Chem. Rev.*, 1990, **100**, 403 and references therein.

[6] G. N. Lewis, *J. Am. Chem. Soc.*, 1913, **35**, 1448; S. Ahrland, J. Chatt and N. R. Davies, *Q. Rev. Chem. Soc.*, 1958, **12**, 265.

[7] G. E. Kemball, *J. Chem. Phys.*, 1940, **8**, 188.

[8] R. J. Hach and R. E. Rundle, *J. Am. Chem. Soc.*, 1951, **73**, 4321.

[9] G. C. Pimental, *J. Chem. Phys.*, 1951, **19**, 446.

[10] P. v. R. Schleyer and A. E. Reed, *J. Am. Chem. Soc.*, 1990, **112**, 1434; W. Kutzelnigg, *Angew. Chem. Int. Ed. Engl.*, 1984, **23**, 272.

[11] C. J. Carmalt and N. C. Norman in *The Chemistry of Arsenic, Antimony and Bismuth*, (Ed. N. C. Norman), Blackie, New York, 1998 and references therein.

[12] G. A. Landrum, N. Goldberg and R. Hoffmann, *J. Chem. Soc., Dalton Trans.*, 1997, 3605.

[13] G. A. Landrum, N. Goldberg, R. Hoffmann and R. M. Minyaev, *New. J. Chem.*, 1998, 883. G. A. Landrum and R. Hoffmann, *Angew. Chem. Int. Ed. Engl.*, 1998, **13**, 1887.

[14] N. W. Alcock, *Adv. Inorg. Chem. Radio. Chem.*, 1972, **15**, 1.

[15] J. Starbuck, N. C. Norman and A. G. Orpen, *New. J. Chem.*, 1999, **23**, 969 and references therein.

[16] M. L. Munzarová and R. Hoffmann, *J. Am. Chem. Soc.*, 2002, **124**, 4787.

[17] J. Chatt, *Nature (London)*, 1950, **165**, 637.

[18] A. G. Orpen and N. G. Connelly, *Chem. Commun.*, 1985, 1310.

[19] W. Levason in *The Chemistry of Organophosphorus Compounds*, (Ed. F. R. Hartley), Volume 1, Wiley, New York, 1990.

[20] For a recent example, see R. G. Baker and P. G. Edwards, *J. Chem. Soc., Dalton Trans.*, 2002, 2960.

[21] C. A. Tolman, *J. Am. Chem. Soc.*, 1970, **92**, 2956; C. A. Tolman, *Chem. Rev.*, 1977, **77**, 313.

[22] N. R. Champness and W. Levason, *Coord. Chem. Rev.*, 1994, **133**, 115.

[23] D. G. Gilheany and C. M. Mitchell in *The Chemistry of Organophosphorus Compounds*, (Ed. F. R. Hartley), Volume 1, p. 152, Wiley, New York, 1990.

[24] O. Stelzer and K. P. Langhans in *The Chemistry of Organophosphorus Compounds*, (Ed. F. R. Hartley), Volume 1, p. 192, Wiley, New York, 1990.

[25] C. A. McAuliffe in *Comprehensive Coordination Chemistry* (Eds. G. Wilkinson, R. D. Gillard and J. McCleverty), Volume 2, p. 989, Pergamon, Oxford, England, 1987.

[26] H. C. E. McFarlane and W. McFarlane, *Polyhedron*, 1983, **2**, 303; H. C. E. McFarlane and W. McFarlane, *Polyhedron*, 1988, **7**, 1875.

[27] F. A. Hart, *J. Chem. Soc.*, 1960, 3324.

[28] R. Talay and D. Rehder, *Z. Naturforsch.*, 1981, **36b**, 451; B. Chiswell and L. M. Venanzi, *J. Chem. Soc. (A)*, 1966, 417.

[29] E. P. Kyba, S. T. Liu and R. L. Harris, *Organometallics*, 1983, **2**, 1877.

[30] W. Levason, K. G. Smith, C. A. McAuliffe, F. P. McCullough, R. D. Sedgwick and S. G. Murray, *J. Chem. Soc., Dalton Trans.*, 1979, 1718.

[31] R. D. Feltham, A. Kasenally and R. S. Nyholm, *J. Organomet. Chem.*, 1967, **7**, 285.

[32] J. Chatt and F. G. Mann, *J. Chem. Soc.*, 1939, 610.

[33] F. R. Hartley and S. G. Murray, *Chem. Rev.*, 1981, **81**, 365.

[34] E. G. Hope and W. Levason, *Coord. Chem. Rev.*, 1993, **122**, 109.

[35] A. J. Blake and M. Schröder, *Adv. Inorg. Chem.*, 1990, **37**, 1; S. R. Cooper and S. C. Rawle, *Struct. Bonding (Berlin),* 1990, **72**, 1.

[36] W. Levason, S. D. Orchard and G. Reid, *Coord. Chem. Rev.*, 2002, **225**, 159.

[37] F. R. Hartley, W. Levason, C. A. McAuliffe, S. G. Murray and H. E. Soutter, *Inorg. Chim. Acta*, 1979, **35**, 265.

[38] D. J. Gulliver, E. G. Hope, W. Levason, G. L. Marshall, S. G. Murray and D. M. Potter, *J. Chem. Soc., Perkin Trans. 2*, 1984, 429.

[39] E. E. Aynsley, N. N. Greenwood and J. B. Leach, *Chem. Ind. (London),* 1966, 379.

[40] A. D. Westland and L. Westland, *Can. J. Chem.*, 1965, **43**, 426.

[41] E. G. Hope, T. Kemmitt and W. Levason, *Organometallics*, 1988, **7**, 78.

[42] S. R. Cooper, *Acc. Chem. Res.*, 1988, **21**, 141 and references therein.

[43] L. Ochrymowycz, C.-P. Mak and J. D. Michna, *J. Org. Chem.*, 1974, **29**, 2079.

[44] L. F. Lindoy, *The Chemistry of Macrocyclic Ligand Complexes*, Cambridge University Press, Cambridge, 1989.

[45] J. Buter and R. M. Kellogg, *J. Org. Chem.*, 1981, **46**, 4481; J. Buter and R. M. Kellogg, *Chem. Commun.*, 1980, 466.

[46] P. J. Blower and S. R. Cooper, *Inorg. Chem.*, 1987, **26**, 2009.

[47] D. Sellmann and L. Zapf, *J. Organomet. Chem.*, 1985, **289**, 57.

[48] T. Tsuchiya, T. Shimizu and N. Kamitaga, *J. Am. Chem. Soc.*, 2001, **123**, 11534.

[49] R. J. Batchelor, F. W. B. Einstein, I. D. Gay, J. –H. Gu, B. D. Johnston and B. M. Pinto, *J. Am. Chem. Soc.*, 1989, **111**, 6582.

[50] I. Cordova-Reyes, H. Hu, J.-H Gu, E. VandenHoven, A. Mohammed, S. Holdcroft and B. M. Pinto, *Can. J. Chem.*, 1996, **74**, 533.

[51] H. Schumann, A. A. Arif, A. L. Rheingold, C. Janiak, R. Hoffmann and N. Kuhn, *Inorg. Chem.*, 1991, **30**, 1618.

[52] W. Levason, S. D. Orchard and G. Reid, *Organometallics*, 1999, **18**, 1275.

[53] E. W. Abel, R. P. Bush, F. J. Hopton and C. R. Jenkins, *Chem. Commun.*, 1966, 58.

[54] K. G. Orrell, *Coord. Chem. Rev.*, 1989, **96**, 1.

[55] M. Webster and S. Keats, *J. Chem. Soc.* (A), 1971, 836.

[56] R. Hulme and J. S. Scruton, *J. Chem. Soc.* (A), 1968, 2448.

[57] L. P. Battaglia, A. B. Corradi, G. Pelosi, A. Cantoni, G. Alonzo and N. Bertazzi, *J. Chem. Soc., Dalton Trans.*, 1991, 3153.

[58] H. Wunderlich and A. Lipka, *Z. Naturforsch.*, 1980, **35b**, 1548.

[59] D. V. Khasnis, H. Zhang and M. Lattman, *Organometallics*, 1992, **11**, 3748.

[60] G. R. Willey, L. T. Daley, M. D. Rudd and M. G. B. Drew, *Polyhedron*, 1995, **14**, 315.

[61] R. Luckay, I. Cukrowski, J. Mashishi, J. H. Reibenspies, A. H. Bond, R. D. Rogers and R. D. Hancock, *J. Chem. Soc., Dalton Trans.*, 1997, 901.

[62] S. C. James, N. C. Norman and A. G. Orpen, *J. Chem. Soc., Dalton Trans.*, 1999, 2837.

[63] S. C. James, N. C. Norman, A. G. Orpen and J. Starbuck, *Cryst. Eng. Comm.*, 2000, 10.

[64] S. C. James, N. C. Norman, A. G. Orpen and M. J. Quayle, *Acta Crystallogr.*, 1997, **C53**, 1024.

[65] J. R. Eveland and K. H. Whitmire, *Inorg. Chim. Acta*, 1996, **249**, 41.

[66] C. J. Carmalt, W. Clegg, M. R. J. Elsegood, R. J. Errington, J. Havelock, P. Lightfoot, N. C. Norman and A. J. Scott, *Inorg. Chem.*, 1996, **35**, 3709.

[67] G. A. Bowmaker, J. M. Harrowfiled, P. C. Junk, B. W. Skelton and A. H. White, *Aust. J. Chem.*, 1998, **51**, 285.

[68] L. Golic and S. Milicev, *Acta Crystallogr.*, 1978, **B34**, 3379.

[69] M. Vijjulatha, K. C. Kumara Swamy, V. Huch and M. Veith, *Acta Crystallogr.*, 1997, **C53**, 1789.

[70] F. Lazarini and S. Milicev, *Acta Crystallogr.*, 1976, **B31**, 2863.

[71] F. Lazarini, L. Golic and G. Pelizzi, *Acta Crystallogr.*, 1975, **A31**, 5140.

[72] W. Clegg, L. J. Farrugia, A. McCamley, N. C. Norman, A. G. Orpen, N. L. Pickett and S. E. Stratford, *J. Chem. Soc., Dalton Trans.*, 1993, 2579.

[73] G. R. Willey, M. D. Rudd, C. J. Samuel and M. G. B. Drew, *J. Chem. Soc., Dalton Trans.*, 1995, 759.

[74] E. Hough, D. G. Nicholson and A. K. Vasudevan, *J. Chem. Soc., Dalton Trans.*, 1997, 427; N. W. Alcock, M. Ravindran, S. M. Roe and G. R. Willey, *Inorg. Chim. Acta*, 1990, **167**, 115; M. Takahashi, T. Kitazawa and M. Takeda, *Chem. Commun.*, 1993, 1779; I. Becker, M. Windhaus, R. Mattes, *Z. Naturforsch.*, 1994, **49b**, 870.

[75] N. W. Alcock, M. Ravindran and G. R. Willey, *Chem. Commun.*, 1989, 1063; M. G. B. Drew, D. G. Nicholson, I. Sylte and A. Vasudevan, *Inorg. Chim. Acta*, 1990, **171**, 11; N. W. Alcock, M. Ravindran and G. R. Willey, *Acta Crystallogr.*, 1993, **B49**, 507.

[76] R. D. Rogers, A. H. Bond, S. Aguinaga and A. Reyes, *J. Am. Chem. Soc.*, 1992, **114**, 2967.

[77] R. Garbe, B. Vollmer, B. Neumüller, J. Pebler and K. Dehnicke, *Z. Anorg. Allg. Chem.*, 1993, **619**, 271.

[78] A. Nerhaus, G. Frenzen, J. Pebler and K. Dehnicke, *Z. Anorg. Allg. Chem.*, 1993, **618**, 93.

[79] G. R. Willey, D. R. Aris and W. Errington, *Inorg. Chim. Acta*, 2000, **1004**, 1013.

[80] Examples include: V. Venkatachalam, K. Ramalingam, U. Casalleto, R. Graziani, *Polyhedron,* 1997, **16**, 1211; V. Venkatachalam, K. Ramalingam, G. Bocelli and A. Cantoni, *Inorg. Chim. Acta*, 1997, **261**, 23; C. L. Raston and A. H. White, *J. Chem. Soc., Dalton Trans.*, 1976, 791; M. R. Snow and E. R. T. Tienkink, *Aust. J. Chem.*, 1987, **40**, 743; F. Knoedler, W. Schwartz and A. Schmidt, *Z. Naturforsch.*, 1987, **42b**, 1282.

[81] D. J. Williams, T. Carter, K. L. Fahn and D. VanDerveer, *Inorg. Chim. Acta*, 1995, **228**, 69.

[82] W. Clegg, M. R. J. Elsegood, L.J. Farrugia, F. J. Lawlor, N. C. Norman and A. J. Scott, *J. Chem. Soc., Dalton Trans.*, 1995, 2129.

[83] G. R. Willey, J. R. Barras, M. D. Rudd and M. G. B. Drew, *J. Chem. Soc., Dalton Trans.*, 1994, 3025.

[84] S. Pohl, W. Saak, R. Lotz and D. Haase, *Z. Naturforsch.*, 1990, **45b**, 1355.

[85] G. R. Willey, J. R. Barras, M. D. Rudd and M. G. B. Drew, *J. Chem. Soc., Dalton Trans.*, 1994, 3025.

[86] G. E. Manoussakis, A. G. Christophides and M. Lalia-Kantouri, *Inorg. Chim. Acta*, 1977, **25**, 219.

[87] M. Bochmann, X. Song, M. B. Hursthouse and A. Karaulov, *J. Chem. Soc., Dalton Trans.*, 1995, 1649.

[88] H. J. Breunig, S. Gülec, b. Krebs and M. Dartmann, *Z. Naturforsch.*, 1989, **44b**, 1351.

[89] W. W. du Mont, T. Severengiz, H. J. Breunig and D. Müller, *Z. Naturforsch.*, 1985, **40b**, 848.

[90] A. J. Barton, A. R. J. Genge, W. Levason and G. Reid, *J. Chem. Soc., Dalton. Trans.*, 2000, 859; A. R. J. Genge, W. Levason and G. Reid, *Chem. Commun.*, 1998, 2159.

[91] A. J. Barton, A. R. J. Genge, W. Levason and G. Reid, *J. Chem. Soc., Dalton. Trans.*, 2000, 2163.

[92] A. J. Barton, W. Levason, G. Reid and A. J. Ward, *Organometallics*, 2001, **20**, 364 and references therein.

Chapter 2

Group 15 Halide Complexes of Phosphines and Arsines

2.1 Introduction

Initial studies of main group metal-phosphine complexes concentrated upon the group 13 and 14 metals, particularly aluminium(III), gallium(III) and tin(IV). Levason and McAuliffe reviewed the phosphine complexes of these and other p-block elements in 1976.[1] A further review, covering developments up to 1994, has also appeared.[2] As discussed in Chapter 1, there are few reports of arsine, stibine and bismuthine complexes of main group elements. This chapter describes a synthetic and structural study upon a range of coordination complexes of arsenic(III), antimony(III) and bismuth(III) halides with mono- and bidentate tertiary phosphine and arsine ligands.

2.1.1 Bismuth(III) Complexes

Early work upon phosphine complexes of the group 15 element halides concerned complexes of the type $[MCl_3(PMe_3)_n]$ (M = P, As or Sb, n = 1 or 2), with the results based mainly upon vapour pressure measurements.[3] However, this work did little to spark continued interest in the coordination chemistry of the group. Complexes of BiX_3 (X = Cl, Br or I) with dppe were reported by Alonzo *et al*, and were characterised by microanalysis, infrared spectroscopy and mass spectrometry.[4] Although no X-ray structural data were obtained, the authors proposed a ligand-bridged dimer structure for the chloro-complex. A report of the polymeric $[\{Bi_2Br_7(PMe_3)_2\}_n]^{n-}$ anion by Norman and co-workers marked the first example of a structurally characterized bismuth-phosphine complex (and indeed, the first structurally characterised Bi-P bond).[5] The $[BiI_4(PMe_2Ph)_2]^-$ species has also been reported.[6]

Norman *et al* also reported the first structurally characterised neutral bismuth(III) complex of a tertiary phosphine, $[Bi_2Br_6(PMe_3)_4]$ (Figure 2.1).[7] This species was obtained by reaction of $BiBr_3$ in neat PMe_3, and adopts a halide-bridged, edge-shared, bioctahedral dimer structure (Bi-P 2.716(3) – 2.865(3) Å), as does the mixed phosphine/phosphine oxide complex $[Bi_2Br_6(PPhMe_2)_2(OPPhMe_2)_2]$.[6]

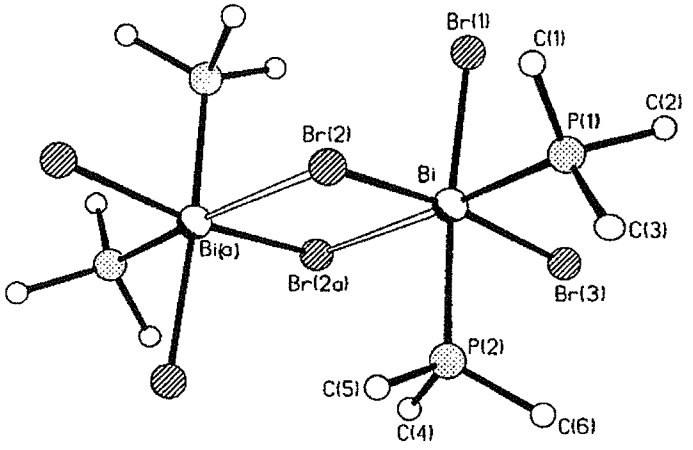

Figure 2.1 View of the structure of the $[Bi_2Br_6(PMe_3)_4]$ complex.[7]

However, the reaction of $BiBr_3$ with two equivalents of PEt_3 in THF yielded the tetrameric $[Bi_4Br_{12}(PEt_3)_4]$ complex.[8] The structure of this species is similar to that adopted by the tetrameric antimony and bismuth halogenoanions $[E_4X_{16}]^{4-}$,[9] and is best described as two halide linked, edge-shared bioctahedral units containing both μ^2- and μ^3-bridging bromine atoms (Figure 2.2). The two crystallographically independent bismuth atoms are each bound to five bromines and one phosphorus atom, with no significant departure from octahedral geometry.

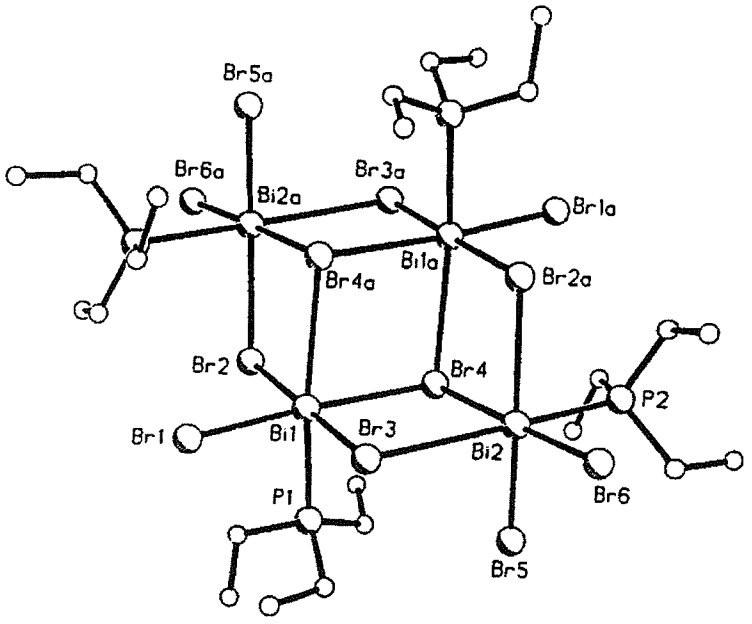

Figure 2.2 View of the structure of the $[Bi_4Br_{12}(PEt_3)_4]$ complex.[8]

Complexes of aliphatic-backboned diphosphine ligands have also been reported, with the structure of the $[Bi_2Br_6(dmpe)_2]$ complex shown to be closely related to the $[Bi_2Br_6(PPhMe_2)_2(OPPhMe_2)_2]$ and $[Bi_2Br_6(PMe_3)_4]$ species.[8] This structural motif is common in MX_3 complexes of tertiary phosphines and arsines, and merits further discussion.

Norman has noted that two trends arise from the above examples.[2] Firstly, the greater *trans* influence of a phosphine compared to a halide is apparent in the lengths of M-X bonds *trans* to M-P bonds (in general, such a bond is *ca.* 0.2 Å longer than a M-X bond *trans* to a halide). Secondly, only the structural isomer A (of the four, A-D, shown in Figure 2.3) is commonly observed. Isomer C would be predicted on stereochemical grounds, and is observed for phosphine complexes of the Group 5 - 9 metals.[2]

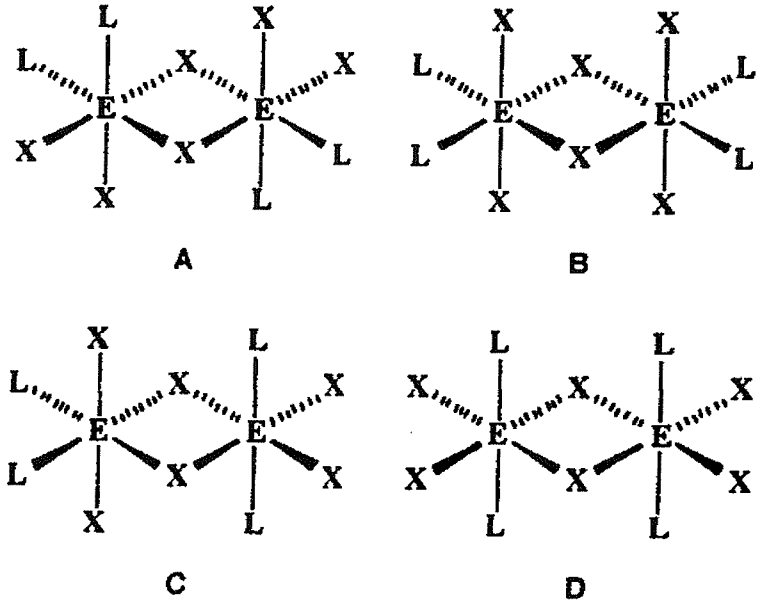

Figure 2.3 Isomers A to D.[2]

As discussed in Chapter 1, the d-orbitals play little part in M-P bonding, with the vacant M-X σ^* anti-bonding orbitals being the acceptors of electron donation. These orbitals are of lower energy than M-P σ^*-antibonding orbitals, and so the phosphine ligand bonds *trans* to a halide, hence isomers C and D are discounted. Norman and Pickett propose that the preference for isomer A over isomer B is due to an electronic effect attributable to the large *trans* influence of the phosphine ligand.[2]

If such a ligand were coordinated *trans* to a bridging halide, as is the case for isomer B, the bridges would weaken to such an extent as to create a pair of adjacent $[MX_2L_2]^+$ species, along with a pair of X^- anions. The close proximity of these ions is energetically unfavorable. The M(III) lone pairs, now more stereochemically active due to the decrease in formal coordination number, would point toward each other, leading to further repulsive effects (Figure 2.4). As is observed in practice, isomer A is the more common (but not exclusive) form in the solid state.

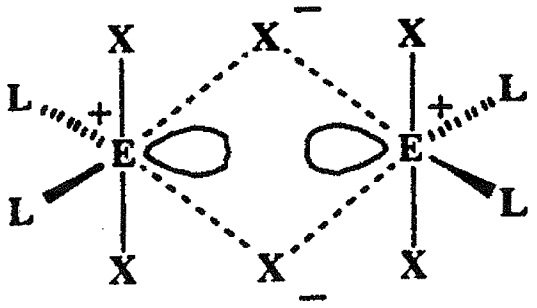

Figure 2.4 Weakening of the M-X-M bridge in an isomer B structure.[2]

Bismuth(III) complexes involving dppm and dppe ligands have been prepared and structurally characterised by Willey and co-workers.[10] The structures of these species do not conform to the above rationale regarding preference for the isomer A motif. The $[Bi_2Cl_6(dppm)_2]$ species consists of two bidentate dppm molecules spanning a coplanar, halide-bridged Bi_2Cl_6 unit in an isomer D arrangement (Bi-P 2.872(3) – 3.090(3) Å) (Figure 2.5). Chelation of this ligand to a single bismuth(III) centre (which would lead to a strained four-membered ring) is disfavoured hence the preference toward a bridging mode and adoption of a less strained six-membered ring.[10]

For the dppe complex two independent molecules exist in the asymmetric unit, identified as $[Bi_2Cl_6(dppe)_2]$ and $[Bi_2Cl_6(dppe)_3]$.[10] The former adopts the isomer A structure, while the latter is a centrosymmetric dimer containing two *mer*-octahedral $BiCl_3(dppe)$ moieties bridged by a dppe molecule (Bi-P 2.654(8) – 2.973(9) Å) (Figure 2.6).

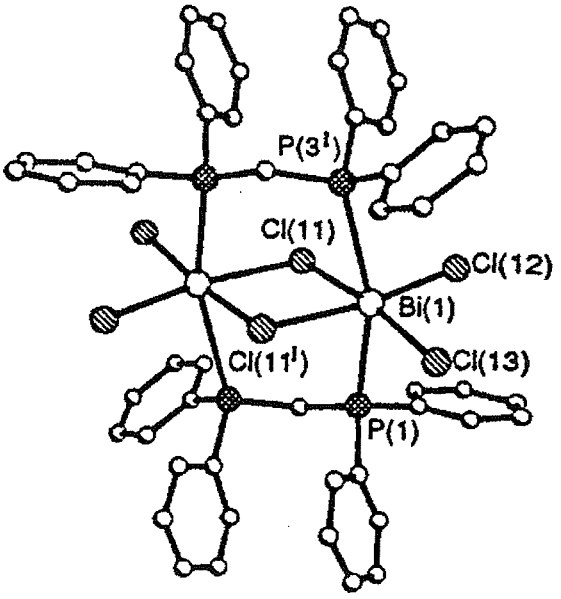

Figure 2.5 View of the $[Bi_2Cl_6(dppm)_2]$ complex.[10]

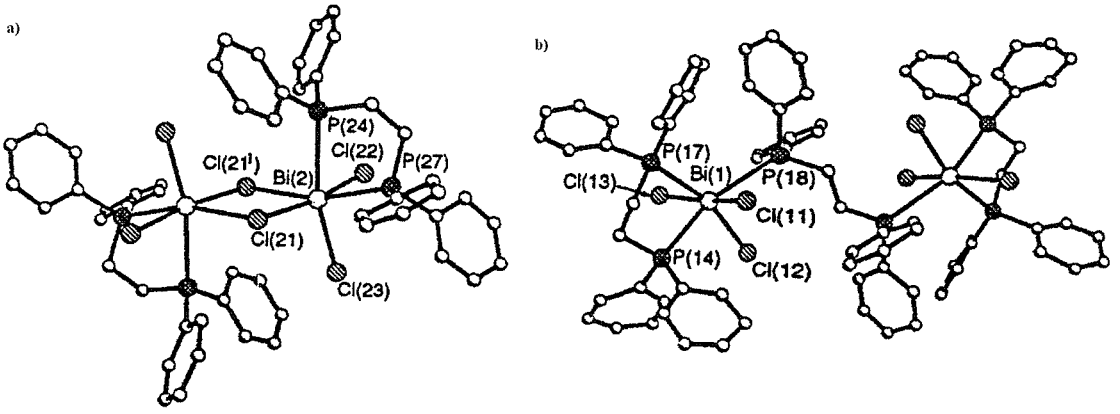

Figure 2.6 View of the a) $[Bi_2Cl_6(dppe)_2]$ and b) $[Bi_2Cl_6(dppe)_3]$ complexes.[10]

There has been little work upon tertiary arsine complexes of bismuth(III) or antimony(III) halides. Sutton studied the reactions of BiX_3 and SbX_3 with diars and concluded, on the basis of molecular weight and conductivity data, that the 1:1 complexes were trigonal pyramidal monomers.[11] However, the $[Bi_2I_6(diars)_2]$ complex was recently shown to adopt the dimeric isomer A structure (Bi-As 2.801(2) – 2.974(2) Å).[12] There are no examples of BiX_3 complexes of tertiary stibines or bismuthines in the literature.

2.1.2 Antimony(III) Complexes

Like the BiX_3 analogues, antimony(III) halide complexes of tertiary phosphines have only recently been isolated, though the formation of such complexes was postulated from NMR evidence by both Summers and Holmes.[3] The first species to be structurally characterised was the monomeric $[SbI_4(dmpe)]^-$ anion, obtained from dissolution of the $[SbI_3(dmpe)]$ complex in pyridine.[13] The antimony atom is coordinated to four iodine and one diphosphine ligand, and shows significant distortion from octahedral geometry. This was rationalised in terms of an arrested double S_N2 transition state for the nucleophillic substitution of two iodide ligands by a dmpe molecule. The anion $[Sb_2Br_7(PEt_3)_2]^-$ has also been reported, and consists of discrete dinuclear units containing three μ^2-bridging bromides.[6]

The direct reaction of SbI_3 and PMe_3 in THF yielded the $[Sb_2I_6(PMe_3)_2]$. THF adduct.[8] Single crystal X-ray diffraction revealed the structure to consist of a weakly interacting polymer of dimers, with one unbound THF molecule of crystallisation per dimer (Figure 2.7). Each dimeric unit is comprised of two edge-sharing square pyramidal antimony atoms coordinated to an apical phosphine (2.633(6) – 2.627(5) Å) and four basal iodines. Two weak, intermolecular antimony-iodine bridges form the polymer (3.547(2) – 3.698(2) Å).

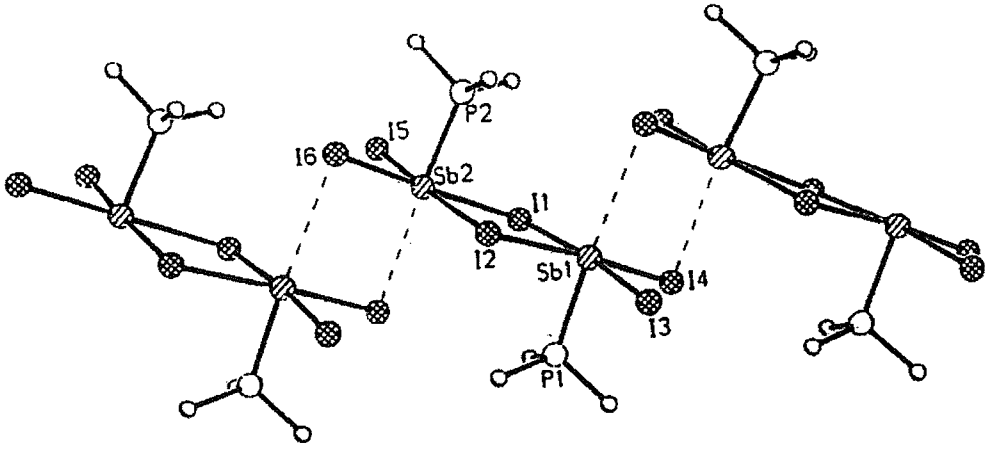

Figure 2.7 View of the $[Sb_2I_6(PMe_3)_2]$ complex (THF molecules not shown).[8]

The same authors have reported two independent polymorphs of $[SbBr_3(dmpe)]$.[8] The first of these, $[Sb_2Br_6(dmpe)_2]$, is isomorphous with the corresponding bismuth(III) complex (i.e. an isomer A dimer), however the second isomer, $[Sb_4Br_{12}(dmpe)_4]$, adopts a tetrameric arrangment (Figure 2.8). The central part of the tetramer is similar to the isomer A dimer, although the halide bridge is highly asymmetric. This unit is linked through near-linear Br-Sb-Br bridges to two $SbBr_3(dmpe)$ species. The Br-Sb-Br bridges are both *trans* to a coordinated phosphine and thus long (3.000(2) – 3.333(2) Å), and the authors suggest that the greater Sb-Sb separation (due to near-linear Br-Sb-Br bridges) serves to reduce the effect of any destabilising lone pair-lone pair repulsion (akin to that proposed in Figure 2.4).[8]

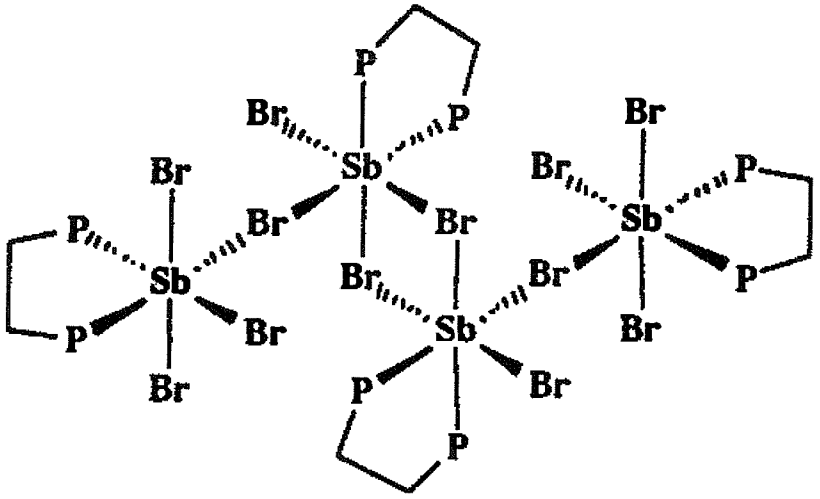

Figure 2.8 View of one of the polymorphs of the $[Sb_4Br_{12}(dmpe)_4]$ complex (methyl groups omitted).[8]

Denker *et al* have reported the synthesis and crystal structures of the $[SbI_2Me(SbMe_3)]$ and $[SbI_3(SbMe_3)(THF)]_2$ complexes.[14, 15] The former contains two crystallographically independent molecules of similar geometry but in different environments. Both of these species adopt a distorted pseudo-trigonal bipyramidal structure with trimethylstibine, the methyl group and the lone pair in the equatorial positions and iodine atoms bound axially.[14] The difference between the two molecules is the extent of the secondary interactions, with one molecule forming an Sb---I contact of 3.480(1) Å *trans* to the Sb-Sb bond and two further such contacts (3.903(1) – 3.970(1) Å) to give an array of tetrameric units. The other molecule is associated with only one neighbour, through a Sb---I contact of 4.234(1) Å, to give a dimer (Figure 2.9). The Sb-Sb distances are similar in each molecule (2.859(1) – 2.868(1) Å).

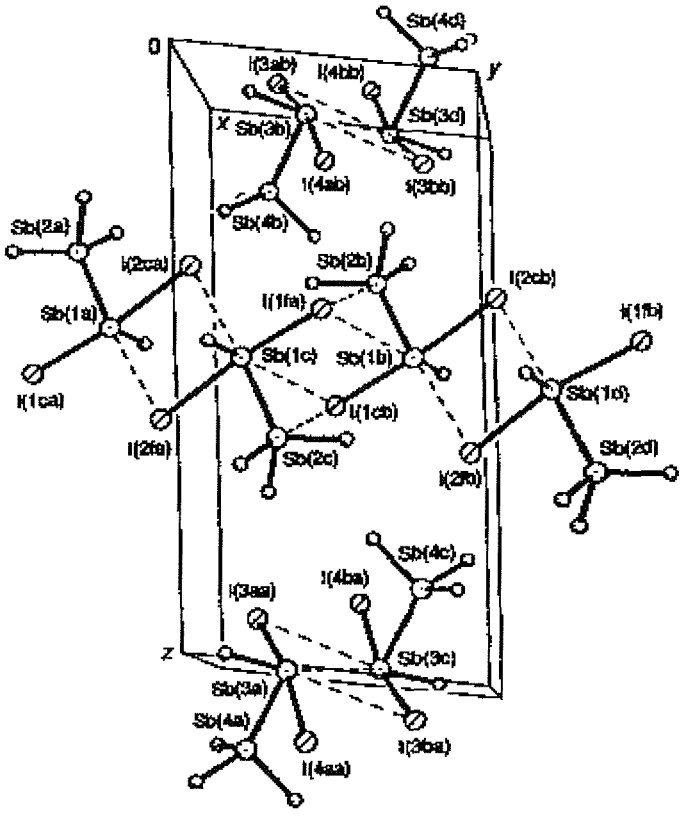

Figure 2.9 View of the secondary interactions in the $[SbI_2Me(SbMe_3)]$ complex.[14]

The $[SbI_3(SbMe_3)(THF)]_2$ complex exists as a centrosymmetric, edge-sharing bioctahedral dimer, comprised of two terminal and two bridging iodines in equatorial positions with $SbMe_3$ and THF molecules bound axially (Sb-Sb 2.8430(10) Å, Sb-O

2.850(10) Å) to give a slightly distorted octahedral geometry (Figure 2.10).[15] This structure can be viewed as being similar to that of the $[SbI_3(PMe_3)_2]$.THF adduct reported by Norman, the major difference being that the coordinated THF molecule in the present complex prevents the formation of intermolecular Sb---I contacts.

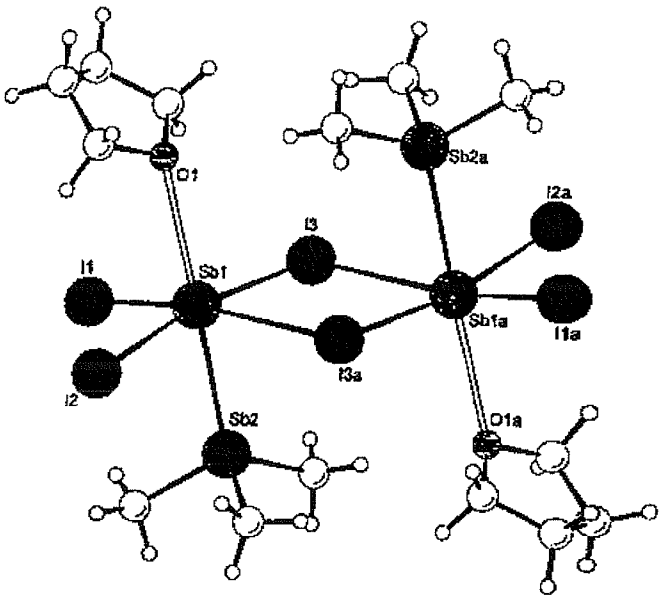

Figure 2.10 View of the structure of $[SbI_3(SbMe_3)(THF)]$.[15]

2.1.3 Arsenic(III) and Phosphorus(III) Complexes

Studies involving arsenic(III) halides acting as Lewis acids towards either amine, phosphine or arsine species are very rare. The $[AsX_3\{o\text{-}C_6H_4(AsMe_2)_2\}]$ complexes were isolated by Sutton and assigned the same structure as those for the corresponding SbX_3 and BiX_3 species.[11] In later work, Summers and Sisler studied the reactions of AsX_3 with PMe_3 and $AsMe_3$.[3] Depending upon the AsX_3 : ligand ratio used for the PMe_3 species, the 1:1 or 1:2 adducts were obtained, however only the 1:1 product was obtained from the $AsMe_3$ system. These adducts were characterised by ^{1}H-NMR spectroscopy, conductivity and microanalysis, although no structural predictions were made.

Recently, Baum and co-workers reported the first structurally characterised AsX_3 complex of a tertiary arsine (Figure 2.11).[16] The $[As_2Cl_6(AsEt_3)_2]$ species adopts a dimeric μ^2-dichloro edge-bridged motif showing a distorted square pyramidal arsenic geometry with two terminal and two bridging halides in the basal plane and two $AsEt_3$ molecules bound in axial, mutually *anti* positions (As-As 2.469(3) Å), similar to the $[SbI_3(PMe_3)_2]$.THF adduct. However, in the present case there is no evidence for intermolecular As---Cl interactions. The angles about the $As(Cl)_2As$ bridge are highly distorted from 90 ° (As1-Cl1-As1' 99.45(5), Cl1-As1-Cl1' 80.55(5) °) and the $AsEt_3$ groups appear to tilt toward the vacant site on the opposite arsenic atom, suggesting that the arsenic-based lone pair is localized along the vector of the bridge. This product was obtained regardless of the reaction stoichiometry. Prior to the work reported in this chapter, there were no structurally characterised $[AsX_3(phosphine)]$ complexes in the literature.

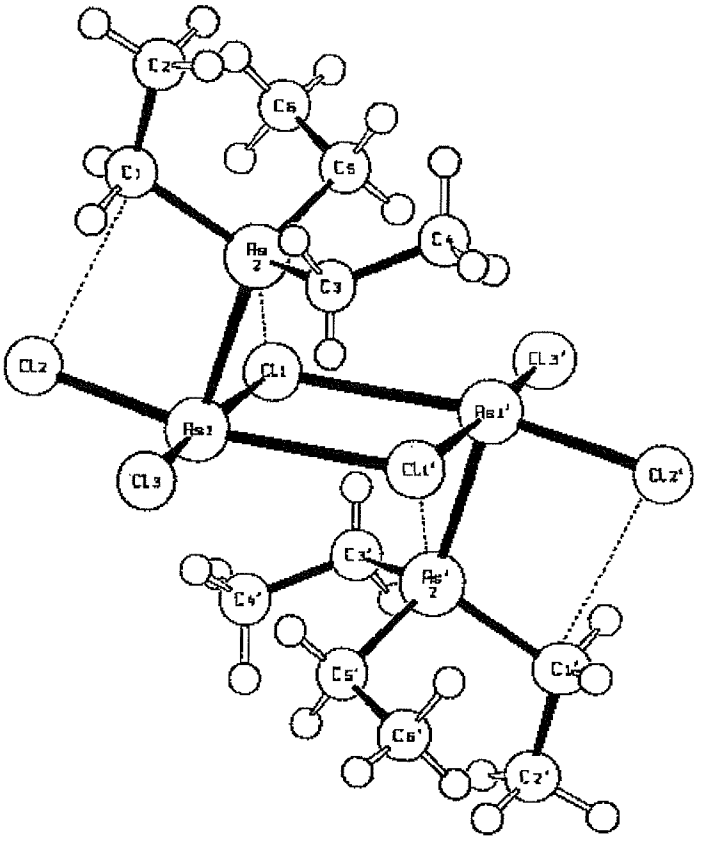

Figure 2.11 View of the $[As_2Cl_6(AsEt_3)_2]$ complex.[16]

As recently as 2002, Müller and co-workers reported the X-ray crystal structures of $[PBr_3(PMe_3)]$ and $[PBr_2Bz(PMe_3)]$, the first such complexes to be structurally characterised (Bz = 3, 5-dimethylbenzyl) (Figure 2.12).[17] The $[PBr_3(PMe_3)]$ adduct exists as dimer, similar to the $[SbI_3(PMe_3)_2].THF$ and $[As_2Cl_6(AsEt_3)_2]$ species, although without the intermolecular contacts of the former. The $[PBr_2Bz(PMe_3)]$ complex adopts a pseudo-trigonal bipyramidal geometry with the phosphorus-based lone pair occupying one of the equatorial positions. The bonding in these species was described as intermediate between the two extremes of a neutral donor-acceptor complex and an ion pair. Of the two adducts, the $[PBr_2Bz(PMe_3)]$ complex was more extensively dissociated, the longest P-Br bond being 2.957(2) Å as opposed to 2.677(2) Å in $[PBr_3(PMe_3)]$. The authors ascribe this difference to the poorer acceptor properties of PBr_2Bz compared to PBr_3. There are no examples of PX_3-AsR_3 complexes in the literature.

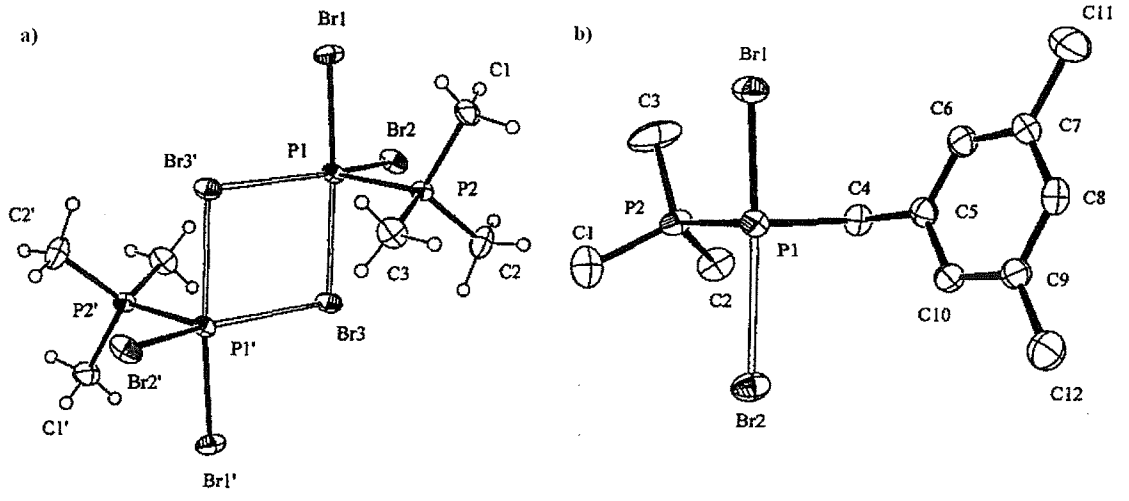

Figure 2.12 View of the a) $[PBr_3(PMe_3)]$ and b) $[PBr_2Bz(PMe_3)]$ complexes.[17]

2.2 Results and Discussion

2.2.1 Antimony(III) and Bismuth(III) – Phosphine Complexes

The reaction of MX_3 (M = Sb or Bi; X = Cl, Br or I) in anhydrous MeCN (X = Cl, Br) or THF (X = I) solutions with one molar equivalent of L (L = o-$C_6H_4(PMe_2)_2$ or o-$C_6H_4(PPh_2)$) in anhydrous CH_2Cl_2 solution immediately produced a yellow or orange solid of general formula $[MX_3(L)]$ in moderate yield. Use of a two-fold excess of ligand failed to produce 1:2 complexes. The solids were filtered under vacuum, washed with anhydrous hexane and dried *in vacuo*. Anhydrous EtOH was occasionally used as solvent, the products obtained being independent of solvent. On account of the moisture sensitivity of MX_3 and the $[MX_3(L)]$ adducts, all reactions were performed under an atmosphere of dry N_2 using standard Schlenk techniques, and the complexes were stored in a dry, N_2-filled glove box.

In general, the $[MX_3(L)]$ complexes were very poorly soluble in chlorocarbons, $MeNO_2$ or MeCN. ^{1}H-NMR spectra (where obtainable) showed resonances little shifted from those for the uncomplexed ligand, indicating solution lability. The $[SbX_3\{o\text{-}C_6H_4(PMe_2)_2\}]$ complexes (X = Cl or Br) were slightly soluble in $MeNO_2$, although $^{31}P\{^1H\}$-NMR spectra recorded at 300 K showed only weak signals due to diphosphine dioxide and, at higher frequencies, halogenated phosphine impurities (R_3PX^+). Spectra obtained at 250 K revealed a sharp singlet at 4.0 ppm (X = Cl) and -6.5 ppm (X = Br) due to the coordinated ligand. These values are shifted from the free ligand resonance of –55.3 ppm. The other complexes were not sufficiently soluble to allow useful low temperature NMR studies.

The infrared spectra of the chloro-derivatives, obtained in nujol, show weak, broad features in the range 230 - 280 cm^{-1} which may be attributed to ν(M-Cl) modes; analogous modes for the parent $BiCl_3$ species were assigned at 242 and 288 cm^{-1} by Oertal.[18] The absence of a strong peak in the range 1200-1100 cm^{-1}, due to phosphine oxide, indicates that the solids do not undergo rapid oxidation. The complexes degrade upon prolonged exposure to air, indicated by a colour change from pale yellow orange to brown and the growth of a broad peak *ca.* 1200-1100 cm^{-1} in the IR spectrum.

Diffuse reflectance UV-visible spectra were obtained for the $[BiX_3\{o\text{-}C_6H_4(PPh_2)_2\}]$ adducts, but show only weak, ill-defined absorptions tailing into the visible region.

Since IR, NMR and UV spectroscopy provided little structural information, single crystal X-ray diffraction studies were required for more complete structural characterisation. The very poor solubility of the complexes in non-coordinating solvents meant that crystals were only obtainable direct from the reaction mixture. A typical crystallisation attempt involved the slow evaporation of solvent from a solution of the starting materials in a N_2-filled glove box. By this procedure, a set of pale yellow block crystals was obtained for the $[SbBr_3\{o\text{-}C_6H_4(PPh_2)_2\}]$ adduct.

The $[SbBr_3\{o\text{-}C_6H_4(PPh_2)_2\}]$ complex adopts an edge-shared, μ-dichloro-bridged, bioctahedral dimer structure (Figure 2.13, Table 2.1), as observed by Norman and others for species such as $[M_2Br_6(dmpe)_2]$ and $[Bi_2Br_6(PMe_3)_4]$.[7, 8]

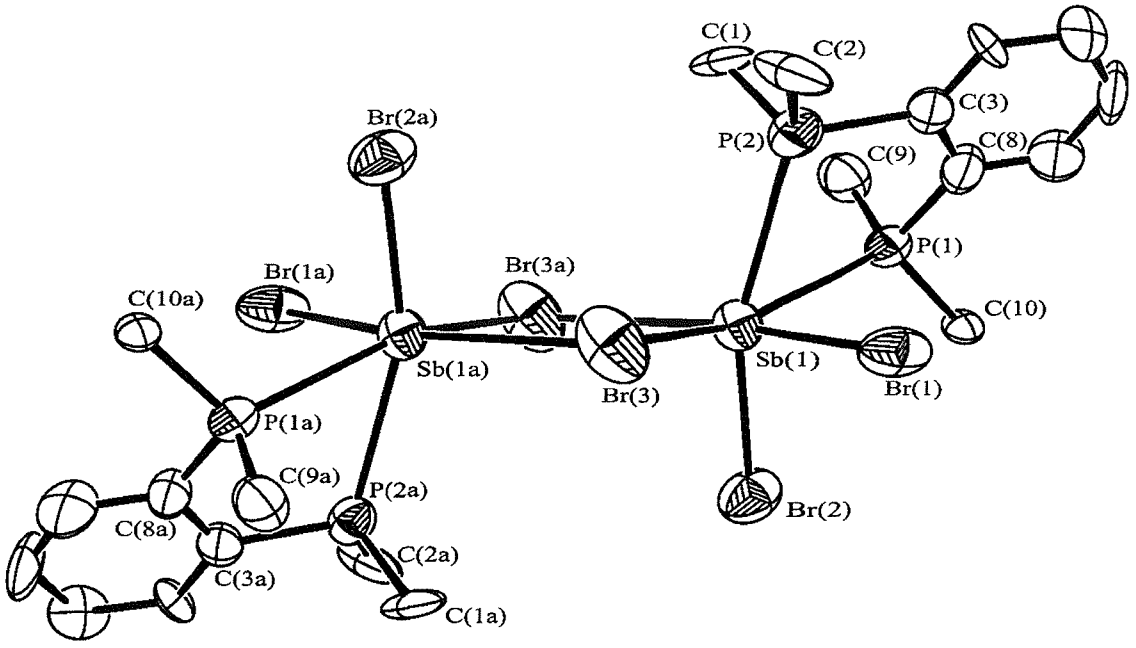

Figure 2.13 View of the structure of $[SbBr_3\{o\text{-}C_6H_4(PPh_2)_2\}]$ with the numbering scheme adopted. Ellipsoids drawn at 40 % probability, with phenyl groups and H-atoms omitted for clarity.

The Sb-P bond lengths (2.91(2) - 3.01(2) Å) are somewhat longer than those observed in the isomorphous $[Sb_2Br_6(dmpe)_2]$ complex (2.575(3) - 2.659(3) Å), indicating that the alkyl substituted phosphine is a stronger donor toward $SbBr_3$.[8] The P-C bond distances are little changed from those observed in the uncoordinated phosphine (average 1.820 *vs.* 1.842 Å).[19] However, the Sb-Br distances and Sb(μ-Br)$_2$Sb bridge asymmetry (2.540(9) - 2.657(9) and 2.679(8) - 3.51(1) Å, Δ = 0.83 Å) are similar to those in the $[Sb_2Br_6\{Me_2P(CH_2)_2PMe_2\}_2$ adduct (2.695(1) - 2.828(1) and 3.003(1) - 3.595(1) Å, Δ = 0.77 Å).[8] Thus the bridges in these SbX_3 adducts are much more distorted than in $[Bi_2Br_6\{Me_2P(CH_2)_2PMe_2\}_2]$ (Δ = 0.46 Å).

Sb(1)	Br(1)	2.540(9)	Sb(1)	Br(3a)	3.513(1)
Sb(1)	Br(2)	2.657(9)	Sb(1)	P(1)	3.011(2)
Sb(1)	Br(3)	2.679(8)	Sb(1)	P(2)	2.919(2)
Br(1)	Sb(1) Br(2)	88.01(3)	Br(1)	Sb(1) Br(3)	91.49(3)
Br(1)	Sb(1) Br(3a)	172.21(2)	Br(1)	Sb(1) P(1)	81.90(4)
Br(1)	Sb(1) P(2)	79.36(4)	Br(2)	Sb(1) Br(3)	100.02(3)
Br(2)	Sb(1) Br(3a)	87.22(3)	Br(2)	Sb(1) P(1)	98.82(4)
Br(2)	Sb(1) P(2)	160.56(4)	Br(3)	Sb(1) Br(3a)	83.31(3)
Br(3)	Sb(1) P(1)	159.85(4)	Br(3)	Sb(1) P(2)	95.13(4)
Br(3a)	Sb(1) P(1)	104.93(4)	Br(3a)	Sb(1) P(2)	106.8(2)

Table 2.1 Selected bond distances (Å) and angles (°) with e.s.d.'s for $[Sb_2Br_6\{o\text{-}C_6H_4(PPh_2)_2\}_2]$

In an attempt to obtain a crystalline sample of the $[BiCl_3\{o\text{-}C_6H_4(PPh_2)_2\}]$ complex, a 1:1 ratio of the starting materials was dissolved in anhydrous THF and the solution layered with anhydrous hexane. A set of crystals suitable for X-ray diffraction studies were obtained, however the complex contained the diphosphine dioxide species, $o\text{-}C_6H_4(P(O)Ph_2)_2$. IR spectra of the free $o\text{-}C_6H_4(PPh_2)_2$ ligand did not show bands in the 1200 cm^{-1} region due to P=O, thus adventitious air is the most likely oxygen source. Similar *in situ* oxidation of the $[BiCl_3(\{Ph_2PCH_2PPh_2\})]$ and $[BiCl_3(Ph_2As(CH_2)_2AsPh_2)]$ complexes has been reported by Willey and co-workers.[20]

The X-ray crystal structure of the $[BiCl_3\{o\text{-}C_6H_4(P(O)Ph_2)_2\}(THF)]$ species shows a distorted octahedral geometry around the bismuth atom (Figure 2.14, Table 2.2), and is similar to that recently reported for the $[SnI_4(o\text{-}C_6H_4\{P(O)Ph_2\}_2)_2]$ complex.[21] Coordination of the diphosphine dioxide ligand to the bismuth atom is through two mutually *cis* oxygen atoms (Bi-O_P 2.444(2) - 2.470(3) Å), forming a seven-membered chelate ring. These bonds are significantly longer than analogous bonds in the complex $[BiCl_3\{Ph_2P(O)CH_2P(O)Ph_2\}]$ (2.31(3) - 2.42(1) Å) which, unlike the present complex, has close to idealised octahedral geometry and adopts the isomer A structure.[20] The Bi-O_P bond length is also longer than that found in the $(\mu\text{-}Br)_2$ bridged square pyramidal $[(BiPhBr_2)_2(OPPh_3)_2]$ complex (2.390(9) Å).[22]

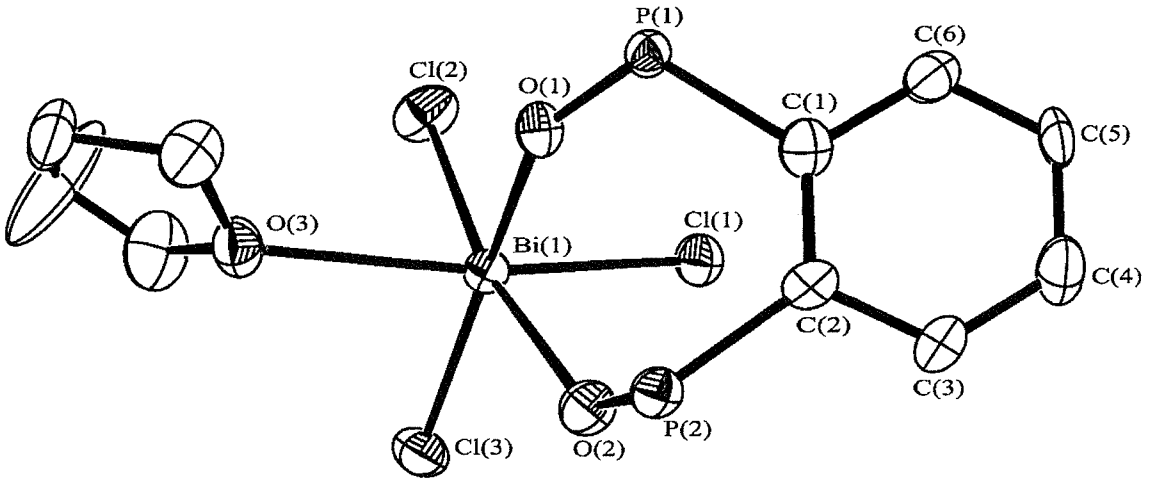

Figure 2.14 View of the structure of $[BiCl_3\{o\text{-}C_6H_4(P(O)Ph_2)_2\}(THF)]$. Details as for Figure 2.13, phenyl groups omitted for clarity.

The Bi-O_{THF} bond distance is 2.709(6) Å, similar to the maximum Bi-O_{THF} bond length of 2.700(7) Å observed in recent structural studies upon THF adducts of BiX_3, although the average Bi-O_{THF} distance was *ca.* 2.62 Å in these species.[23]

Bi(1)	Cl(1)	2.518(2)	Bi(1)	O(1)	2.470(5)
Bi(1)	Cl(2)	2.576(2)	Bi(1)	O(2)	2.444(5)
Bi(1)	Cl(3)	2.593(2)	Bi(1)	O(3)	2.709(6)
Cl(1)	Bi(1) Cl(2)	89.11(8)	Cl(1)	Bi(1) Cl(3)	96.19(7)
Cl(1)	Bi(1) O(1)	92.9(1)	Cl(1)	Bi(1) O(2)	83.0(1)
Cl(1)	Bi(1) O(3)	168.6(1)	Cl(2)	Bi(1) Cl(3)	99.26(8)
Cl(2)	Bi(1) O(1)	97.0(1)	Cl(2)	Bi(1) O(2)	168.7(1)
Cl(2)	Bi(1) O(3)	79.5(1)	Cl(3)	Bi(1) O(1)	161.5(1)
Cl(3)	Bi(1) O(2)	89.7(1)	Cl(3)	Bi(1) O(3)	86.4(1)
O(1)	Bi(1) O(2)	75.4(3)	O(1)	Bi(1) O(3)	87.9(2)
O(2)	Bi(1) O(3)	108.2(2)			

Table 2.2 Selected bond distances (Å) and angles (°) with e.s.d.'s for [$BiCl_3${o-$C_6H_4(POPh_2)_2$}(THF)].

Bulk samples of the diphosphine dioxide complexes were obtained, in moderate yield, as white or pale yellow solids by addition of an anhydrous THF solution of BiX_3 (X = Cl or Br) to an equimolar THF solution of the diphosphine dioxide ligand followed by treatment of the mixture with hexane. Microanalyses corresponding to 1:1 stoichiometry were obtained for all freshly prepared solids. A strong, broad peak *ca.* 1150 cm^{-1} in the nujol IR spectra confirmed the presence of the coordinated diphosphine dioxide ligand, shifted from *ca.* 1200 cm^{-1} for the uncoordinated ligand. Features in the range 230-280 cm^{-1}, attributable to Bi-Cl stretches, were also observed in the chloro-derivative. The diphosphine dioxide complexes were more soluble in

halocarbon solvents than the analogous phosphine species and were thus amenable to both ^{1}H and $^{31}P\{^{1}H\}$ NMR spectroscopy. The ^{1}H NMR spectrum confirms the presence (X = Cl) or absence (X = Br) of a coordinated THF molecule, while the $^{31}P\{^{1}H\}$ NMR spectrum, obtained in CH_2Cl_2 at room temperature, reveals a sharp singlet at δ 34.5 ppm. This value is only slightly shifted from the resonance of uncoordinated o-$C_6H_4(POPh_2)_2$ (δ 33.6 ppm), consistent with other complexes of this ligand.[21, 24] Despite the enhanced solubility of the phosphine oxide complexes, no crystals of the bromo-complex could be isolated. It is likely that the THF-free bromide analogue adopts the isomer A structure, with dimerisation *via* bridging bromide ligands replacing the weak Bi-THF interaction. In effect, the weakly bound THF molecule blocks the bridging site.

Very small, pale yellow plate crystals of [$BiCl_3${o-$C_6H_4(PPh_2)_2$}] were obtained as for the [$SbBr_3${o-$C_6H_4(PPh_2)_2$}] complex. Although weakly diffracting, the crystals were of suitable quality for X-ray diffraction studies. Unfortunately the data obtained were of rather low quality (R = 0.12) and thus comparisons of bond distances and angles with other similar MX_3 species are not warranted. However, the data were sufficient to establish the overall coordination geometry at the bismuth atom, revealing that the structure is very similar to that of the [$SbBr_3${o-$C_6H_4(PPh_2)_2$}] complex (i.e. a bioctahedral dimer in the isomer A motif).

2.2.2 Antimony(III) – Arsine Complexes

The reaction of SbX_3 (X = Cl, Br or I) with one molar equivalent of L (L = o-$C_6H_4(AsMe_2)_2$, $Ph_2As(CH_2)_2AsPh_2$ or $MeC(CH_2AsMe_2)_3$), both in anhydrous EtOH solution, produced white or yellow solids of general formula $[SbX_3(L)]$ in moderate yield. Use of a twofold excess of ligand failed to produce 1:2 complexes. The solids were isolated and stored as for the SbX_3 and BiX_3 complexes discussed in section 2.2.1. Microanalytical data corresponding to 1:1 stoichiometry were recorded for all freshly prepared solids, and nujol IR spectra revealed weak, broad bands in the range 230 –270 cm^{-1} due to Sb-Cl stretches. Again, very low solubility in non-donor solvents prevented NMR studies and production of crystals by normal recrystalisation techniques. However, slow evaporation of solvent from the $SbCl_3$-o-$C_6H_4(AsMe_2)_2$ reaction solution yielded a set of colourless, block crystals of the $[Sb_2Cl_6$ {o-$C_6H_4(AsMe_2)_2$}] adduct suitable for X-ray diffraction studies.

The solid-state structure of the complex reveals an extended coordination network, consisting of $SbCl_2${o-$C_6H_4(AsMe_2)$} fragments weakly cross-linked into a two-dimensional chain by $SbCl_4$ units (Figures 2.15 and 2.16, Table 2.3). Such a motif is unexpected and in stark contrast to the analogous $[BiI_3${o-$C_6H_4(AsMe_2)_2$}] complex.[15] The donor set of the $SbCl_2${o-$C_6H_4(AsMe_2)$} moiety is comprised of the terminal chlorine Cl(1) (2.580(2) Å), the bridging primary chlorine Cl(2) (2.573(2) Å), two weakly bonded bridging chlorine atoms Cl(3) and Cl(5a) (3.141(2), 3.020(3) Å) and a symmetrically bound, chelating diarsine (2.664(1) Å), with the $SbCl_2${o-$C_6H_4(AsMe_2)$} fragments linked to $SbCl_4$ units by Sb(μ-Cl)Sb bridges. The geometry about the central antimony atom is severely distorted from octahedral, although it is unclear as to whether the distortion is due to lone pair effects or a consequence of the novel coordination environment. The $SbCl_4$ unit consists of terminal chlorines Cl(4) and Cl(6) (2.352(3) - 2.366(3) Å) and primary bridging chlorines Cl(3) and Cl(5) (2.603(3) - 2.618(2) 2.603(3)), with a weak, secondary Sb-Cl contact Cl(2) (3.267(3) Å) completing the square pyramidal donor set. Microanalytical data consistent with a 2:1 $SbCl_3$:o-$C_6H_4(AsMe_2)_2$ ratio were obtained.

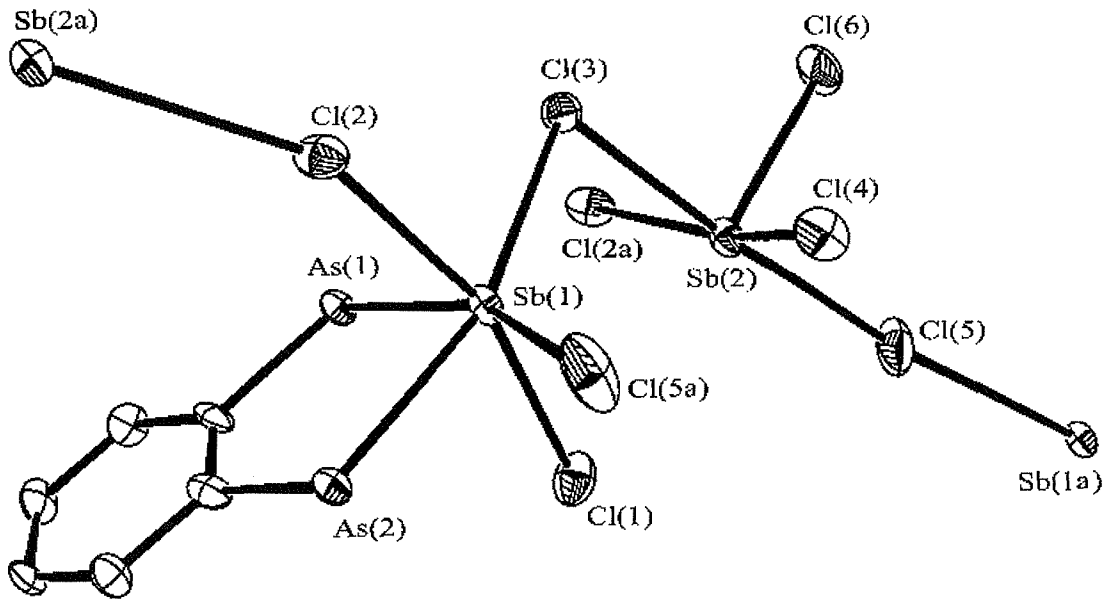

Figure 2.15 View of the structure of the asymmetric unit of $[Sb_2Cl_6\text{-}\{o\text{-}C_6H_4(AsMe_2)_2\}]$. Details as for Figure 2.12, methyl groups omitted for clarity.

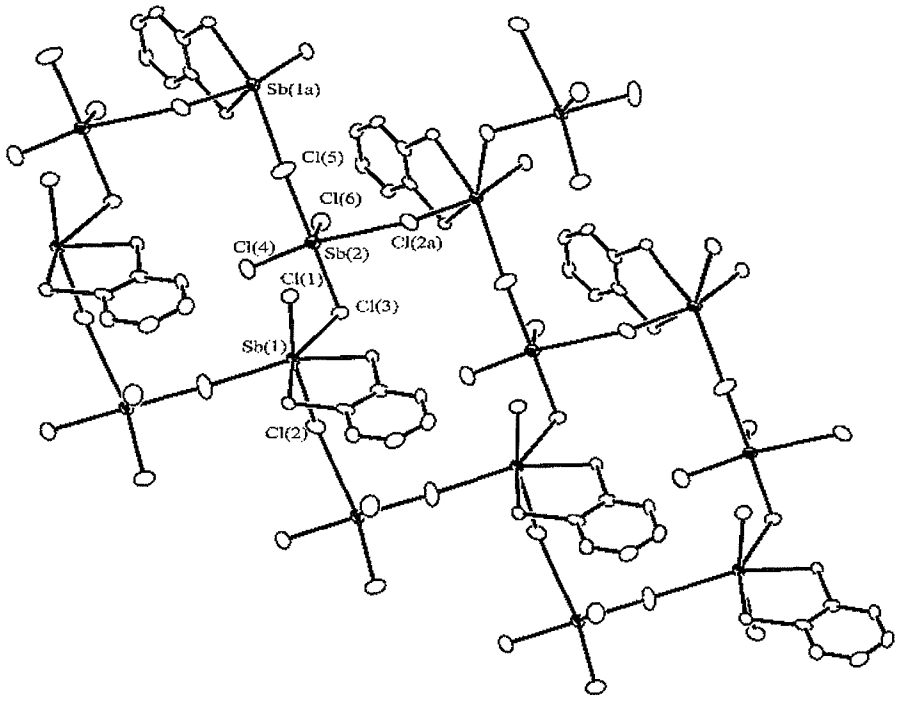

Figure 2.16 View of a portion of the extended network adopted by $[Sb_2Cl_6\{o\text{-}C_6H_4(AsMe_2)_2\}]$.

Sb(1) As(1)	2.663(1)	Sb(1) As(2)	2.664(1)
Sb(1) Cl(1)	2.580(2)	Sb(1) Cl(2)	2.573(2)
Sb(1) Cl(3)	3.141(2)	Sb(1) Cl(5a)	3.020(3)
Sb(2) Cl(3)	2.618(2)	Sb(2) Cl(4)	2.366(3)
Sb(2) Cl(5)	2.603(3)	Sb(2) Cl(6)	2.352(3)
Sb(2) Cl(2a)	3.267(3)		
As(1) Sb(1) As(2)	81.23(3)	As(1) Sb(1) Cl(1)	82.45(6)
As(1) Sb(1) Cl(2)	80.69(7)	As(1) Sb(1) Cl(3)	72.06(6)
As(1) Sb(1) Cl(5a)	156.49(6)	As(2) Sb(1) Cl(1)	84.07(7)
As(2) Sb(1) Cl(2)	82.51(6)	As(2) Sb(1) Cl(3)	153.21(6)
As(2) Sb(1) Cl(5a)	75.65(6)	Cl(1) Sb(1) Cl(2)	159.84(9)
Cl(1) Sb(1) Cl(3)	94.17(7)	Cl(1) Sb(1) Cl(5a)	99.14(9)
Cl(2) Sb(1) Cl(3)	91.08(7)	Cl(2) Sb(1) Cl(5a)	92.04(9)
Cl(3) Sb(1) Cl(5a)	130.77(8)	Cl(3) Sb(2) Cl(4)	87.83(9)
Cl(3) Sb(2) Cl(6)	89.27(9)	Cl(3) Sb(2) Cl(5a)	177.20(9)
Cl(3) Sb(2) Cl(2a)	81.22(7)	Cl(4) Sb(1) Cl(5)	90.81(1)
Cl(4) Sb(2) Cl(2a)	168.81(9)	Cl(5) Sb(2) Cl(2a)	100.02(9)
Cl(6) Sb(2) Cl(4)	94.19(9)	Cl(6) Sb(2) Cl(5)	88.48(1)
Cl(6) Sb(2) Cl(2a)	83.57(9)	Sb(1) Cl(2) Sb(2a)	156.55(1)
Sb(2) Cl(5) Sb(1a)	172.53(1)		

Table 2.3 Selected bond distances (Å) and angles (°) for $[Sb_2Cl_6\{o\text{-}C_6H_4(AsMe_2)_2\}]$.

The present structure provides the first example of a coordination polymer derived from an $[MX_3(L)]$ complex although, in view of the preference for the isomer A dimer structure in the solid state, it is likely that the extended chain structure is due to degradation of a parent dimeric molecule.

Attempts to crystallise the $[SbCl_3(Ph_2As(CH_2)_2AsPh_2)]$ complexes produced a few large, colourless needle crystals suitable for X-ray diffraction studies. However, data analysis revealed the crystals to be uncomplexed 1,2-bis(diphenylarsino)ethane and subsequent attempts produced crystal of insufficient quality.[25] Attempts to isolate crystals of the $[BiCl_3\{o\text{-}C_6H_4(AsMe_2)_2\}]$ complex for comparison with $[BiI_3\{o\text{-}C_6H_4(AsMe_2)_2\}]$ were plagued by similar problems, although microanalytical data confirms a 1:1 stoichiometry for the bulk sample.

2.2.3 Arsenic(III) – Phosphine and Arsine Complexes

Reaction of AsX_3 (X = Cl, Br and I) with one molar equivalent of L (L = PMe_3, $AsMe_3$, o-$C_6H_4(PMe_2)_2$, o-$C_6H_4(PPh_2)_2$, o-$C_6H_4(AsMe_2)_2$ or $MeC(CH_2AsMe_2)_3$) in anhydrous CH_2Cl_2 or Et_2O (X = Cl and Br) or THF solutions (X = I) produced white or pale yellow solids in moderate to good yield. In some cases (L = PMe_3, $AsMe_3$, o-$C_6H_4(PMe_2)_2$) the reactions were performed at low temperature (*ca.* -30° C) using a solid CO_2/CCl_4 slush bath. The solids were isolated and stored as previously. Use of two molar equivalents of PMe_3 affords products of composition $[AsX_3(PMe_3)_2]$ (X = Cl, Br) whereas reaction of $AsCl_3$ with one equivalent of PMe_3 gives the 1:1 product. No 1:1 adduct was obtained from the reaction of $AsBr_3$ with PMe_3. Reaction of AsX_3 with $AsMe_3$ affords only the 1:1 product $[AsX_3(AsMe_3)]$, using either a 1:1 or 1:2 AsX_3:$AsMe_3$ ratio. These observations are in accord with those of Summers and Sisler.[3]

The complexes were very poorly soluble in non-donor solvents, however $^{31}P\{^1H\}$ NMR spectra of the $[AsCl_3(PMe_3)_n]$ (n = 1 or 2) adducts each showed a broad singlet at 27 ppm. This signal is lost upon addition of excess PMe_3, with a broad resonance developing at lower frequency, indicative of fast-exchange with free PMe_3 (- 62 ppm). The $^{31}P\{^1H\}$-NMR spectra of $[AsBr_3(PMe_3)_2]$ showed a singlet at 16 ppm. ^1H-NMR spectra show two overlapping doublets for $[AsCl_3(PMe_3\}]$ and $[AsCl_3(PMe_3)_2]$, consistent with the presence of both 1:1 and 1:2 species in each case.

Only one doublet is observed for $[AsBr_3(PMe_3)_2]$ (J_{PH} = 12 Hz). For the $[AsX_3\{o\text{-}C_6H_4(PPh_2)_2\}]$ complexes $^{31}P\{^1H\}$-NMR spectra show a mixture of products, including halogenated o-$C_6H_4(PPh_2)_2$, indicating that these adducts rapidly decompose in solution Infrared spectra of the chloro- and bromo-complexes show very broad features in the ranges 420-380 and 270-260 cm^{-1} respectively, which are assigned as ν(As-X) bands.[26] The IR spectra are otherwise uninformative. Satisfactory microanalytical data were obtained for all freshly prepared solids.

As for the insoluble SbX_3 and BiX_3 complexes discussed previously, the techniques of NMR and IR spectroscopy provide very little information regarding the structural properties of these $[AsX_3L]$ complexes. Thus, emphasis was placed upon production of single crystals suitable for X-ray diffraction studies. A set of modest quality crystals of $[AsCl_3(PMe_3)]$ was obtained by slow evaporation of a solution of $AsCl_3$ in anhydrous CH_2Cl_2 layered onto a solution of PMe_3 in toluene in an N_2 purged glove box.

The asymmetric unit contains two discrete, crystallographically independent $[AsCl_3(PMe_3)]$ units, and the As-P bond distances are very similar (As(1)-P(1) 2.380(5), As(2)-P(2) 2.388(5) Å). The $[AsCl_3(PMe_3)]$ complex exists in the solid state as an edge-shared, μ-dichloro-bridged dimer with a planar $Cl_2As(\mu\text{-}Cl)_2AsCl_2$ core and a single PMe_3 ligand axially coordinated to each As atom, the phosphines adopting mutually *anti* positions (Figure 2.17, Table 2.4).

The $As(\mu\text{-}Cl)_2As$ core of the dimer containing As(2) is quite symmetrical (2.795(5), 2.908(5) Å, Δ = 0.113 Å), with terminal As-Cl bond distances of 2.298(5) and 2.270(5) Å. The bond angles about the As(2) atom show no significant departure from a regular octahedron (although the bridge angles are somewhat distorted), and the arsenic-based lone pair is likely to occupy the vacant axial coordination site. The bond length distribution at As(1) is more distorted with an asymmetric $As(\mu\text{-}Cl)_2As$ bridging unit (2.625(6), 2.907(6) Å, Δ = 0.282 Å), while the terminal As-Cl distances differ by *ca.* 0.1 Å (2.333(6), 2.242(5) Å), although the angles about As(1) are similar to those in the As(2) dimer.

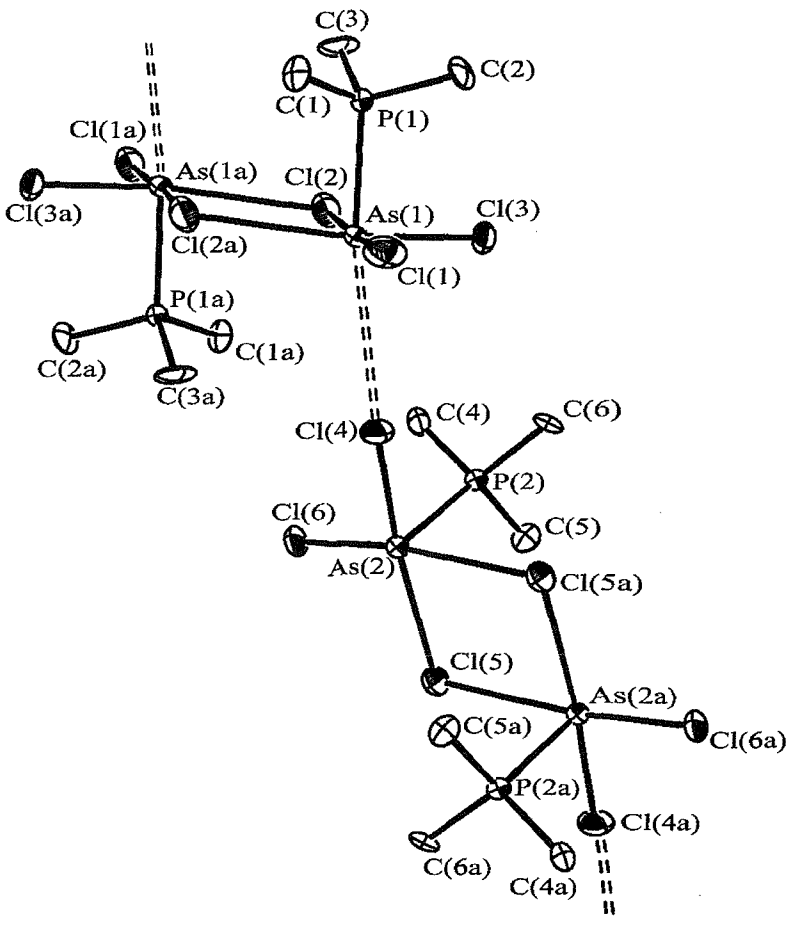

Figure 2.17 View of the packing of $[AsCl_3(PMe_3)]$ showing the long range As(1)···Cl(4) intermolecular contact and orthogonal arrangement of dimer units. Ellipsoids shown at 40 % probability, H-atoms omitted for clarity. Atoms marked (a) are related by the symmetry operation -x, -y, -z.

The packing of the two discrete dimeric units is unusual, with the As(1) and As(2) dimers disposed almost orthogonally and a long range, intermolecular As-Cl contact of *ca.* 3.43 Å between As(1) and Cl(4). This motif is repeated to give infinite chains of weakly associated dimers (Figure 2.18). This intermolecular As-Cl contact is within the sum of the van der Waal's radii for As and Cl (3.60 Å),[27] and indicates that the sixth coordination site on As(1) is occupied by a secondary interaction, which probably stabilizes the observed orthogonal chain arrangement. Thus, As(1) adopts a [5+1] coordination environment.

As(1)	P(1)	2.380(5)	As(1)	Cl(1)	2.333(6)
As(1)	Cl(2)	2.625(6)	As(1)	Cl(2a)	2.907(6)
As(1)	Cl(3)	2.242(5)	As(1)	Cl(4)	3.432(5)
As(2)	P(2)	2.388(5)	As(2)	Cl(4)	2.298(5)
As(2)	Cl(5)	2.795(5)	As(2)	Cl(5a)	2.809(5)
As(2)	Cl(6)	2.270(5)	P(1)	C(1)	1.776(3)
Cl(1)	As(1) Cl(2)	175.6(2)	Cl(1)	As(1) Cl(2a)	98.0(2)
Cl(1)	As(1) Cl(3)	92.8(2)	Cl(1)	As(1) P(1)	84.4(2)
Cl(1)	As(1) Cl(4)	81.3(1)	Cl(2)	As(1) Cl(2a)	81.4(2)
Cl(2)	As(1) Cl(3)	87.4(2)	Cl(2)	As(1) Cl(4)	103.1(2)
Cl(2)	As(1) P(1)	91.1(2)	Cl(2a)	As(1) Cl(3)	167.5(2)
Cl(2a)	As(1) P(1)	91.9(2)	Cl(3)	As(1) P(1)	91.9(2)
Cl(3)	As(1) Cl(4)	83.0(3)	Cl(4)	As(1) P(1)	164.6(2)
Cl(4)	As(2) Cl(5)	174.7(2)	Cl(4)	As(2) Cl(5a)	94.3(2)
Cl(4)	As(2) Cl(6)	95.6(2)	Cl(4)	As(2) P(2)	86.1(2)
Cl(5)	As(2) Cl(5a)	81.2(2)	Cl(5)	As(2) Cl(6)	88.7(2)
Cl(5)	As(2) P(2)	90.8(2)	Cl(5a)	As(2) Cl(6)	169.4(2)
Cl(5a)	As(2) P(2)	85.7(2)	Cl(6)	As(2) P(2)	91.2(5)
As(1)	Cl(2) As(1a)	98.6(2)	As(2)	Cl(5) As(2a)	98.8(2)

Table 2.4 Selected bond distances (Å) and angles (°) for $[AsCl_3(PMe_3)]$.

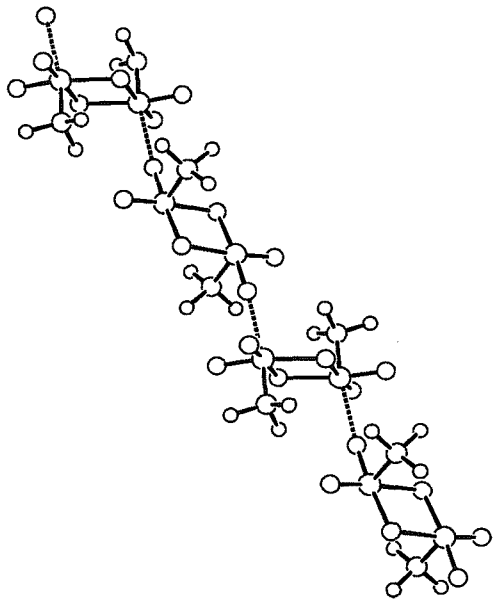

Figure 2.18 View of the extended chain structure of the $[AsCl_3(PMe_3)]$ complex.

No such long range As---Cl interaction is observed for As(2), and this arsenic atom is thus regarded as five-coordinate (hence the weakly bound chains are not cross-linked). The occupation of the sixth As(1) coordination site by a secondary interaction has implications for the stereochemical activity of the As(1)-based lone pair, since it cannot occupy an open vertex (as is observed in the As(2) dimer), and hence the distorted bond length distribution about As(1) may be evidence of a lone pair effect.

It is useful to compare the structure of the $[Sb_2I_6(PMe_3)_2].THF$ complex to $[AsCl_3(PMe_3)]$, since the antimony species also shows secondary interactions (Figure 2.7).[8] In this case, long range Sb---I contacts between dimer units form a loosely bound polymer but the individual dimers are crystallographically identical and they align in a parallel (rather than orthogonal) fashion. The individual $[AsCl_3(PMe_3)]$ dimer units may also be compared to the structure of $[AsCl_3(AsEt_3)]$ reported by Baum (Figure 2.11).[16] The latter species is similar to $[AsCl_3(PMe_3)]$ in that it adopts a $(\mu\text{-}Cl)_2$ bridged square pyramidal geometry with four terminal chlorine atoms in the basal plane and apical, mutually *anti* $AsEt_3$ ligands. However, the latter are tilted slightly toward (and thus partially block) the vacant coordination site on the arsenic atom, hence no intermolecular interaction is observed. A final comparison may be made to the recently reported $[PBr_3(PMe_3)]$ species (Figure 2.12),[17] the structure of which is very similar to the individual $[AsCl_3(PMe_3)]$ dimer. A major difference, however, is the much higher

degree of asymmetry in the bridging P(μ-Br)$_2$P unit (3.327(2), 2.677(2) Å, Δ = 0.650 Å *cf.* Δ = 0.282 Å for the most distorted [AsCl$_3$(PMe$_3$)] dimer). This reflects the bonding situation in the [PBr$_3$(PMe$_3$)] adduct, which is considered to be intermediate between neutral covalent and ionic.[17] No intermolecular contacts were observed for this species.

Crystals of [AsX$_3${o-C$_6$H$_4$(AsMe$_2$)$_2$}] (X = Br and I) were obtained by slow evaporation of a solution of the appropriate complex in CH_2Cl_2 in a N_2 purged glove box. Although not formally isostructural, the complexes [AsBr$_3${o-C$_6$H$_4$(AsMe$_2$)$_2$}] (Figure 2.19, Table 2.7) and [AsI$_3${o-C$_6$H$_4$(AsMe$_2$)$_2$}] (Figure 2.19, Table 2.8) adopt very similar structures. Like the [Bi$_2$I$_6${o-C$_6$H$_4$(AsMe$_2$)$_2$}] adduct, both complexes exist as isomer A, edge-shared, bioctahedral μ-dihalo-bridged dimers with each As atom bound to two bridging halides, two *cis* terminal halides and two As donor atoms from the chelating diarsine ligand.

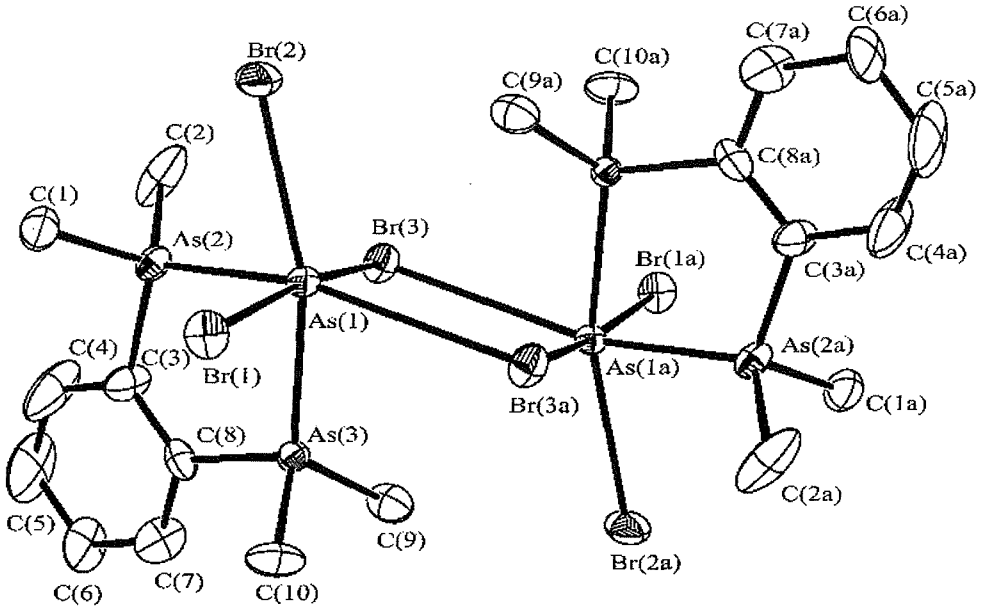

Figure 2.19 View of the structure of [AsBr$_3${o-C$_6$H$_4$(AsMe$_2$)$_2$}]. Ellipsoids shown at 40 % probability, H-atoms omitted for clarity. Atoms marked (a) are related by the symmetry operation -x, -y, -z.

The range of bond distances at each central As atom is noteworthy. The As(μ-X)$_2$As bridging unit is highly asymmetric (2.830(2), 3.345(2) Å, Δ = 0.515 Å for X= Br; 2.845(1), 3.434(1) Å, Δ = 0.588 Å for X = I), while the terminal As-X distances differ by *ca.* 0.4 Å in the bromo-species (2.463(2), 2.886(2) Å) and *ca.* 0.2 Å in the

iodo-analogue (2.8376(11), 3.0202(11) Å). The As-As distances involving the AsX_3 unit and the chelating diarsine ligand are also unequal, differing by *ca.* 0.1 Å in both complexes (2.448(2), 2.537(2) Å for X = Br; 2.4785(12), 2.6067(12) Å for X = I). These As-As distances are comparable to the only other structurally characterised arsenic-arsine bond length of 2.469(3) Å (in the $[AsCl_3(AsEt_3)]$ complex), and also lie in the range observed in various tetra-alkyl and tetra-aryl diarsines. For example, the As-As bond distance in $Me_2AsAsMe_2$ is 2.429(1) Å, while that in $Mes_2AsAsMes_2$ is 2.472(3) Å (Mes = $C_6H_2(Me)_3$).[28]

As(1)	Br(1)	2.463(2)		As(1)	Br(2)	2.886(2)	
As(1)	Br(3)	2.830(2)		As(1)	Br(3a)	3.345(2)	
As(1)	As(2)	2.448(2)		As(1)	As(3)	2.537(2)	
Br(1)	As(1)	Br(2)	90.56(6)	Br(1)	As(1)	Br(3)	167.30(7)
Br(1)	As(1)	Br(3a)	99.87(7)	Br(1)	As(1)	As(2)	90.00(7)
Br(1)	As(1)	As(3)	86.67(6)	Br(2)	As(1)	Br(3)	98.85(6)
Br(2)	As(1)	Br(3a)	118.56(6)	Br(2)	As(1)	As(2)	78.37(6)
Br(2)	As(1)	As(3)	163.85(8)	Br(3)	As(1)	Br(3a)	83.16(6)
Br(3)	As(1)	As(2)	83.62(7)	Br(3)	As(1)	As(3)	81.93(6)
Br(3a)	As(1)	As(2)	159.97(7)	Br(3a)	As(1)	As(3)	77.58(5)
As(2)	As(1)	As(3)	85.72(6)	As(1)	Br(3)	As(1a)	96.84(6)

Table 2.7 Selected bond distances (Å) and angles (°) with e.s.d.'s for $[AsBr_3\{o\text{-}C_6H_4(AsMe_2)_2\}]$.

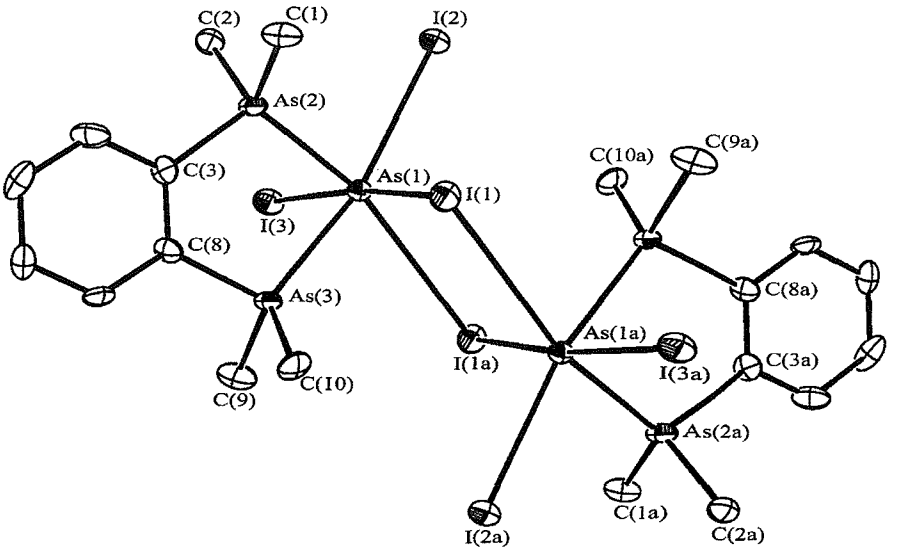

Figure 2.20 View of the structure of $[AsI_3\{o\text{-}C_6H_4(AsMe_2)_2\}]$. Details as for Figure 2.19.

As(1)	I(1)	2.8456(11)	As(1)	I(1a)	3.434(1)
As(1)	I(2)	2.8376(11)	As(1)	I(3)	3.0202(11)
As(1)	As(2)	2.6067(12)	As(1)	As(3)	2.4785(12)
I(1)	As(1) I(1a)	84.52(3)	I(1)	As(1) I(2)	171.52(4)
I(1)	As(1) I(3)	89.24(3)	I(1)	As(1) As(2)	87.29(4)
I(1)	As(1) As(3)	92.74(4)	I(2)	As(1) I(1a)	94.19(3)
I(2)	As(1) I(3)	98.91(3)	I(2)	As(1) As(2)	84.23(4)
I(2)	As(1) As(2)	86.27(4)	I(3)	As(1) I(1a)	114.36(3)
I(3)	As(1) As(2)	164.40(4)	I(3)	As(1) As(3)	80.79(3)
As(2)	As(1) I(1a)	80.44(3)	As(2)	As(1) As(3)	84.19(4)
As(1)	As(1) I(1a)	164.49(4)	As(1)	I(1) As(1a)	95.48(3)

Table 2.8 Selected bond distances (Å) and angles (°) for $[AsI_3\{o\text{-}C_6H_4(AsMe_2)_2\}]$.

The bond length distribution parallels that seen in the $[M_2Br_6(dmpe)_2]$, $[Bi_2I_6\{o\text{-}C_6H_4(AsMe_2)_2\}_2]$ and $[Sb_2Br_6\{o\text{-}C_6H_4(PPh_2)_2\}_2]$ species, in that there is one short and one long bond within each of the three bond types, M-X bridging, M-X terminal and M-E (M = As, Sb or Bi; X = Cl, Br or I; E = P or As donor atom).[8, 12] Two main factors appear to be responsible for this. Firstly, the dimer units are formed through weak association of two square pyramidal units hence the asymmetry of the μ-halo bridges arises from a combination of primary and secondary bonding. In addition, a phosphine or arsine donor atom exerts a greater *trans* influence than a halide.[2] The distortion in bond distances and angles about the central As atoms could be due to stereochemical activity of the lone pair, localised particularly within the triangular face defined by Br(1), Br(2) and Br(3a) for $[AsBr_3\{o\text{-}C_6H_4(AsMe_2)_2\}]$ and I(1a), I(2) and I(3) for $[AsI_3\{o\text{-}C_6H_4(AsMe_2)_2\}]$.

The bonding within the $[SbBr_3\{o\text{-}C_6H_4(PPh_2)_2\}]$, $[BiCl_3\{o\text{-}C_6H_4(POPh_2)_2\}(THF)]$, $[Sb_2Cl_6\{o\text{-}C_6H_4(AsMe_2)_2\}]$ and $[AsX_3\{o\text{-}C_6H_4(AsMe_2)_2\}]$ complexes can be rationalized in terms of the simple DA model outlined in chapter 1, where the M-X σ^* anti-bonding orbitals function as acceptors toward electron density from a donor. The ligand donor atoms are bound *trans* to an M-X bond, indicating donation into an M-X σ^* anti-bonding orbital. However, the $[AsCl_3(PMe_3)]$ dimer does not adopt the isomer A structure and instead exists as a planar As_2Cl_6 unit with axial, mutually *anti* phosphines. This structure is also adopted by the $[Bi_2Cl_6(dppm)_2]$, $[Sb_2I_6(PMe_3)_2]$, $[As_2Cl_6(AsEt_3)_2]$ and $[PBr_3(PMe_3)]$ complexes (although the structure of $[Bi_2Cl_6(dppm)_2]$ is probably governed by steric factors).

It is very unlikely that an orbital other than the M-X σ^* anti-bonding orbital acts as an acceptor in these examples, since this is the lowest energy orbital available. Indeed, the weak, near linear As(1)---Cl(4) contact which links the $[AsCl_3(PMe_3)]$ dimers suggests that the PMe_3 ligand does, in fact, donate into an As-Cl σ^* orbital. This As---Cl interaction may be weakened by the strong *trans* influence of PMe_3. A similar situation is observed in the $[Sb_2I_6(PMe_3)_2]$ complex (i.e. donation into a σ^* orbital derived from a secondary M---X bond) (Figure 2.7).[8] However, this is not so for the As(2) dimer where the As-based lone pair is assumed to occupy the vacant sixth coordiniation site *trans* to the PMe_3 ligand.

2.3 Conclusions

The reaction of MX_3 with o-$C_6H_4(ER_2)_2$ and $MeC(CH_2ER_2)_3$ ligands (E = P or As; R = Me or Ph) produces 1:1 adducts regardless of reaction stoichiometry. It was anticipated that the rigid aromatic back-bone of the o-$C_6H_4(ER_2)_2$ ligands may induce higher ligand: MX_3 ratios compared to those established in complexes of the flexible aliphatic back-boned ligands (a consequence of the so-called "o-phenylene backbone" effect).[29] The failure to observe anything other than 1:1 stoichiometry is probably due to the nature of the primary bonding interactions in these systems. These occur in the pyramidal MX_3 unit, with the remaining sites on the (distorted) octahedral coordination sphere being filled by weaker secondary bonds to the neutral ligand and bridging halide atom. With such a bonding scheme, alterations in donor atom, ligand geometry and/or organyl substituent have much less effect on the present complexes than is observed for d-block metal complexes of these ligands (although a trend toward flattened M_2X_6 units is observed when the ligand is PMe_3).

The fact that the $[SbBr_3\{o\text{-}C_6H_4(PPh_2)_2\}]$, $[BiCl_3\{o\text{-}C_6H_4(PPh_2)_2\}]$ and $[AsX_3\{o\text{-}C_6H_4(AsMe_2)_2\}]$ (X = Br or I) complexes adopt the isomer A dimer structure implies that the other $[MX_3(dipnictine)]$ adducts are likely to exist in this motif. Indeed it is likely that this also applies to the $[SbX_3\{o\text{-}C_6H_4(AsMe_2)_2\}]$ complexes, despite the extended structure observed for the 2:1 chloro-species. However, it is equally likely that other structural motifs exist for this range of MX_3 adducts, particularly in view of the increased secondary bonding capacity of the MX_3 fragment as group 15 is descended. In other words it appears that, in solution, a range of structures exist in dynamic equilibrium, with solubility and stability factors (and experimental conditions) governing the structure of the species obtained in the solid-state.

The synthesis of a series of AsX_3 complexes of phosphines and arsines demonstrate that the non-metallic AsX_3 fragment is a reasonable Lewis acid, giving modest yields of products. The crystal structure of $[AsCl_3(PMe_3)]$ reveals a weakly linked extended chain motif, and it is tempting to propose such a structure for the analogous $[AsX_3(AsMe_3)]$ species. However, it is equally likely that the latter is structurally very similar to the $[AsCl_3(AsEt_3)]$ complex.[16]

2.4 Experimental

General experimental conditions are given in the Appendix. Phosphine and arsine ligands were prepared using literature methods,[31-33] except PMe_3 and $AsMe_3$ which were obtained commercially (Aldrich and Strem). Anhydrous arsenic, antimony and bismuth(III) halides were obtained from Aldrich and used as received. Standard Schlenk techniques were used throughout, and all preparations and manipulations were performed under a N_2 atmosphere. All preparations used the same general method, with minor modifications noted under individual complexes.

Bismuth Halide Complexes

[$BiCl_3${o-$C_6H_4(PPh_2)_2$}]. A solution of o-$C_6H_4(PPh_2)_2$ (0.20 g, 0.45 mmol) in CH_2Cl_2 (10 cm^3) was added dropwise at room temperature to a stirred solution of $BiCl_3$ (0.14 g, 0.45 mmol) in MeCN (10 cm^3). The resultant bright yellow precipitate was filtered off, washed with CH_2Cl_2 and dried *in vacuo*. 0.28 g, 83 %. Calculated for $C_{30}H_{24}BiCl_3P_2$: C, 47.3; H, 3.1; Found C, 47.0; H, 3.0 %. IR/cm^{-1}: 260, 250, 236 ν(Bi-Cl).

[$BiBr_3${o-$C_6H_4(PPh_2)_2$}]. Procedure as above. Yellow powder. Yield 75 %. Calculated for $C_{30}H_{24}BiBr_3P_2$: C, 40.3; H, 2.7; Found C, 40.0; H. 2.6 %.

[BiI_3{o-$C_6H_4(PPh_2)_2$}]. Procedure as above, using THF solutions of BiI_3 and o-$C_6H_4(PPh_2)_2$. Orange powder. Yield 54 %. Calculated For $C_{30}H_{24}BiI_3P_2$: C, 34.8; H, 2.3; Found C, 34.8; H, 2.0 %

[$BiCl_3${o-$C_6H_4(PMe_2)_2$}]. To an anhydrous MeCN solution (10 cm^3) of $BiCl_3$ (0.053 g, 0.17 mmol) was added an equimolar solution of o-$C_6H_4(PMe_2)_2$ in MeCN (3 cm^3). The solution was concentrated *in vacuo* and the cream coloured solid separated, washed with CH_2Cl_2 and dried *in vacuo*. Yield 75 %. Calculated for $C_{10}H_{16}BiCl_3P_2$: C, 23.4; H, 3.1; Found: C, 23.2; H, 3.2 %. IR/cm^{-1}: 263, 251, 237 ν(Bi-Cl).

[$BiBr_3${o-$C_6H_4(PMe_2)_2$}]. Procedure as above. Pale brown solid. Yield 67 %. Calculated for $C_{10}H_{16}BiBr_3P_2$: C, 18.6; H, 2.5; Found: C, 18.2; H, 2.4 %.

[BiI_3{o-$C_6H_4(PMe_2)_2$}]. Procedure as above, using THF solutions of BiI_3 and o-$C_6H_4(PMe_2)_2$.Yellow-green solid. Yield 45 %. Calculated for $C_{10}H_{16}BiI_3P_2$: C, 15.2; H, 2.0; Found: C, 15.3; H, 2.0 %.

[$BiCl_3$(THF){o-$C_6H_4(POPh_2)_2$}]. A solution of o-$C_6H_4(PPh_2)_2$ (0.14 g, 0.30 mmol) in THF (10 cm^3) was added dropwise to a stirred solution of $BiCl_3$ (0.09 g, 0.30 mmol) in THF (10 cm^3). Hexane (10 cm^3) was added and the solution allowed to stand overnight. The resultant white solid was filtered off, washed with hexane and dried *in vacuo*. Yield 52 %. Calculated for $C_{34}H_{32}BiCl_3O_3P_2$ C, 47.1; H, 3.7; Found: C, 48.1; H, 4.3 %. ^{1}H-NMR: δ 1.87 (m), 3.7 (m), 7.3 –7.6 (m) ppm. $^{31}P\{^1H\}$-NMR (300K) δ 34.5 ppm. IR/cm^{-1}: 1165 sh, 1156 ν(P-O); 274, 236 ν(Bi-Cl).

[$BiBr_3${o-$C_6H_4(POPh_2)_2$}]. Procedure as above. Pale yellow solid. Yield 65 %. Calculated for $C_{30}H_{24}BiBr_3O_2P_2$ C, 38.8; H, 2.6; Found: C, 38.4; H, 2.8 %. ^{1}H-NMR: δ 7.3 –7.6(m). $^{31}P\{^1H\}$-NMR (300K, CH_2Cl_2) δ 35.0. IR/cm^{-1}: 1160 sh, 1148 ν(P-O)

Antimony Halide Complexes

[$SbCl_3${o-$C_6H_4(PPh_2)_2$}]. To an anhydrous MeCN solution (10 cm^3) of $SbCl_3$ (0.09 g, 0.37 mmol) was added an anhydrous CH_2Cl_2 solution (5 cm^3) of o-$C_6H_4(PPh_2)_2$ (0.17 g, 0.37 mmol). The resultant pale yellow solution was concentrated *in vacuo* to produce a grey powder, isolated as above. Yield 67 %. Calculated for $C_{30}H_{24}Cl_3P_2Sb$: C, 53.4; H, 3.6; Found: C, 53.6; H, 3.6 %. IR/cm^{-1}: 267, 240, 228 ν(Sb-Cl).

[$SbBr_3${o-$C_6H_4(PPh_2)_2$}]. Procedure as above. Yellow powder. Yield 83 %. Calculated for $C_{32}H_{28}Br_3P_2Sb$: C, 39.3; H, 2.9; Found: C, 40.6; H, 2.7 %.

[SbI_3{o-$C_6H_4(PPh_2)_2$}]. Procedure as above, using THF solutions of SbI_3 and o-$C_6H_4(PPh_2)_2$. Yellow powder. Yield 49 %. Calculated for $C_{31}H_{26}I_3Sb$: C, 36.0; H, 2.5; Found: C, 36.6; H, 2.5 %.

[$SbCl_3${o-$C_6H_4(PMe_2)_2$}]. To an anhydrous THF solution (10 cm^3) of $SbCl_3$ (0.25 mmol) was added an equimolar solution of o-$C_6H_4(PMe_2)_2$ in CH_2Cl_2 (3 cm^3). The resultant white solid was filtered, washed with CH_2Cl_2 and dried *in vacuo*. Yield 80%. Calculated for $C_{10}H_{16}Cl_3P_2Sb$: C, 28.2; H, 3.8; Found: C, 28.5; H, 3.8 %. $^{31}P\{^1H\}$-NMR ($MeNO_2$, 250 K): δ 4.0 ppm. IR/cm^{-1}: 257, 243, 230 *ν*(Sb-Cl).

[$SbBr_3${o-$C_6H_4(PMe_2)_2$}]. Procedure as above. Yellow powder. Yield 51 %. Calculated for $C_{10}H_{16}Br_3P_2Sb$: C, 21.5; H, 2.9; Found: C, 22.4; H, 3.0 %. $^{31}P\{^1H\}$-NMR ($MeNO_2$, 250 K): δ -6.5 ppm.

[SbI_3{o-$C_6H_4(PMe_2)_2$}]. Procedure as above, using THF solutions of SbI_3 and o-$C_6H_4(PMe_2)_2$. Orange powder. Yield 64 %. Calculated for $C_{10}H_{16}I_3P_2Sb$: C, 17.1; H, 2.3; Found: C, 16.7; H, 2.3 %.

[$SbCl_3${o-$C_6H_4(AsMe_2)_2$}]. To an anhydrous ethanol solution (10 cm^3) of $SbCl_3$ (0.124 g, 0.54 mmol) was added an ethanol solution (3 cm^3) of o-$C_6H_4(AsMe_2)_2$ (0.154 g, 0.54 mmol) resulting in a white crystalline precipitate which was filtered and dried *in vacuo*. Yield 68 %. Calculated for $C_{10}H_{16}As_2Cl_3Sb$: C, 23.2; H, 3.5; Found: C, 23.0; H, 3.1 %. IR/cm^{-1}: 265, 240, 230 *ν*(Sb-Cl).

[$SbBr_3${o-$C_6H_4(AsMe_2)_2$}]. Procedure as above. Yellow powder. Yield 82 %. Calculated for $C_{10}H_{16}As_2Br_3Sb$: C, 18.5; H, 2.8; Found: C, 18.6; H, 2.4 %.

[SbI_3{o-$C_6H_4(AsMe_2)_2$}]. Procedure as above, using THF solutions of SbI_3 and o-$C_6H_4(AsMe_2)_2$. Bright yellow powder. Yield 60 %. Calculated for $C_{10}H_{16}As_2I_3Sb$: C, 15.2; H, 2.3; Found: C, 15.3; H, 1.9 %.

[Sb_2Cl_6{o-$C_6H_4(AsMe_2)_2$}]. Slow evaporation of solvent from a warm solution of [$SbCl_3${o-$C_6H_4(AsMe_2)_2$}] yielded colourless, block crystals. Yield 60 %. Calculated for $C_{10}H_{16}As_2Cl_6Sb_2$: C, 16.2; H, 2.2; Found: C, 15.8; H, 2.0 %. IR/cm^{-1}: 264, 251, 231 *ν*(Sb-Cl).

[$SbCl_3\{Ph_2As(CH_2)_2AsPh_2\}$]. Procedure as above, using an ethanol solution of $SbCl_3$ and a CH_2Cl_2 solution of $Ph_2As(CH_2)_2AsPh_2$. White powder. Yield 57%. Calculated for $C_{26}H_{24}As_2Cl_3Sb$: C, 43.7; H, 3.4; Found: C, 43.6; H, 3.1 %. IR/cm^{-1}: 256, 244, 230 ν(Sb-Cl).

[$SbBr_3\{Ph_2As(CH_2)_2AsPh_2\}$]. Procedure as above. Yellow powder. Yield 72%. Calculated for $C_{26}H_{24}As_2Br_3Sb$: C, 36.8; H, 2.9; Found: C, 37.0; H, 3.2 %.

[$SbCl_3\{MeC(CH_2AsMe_2)_3\}$]. Procedure as above. White powder. Yield 56 %. Calculated for $C_{11}H_{27}As_3Cl_3Sb$: C, 21.6; H, 4.5; Found: C, 21.1; H, 4.3; %. IR/cm^{-1}: 265, 249, 232 ν(Sb-Cl) .

[$SbBr_3\{MeC(CH_2AsMe_2)_3\}$]. Procedure as above. Yellow powder. Yield 34 %. Calculated for $C_{11}H_{27}As_3Br_3Sb$: C, 17.7; H, 3.7; Found: C, 17.7; H, 3.5 %.

Arsenic Halide Complexes

[$AsCl_3\{o\text{-}C_6H_4(AsMe_2)_2\}$]. Addition of a CH_2Cl_2 solution (10 cm^3) of o-$C_6H_4(AsMe_2)_2$ (0.071 g, 0.25 mmol) to a CH_2Cl_2 solution (10 cm^3) of $AsCl_3$ (0.045 g, 0.25 mmol) immediately produced a white powder which was filtered, washed with hexane dried *in vacuo*. Yield 0.08g, 68 %. Calculated for $C_{10}H_{16}As_3Cl_3$: C, 25.7; H, 3.5; Found: C, 25.4; H, 3.6 %. ^{1}H-NMR: δ 1.55 (br, AsMe, 12H), 7.3 – 7.6 (br m, o-C_6H_4, 4H) ppm. IR/cm^{-1}: 419, 386 ν(As-Cl).

[$AsBr_3\{o\text{-}C_6H_4(AsMe_2)_2\}$]. White powder. Yield 82 %. Calculated for $C_{10}H_{16}As_2Br_3$: C, 20.0; H, 2.7; Found: C, 20.2; H, 3.0 %. ^{1}H-NMR: δ 1.25 (s, AsMe, 12H), 7.2 – 7.6 (m, o-C_6H_4, 4H) ppm. IR/cm^{-1}: 263 ν(As-Br).

[$AsI_3\{o\text{-}C_6H_4(AsMe_2)_2\}$]. Procedure as above, using anhydrous THF solutions of AsI_3 and o-$C_6H_4(AsMe_2)_2$. Yellow powder. Yield 81 %. Calculated for $C_{10}H_{16}As_3I_3$: C, 16.2; H, 2.2; Found: C, 16.6; H, 2.5 %. ^{1}H-NMR: δ 1.22 (s, AsMe, 12H), 7.2 – 7.6 (m, o-C_6H_4, 4H) ppm.

[$AsBr_3${$MeC(CH_2AsMe_2)_3$}]. Procedure as for [$AsBr_3${o-$C_6H_4(AsMe_2)_2$}]. Yellow powder. Yield 53 %. Calculated for $C_{11}H_{27}As_4Br_3$: C, 18.9; H, 3.9; Found: C, 18.9; H, 3.8 %. ^{1}H-NMR: δ 1.12 (s, CMe, 3H), 1.62 (br, AsMe, 9H), 2.15 (br, CH_2, 6H) ppm. IR/cm^{-1}: 265 *ν*(As-Br)

[AsI_3{$MeC(CH_2AsMe_2)_3$}]. Addition of a CH_2Cl_2 solution (10 cm^3) of $MeC(CH_2AsMe_2)_3$ to a THF solution (10 cm^3) of AsI_3 gave a yellow solution. This solution was slowly concentrated *in vacuo* to leave a yellow powder which was filtered, washed with CH_2Cl_2 and dried *in vacuo*. Yield 82 %. Calculated for $C_{11}H_{27}As_4I_3$: C, 15.7; H, 3.2; Found: C, 16.2; H, 3.5 %. ^{1}H-NMR: δ 1.10 (s, CMe, 3H), 1.32 (br, AsMe, 9H), 1.97 (br, CH_2, 6H) ppm.

[$AsCl_3${o-$C_6H_4(PPh_2)_2$}]. Addition of a CH_2Cl_2 solution (10cm^3) of o-$C_6H_4(PPh_2)_2$ (0.156 g, 0.35 mmol) to an equimolar CH_2Cl_2 solution (10 cm^3) of $AsCl_3$ (0.064 g, 0.35 mmol) produced a pale green solution. Removal of solvent *in vacuo* gave a yellow-green waxy solid, which was triturated in anhydrous hexane to obtain a yellow powder, which was filtered, washed with CH_2Cl_2 and dried *in vacuo*. Yield 74 %. Calculated for $C_{30}H_{24}AsCl_3P_2$: C, 57.4; H, 3.9; Found: C, 57.0; H, 3.6 %. IR/cm^{-1}: 412, 388 *ν*(As-Cl).

[$AsBr_3${o-$C_6H_4(PPh_2)_2$}]. Procedure as above. Yellow powder. Yield 64 %. Calculated for $C_{30}H_{24}AsBr_3P_2$: C, 47.3; H, 3.2; Found: C, 48.0; H, 3.3 %. IR/cm^{-1}: 268 *ν*(As-Br).

[AsI_3{o-$C_6H_4(PPh_2)_2$}]. Procedure as above, using THF solutions of AsI_3 and o-$C_6H_4(PPh_2)_2$. Yellow powder. Yield 78 %. Calculated for $C_{30}H_{24}AsI_3P_2$: C, 39.9; H, 2.7; Found: C, 40.2; H, 2.7 %.

[$AsCl_3${o-$C_6H_4(PMe_2)_2$}]. Addition of a chilled diethyl ether solution (10 cm^3) of $AsCl_3$ (0.036 g, 0.20 mmol) to a cold (-30 ° C) diethyl ether solution (10 cm^3) of o-$C_6H_4(PMe_2)_2$ (0.039 g, 0.20 mmol) immediately produced a white powder. The solvent was removed and the solid dried *in vacuo*. Yield 58 %. Calculated for $C_{10}H_{16}AsCl_3P_2$.¼ Et_2O; C, 33.2; H, 4.7; Found: C, 33.1; H, 4.8 %. ^{1}H-NMR: δ 1.20 (t, CH_3CH_2O 6H), 2.0 (m, Me, 12H), 3.45 (q, CH_3CH_2O, 4H), 7.6 – 8.1 (m, o-C_6H_4, 4H) ppm. $^{31}P\{^1H\}$-NMR: δ 32 ppm. IR/cm^{-1}: 412, 388 *ν*(As-Cl).

[$AsCl_3(PMe_3)$]. Addition of a chilled diethyl ether solution (10cm^3) of $AsCl_3$ (0.09g, 0.50 mmol) to a cold toluene solution of PMe_3 (0.5 mmol, 0.50 cm^3 1.0 $moldm^{-3}$ solution of PMe_3 in toluene) immediately produced a white powder. Solvent removed and product dried *in vacuo*. Yield 40 %. Calculated for $C_3H_9AsCl_3P$: C, 14.0; H, 3.5; Found: C, 13.0; H, 3.5 %. ^{1}H-NMR: δ 2.15 (d, 12Hz), 2.20 (d, 12Hz), $^{31}P\{^1H\}$-NMR: δ 27 ppm. IR/cm^{-1}: 409, 380 *ν*(As-Cl).

[$AsCl_3(PMe_3)_2$]. Procedure as above, using 2 equivalents of PMe_3. White powder. Yield 65 %. Calculated for $C_6H_{18}AsCl_3P_2$: C, 21.6; H, 5.4; Found: C, 21.8; H, 5.3 %. $^{31}P\{^1H\}$ NMR δ: 28 ppm. ^{1}H-NMR: δ 2.15 (d, 12Hz), 2.20 (d, 12Hz). $^{31}P\{^1H\}$-NMR: δ 28 ppm. IR/cm^{-1}: 413, 382 *ν*(As-Cl)..

[$AsBr_3(PMe_3)_2$]. Procedure as above. White powder. Yield 61 %. Calculated for $C_6H_{18}AsBr_3P_2$: C, 15.4; H, 3.9; Found: C, 15.5; H, 3.6 %. ^{1}H-NMR: δ 2.20 (d, 12Hz). $^{31}P\{^1H\}$-NMR δ: 16 ppm. IR/cm^{-1}: 267 *ν*(As-Br)

[$AsCl_3(AsMe_3)$]. Procedure as for [$AsCl_3(PMe_3)$]. 1:1 product obtained irrespective of the reaction stoichiometry. White powder. Yield 67 %. Calculated for $C_3H_9As_2Cl_3$: C, 11.9; H, 3.0; Found: C, 11.6; H, 2.7 %. IR/cm^{-1}: 419, 382 *ν*(As-Cl).

[$AsI_3(AsMe_3)$]. Procedure as for [$AsCl_3(PMe_3)_2$], using THF solutions of AsI_3 and $AsMe_3$. Yellow powder. Yield 47 %. Calculated for $C_3H_9As_2I_3$: C, 6.3; H, 1.6; Found: C, 5.9; H, 1.8 %. ^{1}H-NMR: δ 1.20 (S, Me) ppm.

2.5 X-ray Crystallography

General experimental X-ray data collection conditions are given in the Appendix. Details of the crystallographic data collection and refinement parameters for data discussed in this Chapter are given in Tables 2.9 to 2.11. Data collection used a Rigaku AFC7S four-circle diffractometer. No significant crystal decay or movement was detected during data collection.

Structure solution and refinement were routine except for [$SbBr_3${o-$C_6H_4(PPh_2)_2$}], where DIFABS absorption correction was applied.[34-37] For all structures, fully occupied non-hydrogen atoms were refined anisotropically. Hydrogen atoms were added in fixed, calculated positions with d(C-H) = 0.96 Å.

	$[SbBr_3\{o\text{-}C_6H_4(PPh_2)_2\}_2]$	**$[BiCl_3\{oC_6H_4(P(O)Ph_2)_2\}_2(THF)]$**
Formula	$C_{30}H_{24}Br_3P_2Sb$	$C_{34}H_{32}BiCl_3O_3P_2$
Formula Weight	807.93	865.88
Crystal System	Triclinic	Monoclinic
Space Group	*P*-1 (# 2)	$P2_1/n$ (# 14)
a/ Å	11.025(5)	12.043(2)
b/ Å	13.726(5)	19.467(2)
c/ Å	10.797(4)	14.530(2)
α / °	92.83(4)	90
β / °	106.39(4)	101.80(2)
γ / °	107.59(3)	90
U / Å^3	1478(1)	3334.7(9)
Z	4	4
μ (Mo-K_α)/ cm^{-1}	51.32	56.47
Unique obs. reflns.	5503	6074
Obs. reflns.		
$[I > 2\sigma(I)]$	5205	3648
R	0.108	0.033
R_w	0.121	0.033

Table 2.9 X-ray data collection and refinement parameters for the $[SbCl_3\{o\text{-}C_6H_4(PPh_2)_2\}]$ and $[BiCl_3\{o\text{-}C_6H_4(P(O)Ph_2)_2\}_2(THF)]$ complexes.

	[$BiCl_3${o-$C_6H_4(PPh_2)_2$}]	**[$AsCl_3(PMe_3)$]**
Formula	$C_{30}H_{24}BiCl_3P_2$	$C_3H_9AsCl_3P$
Formula Weight	761.81	257.36
Crystal System	Monoclinic	Monoclinic
Space Group	$P2_1/c$ (# 14)	$P2_1/a$ (# 14)
a/ Å	22.770(1)	12.002(6)
b/ Å	10.911(5)	12.297(6)
c/ Å	24.243(2)	12.328(4)
α / °	90	90
β / °	93.582(3)	91.97(4)
γ / °	90	90
U / Å^3	6011.4(5)	1819(1)
Z	8	8
μ (Mo-K_α)/ cm^{-1}	62.457	47.09
Unique obs. reflns.	13491	3377
Obs. reflns. [$I > 2\sigma(I)$]	4254	1706
R	0.119	0.073
R_w	0.122	0.089

Table 2.10 X-ray data collection and refinement parameters for the [$BiCl_3${o-$C_6H_4(PPh_2)_2$}] and [$AsCl_3(PMe_3)$] complexes.

	[$AsBr_3${o-$C_6H_4(AsMe_2)_2$}]	**[AsI_3{o-$C_6H_4(AsMe_2)_2$}]**
Formula	$C_{10}H_{16}As_3Br_3$	$C_{10}H_{16}As_3I_3$
Formula Weight	600.71	741.71
Crystal System	Monoclinic	Monoclinic
Space Group	$P2_1/n$ (# 14)	$P2_1/n$ (# 14)
a/ Å	9.8794(3)	8.7874(2)
b/ Å	16.0455(6)	12.0405(3)
c/ Å	11.3094(4)	16.7508(5)
α / °	90	90
β / °	110.973(1)	90.9090(7)
γ / °	90	90
U / Å^3	1673.99(9)	1772.09(7)
Z	4	4
μ (Mo-K_α)/ cm^{-1}	153.43	108.33
Unique obs. reflns.	3929	3757
Obs. reflns.[$I > 2\sigma(I)$]	2324	2525
R	0.073	0.037
R_w	0.078	0.046

Table 2.11 X-ray data collection and refinement parameters for the [$AsBr_3${o-$C_6H_4(AsMe_2)_2$}] and [AsI_3{o-$C_6H_4(AsMe_2)_2$}] complexes.

2.6 References

[1] W. Levason and C. A. McAullife, *Coord. Chem. Rev.*, 1976, **19**, 173.

[2] N. C. Norman and N. L. Pickett, *Coord. Chem. Rev.*, 1995, **145**, 27.

[3] J. C. Summers and H. H. Sisler, *Inorg. Chem.*, 1970, **9**, 862; R. R. Holmes and E. F. Bertaut, *J. Am. Chem. Soc.*, 1958, **80**, 2980.

[4] G. Alonzo, M. Consiglio, N. Bertazzi and C. Preti, *Inorg. Chim. Acta*, 1985, **105**, 51.

[5] W. Clegg, R. J. Errington, G. A. Fisher, M. E. Green, D. C. R. Hockless and N. Norman, *Chem. Ber.*, 1991, **124**, 2457.

[6] W. Clegg, M. R. J. Elsegood, N. C. Norman and N. L. Pickett, *J. Chem. Soc., Dalton Trans.*, 1994, 1753.

[7] W. Clegg, R. J. Errington, R. J. Flynn, M. E. Green, D. C. R. Hockless, N. C. Norman, V. C. Gibson and K. Tavakkoli, *J. Chem. Soc., Dalton Trans.*, 1992, 1753.

[8] W. Clegg, M. R. J. Elsegood, V. Graham, N. C. Norman, N. L. Pickett and K. Tavakkoli, *J. Chem. Soc., Dalton Trans.*, 1994, 1743.

[9] G. A. Fisher and N. C. Norman, *Adv. Inorg. Chem.*, 1994, **41**, 233.

[10] G. R. Willey, L. T. Daley and M. G. B. Drew, *J. Chem. Soc., Dalton Trans.*, 1996, 1063.

[11] G. J. Sutton, *Aust. J. Chem.*, 1958, **11**, 415; G. J. Sutton, *Aust. J. Chem.*, 1958, **11**, 420.

[12] A. R. J. Genge, N. J. Hill, W. Levason and G. Reid, *J. Chem. Soc., Dalton Trans.*, 2001, 1007.

[13] W. Clegg, M. R. J. Elsegood, V. Graham, N. C. Norman and N. L. Pickett, *J. Chem. Soc., Dalton Trans.*, 1993, 997.

[14] H. J. Breunig, M. Denker and K. H. Ebert, *J. Chem. Soc., Chem. Commun.*, 1994, 875.

[15] H. J. Breunig, M. Denker, R. E. Schulz and E. Lork, *Z. Anorg. Allg. Chem.*, 1998, **624**, 81.

[16] G. Baum, A. Greiling, W. Massa, B. C. Hiu and J. Lorbeth, *Z. Naturforsch.*, 1989, **44b**, 560.

[17] G. Müller, H.-J. Matheus and M. Winkler, *Z. Naturforsch.*, 2002, **56b**, 1155.

[18] R. P. Oertal and R. A. Plane, *Inorg. Chem.*, 1969, **8**, 118.

[19] N. J. Hill, W. Levason and G. Reid, unpublished work, 2001.

[20] G. R. Willey, M. D. Rudd, C. J. Samuel and M. G. B. Drew, *J. Chem. Soc., Dalton Trans.*, 1995, 759.

[21] A. R. J. Genge, W. Levason and G. Reid, *Inorg. Chim. Acta*, 1999, **288**, 142.

[22] C. J. Carmalt, A. H. Cowley, A. Decken and N. C. Norman, *J. Organomet. Chem.*, 1995, **496**, 59.

[23] C. J. Carmalt, W. Clegg, M. R. J. Elsegood, R. J. Errington, J. Havelock, P. Lightfoot, N. C. Norman and A. J. Scott, *Inorg. Chem.*, 1996, **35**, 3709; J. R. Eveland and K. H. Whitmire, *Inorg. Chim. Acta*, 1996, **249**, 41.

[24] N. Bricklebank, S. M. Godfrey, C. A. McAuliffe and K. C. Molloy, *J. Chem. Soc., Dalton Trans.*, 1995, 1593.

[25] N. J. Hill, W. Levason, G. Reid and M. Webster, *Acta Crystallogr.*, 2001, **E57**, o700.

[26] T. Klapotke, *Main Group Met. Chem.*, 1997, **2**, 81.

[27] A. Bondi, *J. Phys. Chem.*, 1964, **68**, 441.

[28] O. Mundt, H. Riffel, G. Becker and A. Simon, *Z. Naturforsch.*, 1988, **43b**, 952; H. Chen, M. M. Olmstead, D. C. Pestana and P. P. Power, *Inorg. Chem.*, 1991, **30**, 1783.

[29] L. F. Warren and M. A. Bennett, *Inorg. Chem.*, 1976, **15**, 3126.

[31] R. D. Feltham, R. S. Nyholm and A. Kasenally, *J. Organomet. Chem.*, 1967, **7**, 285.

[32] E. P. Kyba, S. T. Liu and R. L. Harris, *Organometallics*, 1983, **2**, 1877.

[33] H. C. E. McFarlane and W. McFarlane, *Polyhedron*, 1983, **2**, 203.

[34] SHELXL-97, G. M. Sheldrick, University of Göttingen, 1997.

[35] PATTY, The DIRDIF Program System, P. T. Beurskins, G. Admiraal, G. Beurskins, W. P. Bosman, S. Garcia-Granda, R. O. Gould, J. M. M. Smits and C. Smykalla, Technical Report of the Crystallography Laboratory, University of Nijmegen, The Netherlands, 1992.

[36] DIFABS, N. Walker and N. D. Stuart, *Acta Crystallogr.*, 1983, **A39**, 4158.

[37] TeXsan: Crystal Structure Analysis Package, Molecular Structure Corporation, Texas, 1995.

Chapter 3

Antimony(III) Halide Complexes of Thio- and Seleno-ethers

3.1 Introduction

The preceding chapter described a synthetic and structural study of arsenic(III), antimony(III) and bismuth(III) halide complexes of tertiary phosphine and arsine ligands. In the solid state these complexes displayed a rather limited number of topologies, broadly based upon an edge-shared, bioctahedral dimer motif. Recently, within the Southampton research group, a series of bismuth(III) halide complexes of multidenate thio- and seleno-ether ligands has been synthesised and structurally characterized,[1,2] and shown to adopt a much wider range of structures than the phosphine and arsine complexes discussed in Chapter 2.[3] In order to further develop the coordination chemistry of these chalogenoether ligands with p-block elements, and to probe the effect of changing the stereoelectronic properties of the group 15 atom upon the structural motifs adopted by these adducts in the solid state, a series of antimony(III) halide complexes containing multidentate and macrocyclic thio- and seleno-ether ligands have been prepared. This chapter describes the synthesis and structural properties of such complexes.

Antimony(III) is regarded as a borderline hard/soft acid in terms of the HSAB principle (Table 1.2) and is thus expected to preferentially coordinate ligands bearing softer donor atoms such as sulfur and phosphorus over those containing harder donors, for example, nitrogen or oxygen. Studies of antimony(III) complexes of dithio-oxamide and dithiomalonamide ligands [RHNC(S)C(S)NHR and RHNC(S)CCH_2(S)NHR], where both N and S donor atoms were potentially available to the antimony(III) atom, confirmed this. In all cases, bidentate ligand attachment *via* the two sulfur donor atoms was observed, with the nitrogen donors uncoordinated.[4]

3.1.1 p-Block Complexes of Thioether Ligands

As highlighted by a recent review there are few crown thioether complexes of p-block elements,[5] especially in comparison to the vast number of transition metal complexes reported for these ligands. The only structurally characterised complexes of the group 13 metals containing crown thioether ligands are [$AlMe_3$([12]aneS_4)],[6] [($AlMe_3$)$_4$([14]aneS_4)],[7] [$InCl_3$([9]aneS_3)],[8] [Tl([9]aneS_3)][PF_6],[9]

[Tl([18]aneS$_6$)][PF$_6$],[10] and [Tl([24]aneS$_8$)][PF$_6$],[11] while examples from group 14 are restricted to the tin(IV) and lead(II) complexes [SnCl$_4$(1,5-dithiacyclooctane)$_2$],[12] [(SnCl$_3$)$_3$([9]aneS$_3$)]$_2$[SnCl$_6$],[13] [(SnCl$_4$)$_2$([18]aneS$_6$)],[14] [Pb([9]aneS$_3$)$_2$(ClO$_4$)$_2$][15] and [Pb$_2$([28]aneS$_8$)(ClO$_4$)$_4$].[11] A series of tin(IV) halide complexes containing acyclic thio-, seleno- and telluro-ether ligands have been synthesised and structurally characterised,[16] and a number of diiodine charge transfer adducts of thiacrowns have been reported, for example [N]aneS$_4$.I$_2$ (N = 12, 14 or 16) and [18]aneS$_6$.I$_2$, forming polymeric networks through iodine-sulfur interactions.[17, 18] Aside from the antimony(III) and bismuth(III) halide complexes described in section 3.1.2, these appear to be the only examples of chalcogenoether complexes of the p-block elements.

3.1.2 Bismuth(III) and Antimony(III) Halide Complexes of Thioether Ligands

Prior to the work described herein there were no examples of antimony(III) complexes containing acyclic thio- or seleno-ether ligands. Only complexes of macrocyclic thioethers have received any study, with reports of the synthesis and X-ray structural characterization of [SbCl$_3$([9]aneS$_3$)], [(SbCl$_3$)$_2$([18]aneS$_6$)],[19] [BiCl$_3$([12]aneS$_4$)], [BiCl$_3$([15]aneS$_5$)][20] and [BiCl$_3$([18]aneS$_6$)][21] by Willey *et al*, [SbI$_3$([9]aneS$_3$)] by Pohl[22] and [(BiCl)$_2$([24]aneS$_8$)] by Schröder and co-workers.[11]

In the solid state, [SbCl$_3$([9]aneS$_3$)] adopts a chain structure with each SbCl$_3$ fragment bound in an endocyclic manner to the three sulfur donors of one [9]aneS$_3$ unit and to a bridging sulfur from an adjacent ligand to give seven-coordinate antimony(III) (Figure 3.1). Coordination of antimony to sulfur is weak, with Sb-S distances in the range 3.156(3)-3.460(3) Å.[19]

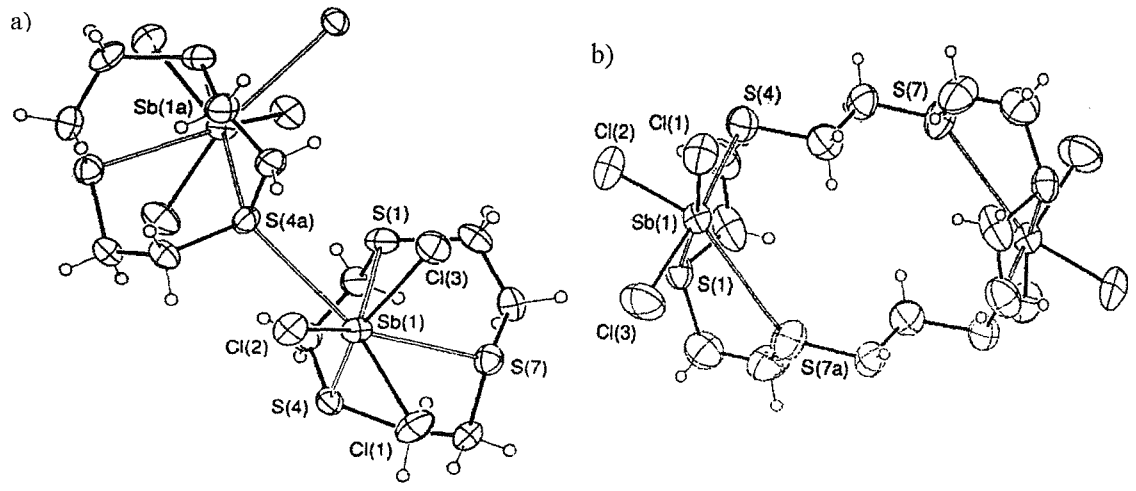

Figure 3.1 View of the structures of a) $[SbCl_3([9]aneS_3)]$ and b) $[(SbCl_3)_2([18]aneS_6)]$.[19]

The $[(SbCl_3)_2([18]aneS_6)]$ complex contains two $SbCl_3$ units each bonded to three separate sulfur atoms in an irregular *fac*-octahedral conformation.[19] A similar geometry was observed for $[SbCl_3(EtNHCSCSNHEt)_{1.5}]$ and $[SbCl_3(1,4\text{-dithiacycloheptane})]$.[23] The crystal structures of the $[SbI_3([9]aneS_3)]$, $[BiCl_3([12]aneS_4)]$, $[BiCl_3([15]aneS_5]$ and $[BiCl_3([18]aneS_6)]$ adducts all show a pyramidal MX_3 unit bound in an endocyclic manner to three, four, five or six co-planar sulfur donors respectively from the macrocycle to give an approximate half-sandwich structure. The Bi-S distances are in the range 2.987(3) – 3.346(8) Å. The structure of the related $[(BiCl_3)_2([24]aneS_8)]$ adduct is comprised of two separate $BiCl_3$ units bound to five sulfur donors (two of which bridge the bismuth atoms). [11] The $BiCl_3$ units are disposed on opposite sides of the mean plane of the crown (Bi-S 3.134(2) – 3.313(2) Å), in a similar manner to the $[(SbCl_3)_2([\text{dibenzo-24-crown-8}])]$ complex (Figure 1.12).

There are no reports of antimony(III) halide complexes of monodentate thio- or seleno-ethers. The sole example of such a bismuth(III) halide adduct, the ionic $[SMe_3]_2[Bi_2I_8(SMe_2)_2]$ species, was reported by Norman and co-workers in 1993.[24] The bismuth-containing dianion was described as a complex of $[Bi_2I_8]^{2-}$ with two molecules of SMe_2, adopting a centrosymmetric, edge-shared bi-octahedral structure in which the SMe_2 ligands are weakly bound (Bi-S 3.054(8) Å) in mutually *anti* positions.

As mentioned above, a series of structurally characterised $[BiX_3(L)]$ complexes was reported recently (L = acyclic bi- or tri-dentate thio- or seleno-ether ligand; X = Cl, Br or I) and it is appropriate to highlight the broad range of unusual structural motifs adopted by these bismuth(III) adducts. The first such compound to be structurally characterised was the $[Bi_4Cl_{12}\{MeS(CH_2)_3SMe\}_4]_n.nH_2O$ species.[1] This compound adopts an infinite three-dimensional lattice with large channels, consisting of an open cradle Bi_4Cl_4 unit connected to other such units by bridging dithioether ligands (2.857(7) – 2.977(7) Å) (Figure 3.2). Each bismuth atom is coordinated to two terminal and two μ-bridging chlorines and two sulfur atoms, giving a highly distorted octahedral environment. Long range Bi---Cl interactions (Bi-Cl 3.268(7) Å) link across the Bi_4Cl_4 units to give a pseduo-cubane core.

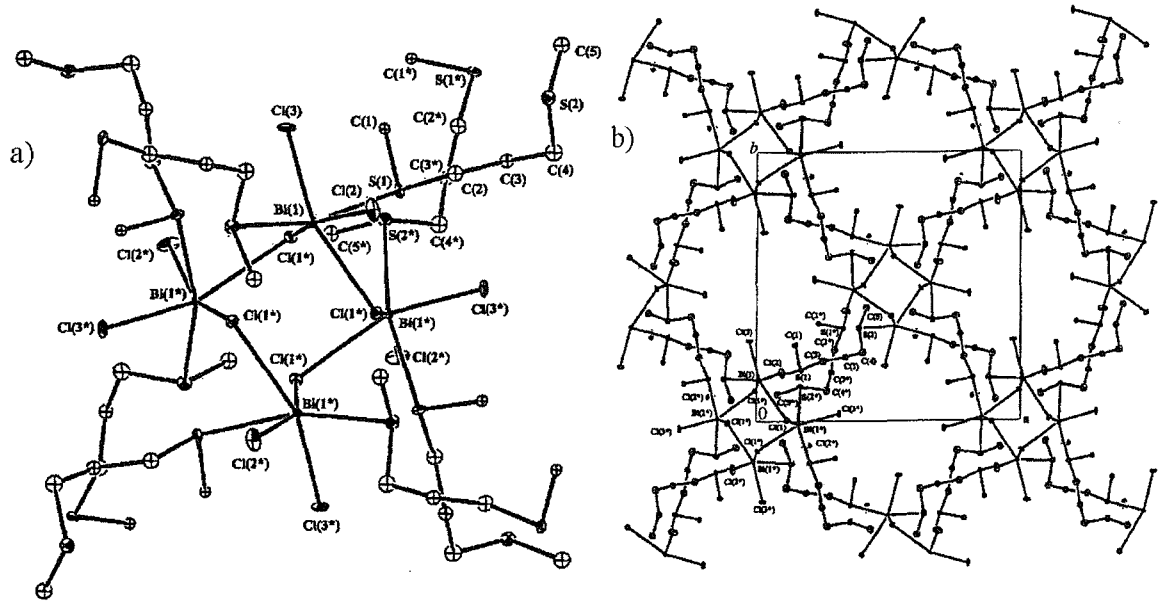

Figure 3.3 View of a) the repeat unit of the $[Bi_4Cl_{12}\{MeS(CH_2)_3SMe)_4]$ complex and b) a portion of the full lattice.[1]

In contrast, the $[BiBr_3\{MeS(CH_2)_2SMe\}_2]$ complex is a discrete molecular compound in the solid state, containing two chelating dithioether ligands.[2] The coordination geometry about the seven-coordinate bismuth(III) atom is distorted pentagonal bipyramidal, with three terminal bromines and four sulfur atoms comprising the donor set (Figure 3.4). Unusually, both the *meso* and DL invertomers of the dithiooether are present in the same molecule. The Bi-S bond lengths are asymmetric, in the range 2.918(5) - 3.090(5) Å.

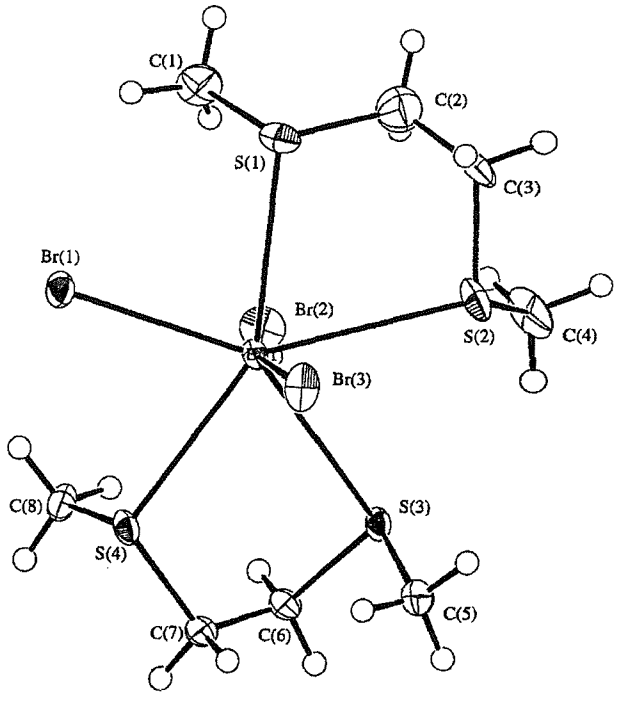

Figure 3.4 View of the structure of the $[BiBr_3\{MeS(CH_2)_2SMe\}_2]$ complex.[2]

The $[BiBr_3\{MeS(CH_2)_3SMe\}]$ complex adopts an infinite two-dimensional sheet motif, derived from planar Bi_2Br_6 units linked by bridging dithioether ligands.[2] The ligands occupy mutually *trans* coordination sites to give a distorted octahedral geometry about the bismuth(III) atom (Bi-S 2.880(4) – 2.931(4) Å) (Figure 3.5).

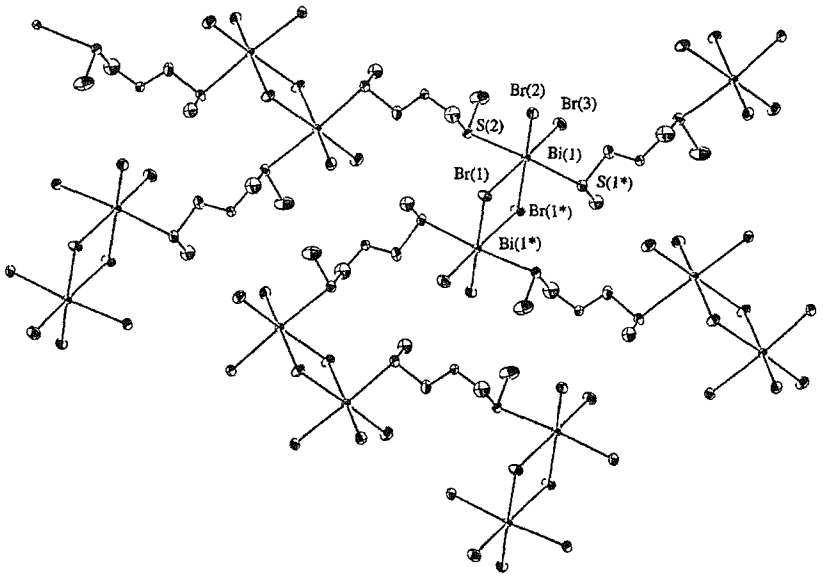

Figure 3.5 View of the extended structure of the $[BiBr_3\{MeS(CH_2)_3SMe\}]$ complex.[2]

Alteration of the terminal substituent of the ligand, from Me to Ph, has a significant effect upon the structural arrangement adopted. The complex $[Bi_2Br_6\{PhS(CH_2)_2SPh\}]$ displays a novel motif in which bridging dithioether ligands crosslink chains of mutually orthogonal Bi_2Br_6 units, giving an infinite sheet array (Figure 3.6). The Bi(III) donor set comprises one sulfur atom and one terminal and four bridging bromine atoms, with the thioether ligand *cis* to the terminal bromine.[2]

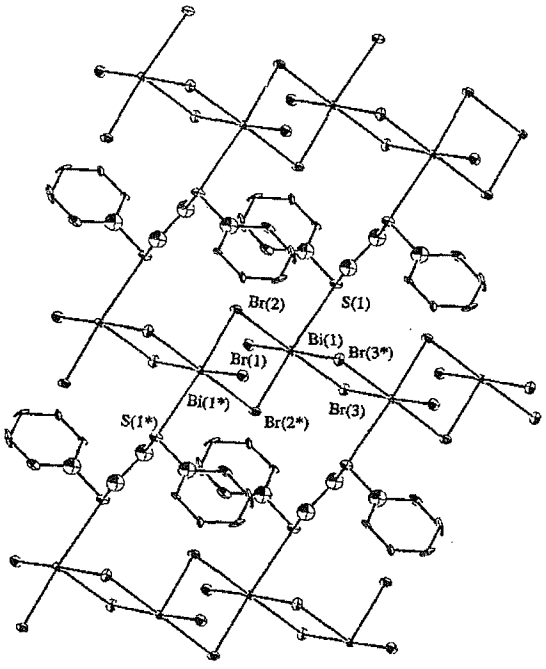

Figure 3.6 View of the extended structure of the $[Bi_2Br_6\{PhS(CH_2)_2SPh\}]$ complex.[2]

A change in the number of donor atoms available per ligand also has a dramatic effect on the observed coordination geometry. The structure of $[SbCl_3\{MeC(CH_2SMe)_3\}]$, containing a tripodal thioether ligand, shows a five-coordinate antimony centre forming an infinite helical structure derived from linking of these units by bridging tripodal ligands (Sb-S 3.106(2) – 3.172(2) Å). The ligand binds as bidentate donor such that each $SbCl_3$ unit coordinates to sulfur atoms from different ligands (Figure 3.7). The remaining sulfur donor is very weakly associated with the antimony atom (3.462(2) Å). The $[SbI_3\{MeC(SCH_2SMe)_3\}]$ adduct also exists as a coordination polymer, but in this case the antimony atoms are six-coordinate *via* two sulfur donors, two bridging iodine atoms and two terminal iodine ligands. Again, one sulfur donor is unbound and thus the ligand acts in a bridging bidentate fashion (Sb-S 2.973(6) – 3.021(6) Å).

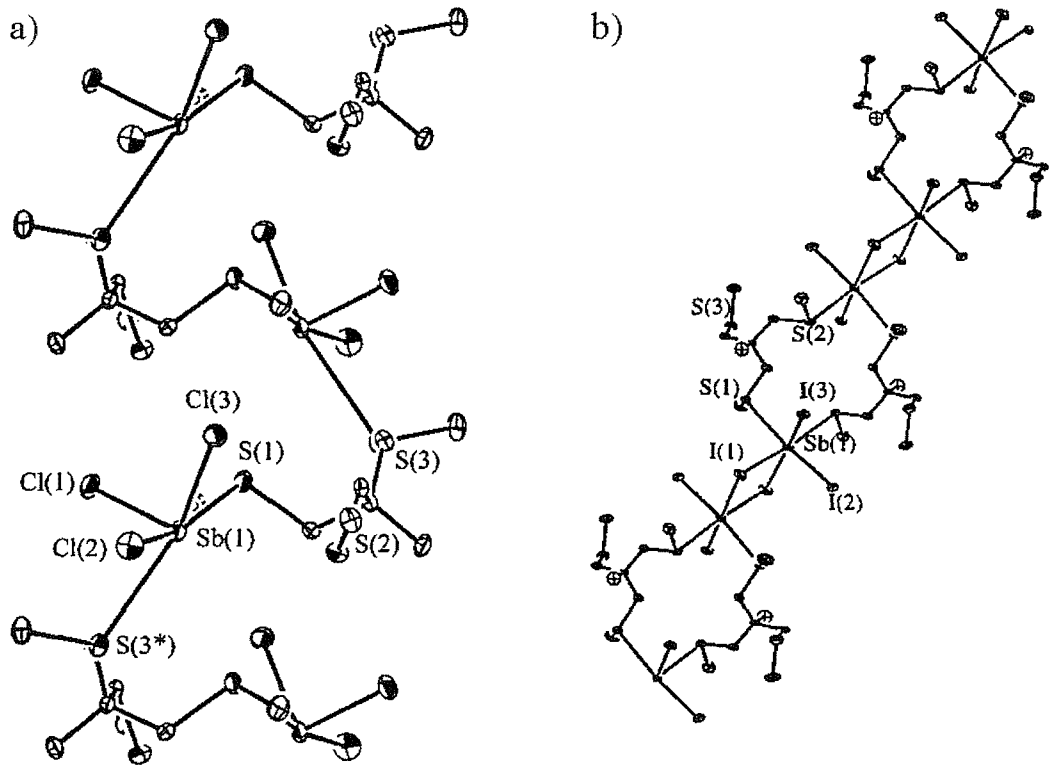

Figure 3.7 View of the extended structures of a) $[SbCl_3\{MeC(CH_2SMe)_3\}$ and b) $[SbI_3\{MeC(SCH_2SMe)_3\}]$ complexes.

In related work, Rabinovich and co-workers observed that the reaction of $BiCl_3$ with the silicon-apex tripodal thioether $MeSi(CH_2SMe)_3$ produced an extended chain structure containing single μ-Cl bridged Cl_2Bi-Cl-$BiCl_2$ fragments.[25] This leads to two distinct octahedral bismuth coordination environments, one with bidentate ligand attachment to one tripod and to one bridging and three terminal chlorines, and the other showing bidentate coordination to a tripod ligand, monodentate attachment to another and three terminal chlorines.

3.1.3 Bismuth(III) and Antimony(III) Halide Complexes of Selenoether Ligands

A series of bismuth(III) and antimony(III) halide complexes of multidentate and macrocyclic seleno-ether ligands has been reported recently by the Southampton research group, many of them structurally characterised.[26, 27] Although a part of the overall synthesis and characterisation program, these complexes were prepared in parallel to the work discussed later in this Chapter (i.e. complexes of bidentate thio- and seleno-ethers and thiacrowns).[28, 29]

The $[BiX_3\{MeSe(CH_2)_3SeMe\}]$ species (X = Cl or Br) adopt very similar structures to the $[BiBr_3\{MeS(CH_2)_3SMe\}]$ complex described above [Bi-Se 2.978(2) – 3.036)2) Å] (Figure 3.5).[2] The $[BiCl_3\{MeC(CH_2SeMe)_3\}]$ adduct contains a seven-coordinate bismuth atom, with Bi_2Cl_6 units bridged by the tripod selenoether to give a two-dimensional network, the ligand chelating to one bismuth centre in a bidentate manner and binding to an adjacent bismuth *via* the remaining Se-donor (Bi-Se 2.962(4) – 3.156(4) Å). In contrast, the $[Bi_2I_6\{MeC(CH_2SeMe)_3\}]$ complex is structurally very similar to the edge-shared, bioctahedral, isomer A dimer $[MX_3(L)]$ complexes discussed in chapter 2 (L = R_3P or R_3As). As in the thioether tripod complexes discussed above, the tripod selenoether behaves as a bidentate chelate to the bismuth atom with one Se-donor uncoordinated, resulting in a discrete molecular species rather than an extended coordination network (Bi-Se 2.96(1) – 3.19(1) Å).[2]

The structures of both the $[BiCl_3([8]aneSe_2)]$ and $[BiBr_3([16]aneSe_4)]$ species show exocyclic coordination of the ligand (Figure 3.8). In both examples, the bismuth atom is at the centre of a *trans* Se_2X_4 donor set, with two selenium donors per ligand uncoordinated in the $[BiBr_3([16]aneSe_4)]$ complex. Both species adopt an unusual one-dimensional ladder arrangement, with the co-planar Bi_2X_6 units ("rungs") linked by *trans* bridging selenoether ligands ("uprights") (Bi-Se 2.952(2) – 3.095(2) Å over both adducts). The $[BiX_3([24]aneSe_6)]$ complexes have also been synthesized and characterized by microanalysis and IR spectroscopy.[3]

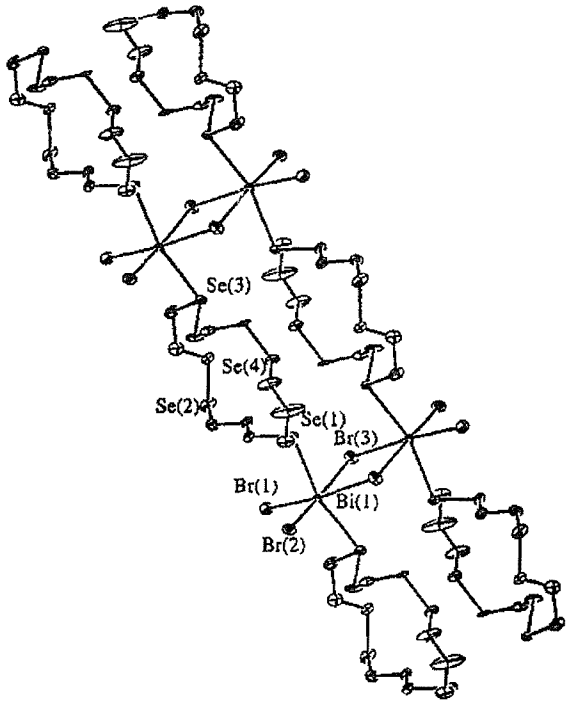

Figure 3.8 View of the ladder-type structure of $[BiBr_3([16]aneSe_4)]$.[3]

The $[SbBr_3\{MeC(CH_2SeMe)_3\}]$ complex exists as a chain polymer, with a six-coordinate antimony atom in a distorted octahedral environment. The donor set comprises three terminal bromines and three *fac*-coordinated selenium atoms. Each tripodal ligand donates all three selenium atoms, two coordinating to an SbX_3 unit in a bidentate manner with the remaining donor attached monodentate to a separate antimony atom. The Sb-Se distances are in the range 3.162(3) – 3.195(4) Å, and thus similar to those observed in the structurally similar $[SbCl_3\{MeC(CH_2SMe)_3\}]$ complex (Figure 3.7a). However, in the latter example, the antimony coordination geometry was described as five-coordinate on account of one of the Sb-S interactions being much

longer than the other two (*ca.* 3.13 Å compared to 3.46 Å) whereas the similarity of the Sb-Se distances in the present complex makes a six-coordinate description more appropriate.

The macrocyclic seleno-ethers [8]aneSe$_2$, [16]aneSe$_4$ and [24]aneSe$_6$ formed either 1:1 or 2:1 M:L complexes, characterised by microanalysis and IR spectroscopy, although only the [(SbBr$_3$)$_2$([16]aneSe$_4$)] adduct was structurally characterised (Figure 3.9). This species adopts a two-dimensional sheet array with SbBr$_3$ units weakly bound to two mutually *cis* selenium donors from separate macrocycles, giving a distorted square pyramidal geometry about the antimony atom (2.989(1) – 3.193(1) Å).

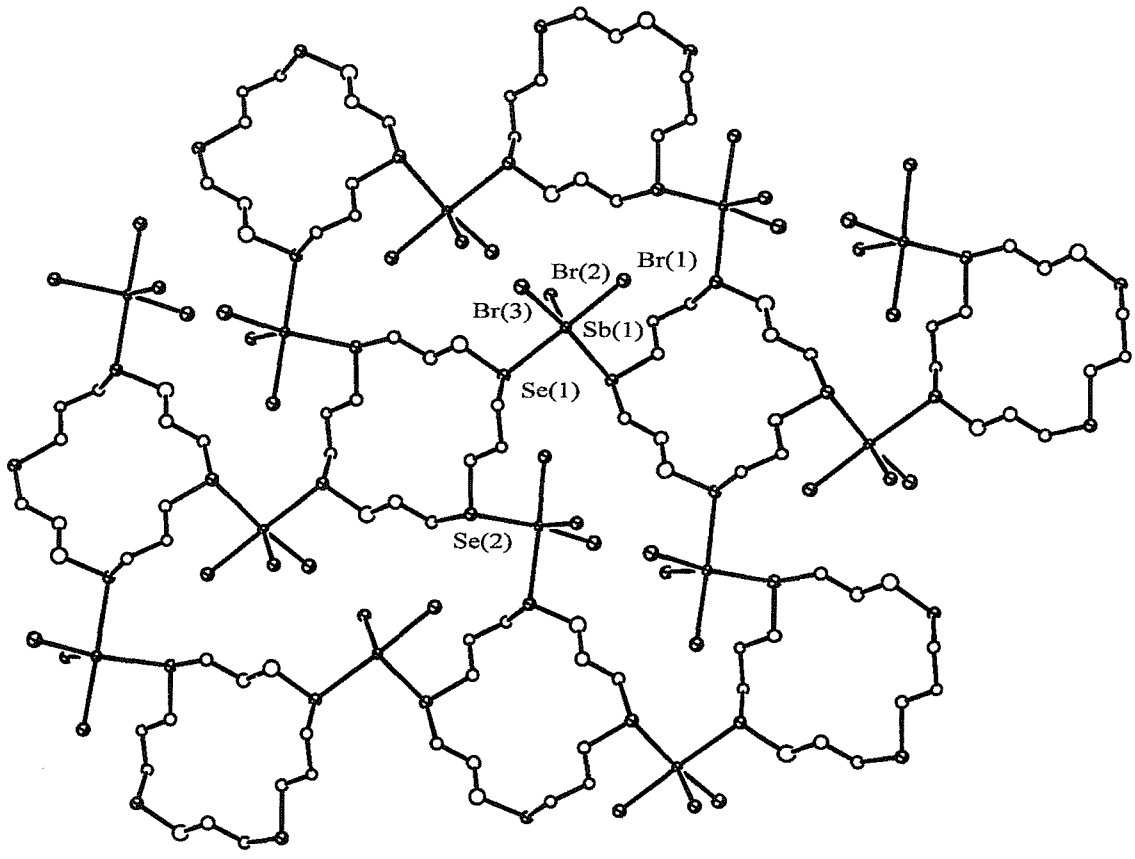

Figure 3.9 View of a portion of the two-dimensional lattice sheet adopted by [(SbBr$_3$)$_2$([16]aneSe$_4$)].[27, 29]

In summary, all but one of the reported MX_3 complexes of acyclic multidentate chalcogenoether ligands display infinite one-, two- or three-dimensional structures comprised of primary M-X bonding and weaker, secondary M---S/Se interactions (the $[BiBr_3\{MeS(CH_2)_2SMe\}_2]$ complex is a discrete, pentagonal bipyramidal molecule). This is in contrast to the examples containing thia-crown ligands where discrete face-capped molecular species predominate, although the M---S bond distances are similar to those in the acyclic complexes. The only structurally characterised selena-crown complex, $[(SbBr_3)_2([16]aneSe_4)]$, adopts a two-dimensional lattice structure.

3.2 Results and Discussion

3.2.1 Antimony(III) Halide Complexes of Thio- and Seleno-ethers

The reaction of SbX_3 (X = Cl, Br or I) in anhydrous MeCN (X = Cl, Br) or THF (X = I) solutions with one molar equivalent of L (L = $MeS(CH_2)_2SMe$, $MeS(CH_2)_3SMe$ $MeSe(CH_2)_2SeMe$ or $MeSe(CH_2)_3SeMe$) in anhydrous CH_2Cl_2 produced, following removal of solvent *in vacuo*, white (X = Cl) or pale orange-yellow (X = Br or I) solids in moderate yield. Most of these reactions yielded oils upon solvent removal and so trituration in anhydrous hexane was necessary in order to isolate a powder, which was isolated by vacuum filtration, washed with anhydrous CH_2Cl_2 and dried *in vacuo*. Satisfactory microanalyses were obtained for all freshly prepared solids, the majority of the adducts having empirical formula $[SbX_3(L)]$. Attempts to obtain a solid product from the reaction of $SbCl_3$ with $MeSe(CH_2)_2SeMe$ produced only an intractable wax, and the attempted reaction of SbF_3 with $MeS(CH_2)_2SMe$ or $MeSe(CH_2)_2SeMe$ resulted only in re-isolation of SbF_3 (as assessed by trace carbon and hydrogen values in the microanalyses).

Due to the moisture sensitivity of the SbX_3 and $[SbX_3(L)]$ species, all reactions were carried out under an atmosphere of dry N_2 using standard Schlenk techniques, and the complexes were stored in a dry, nitrogen filled glove-box. Under these conditions both the acyclic and macrocyclic thioether complexes appeared indefinitely stable, however the selenoether adducts became black and oily after about one week, indicating significant decomposition.

As for the MX_3-phosphine and arsine complexes discussed in Chapter 2, the majority of the thio- and seleno-ether complexes were very poorly soluble in non-coordinating solvents such as $CHCl_3$ and CH_2Cl_2 and thus no useful structural information could be obtained from NMR spectroscopy. Where room temperature ^{1}H-NMR spectra were obtainable only resonances attributable to free ligand were observed, suggesting extensive dissociation. The infrared spectra of the chloro derivatives, obtained as nujol mulls, show very weak, broad features in the range 300-230 cm^{-1} which may be tentatively assigned to ν(Sb-Cl) modes. Crystalline adducts were obtained by slow evaporation of an anhydrous MeCN solution of the reactants (in a 1:1 ratio) in a glove box. This method yielded crystals of sufficient quality for single crystal X-ray diffraction studies of the complexes $[SbCl_3\{MeS(CH_2)_2SMe\}]$, $[SbBr_3\{MeS(CH_2)_3SMe\}]$, and $[SbCl_3\{MeSe(CH_2)_3SeMe\}]$, all of which gave satisfactory microanalyses.

The structure of the $[SbCl_3\{MeS(CH_2)_2SMe\}]$ complex shows a distorted *fac* octahedral coordination environment about the antimony atom, with the donor set comprised of three terminal chlorides from the parent $SbCl_3$ fragment, and one terminal monodentate and two μ^2-bridging sulfur donor atoms (Figure 3.12, Table 3.1). The methyl groups of $MeS(CH_2)_2SMe$ adopt the DL conformation. All of the coordinated sulfur atoms are from separate ligands, thus each dithioether adopts an unusual bonding mode in which one of the sulfurs is bound terminally and the other uses both lone pairs to bridge two adjacent antimony atoms. This bifurcated arrangement generates an infinite three-dimensional coordination network (Figure 3.13). The only previous example of such a bonding mode for these ligands was observed in the $[Ag_n\{MeS(CH_2)_3SMe\}_n][BF_4]_n$ complex, an infinite chain polymer.[18]

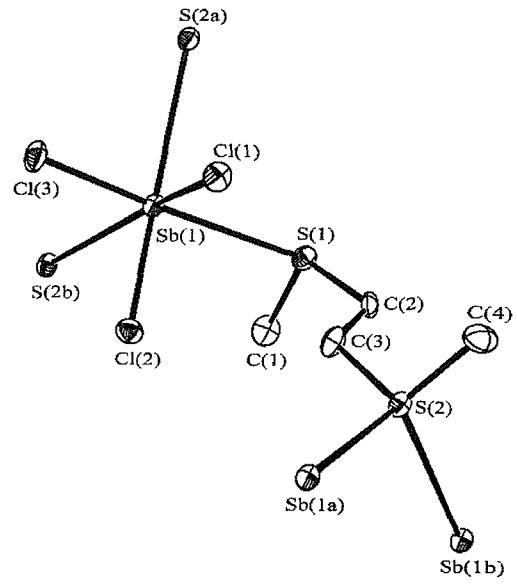

Figure 3.12 View of the asymmetric unit of $[SbCl_3\{MeS(CH_2)_2SMe\}]$ with numbering scheme adopted and nearest symmetry related neighbours. Atoms marked (a) are related by ½ + x, ½ - y, -z, and atoms marked (b) are related by –x, ½ + y, ½ - z.

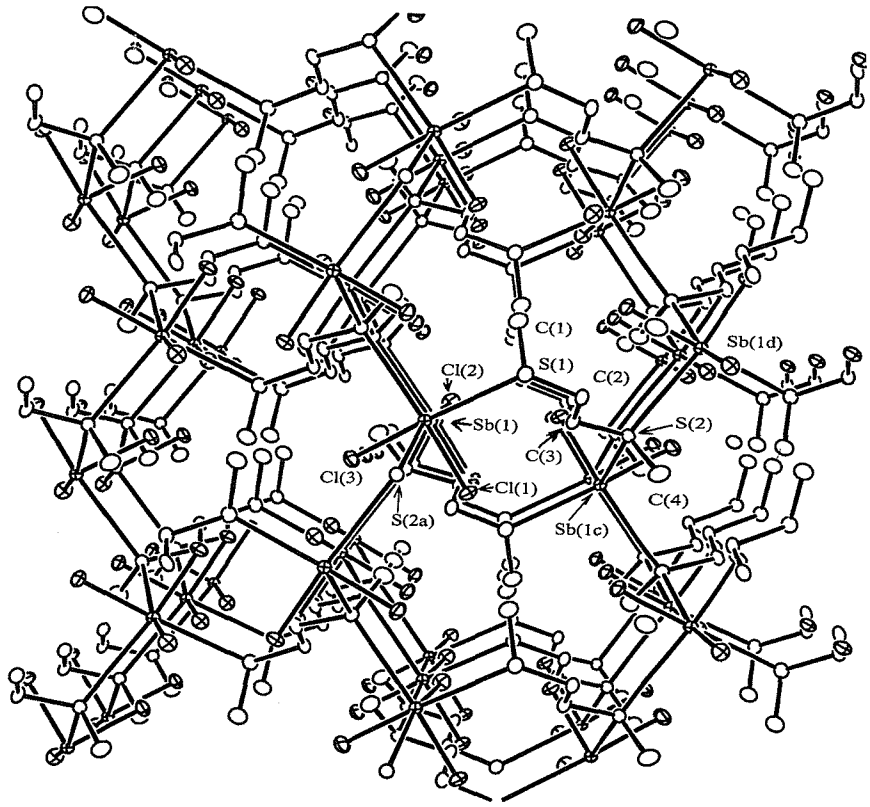

Figure 3.13 View of a portion of the three-dimensional lattice adopted by $[SbCl_3\{MeS(CH_2)_2SMe\}]$.

Sb(1)	Cl(1)	2.384(2)	Sb(1)	S(1)	3.170(2)
Sb(1)	Cl(2)	2.411(2)	Sb(1)	S(2a)	3.094(2)
Sb(1)	Cl(3)	2.428(2)	Sb(1)	S(2b)	3.294(2)
Cl(1)	Sb(1) Cl(2)	90.57(8)	Cl(2)	Sb(1) S(2b)	76.91(7)
Cl(1)	Sb(1) Cl(3)	91.02(7)	Cl(3)	Sb(1) S(1)	176.89(3)
Cl (1)	Sb(1) S(1)	86.69(6)	Cl(3)	Sb(1) S(2a)	80.24(7)
Cl(1)	Sb(1) S(2a)	74.73(7)	Cl(3)	Sb(1) S(2b)	80.62(7)
Cl(1)	Sb(1) S(2b)	164.23(7)	S(1)	Sb(1) S(2a)	97.12(6)
Cl(2)	Sb(1) Cl(3)	94.54(8)	S(1)	Sb(1) S(2b)	102.10(3)
Cl(2)	Sb(1) S(1)	87.58(7)	S(2a)	Sb(1) S(2b)	116.47(2)
Cl(2)	Sb(1) S(2a)	164.20(7)	Sb(1a)	Sb(2) Sb(1b)	108.88(7)

Table 3.1 Selected bond lengths (Å) and angles (°) for $[SbCl_3\{MeS(CH_2)_2SMe\}]$.

The dithioether is weakly bound to antimony, with Sb-S bond distances in the range 3.094(2) – 3.294(2) Å, indicative of secondary interactions. The Sb-Cl bond lengths in the complex (2.384(2) – 2.428(2) Å) are very similar to those observed in the parent pyramidal $SbCl_3$ unit (2.340(2) – 2.368(1) Å), as are the Cl-Sb-Cl bond angles (90.57(8) – 94.58(8)° in the present complex *vs.* 90.98(5) – 95.70(5) ° in $SbCl_3$).[30] The extent of stereochemical activity of the antimony-based lone pair is unclear. The distorted angle of 116.47(4) ° subtended at S(2a)-Sb(1)-S(2b) could indicate that the lone pair is localised in this area, although this may simply be a consequence of the highly unusual bonding mode of the dithioether ligand. The infinite network adopted by $[SbCl_3\{MeS(CH_2)_2SMe\}]$ contrasts sharply with the analogous $BiCl_3$ compound $[BiCl_3\{MeS(CH_2)_2SMe\}_2]$, a discrete molecule containing a seven-coordinate bismuth atom (discussed in section 3.1.2 and shown in Figure 3.4).[2] It seems likely that this

dramatic change in structure for a relatively small alteration in stereoelectronic properties of the central atom is, in the main part, due to the smaller radius of the antimony(III) centre compared to bismuth(III) (covalent radii 1.41 *vs.* 1.52 Å),[31] with the latter more able to accommodate seven-coordination (although $[BiCl_3\{MeS(CH_2)_2SMe\}_2]$ is the only structurally characterised example of an MX_3 complex of an acyclic dichalcogenoether in which the ligand chelates to a single MX_3 unit to give a discrete molecular species).[1-3]

In contrast to the three-dimensional network of $[SbCl_3\{MeS(CH_2)_2SMe\}]$, the $[SbBr_3\{MeS(CH_2)_3SMe\}]$ complex adopts a two-dimensional sheet array. The antimony(III) donor set is similar to that of the $[SbCl_3\{MeS(CH_2)_2SMe\}]$ species, with three mutally *fac* terminal bromines and three sulfur donors from separate dithioether ligands completing a distorted octahedral geometry (Figures 3.14 and 3.15, Table 3.2). The mixed terminal/bridging dithioether bonding mode is again evident, and the Sb-S bond distances are similar to those in $[SbCl_3\{MeS(CH_2)_2SMe\}]$ (Table 3.1), indicative of secondary Sb---S interactions, however in this case the shortest bond is to a terminal sulfur-donor atom (3.155(5) – 3.291(5) Å). The Sb-Br lengths are similar to those in the parent halide. The methyl groups of the dithioether ligands again adopt the DL conformation.

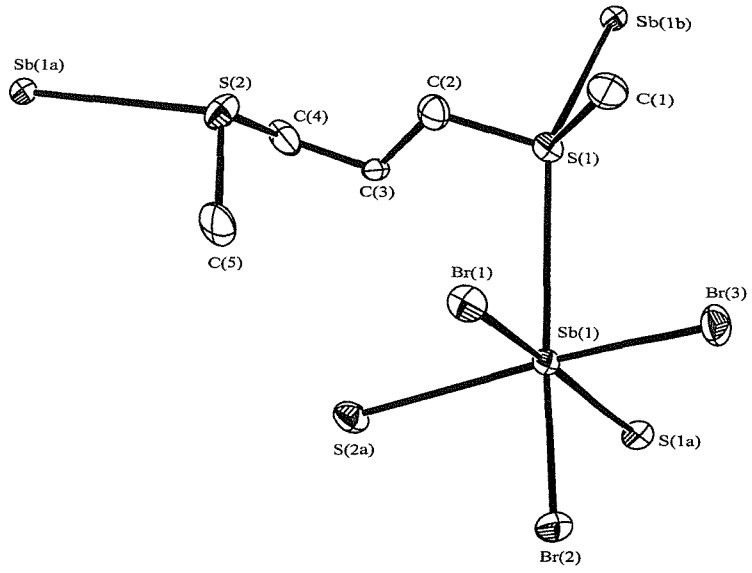

Figure 3.14 View of the asymmetric unit of $[SbBr_3\{MeS(CH_2)_3SMe\}]$ with numbering scheme adopted and nearest symmetry related neighbours. Atoms marked (a) are related by ½ + x, ½ - y, -z, and atoms marked (b) are related by –x, ½ + y, ½ - z.

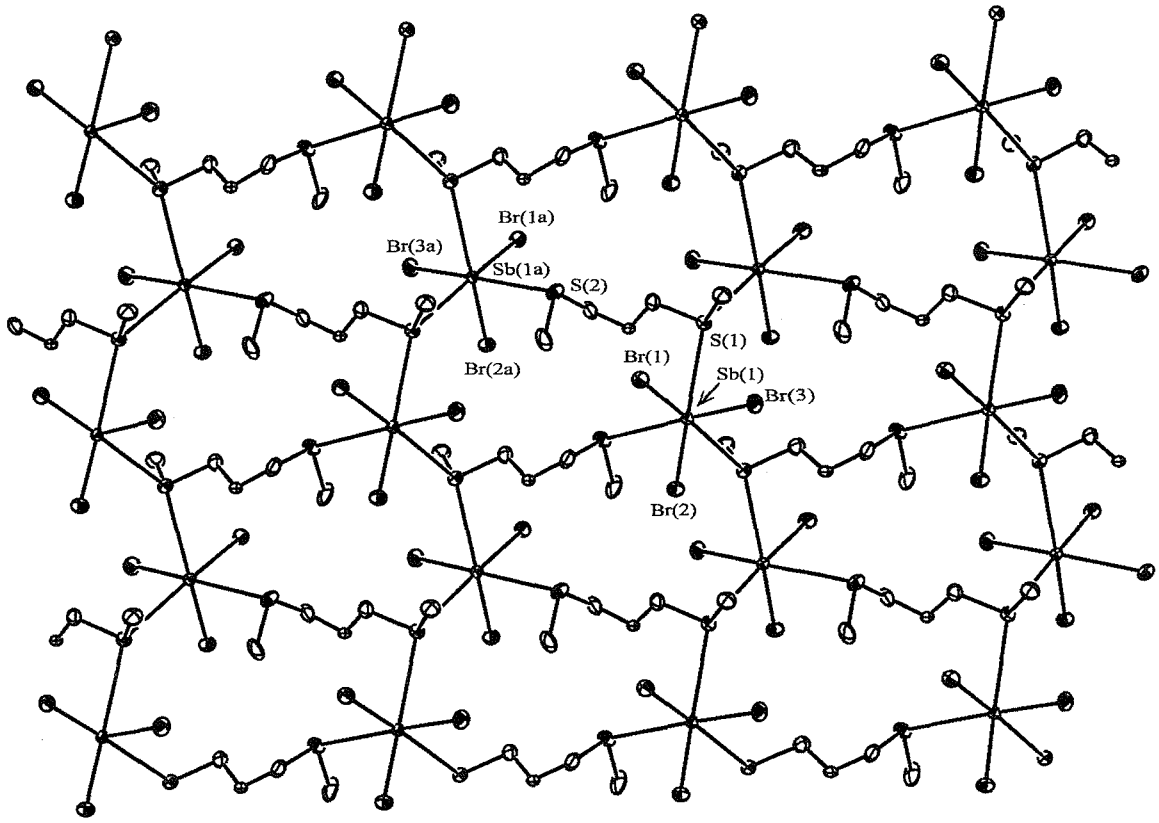

Figure 3.15 View of a portion of the three-dimensional lattice adopted by $[SbBr_3\{MeS(CH_2)_3SMe\}]$.

Sb(1)	Br(1)	2.572(2)	Sb(1)	S(1)	3.291(5)
Sb(1)	Br(2)	2.503(3)	Sb(1)	S(1a)	3.253(5)
Sb(1)	Br(3)	2.575(2)	Sb(1)	S(2)	3.155(5)
Br(1)	Sb(1) Br(2)	95.30(8)	Br(2)	Sb(1) S(2)	82.0(1)
Br(1)	Sb(1) Br(3)	92.49(8)	Br(3)	Sb(1) S(1)	80.3(1)
Br (1)	Sb(1) S(1)	78.2(1)	Br(3)	Sb(1) S(1a)	87.1(1)
Br(1)	Sb(1) S(1a)	177.2(1)	Br (3)	Sb(1) S(2)	173.1(1)
Br(1)	Sb(1) S(2)	82.8(1)	S(1)	Sb(1) S(1a)	104.4(7)
Br(2)	Sb(1) Br(3)	93.46(9)	S(1)	Sb(1) S(2a)	103.6(1)
Br(2)	Sb(1) S(1)	170.6(1)	S(1a)	Sb(1) S(2a)	97.4(1)
Br(2)	Sb(1) S(1a)	81.9(1)			

Table 3.2 Selected bond lengths (Å) and angles (°) for $[SbBr_3\{MeS(CH_2)_3SMe\}]$.

The *cis* angles at antimony are in the range 80.3(1) – 104.4(7) °. It is again uncertain as to the location of the antimony-based lone pair, although substantial distortions from octahedral geometry may suggest that it points out of the face of the triangle defined by the atoms S(1)– S(1a)–S(2a) (S(1)-Sb(1)-S(1a) 104.4(7)°, S(1)-Sb(1)-S(2a) 103.6(1)°, S(1a)-Sb(1)-S(2a) 97.4(1) °). As before, alternative explanations may exist. For example, aside from the constraints imposed by the unusual bonding mode, the lone pair of the terminal sulfur atom S(2a) may cause some distortion of the octahedral antimony(III) environment. Although a coordination network, the analogous bismuth(III) complex $[BiBr_3\{MeS(CH_2)_3SMe\}]$ differs from the present species in that it consists of planar, edge-shared Bi_2Br_6 units bridged by mutually *trans*, terminal dithioether ligands (Figure 3.5).[2]

An alteration in ligand architecture (from a C_2 to C_3 linkage between the donor atoms) appears to have less of an effect upon the structure of SbX_3 complexes than on the analogous BiX_3 species. A change in the ligand donor atom, however, leads to the adoption of an entirely different structure to that of the $[SbCl_3\{MeS(CH_2)_2SMe\}]$ or $[SbBr_3\{MeS(CH_2)_3SMe\}]$ adducts.

The complex $[SbCl_3\{MeSe(CH_2)_3SeMe\}]$ exists as a one-dimensional chain, derived from bridging diselenoether ligands linking $Cl_2Sb(\mu^2\text{-}Cl)_2SbCl_2$ units. The μ^2-bridging chlorines form an edge-shared bioctahedral dimer in the isomer A configuration (discussed in Chapter 2). The octahedral antimony(III) donor set consists of two terminal and two bridging chlorines, and two mutually *cis* selenium atoms from separate $MeSe(CH_2)_3SeMe$ ligands, with the methyl groups of the selenoether adopting the *meso* conformation. This motif is repeated to give an infinite coordination polymer (Figure 3.16, Table 3.3).

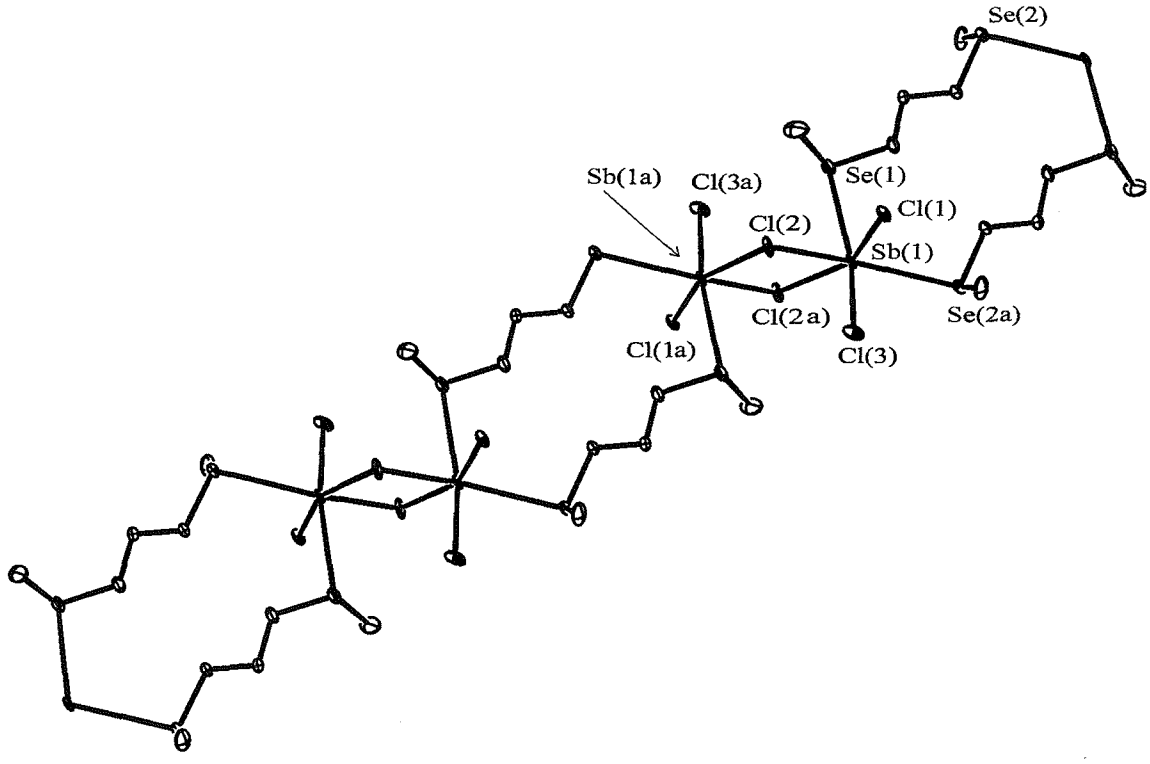

Figure 3.16 View of a portion of the one-dimensional chain structure adopted by $[SbCl_3\{MeSe(CH_2)_3SeMe\}]$ with the numbering scheme adopted. Ellipsoids shown at 40 % probablility, H-atoms omitted for clarity. Atoms labeled (a) are related by the symmetry operation –x, -y, -z

Sb(1)	Cl(1)	2.388(3)	Sb(1)	Cl(3)	2.424(3)
Sb(1)	Cl(2)	2.451(3)	Sb(1)	Se(1)	3.204(2)
Sb(1)	Cl(2a)	3.263(3)	Sb(1)	Se(2)	3.244(2)
Cl(1)	Sb(1) Cl(2)	88.1(1)	Se(1)	Sb(1) Cl(2)	80.42(8)
Cl(1)	Sb(1) Cl(2a)	159.19(9)	Se(1)	Sb(1) Cl(2a)	77.85(7)
Cl(1)	Sb(1) Cl(3)	94.5(1)	Se(1)	Sb(1) Cl(3)	169.69(9)
Cl(2)	Sb(1) Cl(2a)	76.8(1)	Se(2)	Sb(1) Cl(1)	80.66(8)
Cl(2)	Sb(1) Cl(3)	89.3(1)	Se(2)	Sb(1) Cl(2)	163.15(8)
Cl(2a)	Sb(1) Cl(3)	99.5(1)	Se(2)	Sb(1) Cl(2a)	117.01(1)
Se(1)	Sb(1) Se(2)	110.96(5)	Se(2)	Sb(1) Cl(3)	79.18(9)
Se(2)	Sb(1) Cl(1)	85.68(8)			

Table 3.3 Selected bond lengths (Å) and angles (°) for $[SbCl_3\{MeSe(CH_2)_3SeMe\}]$.

The Sb-Se bond distances indicate weak, secondary interactions and are similar to those in the $[SbX_3(dithioether)]$ complexes discussed above (although slightly more symmetric) but much longer than a typical Sb-Se distance of 2.580(2) Å found in, for example, $[Sb(SeMe)_3]$.[32] The Sb-Cl bond lengths in the $Sb(\mu^2\text{-}Cl)_2Sb$ unit are very asymmetric (2.451(3) – 3.236(2) Å, Δ = 0.785 Å), again typical of a bridge derived from a combination of primary and secondary Sb-Cl interactions.

As for the thioether complexes, the antimony coordination geometry is distorted from regular octahedral, but particularly so in the region of the $Sb(\mu^2\text{-}Cl)_2Sb$ bridge (Cl(1)-Sb(1)-Cl(2a) 159.2(6)°, Cl(2)-Sb(1)-Cl(2a) 76.7(7)°). Thus, in the absence of the mixed bridging/terminal bonding mode observed in the $[SbCl_3\{MeS(CH_2)_2SMe\}]$ and $[SbBr_3\{MeS(CH_2)_3SMe\}]$ complexes, the location of the lone pair can be stated with greater (but not absolute) certainty and it is likely to be localised along the vector of the $Sb(\mu^2\text{-}Cl)_2Sb$ bridge. It is noteworthy that the secondary Sb(1)–Cl(2a) interaction

is formed in the general direction of the site attributed to the lone pair (although it is assumed to avoid the direction of maximum lone pair density, in accord with the observations of Sawyer and Gillespie).[33] The structure of the present complex differs markedly from that of the analogous bismuth(III) adduct $[BiBr_3\{MeSe(CH_2)_3SeMe\}]$, which forms a two-dimensional sheet network in which the ligands occupy mutually *trans* coordination sites, isostructural with $[BiBr_3\{MeS(CH_2)_3SMe\}]$ (Figure 3.5).[2]

All members of the range of complexes $[MX_3\{MeE(CH_2)_3EMe\}]$ (M = Sb or Bi; X = Cl or Br; E = S or Se) contain a six-coordinate central atom, thus it is unlikely that the broad differences in structure can be rationalised solely in terms of the steric properties of the MX_3 unit. Whereas the thio- or seleno-ether ligands are coordinated mutually *trans* in the majority of the bismuth(III) complexes,[1-3] they exclusively adopt a *cis* configuration in the analogous antimony(III) adducts. Furthermore, to date, the mixed terminal/bridging thioether bonding mode has only been observed in SbX_3 complexes. These are both major factors in accounting for the diverse range of structures displayed by the two classes of adducts.

The fact that the mixed terminal/bridging dithioether bonding mode has so far only been observed in SbX_3 complexes may have its origins in the reduced Lewis acidity of the SbX_3 fragment compared to BiX_3. In all of the structurally characterised BiX_3 complexes the chalcogenoether ligand is bound to one (or more) bismuth atom(s) through two fairly symmetrical Bi-S/Se bonds, whereas the Sb-S bonds in $[SbCl_3\{MeS(CH_2)_2SMe\}]$ and $[SbBr_3\{MeS(CH_2)_3SMe\}]$ are asymmetric (ranges of 0.136 Å and 0.200 Å respectively). This could indicate that maximum Lewis acid-base interactions are achieved through the binding of one sulfur atom more strongly than the other two (i.e. one "full" Sb-S bond and two "fractional" Sb-S bonds). The "fractional" sulfur donors still have sufficient electron density available to weakly donate to an adjacent antimony atom, giving rise to the mixed terminal/bridging bonding mode and a coordination network motif. Similar bonding was not observed in the $[SbCl_3\{MeSe(CH_2)_3SeMe\}]$ adduct and the two Sb-Se distances are very symmetric (range 0.04 Å) suggesting that $MeSe(CH_2)_3SeMe$ may be a stronger σ-donor toward SbX_3 than $MeS(CH_2)_nSMe$. In contrast, the Lewis acidity of the BiX_3 species is such that two "full" Bi-S bonds are required to realise maximum donor-acceptor interactions.

It is stressed, however, that the difference between "full" and "fractional" bonding is small, and that M-E bonds in general should be regarded as weak, secondary interactions.

3.2.2 Antimony(III) Halide Complexes of Macrocylic Thioether Ligands

The reaction of SbX_3 (X = Cl or Br) in anhydrous MeCN solution with one molar equivalent of L_C (L_C = [12]aneS_4, [14]aneS_4 or [16]aneS_4) in anhydrous CH_2Cl_2 solution produced white (X = Cl) or pale yellow (X = Br) solids upon slow removal of solvent *in vacuo*. These solids were isolated by vacuum filtration, washed with anhydrous CH_2Cl_2 and dried *in vacuo*. Satisfactory microanalyses were obtained for all freshly prepared solids, the majority of the adducts having empirical formula $[SbX_3(L_C)]$ although for $[(SbBr_3)_2([14]aneS_4)]$ only the 2:1 species was isolated. Reaction of SbF_3 with [14]aneS_4 under similar conditions resulted in the re-isolation of SbF_3.

Only the adduct $[(SbBr_3)_2([14]aneS_4)]$ yielded crystals suitable for X-ray diffraction studies, obtained by slow evaporation of an anhydrous MeCN solution of the reactants in a 1:1 ratio. Like the bidentate thio- and seleno-ether ligand complexes discussed above, the $[(SbBr_3)_2([14]aneS_4)]$ adduct can be described as a coordination network, and in this example the network extends in three dimensions. The repeat unit of the network is derived from weakly associated edge-shared $Sb_2Br_4S_2$ bioctahedra, with each $SbBr_3$ unit bound exocyclic to the [14]aneS_4 ring. The structure of this complex is quite different to those observed for the acyclic dithioethers, with two terminal and two μ^2-bridging bromine atoms and two terminal, mutually *cis* sulfur donors from separate thiacrown ligands completing the octahedral antimony coordination sphere. Each [14]aneS_4 unit contributes one sulfur donor per antimony, with the ligand bridging four distinct antimony atoms in total (Figures 3.16 and 3.17, Table 3.4).

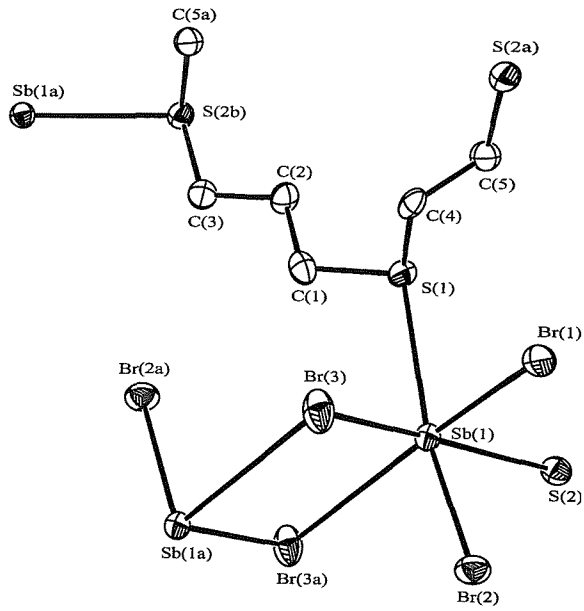

Figure 3.16 View of the asymmetric unit of $[(SbBr_3)_2([14]aneS_4)]$.with numbering scheme adopted and nearest symmetry related neighbours. Atoms marked (a) are related by -x, -y, -z and atoms marked (b) are related by ½ -x, ½ + y, ½ -z.

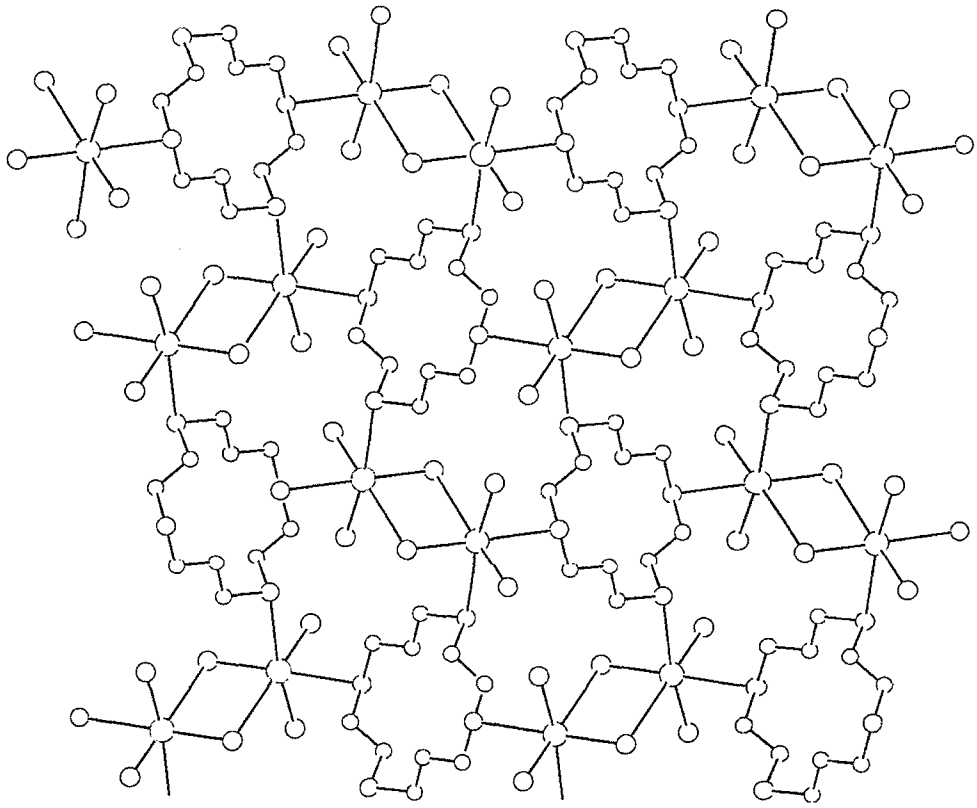

Figure 3.17 View of a portion of the lattice of $[(SbBr_3)_2([14]aneS_4)]$.

Sb(1)	Br(1)	2.5335(2)	Sb(1)	Br(3a)	3.497(2)
Sb(1)	Br(2)	2.2.548(2)	Sb(1)	S(1)	3.143(4)
Sb(1)	Br(3)	2.609(2)	Sb(1)	S(2)	2.954(3)
Br(1)	Sb(1) Br(2)	92.23(7)	Br(2)	Sb(1) S(2)	80.68(8)
Br(1)	Sb(1) Br(3)	93.02(6)	Br(1)	Sb(1) Br(3a)	84.99(6)
Br(1)	Sb(1) Br(3a)	175.56(6)	Br(3)	Sb(1) S(1)	88.79(8)
Br(1)	Sb(1) S(1)	76.60(9)	Br(3)	Sb(1) S(2)	173.68(8)
Br(1)	Sb(1) S(2)	83.00(8)	S(1)	Sb(1) S(2)	95.21(9)
Br(2)	Sb(1) Br(3)	94.62(6)	Br(3a)	Sb(1) S(1)	105.30(8)
Br(2)	Sb(1) Br(3a)	83.99(6)	Br(3a)	Sb(1) S(2)	98.62(7)
Br(2)	Sb(1) S(1)	170.38(8)	Sb(1)	Br(3) Sb(1a)	95.01(6)

Table 3.4 Selected bond lengths (Å) and angles (°) for $[(SbBr_3)_2([14]aneS_4)]$.

The edge-shared bioctahedral dimers adopt the isomer A configuration and the bridging Sb_2Br_2 unit is very asymmetric (2.609(2) – 3.497(2), Δ = 0.888 Å). The thiacrown ligands are bound to antimony through weak, secondary bonds (2.954(3) – 3.143(4) Å) although the coordination is stronger than in the $[SbCl_3([9]aneS_3]$ (X = Cl or I) and $[(SbCl_3)_2([18]aneS_6)]$ species, where the Sb-S distances are in the range 2.968(2) – 3.460(3) Å. The Sb-S bonds are also slightly shorter than those in the acyclic dithioether complexes $[SbCl_3\{MeS(CH_2)_2SMe\}]$ and $[SbBr_3\{MeS(CH_2)_3SMe\}]$ discussed previously.

The crystal structure of the free $[14]aneS_4$ species shows that the molecule exists in an exodentate conformation, with the four sulfur atoms at the corners of the rectangular molecule and the sulfur-based lone pairs pointing away from the macrocyclic cavity.[34] This conformation is also preferred by the similar $[12]aneS_4$ and

[15]aneS$_5$ ligands,[35] however Wiley reported that the $BiCl_3$ moiety in the [$BiCl_3$([12]aneS$_4$)] and [$BiCl_3$([15]aneS$_5$)] complexes was bound below the mean plane of the macrocyclic cavity to give a half-sandwich structure, implying some degree of rearrangement of the ligand backbone upon coordination to bismuth.[20] The inflexible nature of the trigonal pyramidal $BiCl_3$ unit was held responsible for this coordination mode. The thiacrown exists as an exodentate conformer in the [$(SbBr_3)_2$([14]aneS$_4$)] compound, and evidently coordination to the antimony atom has little effect on the conformation of the macrocycle. This implies that the interaction of [14]aneS$_4$ with $SbBr_3$ is substantially less than with BiX_3. A further structural consideration is the different chelate ring sizes available within each thiacrown cavity. For example, endodentate coordination of MX_3 to [9]aneS$_3$, [12]aneS$_4$ or [15]aneS$_5$ gives an energetically favoured five-membered chelate ring (as observed in the [SbI_3([9]aneS$_3$)], [$BiCl_3$([12]aneS$_4$)] and [$BiCl_3$([15]aneS$_5$)] species)[20-22] whereas similar coordination to [14]aneS$_4$ can give both five- and six-membered chelate rings. Since the structures are comprised of very weak Sb-S and Sb-Se interactions, such a chelate effect may influence the overall structure adopted by the complex.

The present complex is structurally very similar to the recently reported [$(SbBr_3)_2$([16]aneSe$_4$)] (Figure 3.9).[27] However an important distinction between the two structures is the lack of secondary Sb---Br bridging interactions in the selenium-donor complex, with the antimony atom adopting a five-coordinate, distorted trigonal bipyramidal geometry. The Sb-Se distances (2.989(1) – 3.193(1) Å) are similar to the Sb-S distances in [$(SbBr_3)_2$([14]aneS$_4$)] (Table 3.4). The [$BiBr_3$([16]aneSe$_4$)] complex adopts an entirely different structure, with near planar Bi_2Br_6 units linked by bridging ligands to generate a one-dimensional ladder-type array (Figure 3.11).[3]

3.3 Conclusions

The work discussed here represents the first structural survey of antimony(III) halide complexes of bidentate thio- and seleno-ethers. The insoluble nature of the adducts is presumably a consequence of their polymeric nature, and limits the available characterisation techniques to microanalysis, IR spectroscopy and single crystal X-ray diffraction, and hence only those species which yielded suitable crystals under the conditions employed can be discussed in detail (although the stoichiometry of the products obtained from all of these reactions is not in question). The fact that X-ray crystallography is the only method available for structural characterisation also limits the extent to which broad conclusions can be drawn, since coordination isomers may be generated under different experimental or crystallisation conditions.

The structures of the SbX_3 complexes containing acyclic bidentate ligands are not generally similar to those of the analogous BiX_3 species. For the dithioether complexes $[SbBr_3\{MeS(CH_2)_3SMe\}]$ and $[SbCl_3\{MeS(CH_2)_2SMe\}]$ complexes infinite two- and three-dimensional coordination networks are obtained respectively, with the sulfur-donors bound *via* an unusual mixed terminal/bridging bonding scheme such that one end of the ligand acts as a bifurcated donor, while the other binds terminally. The adoption of this mode overrides the expected preference for chelation of the flexible bidentate ligand. This bonding mode is not observed in the analogous bismuth(III) complexes.[1-3] The diselenoether complex $[SbCl_3\{MeSe(CH_2)_3SeMe\}]$ displays a more conventional bonding mode with the ligands linking SbX_3 units to generate a one-dimensional chain structure.

Although the $[(SbBr_3)_2([14]aneS_4)]$ complex is the only structurally characterised example of all the $[SbX_3(L_C)]$ complexes prepared in this study (L_C = $[12]aneS_4$, $[14]aneS_4$ or $[16]aneS_4$), comparison to previously reported BiX_3 structures allows some tentative conclusions to be drawn. It seems likely that the combination of weak, secondary Sb---S interactions, the conformation of the free macrocycle and the size of chelate ring potentially available upon endodentate coordination (along with other factors such as solubility) influences the overall structure adopted in the crystal. Hence, $[(SbBr_3)_2([14]aneS_4)]$ exists as a coordination network with *exo*-bound $SbBr_3$ units while the $[BiX_3([12]aneS_4)]$ species, for example, adopts a discrete, half-sandwich

structure with S_4-chelation to the bismuth atom.[20] Examination of the (as yet unreported) [BiX_3([14]aneS_4)] structures would provide insight into the importance of macrocycle conformation relative to M-S bond strength in the determination of overall structure.

The main features in common amongst these complexes is the retention of the trigonal pyramidal SbX_3 unit of the parent halide, and the occurrence of weak, secondary Sb---S or Sb---Se interactions on the opposite face leading to the sulfur- or selenium-donor atoms occupying mutually *cis* coordination sites. The bonding within these complexes is consistent with the DA model outlined in Chapter 1, in that the ligand donates into a M-X σ^* anti-bonding orbital to give delocalised 3-centre 4-electron bonds. The small structural changes in the parent SbX_3 unit indicate that this donation is weak. In view of the few structural examples available it is not yet possible to compile an order of chalcogenoether donor strength toward SbX_3.

3.4 Experimental

General experimental conditions are given in the Appendix. Antimony(III) halides were obtained commercially from Aldrich and used as received. Thio- and seleno-ether ligands were prepared using literature methods[36, 37] except [12]aneS$_4$, [14]aneS$_4$ and [16]aneS$_4$ which were obtained from Aldrich. Standard Schlenk techniques were used throughout, and all preparations and manipulations were performed under a N_2 atmosphere.

[SbCl$_3$(MeS(CH$_2$)$_2$SMe)]. A solution of MeS(CH$_2$)$_2$SMe (0.12 g, 1 mmol) in MeCN (3 cm^3) was added to a stirred and chilled solution of SbCl$_3$ (0.22 g, 1 mmol) in MeCN (10 cm^3). The resultant clear, colourless solution was stirred in an ice bath for 10 minutes, then in a water bath at 50° C for 30 minutes and then stirred at room temperature overnight. Solvent volume was reduced *in vacuo* and the residue layered with anhydrous hexane to produce a crop of colourless block crystals directly suitable for X-ray diffraction studies, which were isolated by vacuum filtration, washed with anhydrous CH_2Cl_2 and dried *in vacuo*. Yield 0.28 g, 80 %. Calculated for $C_4H_{10}Cl_3S_2Sb$: C, 13.7; H, 2.9. Found: C, 13.8; H, 2.9 %. ^{1}H-NMR: δ 2.2 (s, 6H), 2.8 (s, 4H). IR/cm^{-1}: 270, 243 ν(Sb-Cl).

[SbBr$_3${MeS(CH$_2$)$_2$SMe}]. Procedure as above. Removal of solvent yielded a yellow gum, which was triturated in anhydrous hexane (approx. 10 cm^3) to produce a pale yellow powder, isolated as above. Yield 31 %. Calculated for $C_4H_{10}Br_3S_2Sb$: C, 9.9; H, 2.0. Found: C, 9.7; H, 2.0 %. ^{1}H-NMR: δ 2.3 (s, 6H), 2.9 (s, 4H).

[SbI$_3${MeS(CH$_2$)$_2$SMe}]. To a chilled and stirred solution of SbI$_3$ (0.3 g, 0.6 mmol) in anhydrous THF (10 cm^3) was added an equimolar solution of MeS(CH$_2$)$_2$SMe in THF (5 cm^3). The orange-yellow solution was stirred at room temperature for 1 hour and solvent slowly removed *in vacuo* to produce an orange powder, which was isolated as above. Yield 68 %. Calculated for $C_4H_{10}I_3S_2Sb$: C, 7.3; H, 1.5. Found: C, 7.9; H, 1.2 %. ^{1}H-NMR: δ 2.2 (s, 6H), 2.7 (s, 4H).

[$SbCl_3${$MeS(CH_2)_3SMe$}]. Procedure as for [$SbBr_3${$MeS(CH_2)_2SMe$}]. White powder. Yield 67 %. Calculated for $C_5H_{12}Cl_3S_3Sb$: C, 16.5; H, 3.3. Found: C, 16.2; H, 3.2 %. ^{1}H-NMR: δ 1.9 (q, 2H), 2.1 (s, 6H), 2.6 (t, 4H). IR/cm^{-1}: 254, 235 ν(Sb-Cl).

[$SbBr_3${$MeS(CH_2)_3SMe$}]. Procedure as above. White powder. Yield 51 %. Calculated for $C_5H_{12}Br_3S_2Sb$: C, 12.1; H, 2.4. Found: C, 12.6; H, 2.4 %. ^{1}H-NMR: δ 1.9 (q, 2H), 2.1 (s, 6H), 2.6 (t, 4H).

[$SbBr_3${$MeSe(CH_2)_2SeMe$}]. Procedure as above. Yellow solid. Yield 31%. Calculated for $C_4H_{10}Br_3SbSe_2$: C, 8.3; H, 1.8. Found: C, 8.8; H, 1.9 %.

[SbI_3{$MeSe(CH_2)_2SeMe$}]. Procedure as above, using a THF solution of SbI_3 and a CH_2Cl_2 solution of $MeSe(CH_2)_2SeMe$. Orange powder. Yield 82%. Calculated for $C_4H_{10}I_3SbSe_2$: C, 6.7; H, 1.4. Found: C, 6.3; H, 1.3 %. ^{1}H-NMR: δ 2.1 (s, 6H), 2.9 (s, 4H).

[$SbCl_3${$MeSe(CH_2)_3SeMe$}]. A solution of $MeSe(CH_2)_3SeMe$ (0.3 g, 1.30 mmol) in CH_2Cl_2 (5 cm^3) was added to a stirred and chilled solution of $SbCl_3$ (0.3 g, 1.30 mmol) in MeCN (15 cm^3). The resultant clear, colourless solution was stirred for 1 hour at room temperature and solvent slowly removed *in vacuo*, resulting in deposition of colourless block crystals directly suitable for X-ray diffraction studies. Yield 71 %. Calculated for $C_5H_{12}Cl_3SbSe_2$: C, 13.1; H, 2.6. Found: C, 13.4; H 2.5 %. IR/cm^{-1}: 266, 243 ν(Sb-Cl).

[$SbCl_3$([12]aneS_4)]. To an anhydrous MeCN solution of $SbCl_3$ (0.048 g, 0.21 mmol) was added an equimolar MeCN solution of [12]aneS_4. The resultant clear, colourless solution was stirred at room temperature for 1 hour and solvent removed *in vacuo* to leave an off-white powder, isolated as for [$SbCl_3$($MeS(CH_2)_2SMe$)]. Yield 63 %. Calculated for $C_8H_{16}Cl_3S_4Sb$: C, 20.5; H, 3.4. Found: C, 21.0; 3.5 %. IR/cm^{-1}: 253, 244, 230 ν(Sb-Cl).

[$SbBr_3$([12]aneS_4)]. Procedure as above. Pale yellow powder. Yield 57 %. Calculated for $C_8H_{16}Br_3S_4Sb$: C, 16.0; H, 2.7. Found: C, 16.5; 2.6 %.

[$SbCl_3$([14]aneS_4)]. Procedure as above. White powder. Yield 35 %. Calculated for $C_{10}H_{20}Cl_3S_4Sb$: C, 24.2; H, 4.0. Found: C, 23.8; H, 3.9 %. IR/cm^{-1}: 267, 249, 231 ν(Sb-Cl).

[($SbBr_3$)$_2$([14]aneS_4)] Procedure as above. Pale yellow crystals. Yield 40 %. Calculated for $C_{10}H_{20}Br_6S_4Sb_2$.MeCN; C, 14.0; H, 2.2. Found: C, 14.1; 2.3 %.

[$SbCl_3$([16]aneS_4)]. Procedure as above. White powder. Yield 30 %. Calculated for $C_{12}H_{24}Cl_3S_4Sb$: C, 27.5; H, 4.6. Found: C, 27.2; 4.3 %. IR/cm^{-1}: 253, 234 ν(Sb-Cl).

[$SbBr_3$([16]aneS_4)]. Procedure as above. Pale yellow powder. Yield 35 %. Calculated for $C_{12}H_{24}Br_3S_4Sb$: C, 21.9; H, 3.7. Found: C, 21.8; 3.6 %.

3.5 X-ray Crystallography

General experimental X-ray data collection conditions are given in the Appendix. Details of the crystallographic data collection and refinement parameters for data discussed in this Chapter are given in Tables 3.5 and 3.6. Data collection used a Rigaku AFC7S four-circle diffractometer. No significant crystal decay or movement was detected.

Structure solution and refinement were routine[38, 39] except for [$SbCl_3${$MeS(CH_2)_2SMe$}], where a ψ-scan absorption correction was applied,[40] and [$SbBr_3$([14]aneS_4)] where a DIFABS absorption correction was applied.[41] For all structures, fully occupied non-hydrogen atoms were refined anisotropically and hydrogen atoms were added in fixed, calculated positions with *d*(C-H) = 0.96 Å. Refinement of the Flack parameter indicated the correct choice of enantiomorph for [$SbCl_3${$MeS(CH_2)_2SMe$}].[42]

	$[SbCl_3\{MeS(CH_2)_2SMe\}]$	**$[SbBr_3\{MeS(CH_2)_3SMe\}]$**
Formula	$C_4H_{10}Cl_3S_2Sb$	$C_5H_{12}Br_3S_2Sb$
Formula Weight	350.35	497.73
Crystal System	Orthorhombic	Orthorhombic
Space Group	$P2_12_12_1$ (# 19)	$Pna2_1$ (# 33)
a/ Å	8.925(3)	14.105(2)
b/ Å	15.098(2)	9.446(1)
c/ Å	8.224(3)	9.781(1)
α / °	90	90
β / °	90	90
γ / °	90	90
U / Å^3	1108.2(4)	1303.2(3)
Z	4	4
μ (Mo-K_α)/ cm^{-1}	35.22	116.11
Unique obs. reflns.	1169	1364
Obs. reflns.[$I > 2\sigma(I)$]	1093	1022
R	0.028	0.041
R_w	0.029	0.049

Table 3.5 X-ray data collection and refinement parameters for the $[SbCl_3\{MeS(CH_2)_2SMe\}]$ and $[SbBr_3\{MeS(CH_2)_3SMe\}]$ complexes.

	$[SbCl_3\{MeSe(CH_2)_3SeMe\}]$	**$[(SbBr_3)_2([14]aneS_4)]$**
Formula	$C_5H_{12}Cl_3Se_2Sb$	$C_{10}H_{20}Br_6S_4Sb_2$
Formula Weight	458.18	991.43
Crystal System	Monoclinic	Monoclinic
Space Group	$P2_1/c$ (# 14)	$P2_1/n$ (# 14)
a/ Å	9.622(5)	6.897(6)
b/ Å	12.882(3)	13.30(1)
c/ Å	10.376(4)	13.78(1)
α / °	90	90
β / °	101.89(4)	103.27(7)
γ / °	90	90
U / Å^3	1258.5(8)	1230(2)
Z	4	2
μ (Mo-K_α)/ cm^{-1}	85.59	123.02
Unique obs. reflns.	2344	4314
Obs. reflns.[$I > 2\sigma(I)$]	1934	3040
R	0.041	0.065
R_w	0.053	0.072

Table 3.6 X-ray data collection and refinement parameters for the $[SbCl_3\{MeSe(CH_2)_3SeMe\}]$ and $[(SbBr_3)_2([14]aneS_4)]$complexes.

3.6 References

[1] A. R. J. Genge, W. Levason and G. Reid, *Chem. Commun.,* 1998, 2159.

[2] A. J. Barton, A. R. J. Genge, W. Levason and G. Reid, *J. Chem. Soc., Dalton Trans.,* 2000, 859.

[3] A. J. Barton, A. R. J. Genge, W. Levason and G. Reid, *J. Chem. Soc., Dalton Trans.,* 2000, 2163.

[4] M. G. B. Drew, J. M. Kisenyi, G. R. Willey and S. O. Wandiga, *J. Chem. Soc., Dalton Trans.*, 1984, 1717; H. W. Yim, K. C. Lam, A. L. Rheingold and D. Rabinovich, *Polyhedron*, 2000, **19**, 849.

[5] W. Levason and G. Reid, *J. Chem. Soc., Dalton Trans.,* 2001, 2953.

[6] G. H. Robinson and S. A. Sangokoya, *J. Am. Chem. Soc.*, 1988, **110**, 1494.

[7] G. H. Robinson, H. Zhang and J. L. Atwood, *Organometallics*, 1986, **6**, 887.

[8] K. Wieghardt, M. Kleine-Boymann, B. Nuber and J. Weiss, *Inorg. Chem.*, 1986, **25**, 1309.

[9] A. J. Blake, J. A. Grieg and M. Schröder, *J. Chem. Soc., Dalton Trans.*, 1991, 529.

[10] A. J. Blake, G. Reid and M. Schröder, *J. Chem. Soc., Dalton Trans.*, 1992, 2987.

[11] A. J. Blake, D. Fenske, W-S. Li, V. Lippolis and M. Schröder, *J. Chem. Soc., Dalton Trans.,* 1998, 3961.

[12] M. M. Olmstead, K. A. Williams and K. Musker, *J. Am. Chem. Soc.*, 1982, **104**, 5567.

[13] G. R. Willey, A. Jarvis, J. Palin and W. Errington, *J. Chem. Soc., Dalton Trans.*, 1994, 255.

[14] R. D. Shannon, *Acta Crystallogr.,*1976, **A32**, 751.

[15] H.-J. Küppers, K. Wieghardt, B. Nuber and J. Weiss, *Z. Anorg. Allg. Chem.*, 1989, **577**, 155.

[16] S. E. Dann, A. R. J. Genge, W. Levason and G. Reid, *J. Chem. Soc., Dalton Trans.,* 1997, 2207; S. E. Dann, A. R. J. Genge, W. Levason and G. Reid, *J. Chem. Soc., Dalton Trans.,* 1996, 4471; A. R. J. Genge, W. Levason and G. Reid, *J. Chem. Soc., Dalton Trans.,* 1997, 4479; A. R. J. Genge, W. Levason and G. Reid, *J. Chem. Soc., Dalton Trans.,* 1997, 4549.

[17] A. J. Blake, F. Cristiani, F. A. Devillanova, A. Garau, L. M. Gilby, R. O. Gould, F. Isaia, V. Lippolis, S. Parsons, C. Radek and M. Schröder, *J. Chem. Soc., Dalton Trans.*, 1997, 1337.

[18] A. J. Blake, F. A. Devillanova, A. Garau, L. M. Gilby, R. O. Gould, F. Isaia, V. Lippolis, S. Parsons, C. Radek and M. Schröder, *J. Chem. Soc., Dalton Trans.*, 1998, 2037.

[19] G. R. Willey, M. T. Lakin, M. Ravindran and N. W. Alcock, *Chem. Commun.*, 1991, 271.

[20] G. R. Willey, M. T. Lakin and N. W. Alcock, *J. Chem. Soc., Dalton Trans.*, 1992, 591.

[21] G. R. Willey, M. T. Lakin and N. W. Alcock, *J. Chem. Soc., Dalton Trans.*, 1992, 1339.

[22] S. Pohl, D. Haase and M. Peters, *Z. Anorg. Allg. Chem.*, 1993, **619**, 727.

[23] V. M. Schmidt, R. Bender and C. Burschka, *Z. Anorg. Allg. Chem.*, 1979, **454**, 160.

[24] W. Clegg, N. C. Norman and N. L. Pickett, *Polyhedron*, 1993, **12**, 1251.

[25] H.-W. Yim, K. Lam, A. L. Rheingold and D. Rabinovich, *Polyhedron*, 2000, **19**, 849.

[26] A. J. Barton, N. J. Hill, W. Levason and G. Reid, *J. Chem. Soc., Dalton Trans.*, 2001, 1621.

[27] A. J. Barton, N. J. Hill, W. Levason, B. Patel and G. Reid, *Chem. Commun.*, 2001, 95.

[28] A. R. J. Genge, Ph.D Thesis, University of Southampton, 1999.

[29] A. J. Barton, Ph.D Thesis, University of Southampton, 2000.

[30] A. Lipka, *Acta Crystallogr.*, 1979, **B35**, 3020.

[31] "Advanced Inorganic Chemistry", F. A. Cotton, G. Wilkinson, C. A. Murillo and M. Bochmann, 6th Edition, p. 381, Wiley, New York, 1999.

[32] H. J. Breunig, S. Gulec, B. Krebs and M. Dartmann., *Z. Naturforsch.*, 1989, **44b**, 1351.

[33] J. F. Sawyer and R. J. Gillespie, *Prog. Inorg. Chem.*, 1986, **34**, 65.

[34] R. E. DeSimone and M. D. Glick, *J. Am. Chem. Soc.*, 1976, **98**, 762.

[35] R. E. Wolf, Jr., J. R. Hartman, J. M. E. Storey, B. M. Foxman and S. R. Cooper, *J. Am. Chem. Soc.*, 1987, **109**, 4328.

[36] F. R. Hartley, S. G. Murray, W. Levason, H. E. Soutter and C. A. McAuliffe, *Inorg. Chim. Acta*, 1979, **35**, 265.

[37] D. J. Gulliver, E. G. Hope, W. Levason, S. G. Murray, D. M. Potter and G. L. Marshall, *J. Chem. Soc., Perkin Trans. 2*, 1984, 429.

[38] SHELXS-97, G. M. Sheldrick, University of Göttingen, Germany, 1997.

[39] TeXsan: Crystal Structure Analysis Package, Molecular Structure Corporation, The Woodlands, TX, 1995.

[40] PATTY, The DIRDIF Program System, P. T. Beurskens, G. Admiraal, G. Beurskens, W. P. Bosman, S. Garcia-Granda, R. O Gould, J .M. M. Smits and C. Smykalla, Technical Report of the Crystallography Laboratory, University of Nijmegen, The Netherlands, 1992.

[41] N. Walker and D. Stuart, *Acta Crystallogr.*, 1983, **A39**, 158.

[42] H. D. Flack, *Acta Crystallogr.*, 1983, **A39**, 876.

Chapter 4

Arsenic(III) Halide Complexes of Thio- and Seleno-ethers

4.1 Introduction

The previous chapter detailed a synthetic and structural study of antimony(III) halide complexes of multidentate and macrocyclic thio- and seleno-ether ligands. An unexpectedly diverse range of structural motifs was displayed by these adducts; unexpected because the SbX_3 unit demonstrated a reasonably powerful Lewis acidity, similar to that of BiX_3, and diverse due to the variety of coordination modes and geometries displayed by this fragment (often within the same molecule). With this in mind, the next logical step in the study of group 15 halide complexes of chalcogenoethers was to examine the effect of further reducing the acceptor properties of the MX_3 moiety. Given that examples of AsX_3 adducts of phosphine and arsine ligands were reported in Chapter 2, this non-metallic species provides a means of probing the structures adopted by a system lying near the extreme of Lewis acidity for group 15 halides.

The coordination and structural chemistry of arsenic(III) halides has received relatively little coverage in the literature. Aside from the obvious disadvantages of being highly toxic compounds, the lack of structural information is mainly due to the fact that many of the adducts were isolated prior to the advent of modern instrumental techniques (and, in particular, ready access to single crystal X-ray diffraction). The poor acceptor properties of the non-metallic AsX_3 (X = Cl, Br and I) species has also contributed to the lack of comprehensive study. In contrast, the Lewis acidity of antimony(III) and bismuth(III) halides is now well established,[1] with recent work by the Southampton group[2, 3] and others[4] illustrating the broad range of structures adopted by complexes of these species with phosphine, arsine and chalcogenoether ligands. Examples of As(III) functioning as a Lewis base are numerous (e.g. arsine ligands), however there are few reports of As(III) acting as a Lewis acid. Thus, the question of whether AsX_3 displays similar coordination chemistry with chalcogenoether ligands (and thus adopts similar structural motifs) to its heavier congeners still remains. This chapter describes a synthetic and structural study of a range of arsenic(III) halide complexes of bidentate and macrocyclic thio- and seleno-ethers.

4.1.1 Arsenic(III) Halide Complexes of Group 16 Donor Ligands

As stated in Chapter 1, the coordination chemistry of arsenic(III) halides and related species is sparse in comparison to that of SbX_3 and BiX_3. The current literature regarding MX_3 complexes of multidentate and macrocyclic chalcogenoethers has been discussed in Chapter 3, and so this section aims to outline the structural and coordination chemistry of AsX_3 complexes containing chalcogen-donor ligands. Coverage of the literature is not intended to be comprehensive, and the discussion uses selected examples to illustrate trends or key points.

With regard to group 16 donor ligand adducts of arsenic(III) halides, only examples of oxygen- and sulfur-donor systems have appeared in the literature. In terms of oxygen-donor ligands, the IR and Raman spectra of the $[AsX_3\{(OBu)_3P\}_2]$ (X = Cl and Br) adducts were reported by Long.[5] The only subsequent study of oxygen donor ligand complexes was made by Alcock and co-workers, who reported the crystal structures of $[AsCl_3(12\text{-crown-4})]$ and $[AsCl_3(15\text{-crown-5})]$.[6] Like their $SbCl_3$ and $BiCl_3$ analogues, both complexes adopt a half-sandwich structure, with the crown ligand capping the trigonal pyramidal $AsCl_3$ unit and As-O bonds becoming weaker with increasing crown cavity size, in the range 2.776(6) – 2.915(6) Å for $[AsCl_3(12\text{-crown-4})]$ and 2.994(4) – 3.156(4) Å for $[AsCl_3(15\text{-crown-5})]$. No adduct was isolated from the $AsCl_3$/[18]-crown-6 reaction system.[6]

Early work upon sulfur-donor ligands concerned the complexes formed by N, N-dialkyldithiocarbamates, with a non-chelated pyramidal structure proposed for $[As(S_2CNEt_2)_3]$, on the basis of higher than expected dipole moment values.[7] In fact the crystal structure of this complex, obtained some years later, showed the dithiocarbamate ligand to behave as a very asymmetric bidentate chelate, with As-S bond distances ranging from 2.344(3) to 2.904(4) Å) (Figure 4.1).[8]

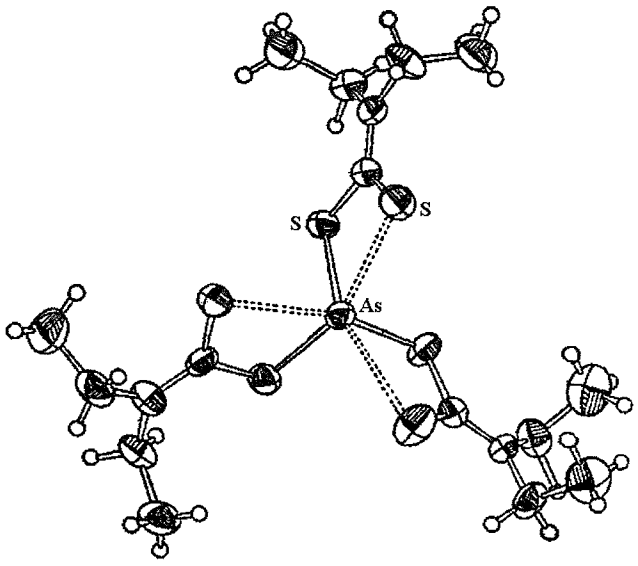

Figure 4.1 View of the $[As(S_2CNEt_2)_3]$ complex.[8a]

An X-ray structural study of the arsenic-xanthate complex $[As(S_2CO^iPr)_3]$ also revealed three asymmetrically chelating xanthate ligands (As-S 2.305(2) and 2.978(2) Å) arranged in a distorted octahedral geometry.[9] A stereochemically active lone pair was held responsible for the distortion.

Dräger reported the crystal structure of 2-chloro-1,3,6,-trithi-2-arsaoctane, which adopts an eight-membered ring in a distorted boat conformation.[10] The coordination geometry about the arsenic(III) atom was considered to be pseudo-trigonal bipyramidal, with a 1, 5-transannular As-S interaction (2.719(2) Å) forming part of the donor set (Figure 4.2).

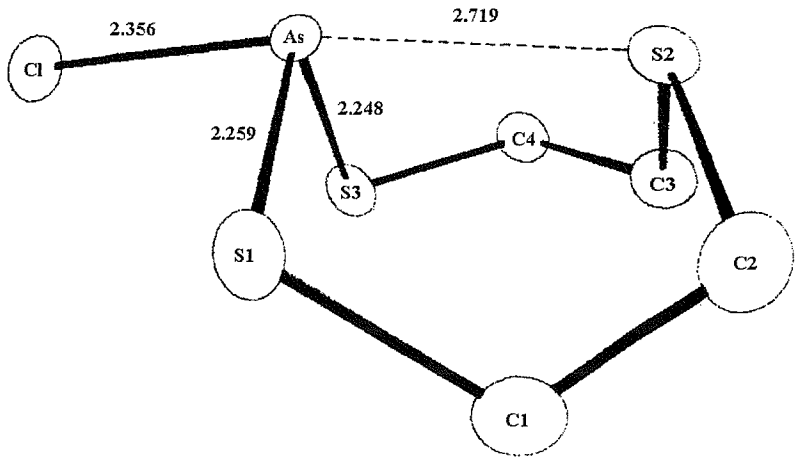

Figure 4.2 View of the $[AsCl\{S(CH_2)_2S(CH_2)_2S\}]$ complex.[10]

The reaction of dimethylarsenic(III) halides with thiourea (tu) produced 1:1 and 1:2 complexes formulated as $[Me_2As(tu)]^+X^-$ and $[Me_2As(tu)]^+X^-.tu$.[11] The cationic nature of these species was confirmed by the absence of an As-X band in the vibrational spectra and a single crystal X-ray structure (As-S 2.320(2) Å). A series of neutral $[AsX_3(tu)]$ complexes was subsequently reported, and characterised by microanalysis, IR, Raman and NMR spectroscopy.[12] A trigonal-bipyramidal geometry was proposed on the basis of vibrational spectroscopic data, although the crystal structure of the $[AsCl_3(dmit)]$ complex revealed a halide-bridged dimer (As-S 2.304 Å) (Figure 4.3).[12]

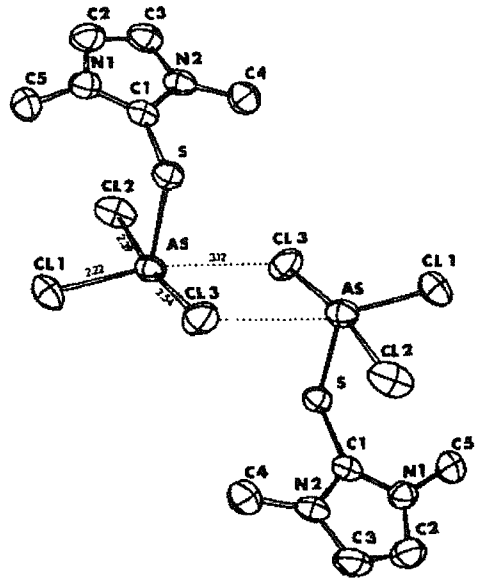

Figure 4.3 View of the $[AsCl_3(dmit)]$ complex.[12]

The reaction of toluene-3,4–dithiol (H_2tdt) with $AsCl_3$, reported by Willey and co-workers, produced the [AsCl(tdt)] adduct.[13] The crystal structure of this species shows a pseudo-tetrahedral arsenic(III) centre, with the dithiol ligand coordinated symmetrically (2.226(3) - 2.209(3) Å) and the lone pair occupying the remaining site (Figure 4.4). The authors suggest that the [AsCl(tdt)] molecules are packed together *via* weak As---Ph interactions, the As-C distances ranging from 3.32(1) to 3.63(1) Å for the six phenyl-ring carbon atoms.

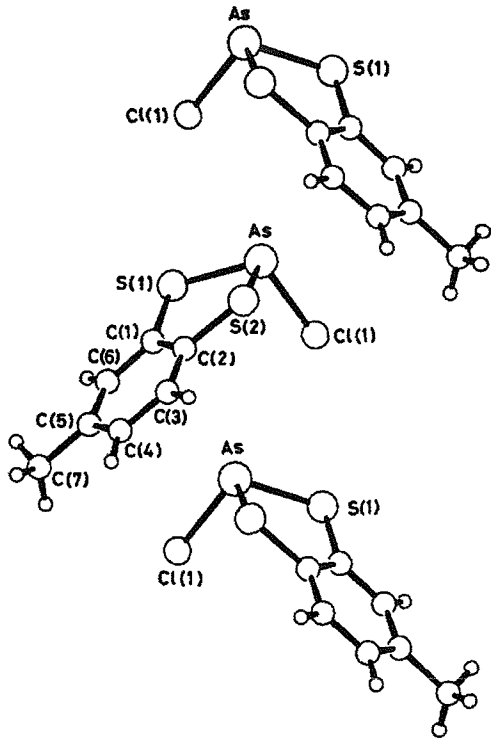

Figure 4.4 View of the stacking arrangement in the [AsCl(TDT)] complex.[13]

In recent work, ethanedithiolato alkyldithiophosphate derivatives of arsenic(III) were obtained by reaction of ethane-1,2-dithiolato arsenic(III) chloride and sodium alkylenedithiophosphate in refluxing benzene (Figure 4.5).[14] From $^{31}P\{^{1}H\}$-NMR and IR data the authors proposed a pseudo-trigonal bipyramidal geometry about the arsenic(III) atom, arising from bidentate chelation of the dithiophosphate ligand to the dithiolato arsenic moiety. A stereochemically active lone pair was assumed to occupy one of the equatorial positions.

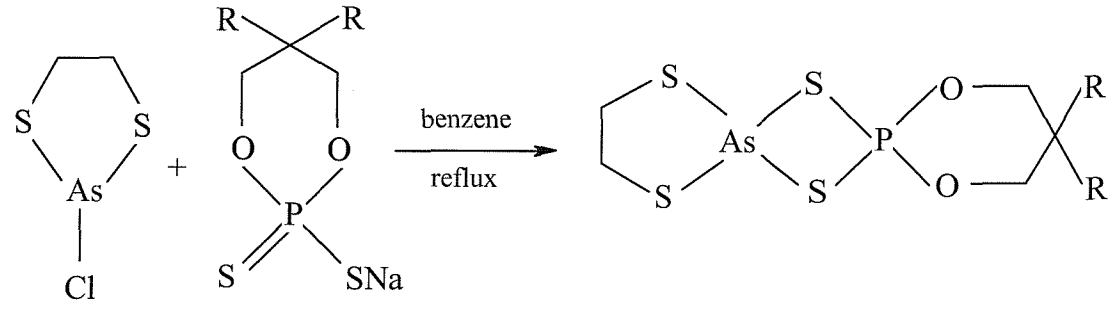

Figure 4.5 Reaction scheme for synthesis of a dithiolatoarsenic(III) alkydithiophosphate (R = Me or Et).[14]

The only example of a thioether complex of AsX_3 is the $[AsI_3(hta)]$ (hta = 1,3,5,7-(tetramethyl)-2,4,6,8,9,10-(hexathia)adamantane) (Figure 4.6).[15] The complex was prepared serendipitously by reaction of AsI_3 with thioacetic acid in water, with hta forming in equilibrium with an acid-derived thione. In the complex, AsI_3 is bound to three of the six sulfur atoms of the hta unit to give an octahedral coordination environment (As-S 3.274(1) – 3.310(1) Å). The As-I distances are similar to those in the parent AsI_3 molecule. The arsenic-based lone pair was assumed to point toward the centre of the six-membered ring formed by the top of the hta molecule.

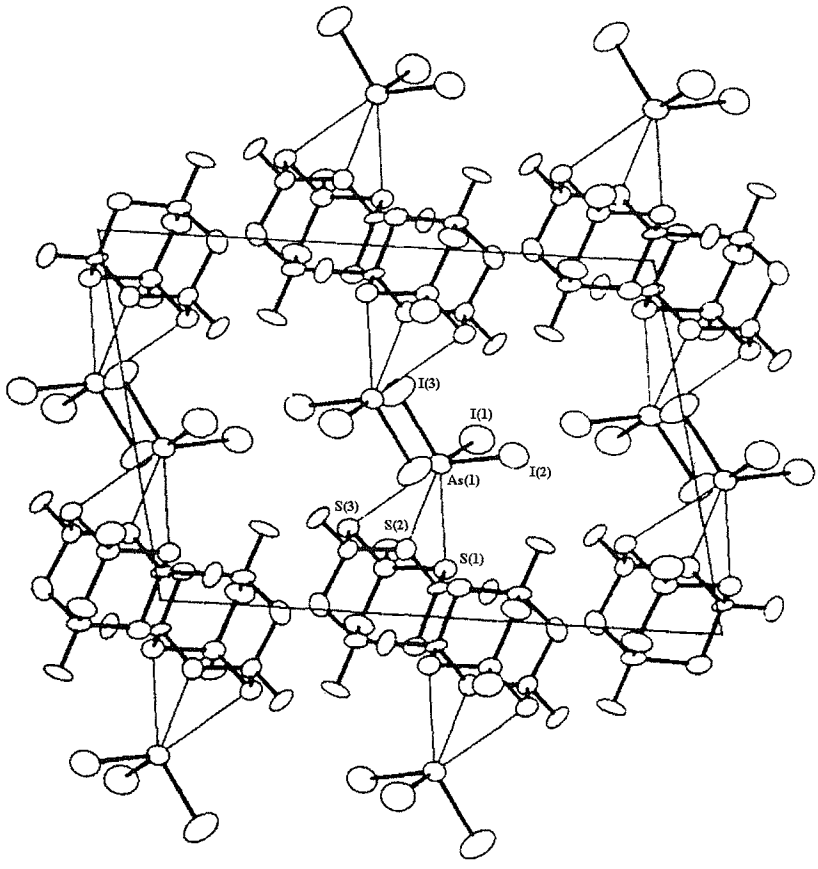

Figure 4.6 Packing diagram for the $[AsI_3(hta)]$ complex.[15]

4.2 Results and Discussion

4.2.1 Arsenic(III) Halide – Thioether Complexes

The reaction of AsX_3 (X = Cl, Br or I) in an anhydrous CH_2Cl_2 (X = Cl, Br) or THF (X = I) solutions with one molar equivalent of L (L = $MeS(CH_2)_2SMe$, [9]aneS_3, [12]aneS_4 or [14]aneS_4) in anhydrous CH_2Cl_2 solution produced, following work-up, an orange or yellow solid of general formula $[AsX_3(L)]$ in good yield. The solids were obtained by concentration of solvent *in vacuo* followed by filtration, washing with anhydrous CH_2Cl_2 and drying *in vacuo*. Attempts to obtain solid complexes from the reaction of AsX_3 with $MeS(CH_2)_3SMe$ and $MeC(CH_2SMe)_3$ produced only an intractable gum or oil. Due to the moisture sensitivity of the AsX_3 and $[AsX_3(L)]$ species, all reactions were carried out under an atmosphere of dry N_2 using standard Schlenk techniques, and the complexes were stored in a dry, nitrogen filled glove-box.

The complexes were sufficiently soluble in $CDCl_3$ and CD_2Cl_2 to allow NMR studies, however ^{1}H-NMR spectra showed resonances little shifted from those for the free ligand. Thus no structural information could be obtained from NMR spectroscopy. The infrared spectra of the chloro- and bromo-derivatives, obtained in nujol, show weak, broad features in the ranges 420-380 and 300-260 cm^{-1} which may be tentatively attributed to ν(As-X) modes for X = Cl and Br respectively.[16] Hence only very limited information on the arsenic coordination environment was forthcoming from NMR and IR spectroscopy. Crystalline adducts were obtained by slow evaporation of an anhydrous CH_2Cl_2 solution (THF for X = I) of the reactants (in a 1:1 ratio) in a N_2 purged glove box. This method yielded X-ray quality crystals for the complexes $[AsX_3\{MeS(CH_2)_2SMe\}]$ (X = Br and I), $[AsX_3([9]aneS_3)]$ (X = Cl and Br) and $[AsCl_3([14]aneS_4)]$. Satisfactory microanalytical data were obtained for all of the bulk solids and crystals except $[AsI_3\{MeS(CH_2)_2SMe\}]$, for which only a only a few deep red crystals were isolated, and thus characterisation of the bulk material was not possible.

The complexes $[AsBr_3\{MeS(CH_2)_2SMe\}]$ (Figure 4.7, Table 4.1) and $[AsI_3\{MeS(CH_2)_2SMe\}]$ (Table 4.2) both adopt an edge-shared, μ^2-dihalo, bioctahedral dimer structure with a dithioether ligand chelated to each arsenic(III) atom, and two *cis* terminal halides. The $MeS(CH_2)_2SMe$ ligand is in the *meso* conformation in each case. The discrete molecule is in the isomer A form observed by Norman and others for MX_3 complexes of tertiary phosphine and arsine ligands (M = As, Sb or Bi).[1] Such complexes were discussed in detail in Chapter 2.

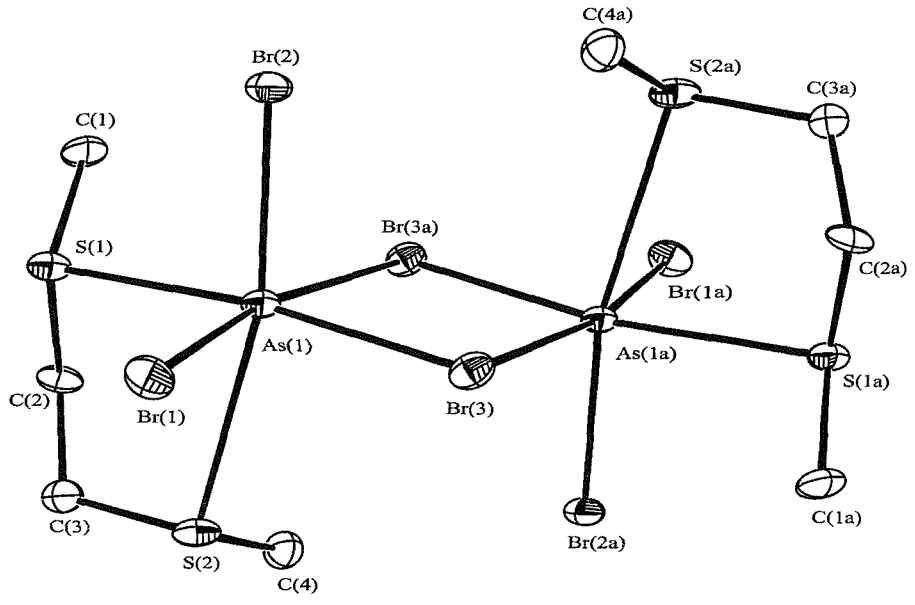

Figure 4.7 View of the $[AsBr_3\{MeS(CH_2)_2SMe\}]$ complex with numbering scheme adopted. Ellipsoids at 40 % probability, H-atoms omitted for clarity. Atoms marked (a) are related by the symmetry operation –x, -y, -z.

The As-S distances are unequal in each molecule, differing by *ca.* 0.1 Å in the iodo- (2.697(2) - 2.792(2) Å) and *ca.* 0.15 Å in the bromo-complex (2.725(3) - 2.876(3) Å). These values are quite similar to the 1,5-transannular interaction in the $[AsCl\{S(CH_2)_2S(CH_2)_2S\}]$ species (*ca.* 2.72 Å) (Figure 4.2),[10] and intermediate between those reported for the arsenic(III)-dithiocarbamate and xanthate complexes, where the two sulfur donors were asymmetrically bound through covalent (*ca.* 2.34 and 2.30 Å) and ionic interactions (*ca.* 2.90 and 2.97 Å).[11, 12] They are substantially shorter than the As-S distances in $[AsI_3(hta)]$ (3.274(1) – 3.310(1) Å) (Figure 4.6).[15] The range of As-X bond distances is noteworthy, with three $As\text{-}X_{terminal}$ bonds of similar length

(*ca.* 2.70 Å for X = I and *ca.* 2.46 Å for X = Br) and one substantially longer As-X_{bridge} interaction, rendering both As(μ-X)$_2$As bridging units highly asymmetric. Thus the asymmetry factor, Δ, (defined in Chapter 1) is 0.562 Å for the iodo-species (3.336(1) - 2.774(1) Å) and 0.708 Å for the bromo-analogue (3.258(1) - 2.550(1) Å). These values are suggestive of a stereochemically active arsenic(III)-based lone pair, probably localized along the vector of the bridging As(1) – X(3a) bond in both examples. In addition, the bridge asymmetry indicates that the dimer motif arises from weak association of square-pyramidal [AsX_3{$MeS(CH_2)_2SMe$}] molecules.

As(1)	Br(1)	2.391(1)	As(1)	Br(3a)	3.258(1)
As(1)	Br(2)	2.453(1)	As(1)	S(1)	2.725(3)
As(1)	Br(3)	2.550(1)	As(1)	S(2)	2.876(3)
Br(1)	As(1) Br(2)	95.21(5)	Br(2)	As(1) S(2)	166.90(7)
Br(1)	As(1) Br(3)	93.48(6)	Br(3)	As(1) Br(3a)	81.00(4)
Br(1)	As(1) Br(3a)	170.59(5)	Br(3)	As(1) S(1)	88.79(8)
Br(1)	As(1) S(1)	87.97(7)	Br(3)	As(1) S(2)	171.38(7)
Br(1)	As(1) S(2)	81.39(6)	S(1)	As(1) S(2)	78.05(8)
Br(2)	As(1) Br(3)	99.09(5)	S(1)	As(1) Br(3a)	93.19(4)
Br(2)	As(1) Br(3a)	93.19(4)	S(2)	As(1) Br(3a)	91.32(6)
Br(2)	As(1) S(1)	89.22(6)	As(1)	Br(3) As(1a)	99.00(4)

Table 4.1 Selected bond distances (Å) and angles (°) with e.s.d.'s for the [$AsBr_3${$MeS(CH_2)_2SMe$}] complex.

The adoption of an isomer A-type dimer arrangement for these adducts contrasts sharply with the structural motifs of the analogous $[SbCl_3\{MeS(CH_2)_2SMe\}]$ and $[BiCl_3\{MeS(CH_2)_2SMe\}_2]$ complexes.[2, 3] The former species exists as a three-dimensional coordination network containing dithioether ligands in an unusual mixed terminal/bridged mode, and was discussed in detail in Chapter 3 (Figures 3.12 and 3.13). The bismuth(III) adduct is monomeric, with chelation of two dithioether ligands enforcing a seven-coordinate pentagonal bipyramidal geometry.[3] This difference is likely to be due to steric factors, with the larger bismuth(III) atom able to accommodate seven-coordination, although the reasons why the AsX_3 complexes differ from the $SbCl_3$ adduct are less clear. In both cases, however, the observed *cis* arrangement of the ligands suggests that M-L bonding is primarily through the M-X σ^* orbitals.

As(1)	I(1)	2.727(1)	As(1)	I(3a)	3.336(1)
As(1)	I(2)	2.620(3)	As(1)	S(1)	2.696(2)
As(1)	I(3)	2.774(1)	As(1)	S(2)	2.792(2)

I(1)	As(1)	I(2)	95.93(3)	I(2)	As(1)	S(2)	90.35(5)
I(1)	As(1)	I(3)	99.40(9)	I(3)	As(1)	I(3a)	86.31(3)
I(1)	As(1)	I(3a)	99.22(3)	I(3)	As(1)	S(1)	172.54(6)
I(1)	As(1)	S(1)	88.00(5)	I(3)	As(1)	S(2)	91.62(5)
I(1)	As(1)	S(2)	166.69(6)	S(1)	As(1)	S(2)	80.91(7)
I(2)	As(1)	I(3)	95.59(3)	S(1)	As(1)	I(3a)	91.61(4)
I(2)	As(1)	I(3a)	164.21(4)	S(2)	As(1)	I(3a)	73.91(5)
I(2)	As(1)	S(1)	84.48(5)	As(1)	I(3)	As(1a)	93.69(4)

Table 4.2 Selected bond distances (Å) and angles (°) with e.s.d.'s for the $[AsI_3\{MeS(CH_2)_2SMe\}]$ complex.

$[AsCl_3([9]aneS_3)]$ also exists as a discrete molecule (Figure 4.7, Table 4.3). The tridentate thiacrown caps the face of the As(III) atom, with three mutually *fac* chlorine atoms completing the donor set to establish a distorted octahedral geometry. The As-S bond distances are in the range 2.715(3) - 2.857(2) Å, similar to those observed in the $[AsX_3\{MeS(CH_2)_2SMe\}]$ series and indicative of secondary As---S interactions, while the As-Cl distances are much shorter (2.304(2) - 2.361(2) Å) despite the similar covalent radii of S and Cl. The weakness of the As-S interactions is manifest in the compressed S-As-S bond angles (76.66(6) – 77.62(7)°). Comparison of the As-S bond lengths in $[AsCl_3([9]aneS_3)]$ to the As-O distance in the $[AsCl_3(12\text{-crown-4})]$ complex shows the thiacrown to be more strongly bound (2.715(3) – 2.857(2) vs. 2.776(6) – 2.915(6) Å respectively). This is quite surprising given that As-O interactions would be favoured over and As-S in terms of the HSAB model. The steric constraints imposed by the ligand coupled with the low Lewis acidity of the $AsCl_3$ fragment probably prevent formation of a dimeric or oligomeric structure.

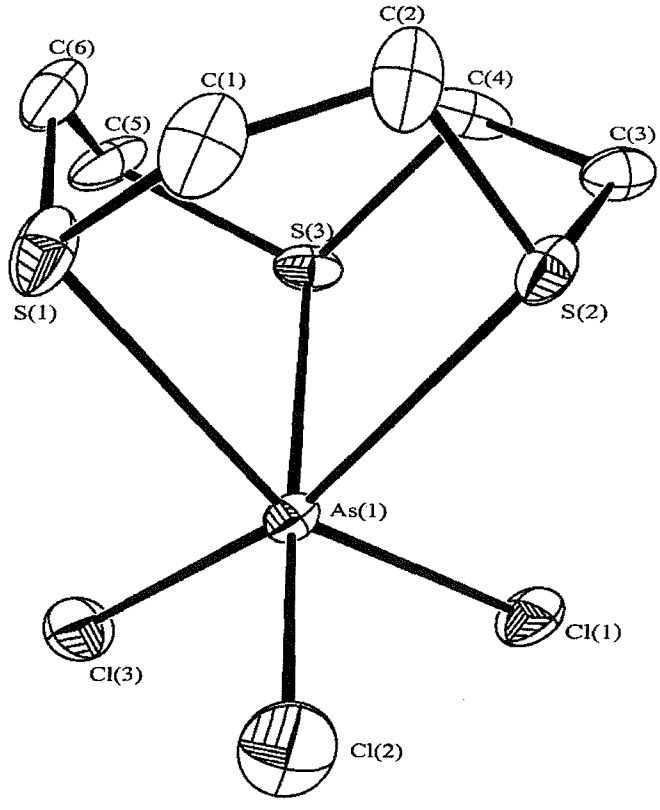

Figure 4.7 View of the $[AsCl_3([9]aneS_3)]$ complex with the numbering scheme adopted. Ellipsoids shown at 40 % probability, H-atoms omitted for clarity.

As(1)	Cl(1)	2.304(2)	As(1)	S(1)	2.857(3)
As(1)	Cl(2)	2.339(3)	As(1)	S(2)	2.776(2)
As(1)	Cl(3)	2.365(1)	As(1)	S(3)	2.715(3)
Cl(1)	As(1) Cl(2)	97.26(9)	Cl(2)	As(1) S(3)	173.7(1)
Cl(1)	As(1) Cl(3)	97.17(8)	Cl(3)	As(1) S(1)	94.66(7)
Cl(1)	As(1) S(1)	157.85(8)	Cl(3)	As(1) S(2)	161.62(8)
Cl(1)	As(1) S(2)	86.19(6)	Cl(3)	As(1) S(3)	85.64(7)
Cl(1)	As(1) S(3)	84.67(7)	S(1)	As(1) S(2)	76.92(6)
Cl(2)	As(1) Cl(3)	100.0(1)	S(1)	As(1) S(3)	77.62(7)
Cl(2)	As(1) S(1)	99.03(9)	S(2)	As(1) S(3)	76.66(6)
Cl(2)	As(1) S(1)	97.44(9)			

Table 4.3 Selected bond distances (Å) and angles (°) with e.s.d.'s for $[AsCl_3([9]aneS_3)]$.

Weakly diffracting crystals of $[AsBr_3([9]aneS_3)]$ were also obtained, with the data indicating that this species also adopts a discrete face-capped arrangement. However, despite a number of attempts using different crystal samples, the data sets were not of sufficient quality to warrant comparison of the bond lengths and angles about the arsenic(III) atom. Microanalytical data consistent with 1:1 As:[9]aneS$_3$ stoichiometry were obtained for the bulk $[AsX_3([9]aneS_3)]$ adducts.

At this point it is appropriate to compare the structure of $[AsCl_3([9]aneS_3)]$ to those observed for the $[SbX_3([9]aneS_3)]$ adducts (X = Cl and I). In the solid state the $[SbCl_3([9]aneS_3)]$ adduct exhibits an infinite chain structure, with each $SbCl_3$ unit bound *endo* to three sulfur donors of one thia-crown and, additionally, to a bridging sulfur atom from an adjacent ligand, *viz*, seven-coordinate antimony(III) (Chapter 3, Figure 3.1a).[17] The antimony-sulfur interactions are weak, in the range 3.156(3) - 3.460(3) Å. The $[SbI_3([9]aneS_3)]$ adduct, in contrast, adopts a very similar structure to

$[AsCl_3([9]aneS_3)]$.[18] The donor set comprises three sulfur and three iodine atoms arranged in a distorted octahedral fashion, with antimony-sulfur distances much shorter than in the corresponding chloro-adduct (2.840(2) – 2.895(2) Å). The difference in the average Sb-S and As-S distances in the six-coordinate systems is *ca.* 0.08 Å. This value is less than the difference between the covalent radii of Sb(III) and As(III) (*ca.* 0.20 Å), and highlights the poorer acceptor properties of $AsCl_3$ compared to SbI_3.

Thus far, all of the structurally characterised chalcogenoether adducts of AsX_3 have existed as discrete molecular species. The $[AsCl_3([14]aneS_4)]$ complex is the first such system to display an extended coordination network in the solid-state (Figures 4.8 and 4.9, Table 4.4). The most obvious difference in the coordination profile of the $AsCl_3$ unit in this adduct with respect to other structurally characterised $[AsX_3(L_C)]$ complexes (L_C = oxa- or thia-crown macrocycle) is the exodentate coordination of the macrocycle. This is likely to be influenced by the conformation of the free macrocycle, in which the sulfur-based lone pairs are arranged pointing out of the ring.[19] Indeed a similar binding mode is observed in the $[(SbBr_3)_2([14]aneS_4)]$ complex (Chapter 3, Figure 3.17), leading to an infinite two-dimensional array. Noteworthy is the fact that reaction of excess $AsCl_3$ with $[14]aneS_4$ yielded only the 1:1 complex, whereas the 2:1 $[(SbBr_3)_2([14]aneS_4)]$ adduct was obtained under all the reactions conditions employed, with no evidence for the formation of a 1:1 $[SbBr_3([14]aneS_4)]$ species.

The structure shows some unusual features. The potentially tetradentate thia-crown binds to separate arsenic atoms through only two of the four sulfur atoms, leaving two sulfurs uncoordinated. The arsenic donor set consists of two mutually *cis* sulfur atoms, two terminal chlorines and two μ^2-bridging chlorine atoms, leading to a distorted octahedral geometry. This distortion is particularly evident in the triangular face defined by S(1), Cl(1a) and S(2a) (e.g. Cl(3) As(1) Cl(1a) 162.74(3) °, S(2a) As(1) Cl(1a) 73.55 °, S(1) As(1) S(2a) 77.10 °) and may indicate that the arsenic-based lone pair is localised in this region.

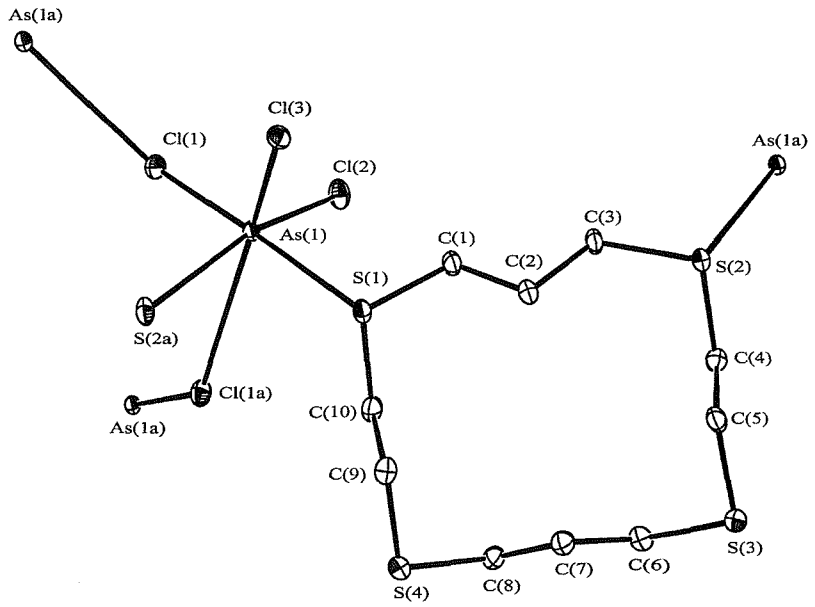

Figure 4.8 View of the asymmetric unit of $[AsCl_3([14]aneS_4)]$ with nearest symmetry related neighbours with the numbering scheme adopted. Ellipsoids at 40 % probability, H-atoms omitted for clarity.

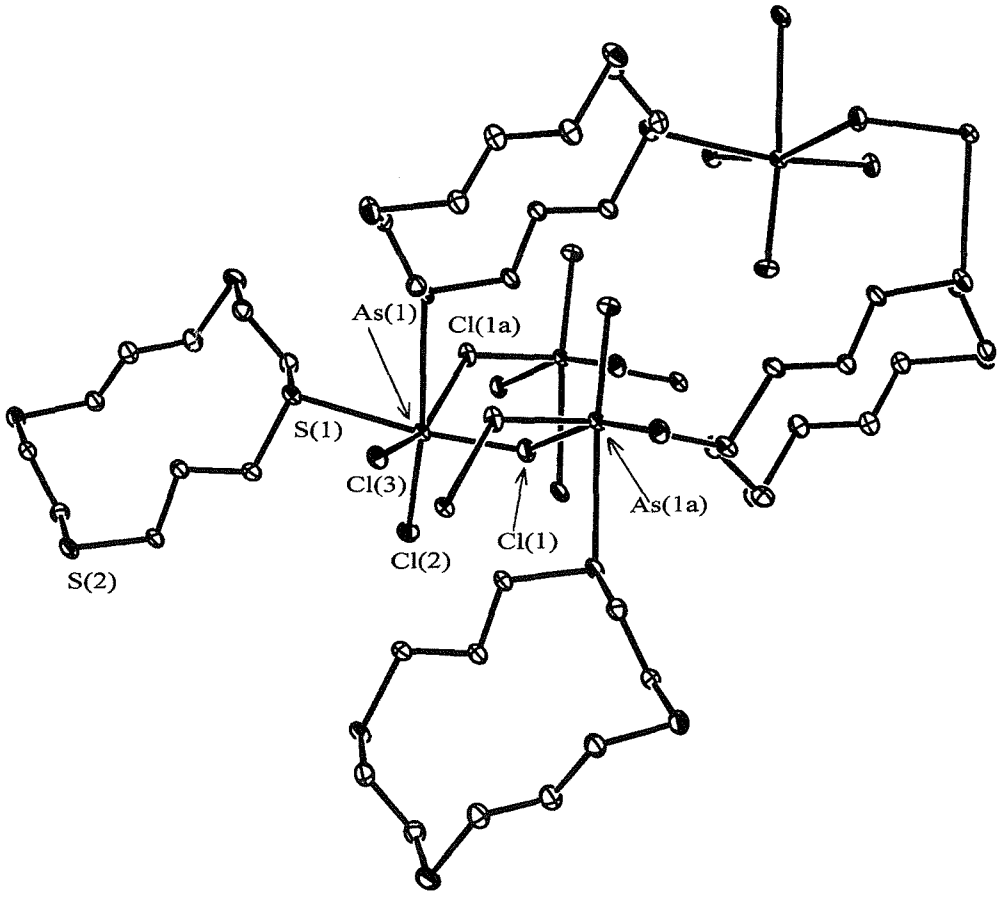

Figure 4.9 View of a portion of the extended lattice of $[AsCl_3([14]aneS_4)]$.

As(1)	Cl(1)	2.2937(8)	As(1)	Cl(3)	2.1889(8)
As(1)	Cl(a)	3.3731(8)	As(1)	S(1)	2.8709(9)
As(1)	Cl(2)	2.2821(9)	As(1)	S(2a)	2.9655(6)
Cl(1)	As(1) Cl(1a)	93.76(2)	Cl(2)	As(1) S(2a)	169.01(3)
Cl(1)	As(1) Cl(2)	94.90(3)	Cl(3)	As(1) Cl(1a)	162.74(3)
Cl(1)	As(1) Cl(3)	94.15(3)	Cl(3)	As(1) S(1)	80.10(3)
Cl(1)	As(1) S(1)	169.50(3)	Cl(3)	As(1) S(2a)	90.58(3)
Cl(1)	As(1) S(2a)	94.29(3)	S(1)	As(1) Cl(1a)	89.58(2)
Cl(2)	As(1) Cl(1a)	99.82(3)	S(1)	As(1) S(2a)	77.10(2)
Cl(2)	As(1) Cl(3)	94.75(3)	S(2a)	As(1) Cl(1a)	73.55(2)
Cl(2)	As(1) S(1)	94.33(3)	As(1)	Cl(1) As(1a)	127.77(3)

Table 4.4 Selected bond distances (Å) and angles (°) with e.s.d's for $[AsCl_3([14]aneS_4)]$.

The sulfur atoms are bound *trans* to As-Cl bonds, indicating that the As-Cl σ^* orbitals function as acceptors. The donor set is similar to that described for the $[AsX_3\{MeS(CH_2)_2SMe\}]$ species (Figure 4.7), however in the present complex the bridging chlorines link to two different arsenic(III) atoms giving rise to an infinite sheet network rather than a discrete dimeric molecule. The bridging thiacrowns span two separate arsenic(III) centres. The As-S bond distances (2.8709(9) – 2.9655(9) Å) are longer than those observed in the $[AsCl_3([9]aneS_3)]$ and $[AsX_3\{MeS(CH_2)_2SMe\}]$ adducts and similar to As-S interactions in thiocarbamate and xanthate AsX_3 complexes (2.904(4) and 2.978(2) Å respectively).[11,12]

4.2.2 Arsenic(III) Halide- Selenoether Complexes

The reaction of AsX_3 (X = Cl, Br or I) with one molar equivalent of L (L = [8]aneS_2, [16]aneSe_4 or [24]aneSe_6) in anhydrous CH_2Cl_2 (or THF for X = I) produced, following work-up, an orange or yellow solid of general formula $[AsX_3(L)]$ in good yield (except for L = [16]aneSe_4 where only a 2:1 ratio and L = [24]aneSe_6 where both 4:1 and 2:1 As:L ratios were obtained for X = Cl and X = Br respectively). Similar attempts to isolate complexes with $MeSe(CH_2)_nSeMe$ (n =2 or 3) and $MeC(CH_2SeMe)_3$ yielded either an oil or intractable gum. The solids were isolated and stored as for the thioether complexes described previously. ^{1}H-NMR spectra again showed signals little shifted from those of the free ligands, and the $^{77}Se\{^1H\}$-NMR spectrum of the $[(AsCl_3)_4([24]aneSe_6)]$ complex revealed a single resonance at δ 153 ppm, identical to that for free [24]aneSe_6.[20] Several broad features around 310 – 380 cm^{-1} were observed in the IR spectrum, assigned to ν(As-Cl).[15] In view of the absence of any reported structural data for arsenic complexes of selenium ligands and to allow comparisons with the thioether adducts described earlier, single crystal X-ray analyses were undertaken on several complexes. Single crystals were obtained by slow evaporation of an anhydrous CH_2Cl_2 solution of the reactants (in a 1:1 ratio) in a N_2 purged glove box. This method produced suitable quality crystals of the $[AsCl_3([8]aneSe_2)]$, $[(AsX_3)_2([16]aneSe_4)]$ (X = Cl and Br) and $[(AsCl_3)_4([24]aneSe_6)]$ complexes.

The $[AsCl_3([8]aneSe_2)]$ complex adopts an infinite one-dimensional ladder motif, consisting of near-planar As_2Cl_6 rungs linked by bridging [8]aneSe_2 molecules (Figure 4.10, Table 4.5). The Se-donor ligands are bound to the As_2Cl_6 units in a mutually *trans* fashion (2.816(7) – 2.752(5) Å) and thus act as the uprights of the ladder. This is an unusual arrangement for an AsX_3-chalcogenoether adduct, since thus far all structurally characterised species in this work have displayed mutually *cis* chalcogen coordination and retention of the pyramidal MX_3 unit (although similar structural features were observed in the $[BiCl_3([8]aneSe_2)]$ and $[BiBr_3([16]aneSe_4)]$ adducts).[3] The geometry about the arsenic(III) atom is only slightly distorted from octahedral, indicating minimal stereochemical activity of the arsenic(III) lone pair (Table 4.5).

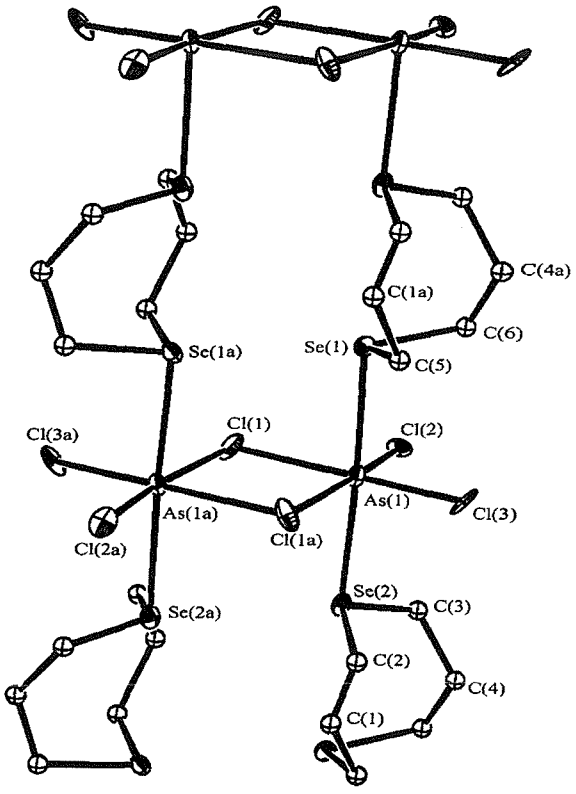

Figure 4.10 View of a portion of the $[AsCl_3([8]aneSe_2)]$ complex with numbering scheme adopted. Ellipsoids shown at 40 % probability, H-atoms omitted for clarity. Atoms marked (a) are related by the symmetry operation -x, -y, -z.

The terminal As-Cl bonds are *ca.* 0.5 Å shorter than the bridging As-Cl bonds (2.257(7) - 2.282(7) *vs.* 2.757(7) – 2.799(7) Å respectively). Of note is the symmetrical nature of the bonding within the bridging As_2Cl_2 unit (Δ = 0.042 Å), contrasting with the highly asymmetric environment in the $[AsX_3\{MeS(CH_2)_2SMe\}]$ complexes discussed previously (Δ = 0.708 and 0.562 Å for X = Br or I respectively). A highly symmetric Bi_2X_2 bridge unit was also observed in the $[BiCl_3([8]aneSe_2)]$ and $[BiBr_3([16]aneSe_4)]$ adducts.

In all of the structurally characterised AsX_3 adducts discussed so far, the chalcogen-donor atoms are bound to As(III) in a mutually *cis* manner, and those complexes containing μ^2-halide bridges enforce an asymmetric coordination environment upon the As(III) atom (Δ = *ca.* 0.75 Å on average). The present complex is an exception to this general trend, with the $[8]aneSe_2$ ligands bound mutually *trans* and a planar As_2Cl_6 bridge unit. Evidently the As-Cl σ^* orbitals are not involved in As-

Se bonding *in the crystalline adduct* (otherwise a *trans* Se-As-Cl geometry would be observed), however it is very unlikely that a different type of acceptor orbital functions in complexes of this particular ligand (especially since the $[BiBr_3([16]aneSe_4)]$ adduct displays a similar structure). Although ligand architecture could be held solely responsible for enforcing the observed *trans* Se-As-Se configuration, it seems more likely that this factor works in concert with a rearrangement and/or inversion mechanism about the $AsCl_3$ unit. Indeed, the planar As_2Cl_6 unit may an example of a trapped transition state of such a mechanism and, given different reaction conditions, this adduct may be a candidate for the observation of coordination isomerism (as yet unrealised in this class of complexes).

As(1)	Cl(1)	2.757(8)	As(1)	Cl(3)	2.282(8)
As(1)	Cl(a)	2.799(8)	As(1)	Se(1)	2.752(9)
As(1)	Cl(2)	2.257(9)	As(1)	Se(2)	2.816(6)
Cl(1)	As(1) Cl(1a)	87.85(2)	Cl(2)	As(1) Se(2)	88.29(3)
Cl(1)	As(1) Cl(2)	87.06(3)	Cl(3)	As(1) Cl(1)	179.56(3)
Cl(1)	As(1) Cl(3)	179.56(3)	Cl(3)	As(1) Cl(1a)	92.50(4)
Cl(1)	As(1) Se(1)	88.12(3)	Cl(3)	As(1) Se(1)	92.14(3)
Cl(1)	As(1) Se(2)	89.05(3)	Cl(3)	As(1) Se(2)	90.70(4)
Cl(2)	As(1) Cl(1a)	174.76(3)	Se(1)	As(1) Se(2)	177.08(2)
Cl(2)	As(1) Cl(3)	92.59(3)	Se(2)	As(1) Cl(1a)	90.40(2)
Cl(2)	As(1) Se(1)	92.27(3)	As(1)	Cl(1) As(1a)	92.14(3)

Table 4.5 Selected bond distances (Å) and angles (°) with e.s.d.s for $[AsCl_3([8]aneSe_2)]$.

Given that the barrier to pyramidal inversion increases down group 15, however, the activation energy for inversion through the planar transition state would be rather large. Alternatively, the increasingly poor mixing of s- and p-orbitals as the group is descended could be held responsible and so M-Se bonding through a pure p-orbital (as described by the simple Rundle-Pimental scheme described in Chapter 1) would satisfy the observed *trans* arrangement. Poor sp-hybridisation is certainly a factor for BiX_3, where relativistic effects stabilise the 6s-orbital. However, it is more likely that a combination of all of these aspects, rather than a single factor, is responsible for the anomalous *trans* Se-M-Se arrangement in these adducts. In the absence of the analogous SbX_3 structure, it is difficult to gauge the relative extent to which ligand architecture, inversion barriers and sp-mixing contribute to the adoption of this geometry. In this regard, it is worth highlighting again that both the $[BiBr_3([8]aneSe_2)]$ and $[BiBr_3([16]aneSe_4)]$ adducts adopt the *trans* Se-Bi-Se arrangement, whereas the Se-Sb-Se configuration is *cis* in $[(SbBr_3)_2([16]aneSe_4)]$.

In contrast to the one-dimensional $[AsCl_3([8]aneSe_2)]$ polymer, the structures of the tetraselenoether macrocyclic complexes $[(AsCl_3)_2([16]aneSe_4)]$ and $[(AsBr_3)_2([16]aneSe_4)]$ extend in all three dimensions. These species exhibit very similar structures, the repeat unit consisting of weakly associated, asymmetric dinuclear μ^2-dihalo As_2X_6 edge-shared bioctahedra, with the As(III) atoms further coordinated to two Se-donors from separate, mutually *cis* macrocycle units to give a distorted octahedral geometry. The repeat unit and lattice structures of the chloro-adduct are shown in Figures 4.11 and 4.12, and bond data for both complexes is given in Tables 4.6 and 4.7. The As-Se bond distances in these two compounds (2.922(1) – 3.163(2) and 2.8876(9) – 3.0854(9) Å for X = Cl and Br respectively) are only *ca* 0.1 Å shorter than the Sb-Se distances in the closely related $[(SbBr)_2([16]aneSe_4)]$ (2.989(1) – 3.193(1) Å).[2a] This is less than the difference in the covalent radii of As(III) vs Sb(III) (1.20 *vs.* 1.41 Å),[21] reflecting the poorer acceptor properties of the former.

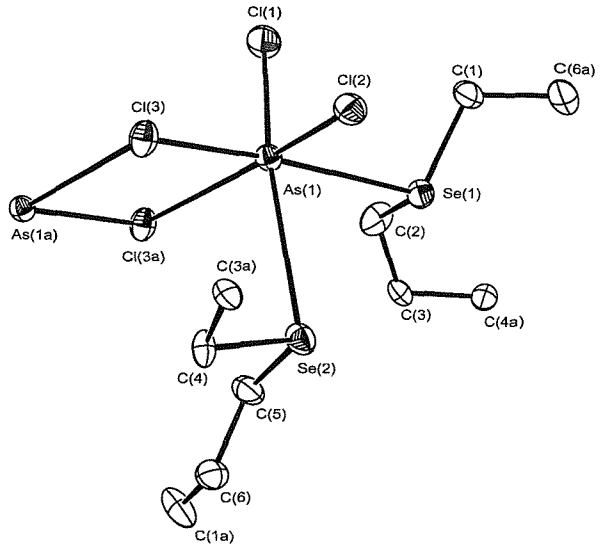

Figure 4.11 View of the asymmetric unit $[(AsCl_3)_2([16]aneSe_4)]$ with nearest symmetry related neighbours and the numbering scheme adopted. Ellipsoids shown at 40 % probablilty, H-atoms omitted for clarity. Atoms marked (a) are related by the symmetry operation -x, -y, -z.

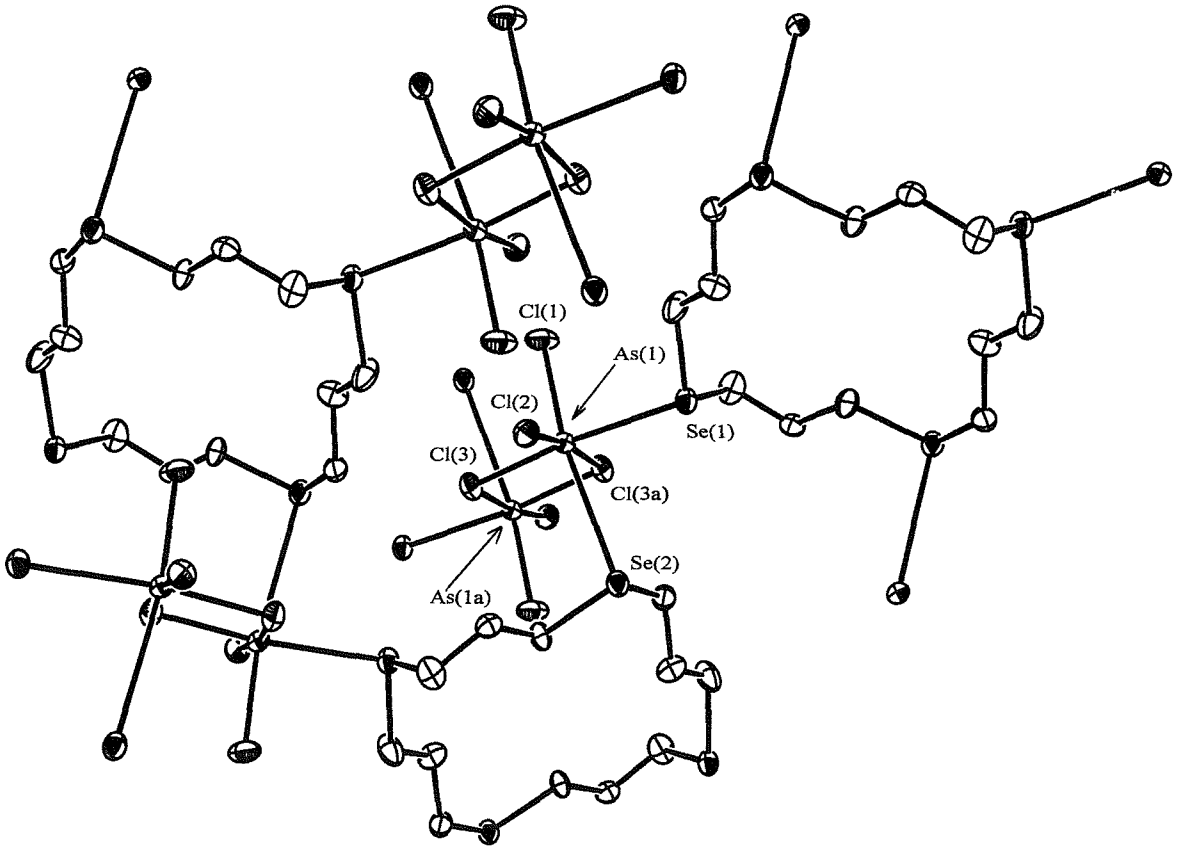

Figure 4.12 View of a portion of the lattice of $[(AsCl_3)_2([16]aneSe_4)]$.

As(1)	Cl(1)	2.243(3)	As(1)	Cl(3a)	3.294(3)
As(1)	Cl(2)	2.196(3)	As(1)	Se(1)	2.922(1)
As(1)	Cl(3)	2.314(3)	As(1)	Se(2)	3.163(2)
Cl(1)	As(1) Cl(2)	94.6(1)	Cl(2)	As(1) Se(2)	86.08(6)
Cl(1)	As(1) Cl(3)	95.1(1)	Cl(3)	As(1) Cl(3a)	79.7(1)
Cl(1)	As(1) Cl(3a)	88.0(1)	Cl(3)	As(1) Se(1)	172.67(9)
Cl(1)	As(1) Se(1)	91.51(9)	Cl(3)	As(1) Se(2)	93.78(8)
Cl(1)	As(1) Se(2)	86.08(9)	Cl(3a)	As(1) Se(1)	103.72(6)
Cl(2)	As(1) Cl(3)	93.3(1)	Cl(3a)	As(1) Se(2)	92.43(6)
Cl(2)	As(1) Cl(3a)	172.7(1)	Se(1)	As(1) Se(2)	79.67(4)
Cl(2)	As(1) Se(1)	83.08(8)	As(1)	Cl(3) As(1a)	100.3(1)

Table 4.6 Selected bond distances (Å) and angles (°) with e.s.d.'s for $[(AsCl_3)_2([16]aneSe_4)]$.

Each ligand contributes one selenium donor per arsenic atom, bridging four separate arsenic centres in total (hence an overall 2:1 As:L stoichiometry) and giving rise to an extended, three-dimensional polymeric motif. The As-X bond distances within each As_2X_6 dinuclear core are very asymmetric (Δ = 0.980 and 0.758 Å for X = Cl and Br respectively) suggesting some degree of stereochemical activity of the arsenic-based lone pair along the long X(3)-As(1) – X(3a) axis.

The series of related complexes $[(AsBr_3)_2([16]aneSe_4)]$, $[(SbBr_3)_2([16]aneSe_4)]$ and $[BiBr_3([16]aneSe_4)]$ have now all been crystallographically characterised, and it is useful to draw some comparisons and distinctions between them. Of immediate note is the structural similarity between the $[(AsBr_3)_2([16]aneSe_4)]$ and $[(SbBr_3)_2([16]aneSe_4)]$ adducts, with both displaying a 2:1 M:L ratio and weak M-Se coordination through two mutually *cis* Se-donors from separate ligands, and existing as extended networks (in

fact these two species occupy the same space group, $P2_1/n$, and have very similar unit cell dimensions). However, whereas the $[(SbBr_3)_2([16]aneSe_4)]$ complex adopts a two-dimensional sheet array with a square pyramidal Br_3Se_2 donor set about each antimony(III) atom, the arsenic(III) analogue is a three-dimensional network due to As_2Br_6 dimeric bioctahedral units cross-linking each sheet. Although the selenacrown behaves as an exodenate ligand in all three examples, the coordination mode differs in $[BiBr_3([16]aneSe_4)]$ in that only two of the four Se-donors per crown are used, the structure being very similar to the $[AsCl_3([8]aneSe_2)]$ and $[BiCl_3([8]aneSe_2)]$ complexes.

As(1)	Br(1)	2.4452(9)	As(1)	Br(3a)	3.279(1)
As(1)	Br(2)	2.3691(9)	As(1)	Se(1)	2.8876(9)
As(1)	Br(3)	2.5209(9)	As(1)	Se(2)	3.085(9)
Br(1)	As(1) Br(2)	95.69(3)	Br(2)	As(1) Se(2)	84.30(3)
Br(1)	As(1) Br(3)	94.49(3)	Br(3)	As(1) Br(3a)	82.52(3)
Br(1)	As(1) Br(3a)	88.17(3)	Br(3)	As(1) Se(1)	173.02(4)
Br(1)	As(1) Se(1)	91.43(3)	Br(3)	As(1) Se(2)	93.76(3)
Br(1)	As(1) Se(2)	171.72(9)	Br(3a)	As(1) Se(1)	101.38(2)
Br(2)	As(1) Br(3)	93.71(3)	Br(3a)	As(1) Se(2)	92.37(2)
Br(2)	As(1) Br(3a)	174.82(3)	Se(1)	As(1) Se(2)	80.37(4)
Br(2)	As(1) Se(1)	82.01(3)	As(1)	Br(3) As(1a)	97.48(3)

Table 4.7 Selected bond distances (Å) and angles (°) with e.s.d.'s for $[(AsBr_3)_2([16]aneSe_4)]$.

In contrast to the $[AsCl_3([8]aneSe_2)]$ and $[(AsX_3)_2([16]aneSe_4)]$ complexes, the $[(AsCl_3)_4([24]aneSe_6)]$ adduct forms as a discrete molecule (Figure 4.13, Table 4.8). The 4:1 As:L stoichiometry arises from monodentate attachment of the ligand to two distinct, exodentate $AsCl_3$ units and bidentate, endodentate chelation to two separate $AsCl_3$ fragments sequestered within the macrocyclic cavity. The latter are linked *via* μ^2-chloro bridges to form an As_2Cl_6 dimer within the ring which, with the selenium atoms bound in a mutually *cis* manner, adopts an edge-shared bioctahedral, isomer A motif. This molecule is the first structurally characterised example of a discrete macrocyclic complex displaying both exo and endo coordination modes. The inclusion of a dinuclear M_2X_6 unit within the macrocylic cavity is also novel.

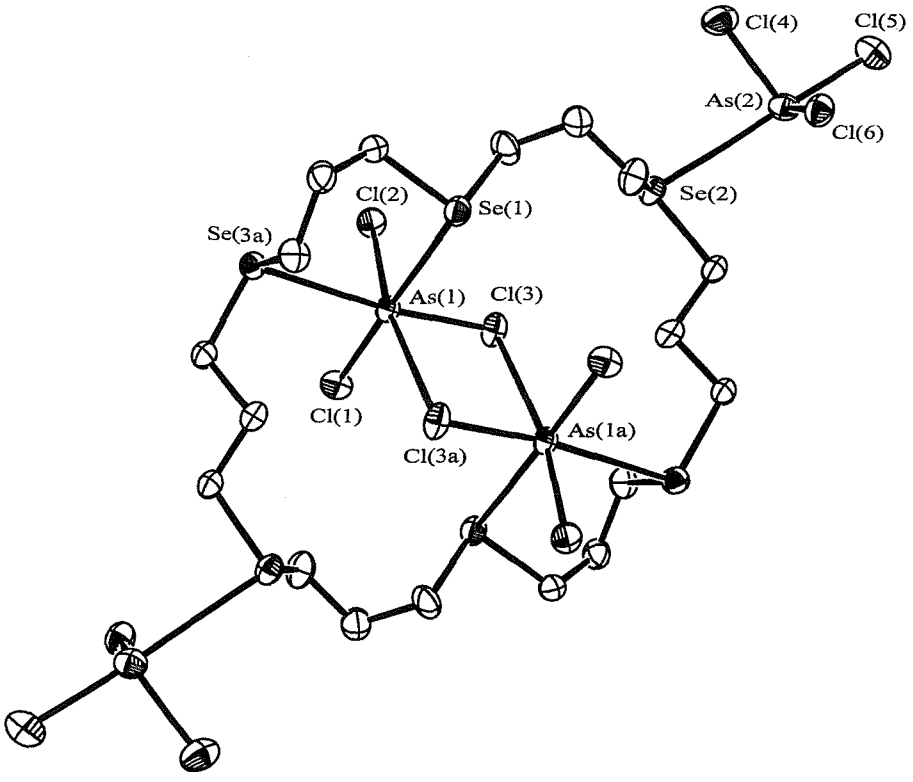

Figure 4.13 View of the $[(AsCl_3)_4([24]aneSe_6)]$ complex with numbering scheme adopted. Ellipsoids at 40 % probability, H-atoms omitted for clarity. Atoms marked (a) are related by the symmetry operation -x, -y, -z.

As(1) Cl(1)	2.292(2)	As(1) Se(3a)	3.0057(14)
As(1) Cl(2)	2.2100(18)	As(2) Cl(4)	2.194(2)
As(1) Cl(3)	2.2862(19)	As(2) Cl(5)	2.250(2)
As(1) Cl(3a)	3.2814(21)	As(2) Cl(6)	2.197(2)
As(1) Se(1)	2.9947(13)	As(2) Se(2)	3.0906(15)
Cl(1) As(1) Cl(2)	95.99(7)	Cl(3) As(1) Se(1)	87.00(6)
Cl(1) As(1) Cl(3)	94.26(7)	Cl(3) As(1) Se(3a)	172.26(6)
Cl(1) As(1) Cl(3a)	96.39(6)	Se(1) As(1) Se(3a)	85.40(4)
Cl(1) As(1) Se(1)	175.52(5)	Cl(4) As(2) Cl(5)	95.35(9)
Cl(1) As(1) Se(3a)	94.43(6)	Cl(4) As(2) Cl(6)	96.95(8)
Cl(2) As(1) Cl(3)	94.03(7)	Cl(4) As(2) Se(2)	86.85(7)
Cl(2) As(1) Cl(3a)	167.45(3)	Cl(5) As(2) Se(2)	175.39(6)
Cl(2) As(1) Se(1)	88.20(6)	Cl(5) As(2) Cl(6)	96.59(8)
Cl(2) As(1) Se(3a)	84.28(6)	Cl(6) As(2) Se(2)	87.15(6)
Cl(3) As(1) Cl(3a)	82.82(4)	As(1) Cl(3) As(1a)	97.18(5)

Table 4.8 Selected bond distances (Å) and angles (°) with e.s.d.'s for $[(AsCl_3)_4([24]aneSe_6)]$.

The exo $AsCl_3$ units adopt a pseudo-trigonal bipyramidal geometry, the donor set consisting of three terminal chloro-ligands (2.250(2) – 2.194(2) Å) and a selenium atom from the selena-crown (3.0906(15) Å), with the arsenic-based lone pair assumed to occupy the remaining equatorial position. Within the cavity, the As-Se distances are similar to those in the *exo* moiety, (3.0057(14) – 2.9947(13) Å), as are the As-$Cl_{terminal}$ bonds (2.292(2) – 2.2100(18) Å). The As-Cl_{bridge} distances are extremely asymmetric (3.2814(21) – 2.2862(19), Δ = 0.9952 Å), indicating very weak, intramolecular

association of the two $AsCl_3$ units, as observed in the previously discussed $[AsX_3\{MeS(CH_2)_2SMe\}]$ species (although the association is much weaker in the present complex). Nevertheless, this weak interaction should be viewed as genuine, given that the formal sum of the van der Waals radii for As and Cl is 3.60 Å;[22] the geometrical constraints imposed by the macrocycle may facilitate the formation of the dimer. There is no clear evidence of a stereochemically active lone-pair operating on the endodentate As_2Cl_6 unit, with the bond angles not significantly distorted from regular octahedral.

The structural characterisation of this complex is significant, since it not only provides another example of an MX_3-selenoether complex but is also only the second X-ray structure containing the [24]aneSe_6 ligand. The only previously crystallographically characterised example, the $[(PdCl)_2([24]aneSe_6)][BF_4]_2$ species, was described by Pinto and co-workers and shows a square planar Se_3Cl donor set at the Pd(II) atoms with no association of the $PdClSe_3$ units.[23]

In an attempt to gauge the Lewis acidity of PX_3 (X = Cl or Br) toward chalcogenoethers, the reactions of these compounds with L (L = Me_2S, $MeE(CH_2)_2EMe$ (E = S or Se) and [9]aneS_3) were carried out. Addition of a rigorously anhydrous CH_2Cl_2 solution of L to an equimolar solution of PX_3 gave no visible reaction. $^{31}P\{^1H\}$-NMR spectra of these samples showed no evidence of any interaction, the resonances being unshifted from free PX_3 even at low temperatures (δ = 220 and 227 ppm for X = Cl and Br respectively). This illustrates the very poor acceptor properties of PX_3 in comparison to the heavier group 15 congeners.

4.3 Conclusions

This work has produced the first examples of AsX_3 functioning as a Lewis acid toward bidentate and macrocyclic thio- and seleno-ethers. A number of the complexes have been structurally characterised, thus allowing comparison to the analogous Sb(III) or Bi(III) adducts, although there are still very few such examples in the literature. The fact that single crystal X-ray diffraction is the only technique available to unambiguously characterise these complexes does not aid matters, since (obviously) only those combinations yielding suitable crystals can be discussed. It is also possible that coordination isomers may be generated under different reaction or crystallisation conditions. Thus it is difficult to draw strong conclusions regarding the reasons for the structural differences and similarities between these species. However, a major factor is undoubtedly the poorer acceptor properties of the AsX_3 fragment compared to either SbX_3 or BiX_3. The structures are assembled from primary As-X bonds and weaker, secondary As---X and/or As---S/Se interactions, with the As-X σ^* orbitals functioning as acceptors toward the halide or group 16 donor. In all but one of the structurally characterised adducts discussed herein the chalcogen-donor atoms are bound to As(III) in a mutually *cis* manner, and those complexes containing μ^2-halide bridges enforce an asymmetric coordination environment upon the As(III) atom (Δ = *ca.* 0.75 Å on average). The exception is the $[AsCl_3([8]aneSe_2)]$ system which, like its $BiBr_3$ analogue, finds the Se-donor ligands disposed *trans* to each other with a symmetrical As_2Cl_6 unit (Δ = 0.042 Å) (Figure 4.10, Table 4.5).

The highly asymmetric μ^2-halide bridges of a number of complexes (except $[AsCl_3([8]aneSe_2)]$) and weakly bound ligand donor atoms indicate that these orbitals behave as poor acceptors toward the chalcogen-donor atoms. Indeed the As-S bond distances are near to the covalent limit, being of similar length to interactions observed in a number of thiocarbamate and xanthate adducts.[11, 12] The stereochemical activity of the arsenic-based lone pair varies between compounds. For example, large distortions in the octahedral arsenic geometry in $[AsCl_3([14]aneS_4)]$ suggest an active lone pair, whereas there is no significant distortion in the coordination spheres of the $[AsCl_3([8]aneSe_2]$ and $[(AsX_3)_2([16]aneSe_4)]$ complexes.

The As(III) atom is much smaller than its heavier congeners, the stereochemical implications of which are illustrated by the fact that while seven-coordination is observed in thio- and seleno-ether complexes of Sb(III) and Bi(III), the maximum coordination number observed for As(III) in this study is six (although examples of seven-coordinate arsenic(III) are known in crown-ether complexes).[6] A consequence of the smaller radius is the increased hardness of the AsX_3 unit compared to SbX_3 or BiX_3 (in terms of the HSAB principle, outlined in Chapter 1). Although difficult to gauge precisely, the overall effect of this is to disfavour interaction between an AsX_3 fragment and softer donor atoms such as sulfur and selenium. The extreme case is seen in PX_3, where the combination of increased hardness, lower Lewis acidity and smaller radius means that no interaction with thio- and seleno-ethers has been detected under the conditions employed. Thus, arsenic(III) halides appear to represent the lower limit of Lewis acidity for MX_3 species toward neutral group 16 donor ligand systems.

4.3.1 General Comparisons and Further Work

Chapters 2 through 4 have described a range of arsenic, antimony and bismuth tri-halide coordination compounds of pnictogen and chalcogenoether ligands, and it is worth outlining the broad conclusions which can be drawn from this range of complexes. In attempting this, however, it is important to realise that the field is relatively new, with the majority of the results being obtained from the early-1990's onward, and hence the number of examples is relatively small. The structures discussed reflect only those species that yielded crystals suitable for X-ray diffraction studies and, since the complexes are derived from weak secondary interactions, different reaction conditions may well produce different structural motifs.

In general, phosphine and arsine ligands have displayed a narrow range of structural coordination modes toward MX_3 species than chalcogenoethers. There are various reasons for this. Since most structurally characterised examples of MX_3-pnicine complexes contain a backbone of two carbon atoms, the chelate effect could be invoked to explain the preference to form a five-membered ring rather than adopt a dinuclear bridging mode. However, the ligand-metal interactions are generally quite weak and thus ligand architecture is unlikely to be the sole influence upon the structure of the complex. More relevant is the fact that chalcogenoether ligands have lower steric demands, greater flexibility and, perhaps most importantly, two lone electron pairs per donor atom (as opposed to one lone pair on phosphines and arsines). This enables the linking of pyramidal MX_3 or dimeric M_2X_6 units into a much wider range of structural motifs, as observed for the majority of MX_3-chalcogenoether complexes.

The wide range of coordination modes and geometries, extent of lone pair stereochemical activity and range of polymeric network motifs observed in these compounds does not lend itself to a simple, all-encompassing explanation. The observed structural diversity probably reflects the very small energy differences between several potential structures, and thus small alterations in metal halide, ligand architecture, donor atom and reaction conditions can lead to profound changes in complex structure. In addition, solubility factors are undoubtedly important – the complex that crystallises is not necessarily the most structurally favoured. Thus, while an isomer A dimer can be predicted with a degree of confidence for MX_3-pnictogen complexes, it is very difficult to make predictions for the chalcogenoether complexes

beyond stating that a coordination network is likely. What can be predicted, however, is that in the majority of cases the bonding can be described in terms of the ligand donating into a vacant M-X σ^* anti-bonding orbital, with the ligand donor atoms disposed mutually *cis*.

With regard to further work, a number of related areas are worthy of study. The coordination and structural chemistry of MX_3 species with macrocyclic tertiary phosphine and arsine ligands remains completely undeveloped (in fact, there are no structurally characterised examples of complexes of such ligands containing any p-block compound). As synthetic routes to these macrocyclic ligands become available, the development of this area would provide structural comparisons with the MX_3 complexes containing acyclic pnictogen-donor ligands discussed in this work, in addition to the thia- and selena-crown complexes. The study of MX_3 complexes containing mixed chalcogen-donor ligands or hybrid pnictogen-chalcogenoether ligands would provide insight as to the relative binding preferences of the MX_3 species when presented with two options. However, this relies more on developments in ligand synthesis than coordination chemistry, and the anticipated low solubility of these complexes (and thus heavy reliance on X-ray crystallography for structural characterisation) would probably still remain a limiting factor. The issue of solubility could be addressed by extension of the coordination chemistry to MX_nR_{3-n} species, which would alter the acceptor properties of the M atom and, potentially, the structures of the complexes formed.

4.4 Experimental

General experimental conditions are given in the Appendix. Arsenic(III) halides were obtained commercially (Aldrich and Alfa) and used as received. Ligands were prepared using literature methods[20, 24, 25] except [9]aneS$_3$ and [14]aneS$_4$ which were supplied commercially (Aldrich). Standard Schlenk techniques were used for all preparations and all preparations and manipulations were performed under a N_2 atmosphere.

[AsCl$_3$([9]aneS$_3$)]. Addition of a CH_2Cl_2 solution of [9]aneS$_3$ (0.045 g, 0.25 mmol) to a CH_2Cl_2 solution of $AsCl_3$ (0.045 g, 0.25 mmol) produced a clear, pale yellow solution. Concentration of solvent *in vacuo* produced a pale yellow solid, which was filtered, washed with CH_2Cl_2 and dried *in vacuo*. Yield 54 %. Calculated for $C_6H_{12}AsCl_3S_3$: C, 19.9; H, 3.3. Found: C, 20.3; H, 3.5 %. ^{1}H-NMR: δ 3.1 (s, SC*H*$_2$) ppm. IR/cm^{-1}: 418 ν(As-Cl).

[AsBr$_3$([9]aneS$_3$)]. Addition of a CH_2Cl_2 solution of [9]aneS$_3$ to $AsBr_3$ solution immediately produced a bright yellow crystalline solid. The product was isolated as described above. Yield 83 %. Calculated for $C_6H_{12}AsBr_3S_3$: C, 14.6; H, 2.4. Found: C, 15.0; H, 2.5 %. ^{1}H-NMR: δ 3.1 (s, SC*H*$_2$) ppm. IR/cm^{-1}: 284 ν(As-Br).

[AsI$_3$([9]aneS$_3$)]. Procedure as above, using THF solutions of AsI_3 and [9]aneS$_3$. Yield 63 %. Calculated for $C_6H_{12}AsI_3S_3$: C, 11.3; H, 1.9. Found: C, 11.4; H, 2.1 %. ^{1}H-NMR: δ 3.1 (s, SC*H*$_2$) ppm.

[AsCl$_3$([14]aneS$_4$)]. Addition of a CH_2Cl_2 solution of $AsCl_3$ (0.024g, 0.14 mmol) to a CH_2Cl_2 solution of [14]aneS$_4$ (0.038g, 0.14 mmol) followed by slow evaporation of solvent by nitrogen flow produced a white crystalline solid, which was filtered, washed with hexane and dried *in vacuo*. Yield 77 %. Calculated for $C_{10}H_{20}AsCl_3S_4$: C, 24.2; H, 4.1; Found: C, 23.9; H, 4.3 %. ^{1}H-NMR: δ 1.94 (quintet, 4H, $CH_2CH_2CH_2$), 2.67 (t, 8H, SC*H*$_2$CH$_2$C*H*$_2$S), 2.78 (s, 8H, SC*H*$_2$C*H*$_2$S) ppm. IR/cm^{-1}: 409, 390 ν(As-Cl).

[$AsCl_3$([8]aneSe_2)]. Addition of a CH_2Cl_2 solution of [8]aneSe_2 to an equimolar CH_2Cl_2 solution of $AsCl_3$ produced a pale yellow solution. Solvent volume was reduced *in vacuo* to produce a deep red gum, which was stirred overnight in anhydrous hexane to give a waxy red solid. This solid was filtered, washed with CH_2Cl_2 and dried *in vacuo*. Yield 45 %. Calculated for $C_6H_{12}AsCl_3Se_2$: C, 17.0; H, 2.9. Found: C, 16.9; H, 3.0 %. ^{1}H-NMR: δ 2.24 (m, 4H, $SeCH_2CH_2CH_2Se$), 2.88 (m, 8H, $SeCH_2CH_2CH_2Se$) ppm. IR/cm^{-1}: 402, 392 ν(As-Cl).

[$AsBr_3$([8]aneSe_2)]. Procedure as above. Burgundy powder. Yield 55 %. Calculated for $C_6H_{12}AsBr_3Se_2$: C, 12.9; H, 2.2 %. Found: C, 12.8; H, 2.2. IR/cm^{-1}: 297, 282 ν(As-Br).

[AsI_3([8]aneSe_2)]. Procedure as above, using THF solutions of [8]aneSe_2 and AsI_3. Burgundy powder. Yield 77 %. Calculated for $C_6H_{12}AsI_3Se_2$: C, 10.3; H, 1.7. Found: C, 10.0; H, 1.9 %.

[($AsCl_3$)$_2$([16]aneSe_4)]. Procedure as for [$AsCl_3$([14]aneS_4)]. Pale yellow crystalline powder. Yield 92 %. Calculated for $C_{12}H_{24}As_2Cl_6Se_4$: C, 17.0; H, 3.1 %. Found: C, 16.7; H, 3.2 %. ^{1}H-NMR: δ 2.07 (quintet, 8H, $SeCH_2CH_2CH_2Se$), 2.70 (t, 16H, $SeCH_2CH_2CH_2Se$) ppm. IR/cm^{-1}: 401br ν(As-Cl).

[($AsBr_3$)$_2$([16]aneSe_4)]. Procedure as above. Yellow crystalline powder. Yield 71 %. Calculated for $C_{12}H_{24}As_2Br_6Se_4$: C, 13.5; H, 2.3. Found: C, 12.9; H, 2.2 %. ^{1}H-NMR: δ 2.07 (quintet, 8H, $SeCH_2CH_2CH_2Se$), 2.70 (t, 16H, $SeCH_2CH_2CH_2Se$) ppm. IR/cm^{-1}: 298, 281, 268 ν(As-Br).

[($AsCl_3$)$_4$([24]aneSe_6)]. Procedure as above. Pale yellow powder. Yield 40 %. Calculated for $C_{18}H_{36}As_4Cl_{12}Se_6$: C, 14.9; H, 2.5. Found: C, 15.2; H, 2.6 %. ^{1}H-NMR: δ 2.04 (quintet, 12H, $SeCH_2CH_2CH_2Se$), 2.70 (t, 24H, $SeCH_2CH_2CH_2Se$) ppm ^{77}Se{^{1}H}-NMR: δ 153 ppm IR/cm^{-1}: 400-380 br ν(As-Cl).

[$(AsBr_3)_2$([24]aneSe$_6$)]. Addition of a CH_2Cl_2 solution of [24]aneSe$_6$ to an equimolar CH_2Cl_2 solution of $AsBr_3$ gave a bright yellow powder. Yield 89 %. Calculated for $C_{18}H_{36}As_2Br_6$ Se$_6$: C, 15.9; H, 2.7. Found: C, 15.7; H, 2.6 %. ^{1}H-NMR: δ: 2.04 (quintet, 12H, $SeCH_2C\mathit{H}_2CH_2Se$), 2.70 (t, 24H, $SeC\mathit{H}_2CH_2C\mathit{H}_2Se$). IR/cm^{-1}: 297, 260 ν(As-Br).

[$AsBr_3$(MeS$(CH_2)_2$SMe)]. Procedure as for [$AsCl_3$([14]aneS$_4$)]. Yellow crystalline powder. Yield 84 %. Calculated for $C_4H_{10}AsBr_3S_2$: C, 11.0; H, 2.3. Found: C, 10.9; H, 2.3 %. ^{1}H-NMR: δ 2.16 (s, 6H, MeS), 2.74 (s, 4H, $SC\mathit{H}_2C\mathit{H}_2S$). IR/cm^{-1}: 298, 281, 261 ν(As-Br).

4.5 X-Ray Crystallography

General experimental X-ray data collection conditions are given in the Appendix. Details of the crystallographic data collection and refinement parameters are given in Tables 4.10 to 4.13. Data collection used a Rigaku AFC7S four-circle diffractometer ([$AsCl_3$([9]aneS$_3$)], [$(AsCl_3)_2$([16]aneSe$_4$)] and [$(AsCl_3)_4$([24]aneSe$_6$)]) (150 K) or an Enraf Nonius Kappa CCD diffractometer (120 K). No significant crystal movement or decay was detected during collection. Structure solution and refinement were routine,[26-31] except for [$AsCl_3$([8]aneSe$_2$)] where the thermal parameters of all carbon atoms were constrained to be equal in order to reduce the effect of disorder. For all other structures, fully occupied non-hydrogen atoms were refined anisotropically, and hydrogen atoms were added in fixed, calculated positions with d(C-H) = 0.96 Å in all cases.

	$[AsBr_3\{MeS(CH_2)_2SMe\}]$	**$[AsI_3\{MeS(CH_2)_2SMe\}]$**
Formula	$C_4H_{10}AsBr_3S_2$	$C_4H_{10}AsI_3S_2$
Formula Weight	436.88	577.88
Crystal System	Monoclinic	Monoclinic
Space Group	$P2_1/c$ (# 14)	$P2_1/n$ (# 14)
a/ Å	10.2818(6)	9.1528(1)
b/ Å	7.8015(5)	11.5622(2)
c/ Å	14.503(1)	12.0939(2)
α / °	90	90
β / °	102.9330(2)	93.863(1)
γ / °	90	90
U / Å ^{3}	1133.8(1)	1276.95(3)
Z	4	4
μ (Mo-K_α)/ cm^{-1}	139.11	101.93
Unique reflections	2435	3035
Obs. reflns.[$I > 2\sigma(I)$]	1689	2560
R	0.061[a]	0.046
R_w	0.146[a]	0.061

Table 4.10 X-ray data collection and refinement parameters for the $[AsBr_3\{MeS(CH_2)_2SMe\}]$ and $[AsI_3\{MeS(CH_2)_2SMe\}]$ complexes.

[a] R_1 (based on *F*) and wR_2 (based on F^2) for $F > 4\sigma(F)$ from SHELXL-97.

	$[AsCl_3([9]aneS_3)]$	**$[AsCl_3([14]aneS_4)]$**
Formula	$C_6H_{12}AsCl_3S_3$	$C_{10}H_{20}AsCl_3S_4$
Formula Weight	361.62	449.49
Crystal System	Tetragonal	Monoclinic
Space Group	$I4_1cd$ (# 110)	$P2_1/n$ (# 14)
a/ Å	17.520(4)	13.5942(2)
b/ Å	17.520(4)	7.7007(1)
c/ Å	16.790(7)	18.1270(3)
α / °	90	90
β / °	90	111.1662(5)
γ / °	90	90
U / Å ^{3}	5153(2)	1769.60(4)
Z	16	4
μ (Mo-K_α)/ cm^{-1}	37.03	28.27
Unique reflections	1322	4282
Obs. reflns.[$I > 2\sigma(I)$]	1080	3246
R	0.036[a]	0.039
R_w	0.095[a]	0.043

Table 4.11 X-ray data collection and refinement parameters for the $[AsCl_3([9]aneS_3)]$ and $[AsCl_3([14]aneS_4)]$complexes.

[a] R_1 (based on F) and wR_2 (based on F^2) for $F > 4\sigma(F)$ from SHELXL-97.

	$[(AsCl_3)_2([16]aneSe_4)]$	**$[(AsBr_3)_2([16]aneSe_4)]$**
Formula	$C_{12}H_{24}As_2Cl_6Se_4$	$C_{12}H_{24}As_2Br_6Se_4$
Formula Weight	846.71	1113.45
Crystal System	Monoclinic	Monoclinic
Space Group	$P2_1/n$ (# 14)	$P2_1/n$ (# 14)
a/ Å	9.764(3)	10.1220(1)
b/ Å	13.164(1)	13.4494(2)
c/ Å	10.627(2)	10.5125(2)
α / °	90	90
β / °	114.90(1)	113.49(2)
γ / °	90	90
U / Å ^{3}	1239.0(4)	1312.48(3)
Z	2	2
μ (Mo-K_α)/ cm^{-1}	92.17	172.24
Unique reflections	2297	2294
Obs. reflns.[$I > 2\sigma(I)$]	1653	2598
R	0.075[a]	0.066[a]
R_w	0.201[a]	0.173[a]

Table 4.12 X-ray data collection and refinement parameters for the $[(AsCl_3)_2([16]aneSe_4)]$ and $[(AsBr_3)_2([16]aneSe_4)]$ complexes.

[a] R_1 (based on *F*) and wR_2 (based on F^2) for $F > 4\sigma(F)$ from SHELXL-97.

	$[AsCl_3([8]aneSe_2)]$	**$[(AsCl_3)_4([24]aneSe_6)]$**
Formula	$C_6H_{12}As_1Cl_3Se_2$	$C_{18}H_{36}As_4Cl_{12}Se_6$
Formula Weight	423.36	1451.36
Crystal System	Orthorhombic	Monoclinic
Space Group	Pnn2 (# 34)	$P2_1/n$ (# 14)
a/ Å	16.5472(8)	8.227(4)
b/ Å	10.2042(4)	25.66(1)
c/ Å	8.8924(3)	9.808(4)
α / °	90	90
β / °	90	95.71(3)
γ / °	90	90
U / Å^3	1501.49	2060(1)
Z	4	2
μ (Mo-K_α)/ cm^{-1}	76.07	93.13
Unique reflections.	1992	3635
Obs. reflns.[$I > 3\sigma(I)$]	945	2449
R	0.071	0.035
R_w	0.089	0.097

Table 4.13 X-ray data collection and refinement parameters for the $[AsCl_3([8]aneSe_2)]$and $[(AsCl_3)_4([24]aneSe_6)]$ complexes.

4.6 References

[1] A. R. J. Genge, N. J. Hill, W. Levason and G. Reid, *J. Chem. Soc., Dalton Trans.*, 2001, 1007.

[2] a) A. J. Barton, N. J. Hill, W. Levason, B. Patel and G. Reid, *Chem. Commun.*, 2001, 95; b) A. J. Barton, N. J. Hill, W. Levason and G. Reid, *J. Chem. Soc., Dalton Trans.*, 2001, 1621

[3] a) A. J. Barton, A. R. J. Genge, W. Levason and G. Reid, *J. Chem. Soc., Dalton Trans.*, 2000, 2163; b) A. J. Barton, A. R. J. Genge, W. Levason and G. Reid, *J. Chem. Soc., Dalton Trans.*, 2000, 859; c) A. R. J. Genge, W. Levason and G. Reid, *Chem. Commun.*, 1998, 2159.

[4] N. C. Norman and N. L. Pickett, *Coord. Chem. Rev.*, 1995, **45**, 5 and references therein.

[5] J. E. D. Davies and D. A. Long, *J. Chem. Soc. (A)*, 1968, 1757.

[6] N. W. Alcock, M. Ravindran and G. R. Willey, *Acta Crystallogr.*, 1993, **B49**, 507.

[7] L. Malatesta, *Gazzetta*, 1939, **69**, 629.

[8] a) C. L. Raston and A. H. White, *J. Chem. Soc., Dalton Trans.*, 1975, 2425; b) M. Colapietro, A. Domenicano, L. Scaramuzza and A. Vaciago, *Chem. Commun.*, 1968, 302.

[9] B. F. Hoskins, E. R. T. Tiekink and G. Winter, *Inorg. Chim. Acta*, 1985, **99**, 177.

[10] M. Dräger, *Chem. Ber.*, 1974, **107**, 2601.

[11] P. H. Javora, E. A. Meyers and R. A. Zingaro, *Inorg. Chem.*, 1976, **15**, 2525.

[12] D. J. Williams and K. J.Wynne, *Inorg. Chem.*, 1978, **17**, 1108.

[13] J. M. Kisenyi, G. R. Willey, M. G. B. Drew and S. O. Wandiga, *J. Chem. Soc., Dalton Trans.*, 1985, 69.

[14] H. P. S. Chauhan, B. Porwal and R. K. Singh, *Phosphorus, Sulfur and Silicon*, 2000, **160**, 93.

[15] R. Kniep and H. D. Reski, *Inorg. Chim. Acta*, 1982, **64**, L83.

[16] T. Klapötke, *Main Group Met. Chem.*, 1997, **2**, 81.

[17] G. R. Willey, M. T. Lakin, M. Ravindran and N. W. Alcock, *Chem. Commun.*, 1991, 272.

[18] S. Pohl, D. Haase and M. Peters, *Z. Anorg. Allg. Chem.*, 1993, **619**, 727.

[19] R. E. DeSimone and M. D. Glick, *J. Am. Chem. Soc.*, 1976, **98**, 762.

[20] R. J. Batchelor, F. W. B. Einstein, I. D. Gay, J.-H. Gu, B. D. Johnston and B. M. Pinto, *J. Am. Chem. Soc.*, 1989, **111**, 6582.

[21] "Advanced Inorganic Chemistry", F. A. Cotton, G. Wilkinson, C. A. Murillo and M. Bochmann, 6th Edition, p. 381, Wiley, New York, 1999.

[22] A. Bondi, *J. Phys. Chem.*, 1964, **48**, 441.

[23] R. J. Batchelor, F. W. B. Einstein, I. D. Gay, J.-H. Gu, B. M. Pinto and X. Zhou, *Inorg. Chem.*, 1996, **35**, 3667.

[24] F. R. Hartley, W. Levason, C. A. McAuliffe, S. G. Murray and H. E. Soutter, *Inorg. Chim. Acta*, 1979, **35**, 265.

[25] D. J. Gulliver, E. G. Hope, W. Levason, G. L. Marshall, S. G. Murray and D. M. Potter, *J. Chem. Soc., Perkin Trans. 2*, 1984, 429.

[26] G. M. Sheldrick, *SHELXL-97*; University of Göttingen, Germany, 1997.

[27] P. T. Beurskens, G. Admiraal, G. Beurskens, W. P. Bosman, S. Garcia-Granda, R. O Gould, J .M. M. Smits and C. Smykalla, *PATTY, The DIRDIF Program System*; Technical Report of the Crystallography Laboratory, University of Nijmegen, The Netherlands, 1992.

[28] *TeXsan: Crystal Structure Analysis Package*, Molecular Structure Corporation, The Woodlands, TX, 1995.

[29] N. Walker and D. Stuart, *Acta Crystallogr.*, 1983, **A39**, 158.

[30] H. D. Flack, *Acta Crystallogr.*, 1983, **A39**, 876.

[31] R. H. Blessing, *Acta Crystallogr.*, 1995, **A51**, 33.

Chapter 5

Reactions of Thallium(I) Salts with Diselenoethers

5.1 Introduction

The preceding chapters have discussed the coordination and structural chemistry of MX_3 species with multidentate and macrocyclic thio- and seleno-ether ligands (M = As, Sb, Bi; X = Cl, Br, I). A series of unusual structural motifs have been identified, ranging from simple monomeric species to complex three-dimensional coordination networks. In the majority of cases the core of the structure was comprised of a pyramidal MX_3 unit weakly bound to a ligand or halide atom through secondary M---L or M---X interactions. These examples have demonstrated that main group compounds such as the group 15 halides do form complexes with these traditionally "modest" donor ligands.

Like Sb(III) and Bi(III), Tl(I) and Tl(III) are regarded as soft acids in terms of the HSAB concept (due to the large size and low charge density) and thus would be expected to demonstrate a reasonably broad coordination chemistry with soft donor ligands. Although a number of Tl(I) and Tl(III) adducts of sulfur donors have been reported,[1] there are no examples of Tl(I) complexes containing selenium-donor ligands. In seeking to further develop the area of p-block coordination complexes of chalcogenoether ligands, this chapter reports the attempted preparation of a range of Tl(I) adducts of acyclic bidentate and macrocyclic selenoether ligands. X-ray crystal structures of the first two examples of such species are discussed.

5.1.1 Thallium(I) Complexes

This section highlights some examples of structurally characterised Tl(I) compounds containing chalcogen-donor ligands.

Thallium(I) complexes of oxygen donors include $[TlOMe]_4$, which contains thallium and oxygen atoms at alternate corners of a cubane-like $[Tl_4O_4]$ framework,[2] and the tetrameric $[Tl(O_2CH)]_4$.[3] Roesky and co-workers used the bulky 2,4,6-tris(trifluoromethyl)phenoxide ligand to enforce an unusual two-fold coordination geometry on the Tl(I) atom in the $[Tl_2O_2]$-bridged $[C_6H_2(CF_3)_3OTl]_2$ dimer (Tl-O 2.469(8) Å) (Figure 5.1).[4]

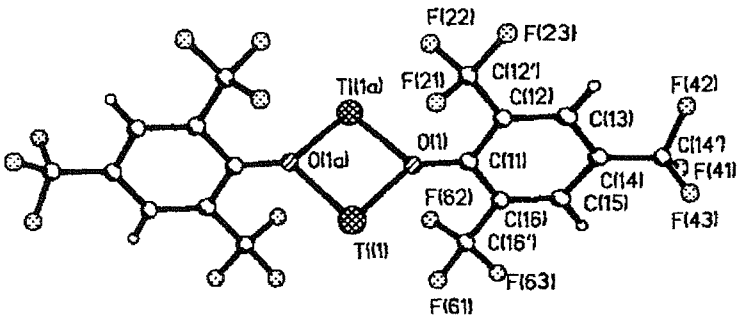

Figure 5.1 View of the $[C_6H_2(CF_3)_3OTl]_2$ dimer.[4]

The [Tl(hfacac)] adduct has been reported (hfacacH = 1,3-bis(trifluoromethyl)propanedione), and the structure is comprised of polymeric chains formed from two distinct structural units.[5] One of the units is monomeric, with the hfacac ligand chelated to the Tl(I) atom (Tl-O 2.62(2) – 2.72(3) Å), which is 0.42 Å below the plane of the ligand. The other unit is dimeric, containing two symmetry-related $Tl(hfacac)_2$ units with the Tl(I) atoms bound 1.56 Å above and below the plane of the hfacac ligands such that the Tl(I) atoms are located at the two axial sites of an octahedron (Tl-O 2.75(3) – 2.96(3) Å) (Figure 5.2a). Weak Tl---O contacts (3.04(3) Å) link the two separate units to give five-coordinate thallium(I). The reaction of $[Tl(O^tBu)]_4$ with $[Sn(O^tBu)_2]_2$ in ^tBuOH gave the mixed Tl(I)-Sn(II) cage compound $[Tl(O^tBu)_3Sn]$ containing trigonal pyramidal metal atoms (Tl-O 2.595(7) Å) (Figure 5.2b).[6]

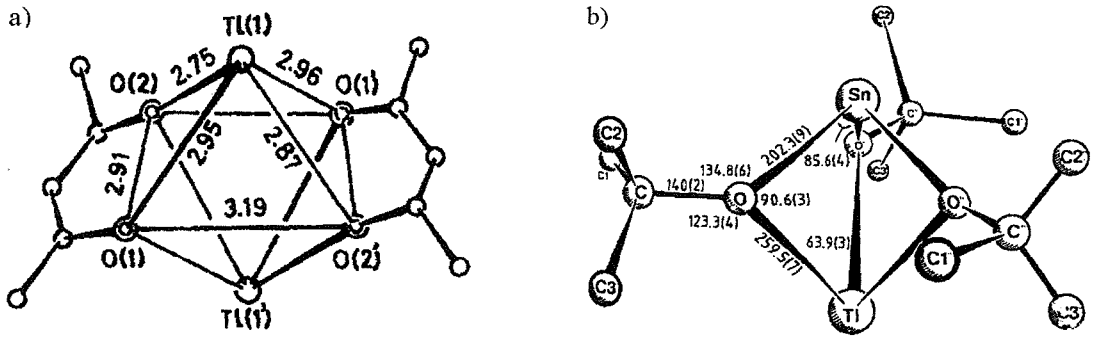

Figure 5.2 a) View of the $[Tl(hfacac)]_2$ dimer[5] and b) view of the $Tl(O^tBu)_3Sn$ adduct.[6]

In terms of sulfur-donor ligands, Krebs and co-workers have reported the synthesis and crystal structures of a series of thallium(I) thiolate cage molecules, obtained from the reaction of Tl_2CO_3 with the precursor sodium thiolate in MeCN or methanol solution.[7, 8] The crystal structure of benzenethiolatothallium(I), [Tl(SPh)], reveals a polymeric motif comprised of two separate structural units, the $[Tl_7(SPh)_6]^+$ and $[Tl_5(SPh)_6]^-$ ions. The $[Tl_5(SPh)_6]^-$ anion (Figure 5.3a) comprises a distorted octahedral array of sulfur atoms in which five of the eight octahedral faces are bridged by Tl(I) atoms, each of which is trigonal-pyramidally coordinated to three separate sulfur atoms, with Tl-S bond distances ranging from 2.876(12) to 3.410(12) Å. The $[Tl_7(SPh)_6]^+$ cation is similar, with seven of the eight octahedral faces bridged by trigonal-pyramidal thallium atoms (Figure 5.3b). Three thallium atoms are additionally bound to a sulfur atom from three neighbouring units of $[Tl_5(SPh)_6]^-$, leading to the polymeric structure. Both ions have C_3 symmetry.[8]

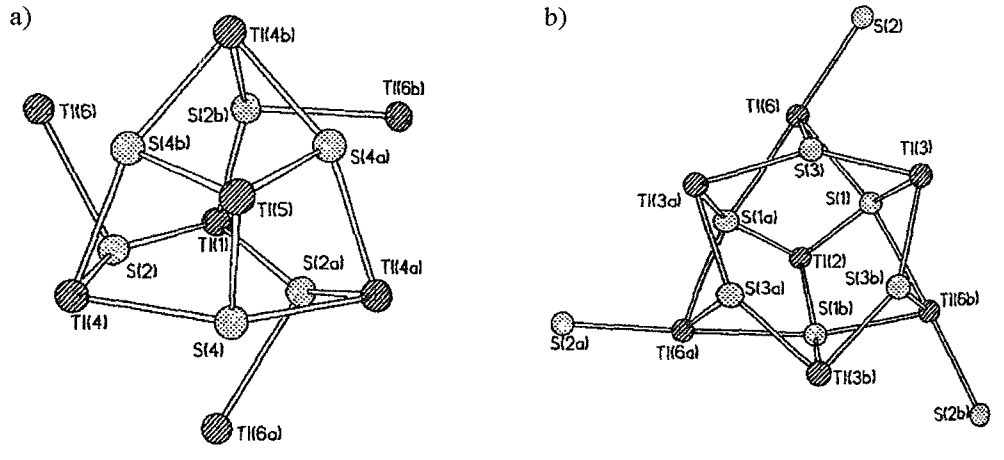

Figure 5.3 a) View of the core of the $[Tl_5(SPh)_6]^-$ anion and b) $[Tl_7(SPh)_6]^+$ cation with phenyl groups omitted for clarity.[8]

The *tert*-butylthiolatothallium(I) complex consists of $[Tl_8(SBu^t)_8]$ molecules comprised of two cubane-like $[Tl_3(SBu^t)_4]$ fragments in which each Tl(I) adopts a trigonal-pyramidal geometry (Figure 5.4a). These fragments are linked by a planar Tl_2S_2 unit containing pseudo-trigonal bipyramidal Tl(I) atoms. The Tl-S distances in the molecule are in the range 2.818(7) - 3.264(6) Å. The $[Tl_8(SBu^t)_8]$ molecules are linked by weak Tl---Tl contacts (3.749(2) – 3.864(3) Å), such that each $[Tl_8(SBu^t)_8]$ unit is in contact with four others.

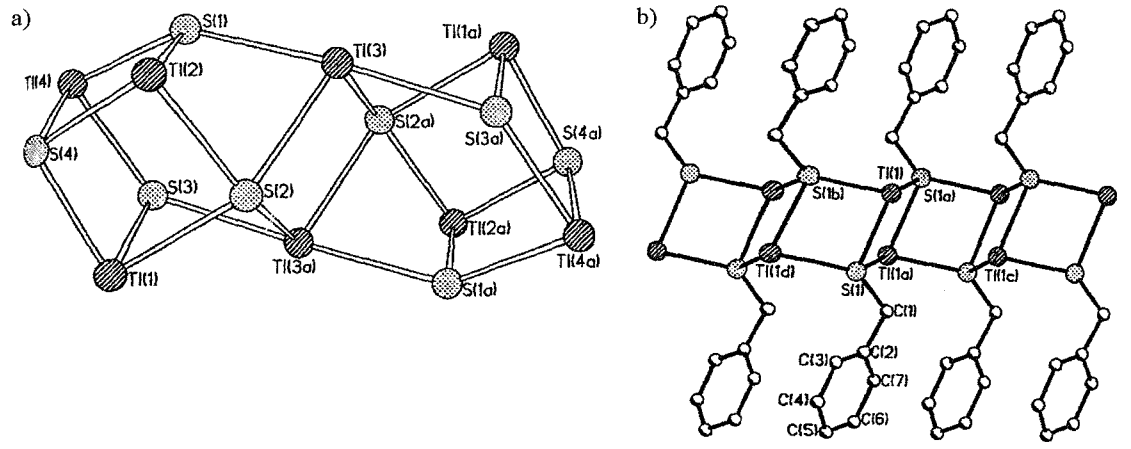

Figure 5.4 a) View of the $[Tl_8(S^tBu)_8]$ cage[8] and b) the infinite chain of $[Tl(SCH_2Ph)]$ with ^{t}Bu groups omitted for clarity.[9]

Benzylthiolatothallium(I) [Tl(SCH$_2$Ph)]] contains chains of Tl_2S_2 rings which are linked through *trans* edges to produce a ladder-type motif, with each Tl(I) atom adopting a distorted trigonal pyramidal geometry (Tl-S 2.867(4) – 2.936(4) Å) (Figure 5.4b) and no evidence for Tl---Tl interactions. The reaction of thallium metal with Ph_2Se_2 in refluxing toluene gave the Tl(SePh) adduct, although Ph_2S_2 did not react with Tl under these conditions.[9]

Similar chemistry involving selenium or tellurium reagents has not been explored; indeed the only structurally characterised example containing a Tl-Te bond appears to be the diamond-shaped $[Tl_2Te_2]^{2-}$ anion.[10] This was obtained by reaction of KTlTe with [2.2.2]cryptate in 1,2-diaminoethane (en) to give $[K([2.2.2]crypt]_2[Tl_2Te_2].en$ (Tl-Te 2.929(3) - 2.984(2) Å).

Few thioether complexes of thallium have been reported, and all contain macrocyclic ligands (i.e. there are no complexes of acyclic thioethers). The first such species to be structurally characterised was $[Tl([9]aneS_3][PF_6]$, prepared by reaction of $TlNO_3$ and $[9]aneS_3$ in MeCN, followed by treatment with NH_4PF_6.[11] The structure consists of the tridentate thiacrown facially bound to a single thallium(I) atom (Tl-S = 3.092(3) - 3.114(3)Å) (Figure 5.6a) The narrow S-Tl-S bond angles (*ca.* 67 °) reflect the relatively long Tl-S bonds in the $[Tl([9]aneS_3]^+$ unit.

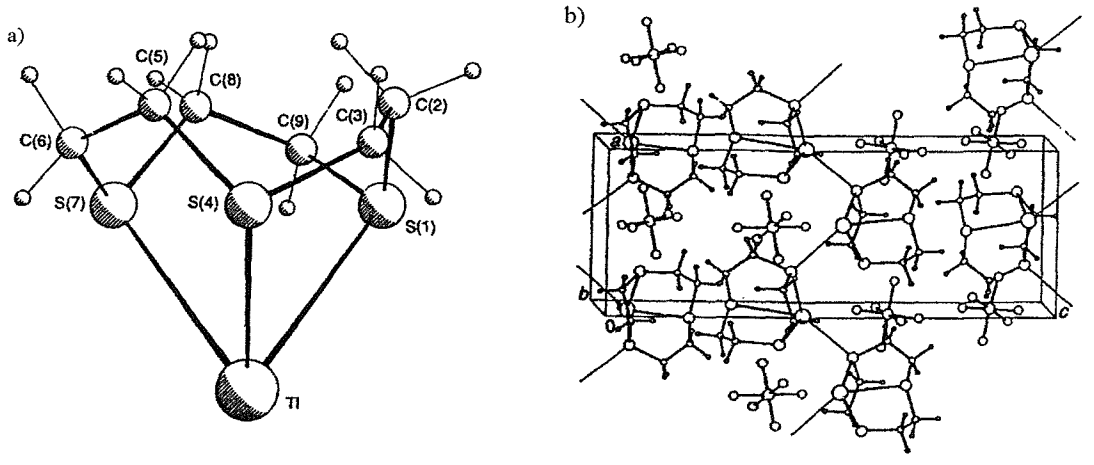

Figure 5.6 a) View of the $[Tl([9]aneS_3)]^+$ cation and b) the packing diagram.[11]

A weaker interaction between the thallium and a sulfur atom from a neighbouring $[Tl([9]aneS_3]^+$ moiety gives an overall [3+1] coordination at Tl(I) (Tl-S 3.431(3) Å) and leads to the formation of infinite helices (Figure 5.6b) In addition, secondary interactions between thallium and fluorine atoms from three separate $[PF_6]^-$ anions give formally eight-coordinate thallium(I) (Tl-F = 3.228(8) - 3.389(8) Å).[11]

The structure of the corresponding complex with $[18]aneS_6$, prepared by direct reaction of $TlPF_6$ with the hexathiacrown, shows Tl(I) bound to all six sulfur atoms (Figure 5.7a).[12] Two of these interactions (3.164(5) - 3.205(7) Å) are substantially shorter than the other four (3.315(6) - 3.370(5) Å). The $[Tl([18]aneS_6)]^+$ cations are weakly associated to two sulfur atoms from adjacent units (Tl-S 3.686(6) - 3.689(6) Å) to give an infinite one-dimensional chain structure (Figure 5.7b) As observed for $[Tl([9]aneS_3)][PF_6]$, Tl-S bond lengths are long (3.164(5) – 3.370(5) Å) and S-Tl-S bond angles are acute (*ca.* 65 °), reflecting a mismatch between the metal ion radius and the macrocycle cavity size The $[Tl([18]aneN_2S_4)][PF_6]$ complex adopts a very similar structure.[12]

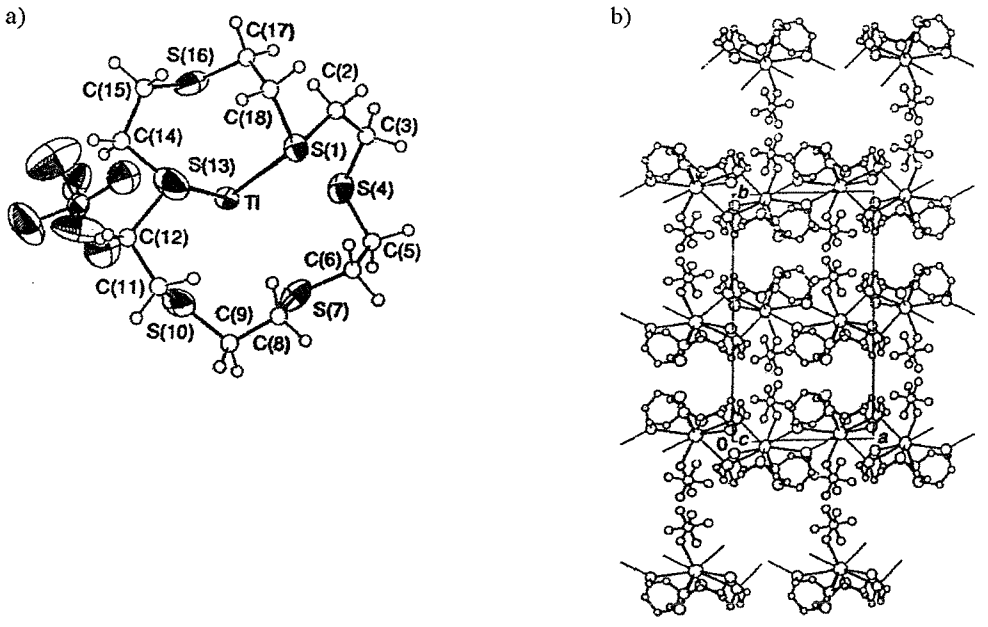

Figure 5.7 a) View of the [Tl([18]aneS$_6$)][PF$_6$] complex and b) the packing diagram.[12]

The [Tl([24]aneS$_8$)][PF$_6$] complex, obtained similarly to [Tl([18]aneS$_6$)][PF$_6$], adopts a polymeric structure in which each Tl(I) is sandwiched by two symmetry-related halves of two thiacrown units to give an infinite sinusoidal chain (Figure 5.8).[13] The thallium atoms are mutually *anti* and an overall [4+4] coordination sphere at the metal centre results, with coordination to each macrocycle occurring via weak Tl---S interactions (3.2413(11) - 3.4734(14) Å) Tl-S bonds.

In summary, there are insufficient examples of thallium(I)-chalcogenoether complexes to discern any general trends. For the complexes reported, ligand architecture and donor characteristics appear to affect the observed coordination environment, and the very weak, long range Tl---S and Tl---F contacts (*ca.* 3.2 Å) lead to extended structures.

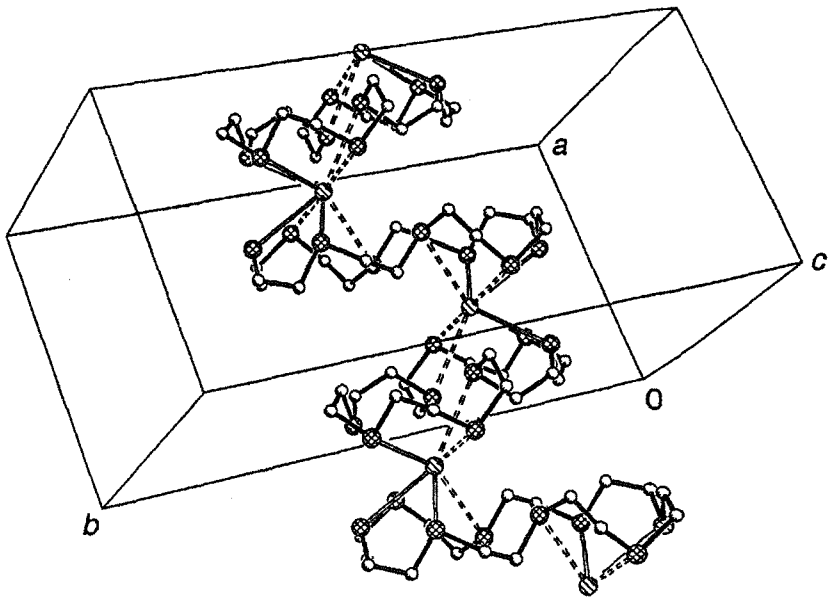

Figure 5.8 Packing diagram for $[Tl([24]aneS_8)]^+$ showing the structure of the infinite one-dimensional polymer ($[PF_6]^-$ anions not shown).[13]

5.2 Results and Discussion

Initial attempts to prepare diselenoether adducts of $TlPF_6$ employed the procedure of Schröder *et al* for thiacrown complexes, involving precipitation of the complex by addition of Et_2O to the reaction solution.[11-13] Thus, following short reflux of an MeCN solution containing $TlPF_6$ and an equimolar amount of L (L = $MeSe(CH_2)_2SeMe$, $MeSe(CH_2)_3SeMe$, o-$C_6H_4(SeMe)_2$, [8]aneSe$_2$, [16]aneSe$_4$ or [24]aneSe$_6$), the solution was allowed to cool and a few drops of diethyl ether added to the colourless solution. A white powder was precipitated immediately and was filtered, washed with MeCN and dried *in vacuo*. In all cases, very low percentage carbon and hydrogen values were obtained from the microanalyses and the IR spectra of these solids, recorded as pressed CsI discs, revealed strong bands *ca.* 830 and 558 cm^{-1} (both indicative of $[PF_6]^-$) but very little evidence for coordinated selenoether. ^{1}H-NMR spectra revealed very weak signals due to the uncoordinated ligand. These results suggest that addition of ether to the reaction solution essentially results in the precipitation of $TlPF_6$.

Slow evaporation of the acetonitrile reaction solution in a small boiling tube at room temperature produced a series of colourless, semi-crystalline solids which were isolated by filtration and rinsed with MeCN, although the crystals produced very weak X-ray diffraction patterns and thus were unsuitable for single crystal diffraction studies. Microanalytical and IR data similar to those discussed above were obtained, indicating that a pure thallium-selenoether complex could not be isolated and that the bulk material is predominantly $TlPF_6$. However, the combination of $TlPF_6$ with $MeSe(CH_2)_nSeMe$ (n = 2 or 3) produced a few colourless crystals which were of suitable quality for X-ray diffraction studies.

The crystal structure of the $[Tl\{MeSe(CH_2)_3SeMe\}][PF_6]$ adduct is comprised of $[Tl\{MeSe(CH_2)_3SeMe\}]^+$ cations and $[PF_6]^-$ anions. In the $[Tl\{MeSe(CH_2)_3SeMe\}]^+$ cation, the Tl(I) atom is coordinated to two selenium atoms from separate $MeSe(CH_2)_3SeMe$ ligands (Figure 5.9) The Se-Tl-Se link is linear (179.89(2)°), and this motif is repeated to generate an infinite one-dimensional chain. The ligand forms an S-shape, and so each individual $[Tl\{MeSe(CH_2)_3SeMe\}]^+$ chain adopts a staircase arrangement (Figure 5.10). The Tl(1)-Se(1) distance is 3.389(1) Å, similar to the longer of the Tl-S distances reported for thallium(I)-thiacrown[11-13] and thallium(I)-thiolate complexes[7, 8] (although the coordination geometries and numbers in both cases are different to the present species). Thus, the structure of the $[Tl\{MeSe(CH_2)_3SeMe\}]^+$ cation is best described as an infinite, one-dimensional chain of $MeSe(CH_2)_3SeMe$ units bridged by thallium(I) atoms. The chains are arranged in stacks, with the layers separated by 5.593(3) Å along the x-axis and 7.911(3) Å along the z-axis.

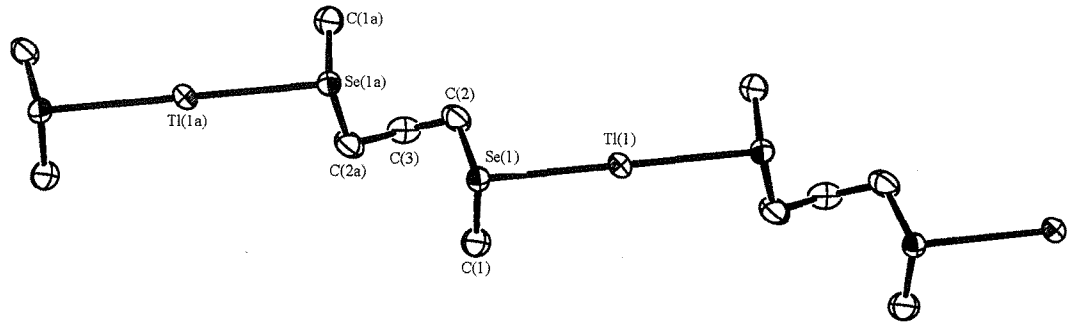

Figure 5.9 View of a portion of a single $[Tl\{MeSe(CH_2)_3SeMe\}]^+$ chain. Ellipsoids shown at 40 % probability, H-atoms omitted for clarity. Atoms marked (a) are related by the symmetry operation –x, -y, -z.

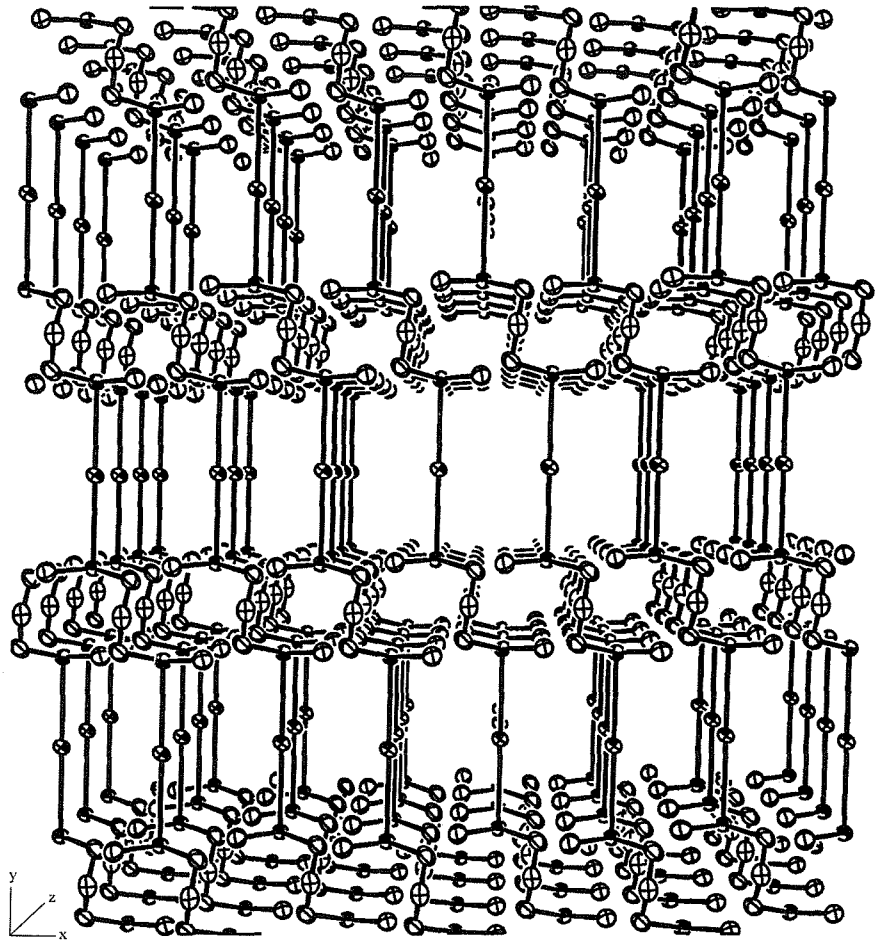

Figure 5.10 View of $[Tl\{MeSe(CH_2)_3SeMe\}]^+$ lattice along the z-axis ($[PF_6]^-$ anions not shown).

The space between the $[Tl\{MeSe(CH_2)_3SeMe\}]^+$ chains is occupied by $[PF_6^-]$ anions, with the phosphorus atoms located along the Tl-Tl vector and the fluorine atoms involved in weak Tl---F interactions. Specifically, there are ten distinct Tl---F contacts derived from four separate $[PF_6^-]$ units; the minimum contact distance is 3.111(4) Å and the maximum is 3.321(4) Å. Figure 5.11 shows the arrangement of these secondary Tl---F interactions as viewed down the y-axis (i.e. along the Se-Tl-Se vector). Each fluorine atom bridges two neighbouring Tl^+ cations to give a network of Tl---F contacts approximately perpendicular to the Tl-Se bonds (Table 3.1). Long range Tl---F contacts have been observed in the $[Tl(Me_3[9]aneN_3)][PF_6]$ (3.23(1) – 3.54(2) Å),[14] $[Tl([18]aneN_2S_4)][PF_6]$ (3.326(4) Å) and $[Tl([18]aneS_6)][PF_6]$ (3.052(24) Å) species,[12] although in these cases the Tl---F interactions were terminal rather than bridging.

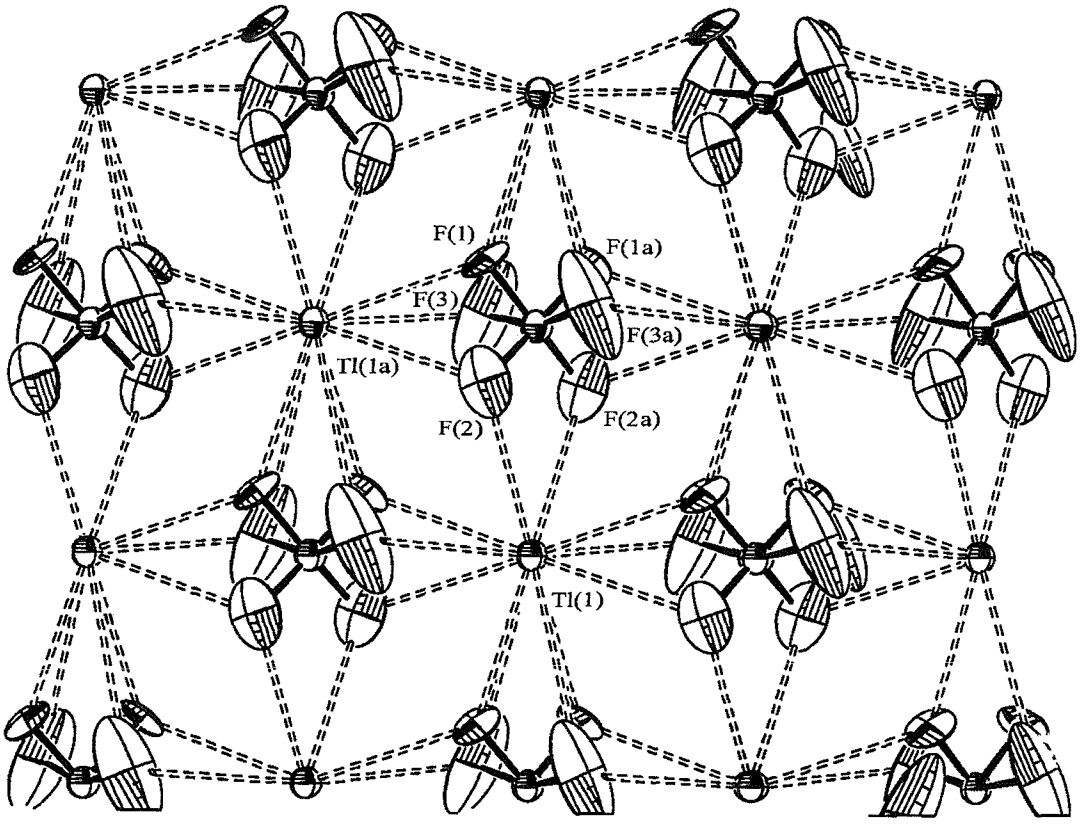

Figure 5.11 View down the y-axis of the long range Tl---F contacts. Details as shown in Figure 5.9.

Tl(1)	Se(1)	3.389(1)	Tl(1a)	F(1)	3.222(1)
Tl(1)	F(2)	3.177(2)	Tl(1a)	F(2)	3.284(1)
Tl(1)	F(2a)	3.111(2)	Tl(1a)	F(3)	3.321(2)
Se(1)	Tl(1) Se(1b)	179.89(2)	C(2)	Se(1) Tl(1)	100.77(1)
C(1)	Se(1) Tl(1)	93.35(2)			

Table 3.1 Selected bond lengths (Å) and angles (°) for $[Tl\{MeSe(CH_2)_3SeMe\}][PF_6]$.

Given that the sum of the ionic radii of Tl^+ and F^- is 3.20 Å,[15] these Tl---F contacts are genuine (albeit weak) and are probably best viewed as supplementary to the Tl---Se bonds. Thus, the one-dimensional $[Tl\{MeSe(CH_2)_3SeMe\}]^+$ chains are stabilised by the weak Tl---F contacts, and the Tl(I) atom can be described as [2 + 10] coordinate, consistent with the ability of thallium to achieve high coordination numbers.

The $[Tl\{MeSe(CH_2)_2SeMe\}][PF_6]$ complex also adopts a coordination network structure, although there are a number of features different to the $[Tl\{MeSe(CH_2)_3SeMe\}][PF_6]$ structure. The most striking difference is the bonding mode of the $MeSe(CH_2)_2SeMe$ ligands, which asymmetrically bridge two separate Tl(I) atoms, leading to a two-dimensional sheet topology (Figure 5.12, Table 5.2). The Tl-Se distances are shorter than in the $[Tl\{MeSe(CH_2)_2SeMe\}]^+$ cation (3.277(3) – 3.332(2) *vs.* 3.389(1) Å). The sheet is comprised of ten-membered, approximately rectangular units containing two $MeSe(CH_2)_2SeMe$ ligands linked at the corners of the rectangle by thallium atoms. These corner thallium and selenium atoms link to four other rectangular units through a Tl-Se bond, such that one selenium atom per ligand bridges two separate thallium atoms. A weaker Tl---Se interaction (Tl(1*)-Se(2*) (3.506(2) Å) gives rise to stacking of the sheets (* indicates a general atom). This contact exists between a thallium atom on one level of the stack and a terminal selenium donor from the next level, such that the thallium atom is four-coordinate (Figure 5.13a). The terminal methyl groups of the ligand adopt the *meso* conformation.

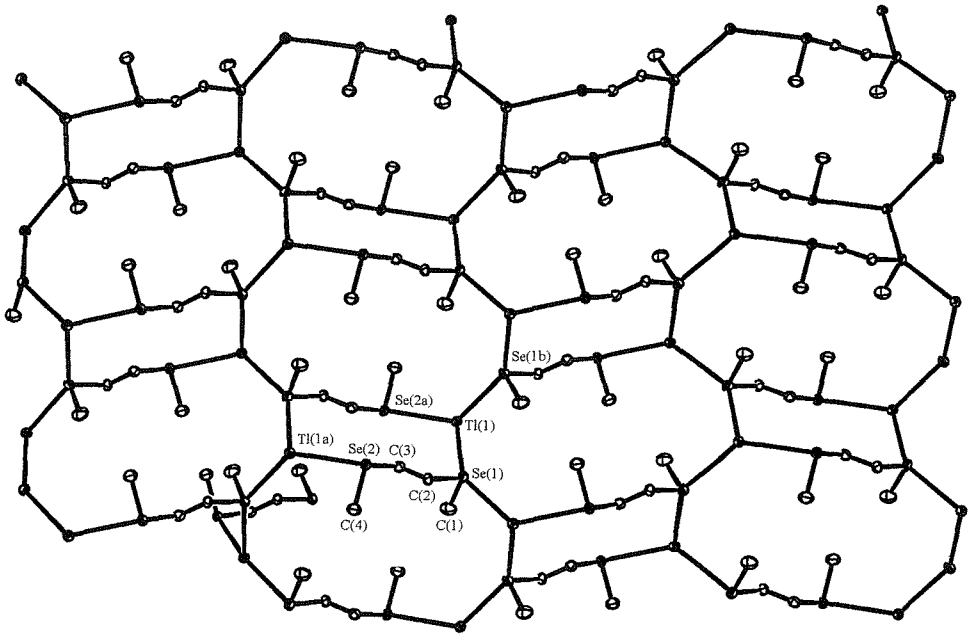

Figure 5.12 View of the sheet structure of $[Tl\{MeSe(CH_2)_2SeMe\}]^+$ ($[PF_6]^-$ anions not shown). Ellipsoids shown at 40 % probability, H-atoms omitted for clarity.

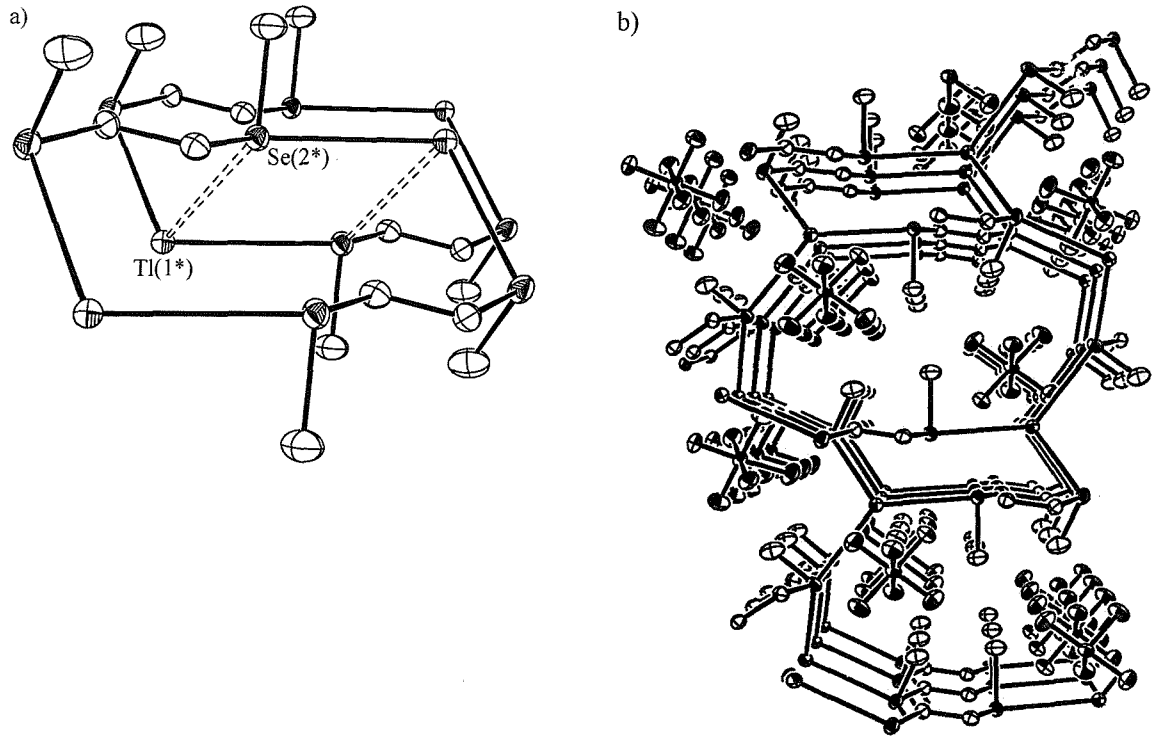

Figure 5.13 a) View of the Tl---Se contacts giving rise to the stacking arrangement and b) view of a portion of the extended lattice structure including the $[PF_6]^-$ anions.

As observed for the $[Tl\{MeSe(CH_2)_3SeMe\}][PF_6]$ species, the $[PF_6]^-$ ions are involved in Tl---F interactions and are significantly shorter than those observed previously (with respect to both the $[Tl\{MeSe(CH_2)_3SeMe\}][PF_6]$ and thiacrown complexes).[11-13] In this example, the anions are located in channels formed by the rectangular $[Tl\{MeSe(CH_2)_3SeMe\}]_2$ units, and are situated approximately equidistant above and below the layers (Figures 5.13b and 5.14). The terminal methyl groups of the $MeSe(CH_2)_3SeMe$ ligand are directed into the centre of the channel. In total, there are five distinct Tl---F interactions per Tl(I) atom, derived from three separate $[PF_6]^-$ anions, with the shortest being 2.985(2) Å and the longest 3.299(3) Å. Thus the thallium atom may be viewed as nine-coordinate, with a $TlSe_4$ core based upon a very distorted tetrahedron supplemented by weak Tl---F contacts.

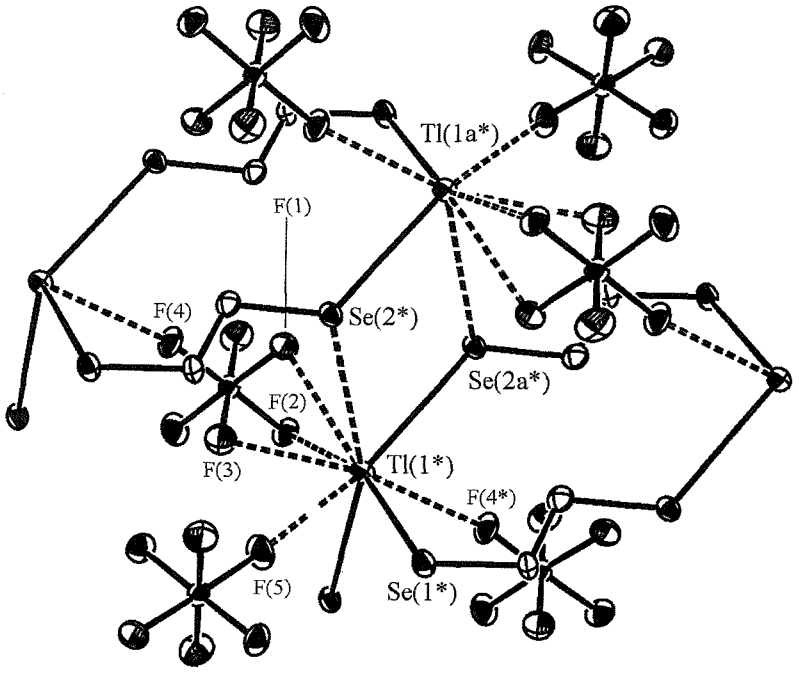

Figure 5.14 View of the Tl---F interactions shown between two layers. Methyl carbon and H-atoms omitted for clarity.

In both examples the stereochemical influence of the thallium-based lone pair is very difficult to ascertain given the range and number of weak Tl---Se and Tl---F contacts (i.e. there is no obvious "hole" in the coordination sphere of Tl(I)). In fact, it is possible that the electronic configuration of the Tl(I) atom in these examples is [Xe] $5d^{10}$ $6s^2$, for which no stereochemical effect would be predicted.

Tl(1)	Se(1)	3.277(3)	Tl(1*)	F(1)	3.299(2)
Tl(1)	Se(1b)	3.314(2)	Tl(1*)	F(2)	3.049(2)
Tl(1)	Se(2a)	3.332(3)	Tl(1*)	F(3)	3.222(3)
Tl(1*)	Se(2*)	3.506(2)	Tl(1*)	F(4*)	2.989(2)
			Tl(1*)	F(5)	2.985(3)
Se(1)	Tl(1) Se(1b)	96.81(2)	Se(1)	Tl(1) Se(2*)	97.43(3)
Se(1)	Tl(1) Se(2a)	107.72(2)	Se(1b)	Tl(1) Se(2*)	157.28(3)
Se(1b)	Tl(1) Se(2a)	125.96(2)	Se(2a)	Tl(1) Se(2*)	65.69(3)
Tl(1*)	Se(2*) Tl(1a*)	114.31(2)			

Table 5.2 Selected bond lengths (Å) and angles (°) for $[Tl\{MeSe(CH_2)_2SeMe\}][PF_6]$.

Using the same experimental procedure, a set of yellow needle crystals was isolated from the reaction of $TlPF_6$ with $PhSe(CH_2)_2SePh$. However, determination of the unit cell parameters revealed the compound to be Ph_2Se_2 rather than the desired selenoether complex. The reaction of $PhSe(CH_2)_2SePh$ with $TlPF_6$ in refluxing MeCN solution was subsequently monitored by $^{77}Se\{^1H\}$-NMR spectroscopy in order to establish the role of Tl(I). Only a signal due to the free diselenoether (333 ppm) was observed upon initial mixing of the solutions.[16] After refluxing for one hour the formerly colourless reaction solution became yellow, and the $^{77}Se\{^1H\}$-NMR spectrum showed a sharp signal at 456 ppm due to Ph_2Se_2.[16] Notably, $PhSe(CH_2)_2SePh$ is unaffected by prolonged reflux in MeCN in the absence of $TlPF_6$.

With little success in obtaining bulk solids of these adducts starting from $TlPF_6$, attempts were made to alter the anion from PF_6^- to ClO_4^- by addition of a few drops of a 70 % $HClO_4$ solution to an MeCN solution of $TlPF_6$ and $MeSe(CH_2)_2SeMe$. This immediately gave a white semi-crystalline precipitate, which gave similar IR, NMR and microanalytical data to the attempts with $TlPF_6$. X-ray crystallography revealed the bulk material to be $Tl(ClO_4)$.

This general failure to isolate bulk samples of selenoether complexes indicates that any such complex is formed in extremely low yield and that the bulk of the isolated product is, in fact, the starting material $TlPF_6$. The strong bands *ca.* 830 and 557 cm^{-1} in the IR spectrum reveal the presence of $[PF_6]^-$ in all cases, however the strongest indication that the adducts are present in only minute amounts is the repeated failure to obtain elemental carbon and hydrogen values for all of the isolated solids. Indeed, in all cases except for the two crystal structures, the isolated product is probably $TlPF_6$ contaminated with a small amount of the selenoether complex.

5.3 Conclusions

This work has seen the synthesis and structural characterisation of the first examples of thallium-selenoether complexes. The crystal structures of the two isolated adducts, $[Tl\{MeSe(CH_2)_nSeMe\}][PF_6]$ (n = 2 and 3) both reveal coordination networks comprised of Tl-Se bonds supplemented by weaker Tl---F contacts. However, characterisation by IR and microanalysis is hampered by the fact that these complexes are formed in very low yield and are thus very difficult to isolate in analytically pure, $TlPF_6$-free form. The majority of attempts to obtain Tl(I) complexes of diselenoethers resulted in the re-isolation of $TlPF_6$, with trace percentage carbon and hydrogen values obtained and no evidence of coordinated ligand by ^{1}H-NMR and IR spectroscopy. Attempts to alter the counter-ion by addition of $HClO_4$ resulted only in precipitation of $TlClO_4$. The general failure to obtain complexes in useful yield indicates that the Tl-SeR_2 interaction is extremely weak in comparison to the M-SeR_2 interactions described in Chapters 2 - 4 (M = As(III), Sb(III) or Bi(III)).

5.4 Experimental

General experimental conditions are given in the Appendix. $TlPF_6$ was obtained commercially (Strem) and used without further purification. Ligands were prepared by literature methods.[16, 17] A typical attempted preparation is described below.

Reaction of $TlPF_6$ with $MeSe(CH_2)_2SeMe$. Addition of an MeCN solution (5 cm^3) of $MeSe(CH_2)_2SeMe$ (0.15 g, 0.70 mmol) to an equimolar MeCN solution of $TlPF_6$ (5 cm^3) gave a colourless solution which was stirred at room temperature for 30 minutes. The solution was then transferred to a small boiling tube and the solvent allowed to evaporate at room temperature, giving a very small crop of colourless crystals amongst a bulk sample of white powder (0.14 g). Calculated for $C_4H_{10}F_6PSe_2Tl$: C, 8.5; H, 1.8. Found: C, 2.1; H, 0.8 % (typical values). ^{1}H-NMR: δ 2.1 (s), 2.9 (s) ppm. IR/cm^{-1}: 830 br, 558 ν(P-F).

5.5 X-ray Crystallography

General experimental X-ray data collection conditions are given in the Appendix. Details of the collection and refinement parameters are given in Table 5.3. Data were collected on an Enraf Nonius Kappa CCD. No significant crystal movement or decay was detected during collection. Structure solution and refinement were routine.[18-24] Fully occupied non-hydrogen atoms were refined anisotropically, and hydrogen atoms were added in fixed, calculated positions with d(C-H) = 0.96 Å.

	[Tl{MeSe(CH$_2$)$_2$SeMe}][PF$_6$]	**[Tl{MeSe(CH$_2$)$_3$SeMe}][PF$_6$]**
Formula	$C_4H_{10}F_6P_1Se_2Tl_1$	$C_5H_{12}F_6P_1Se_2Tl_1$
Formula Mass	565.38	579.40
Crystal System	Monoclinic	Monoclinic
Space Group	$P2_1/n$ (# 14)	$C2$ (# 5)
a / Å	7.3370(2)	7.9081(3)
b / Å	9.0243(2)	7.9111(3)
c / Å	17.8221(4)	10.4005(4)
α/ °	90	90
β/ °	92.3110(8)	101.9320(14)
χ/ °	90	90
U / Å^3	1179.06(5)	636.62(4)
Z	4	2
μ (Mo-K$_\alpha$)/ cm^{-1}	200.282	185.509
Unique Reflections	2655	1314
Obs. reflns.		
[$I > 2\sigma(I)$]	2230	1259
R	0.057	0.044
R_w	0.147	0.154

Table 5.3 Crystallographic data collection and refinement parameters for the complexes [Tl{MeSe(CH$_2$)$_n$SeMe}][PF$_6$] (n = 2 and 3).

5.6 References

[1] D. G. Tuck in *The Chemistry of Aluminium, Gallium, Indium and Thallium*, (Ed. A. J. Downs), Blackie, London, 1993.

[2] L. F. Dahl, G. L. Davis, D. L. Wampler and R. West, *J. Inorg. Nucl. Chem.*, 1962, **24**, 357.

[3] K. Ozutsumi, H. Ohtaki and A. Kusumegi, *Bull. Chem. Soc. Jpn.*, 1984, **57**, 2616.

[4] H. Roesky, M. Schloz, M. Noltenmeyer and F. T. Edelmann, *Inorg. Chem.*, 1989, **28**, 3829.

[5] S. Tachiyashiki, H. Nakayama, R. Kuroda, S. Sato and Y. Saito, *Acta Crystallogr.*, 1975, **B31**, 1483.

[6] M. Veith and R. Rösler, *Angew. Chem. Int. Ed. Engl.*, 1982, **21**, 858.

[7] B. Krebs and A. Brömmelhaus, *Angew. Chem. Int. Ed. Engl.*, 1989, **28**, 1682.

[8] B. Krebs and A. Brömmelhaus, *Z. Anorg. Allg. Chem.*, 1991, **595**, 167.

[9] R. Kumar, H. E. Mabrouk and D. G. Tuck, *J. Chem. Soc., Dalton Trans.*, 1988, 1045.

[10] R. C. Burns and J. D. Corbett, *J. Am. Chem. Soc.*, 1981, **103**, 2627.

[11] A. J. Blake, J. A. Greig and M. Schröder, *J. Chem. Soc., Dalton Trans.*, 1991, 529.

[12] A. J. Blake, G. Reid and M. Schröder, *J. Chem. Soc., Dalton Trans.*, 1992, 2987.

[13] A. J. Blake, D. Fenske, W-S. Li, V. Lippolis and M. Schröder, *J. Chem. Soc., Dalton Trans.*, 1998, 3961.

[14] K. Wieghardt, M. Kleine-Boymann, B. Nuber and J. Weiss, *Inorg. Chem.*, 1986, **25**, 1309.

[15] R. D. Shannon, *Acta Crystallogr.*, 1976, **A32**, 751.

[16] D. J. Gulliver, E. G. Hope, W. Levason, G. L. Marshall, S. G. Murray and D. M. Potter, *J. Chem. Soc., Perkin Trans. 2*, 1984, 429.

[17] R. J. Batchelor, F. W. B. Einstein, I. D. Gay, J.-H. Gu, B. D. Johnston and B. M. Pinto, *J. Am. Chem. Soc.*, 1989, **111**, 6582.

[18] G. M. Sheldrick, *SHELXL-97*; University of Göttingen, Germany, 1997.

[19] P. T. Beurskens, G. Admiraal, G. Beurskens, W. P. Bosman, S. Garcia-Granda, R. O Gould, J .M. M. Smits and C. Smykalla, *PATTY, The DIRDIF Program System*; Technical Report of the Crystallography Laboratory, University of Nijmegen, The Netherlands, 1992.

[20] *TeXsan: Crystal Structure Analysis Package*, Molecular Structure Corporation, The Woodlands, TX, 1995.

[21] N. Walker and D. Stuart, *Acta Crystallogr.*, 1983, **A39**, 158.

Chapter 6

Main Group Complexes and Reactions of Telluroether Ligands

6.1 Introduction

Chapters 3 - 5 have described the coordination and structural chemistry of a series of novel Sb(III), As(III) and Tl(I) complexes of acyclic bidentate and macrocyclic thio- and seleno-ether ligands. As a class of ligands, the corresponding telluroether species have received much less study in terms of both new methods of synthesis and coordination chemistry, although they display quite different behaviour from their lighter analogues. Recently, for example, telluroethers were established as stronger σ-donors than their sulfur and selenium analogues toward low valent d-block metals.[1, 2] The synthesis of telluroethers is generally more difficult than that of analogous thio- and seleno-ethers, with the high reactivity and instability of the tellurium-containing precursors and intermediates posing a major problem. For example, the inherent weakness of the Te-C bond often leads to elimination of the carbon backbone and subsequent telluride formation during ligand synthesis.[3] The ligands are air-sensitive and very malodorous oils, depositing tellurium on prolonged exposure to air, and so it is often convenient to characterise a new telluroether as the telluronium derivative, formed by reaction of the telluroether with an alkyl halide or di-halogen.[3, 4]

Of particular relevance to the current study is the ability of the tellurium atom to participate in secondary Te---X interactions with halogen and pseudo-halogen species, which often gives rise to dimeric or oligomeric assemblies in the solid state.[5] There exist various classes of organotellurium halides, ranging from those of general formula R_3TeX through R_2TeX_2 to $RTeX_3$ (R = alkyl or aryl; X = Cl, Br, I or pseudo-halide).[6]

This chapter focuses upon the synthesis and structural characterisation of R_3TeX and R_2TeX_2 complexes, obtained from the reaction of MeI or I_2 with mono- and ditelluroethers. In addition, the preparation of a series of MX_3 complexes of mono- and ditelluroethers and the structural characterisation of $[BiBr_3(PhTeMe)]$ are reported (M = Sb or Bi; X = Cl, Br or I).

6.2 Organo-tellurium(IV) Complexes

This section highlights the current literature regarding crystallographically characterised R_3TeX and R_2TeX_2 species (X = Cl, Br, I, BPh_4, NCS or NCO; R= Me, Et, ^{i}Bu, Ph or p-C_6H_4(OMe)). All of the R_3TeX structures reported concern mono-telluroethers, and there is only a single example of an R_2TeX_2 species derived from a ditelluroether. As in previous chapters, literature coverage is selective rather than comprehensive.

The crystal structures of the Et_3TeX series have been reported by Drake *et al.*[7, 8] Et_3TeCl and Et_3TeBr are structurally very similar, with the tellurium and halide atoms involved in secondary interactions and occupying alternate corners of a Te_4X_4 cubane skeleton (Te---X = 3.448(4), 3.564(1) Å for X= Cl and X = Br respectively) (Figure 6.1a). Three carbon atoms from ethyl groups complete a distorted octahedral tellurium environment.

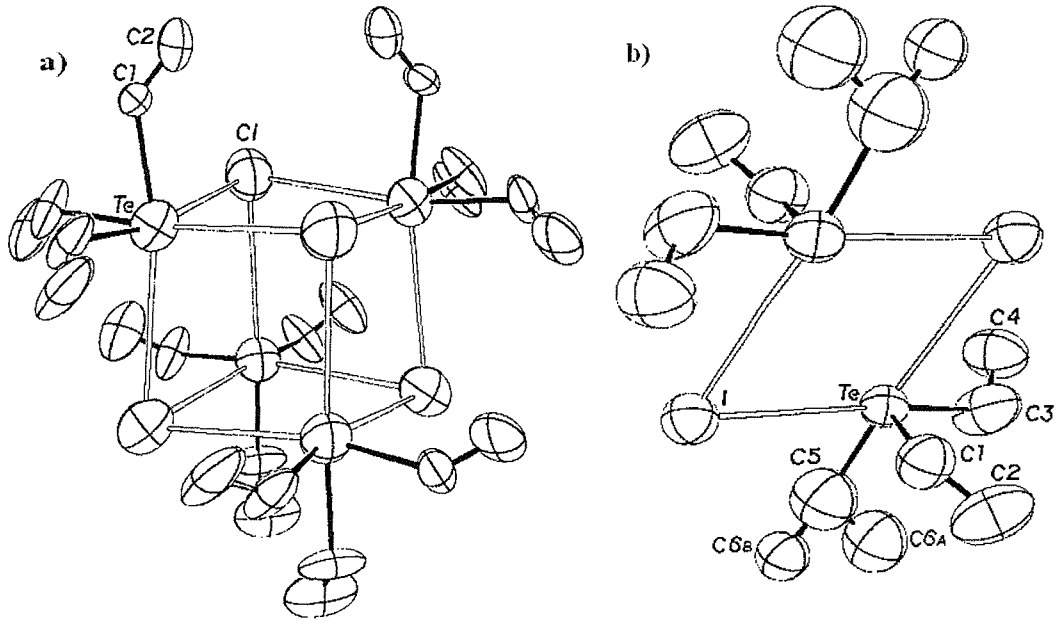

Figure 6.1 View of the structures of a) Et_3TeCl and b) Et_3TeI.

The structure of Et_3TeI is different to the chloride and bromide species, and consists of a pair of Et_3Te^+ cations linked through bridging iodines (3.813(5) – 3.861(5) Å) to give a centrosymmetric $(Et_3TeI)_2$ dimer (Figure 6.1b).[8] Each tellurium is involved

in only two secondary Te---I interactions, giving a square pyramidal geometry and a formally five-coordinate tellurium atom. A similar dimeric structure, containing secondary Te---Cl interactions [3.234(1) – 3.214(1) Å], was reported for the Ph_3TeCl species.[9] The R_3TeBPh_4 adducts (R = Me or Ph) have also been prepared, the crystal structure of Me_3TeBPh_4 consisting of discrete Me_3Te^+ and BPh_4^- ions, with cation-anion interactions absent due to the non-coordinating nature of the BPh_4^- anion, giving a three-coordinate tellurium(IV) atom.[10]

Recently, as part of a ^{125}Te NMR study of various organo-tellurium salts, the crystal structures of Me_3TeI, $^{i}Bu_2PhTeBr$ and $Ph_2MeTeBPh_4$ were reported.[11] The authors suggest that these species exist as ion-pairs (as observed for the R_3TeBPh_4 adducts) and, in support of this, they state "the distance between tellurium and the counter-ion is much longer than that of a normal chemical bond". Suprisingly, the possibility of secondary Te---X interactions was not considered for the halide adducts. This is compounded by an earlier report by Collins *et al* of the crystal structure of Me_3TeI, which shows a distorted octahedral geometry about the tellurium atom arising from three primary Te-C bonds and three secondary Te---I interactions (3.70 – 3.81 Å), leading to an extended structure.[12]

Comparison of the intermolecular Te---Br distances in $^{i}Bu_2PhTeBr$ (3.292(1) Å) with those reported for other R_3TeBr species suggests that the bromide anion is likely to weakly interact with the tellurium atom, and could give rise to a dimeric or oligomeric structure. The X-ray crystal structures of $Me_3TeCl.H_2O$, Me_3TeNO_3, Ph_3TeNO_3, $Ph_3TeCl.½\ CHCl_3$ and $(Ph_3Te)_2SO_4.5H_2O$ were also reported by Collins *et al* as part of a ^{125}Te CP/MAS solid-state NMR study.[12] It is worth noting that, in contrast to solution-phase NMR studies, changes in the environment of the ^{125}Te nucleus imposed by secondary interactions with the various anions were deduced from chemical shift tensors and coupling to neighbouring nuclei.

The diorganotellurium dihalides and pseudo-halides, R_2TeX_2, have received a similar level of study and a number have been structurally characterised Early work upon these species concerned dimethyltellurium di-iodide, Me_2TeI_2, which was proposed to exist in α- and β-forms. These were later concluded to be *cis*- and *trans*-isomers of a square planar structure.[13] Further work suggested that the α-form had the covalent structure Me_2TeI_2 and the β-form was ionic, of formula $[Me_3Te][MeTeI_4]$.[14]

Einstein and co-workers confirmed this crystallographically, and showed that both forms adopt an extended array in the solid state.[15, 16] The α-form contains a tellurium atom in a distorted octahedral geometry, with two iodine atoms in a *trans* arrangement (2.854(3) – 2.994(3) Å), two methyl groups *cis* to each other and two weak, intermolecular Te---I contacts to iodine atoms attached to neighbouring molecules (3.659(3) – 4.030(3) Å).[15] The β-form is derived from trigonal pyramidal Me_3Te^+ cations and square pyramidal $MeTeI_4^-$ anions (2.84 – 2.98 Å). The ions are bridged by four intermolecular Te---I contacts, which complete a distorted octahedral environment about each tellurium atom. Three of the contacts are from the Me_3Te^+ cation to three different iodines of a neighbouring $MeTeI_4^-$ anion (3.84, 3.97, 4.00 Å), with the fourth contact occurring between two $MeTeI_4^-$ anions.[16]

Similarly, Ph_2TeI_2 adopts distinct α- and β-modifications. In both cases the primary geometry is pseudo-trigonal bipyramidal with iodines in the axial positions, and the difference between the two lies in the secondary bonding and packing patterns.[17] In the α-form, two Te---I secondary bonds complete a distorted octahedral geometry about each tellurium linking the molecules into a three-dimensional network.

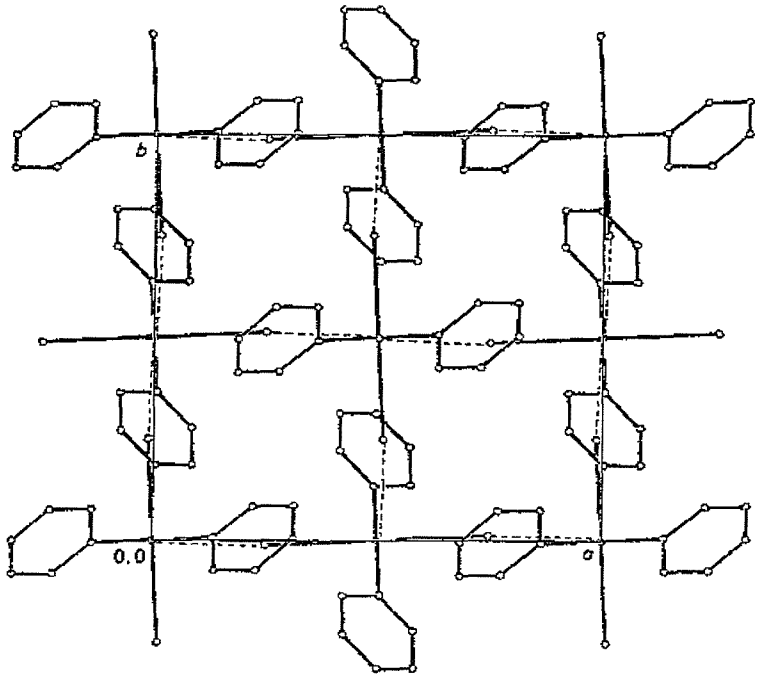

Figure 6.2 Packing diagram of α-Ph_2TeI_2.[15]

The β-modification exists as a more complex three-dimensional network, and is comprised of two crystallographically independent molecules, one of which forms two secondary bonds while the other exists in a pseudo-octahedral geometry with one vacant position.

Farren and co-workers recently reported the preparation and crystal structure of the $\{p\text{-}MeOC_6H_4\}_2TeI_2$ complex, obtained from reaction of $(p\text{-}MeOC_6H_4)_2Te$ with iodine.[18] The geometry at the tellurium atom was described as pseudo-trigonal bi-pyramidal, with the anisyl groups and lone pair in the equatorial plane and iodine atoms in the axial positions (Figure 6.5). The $[\{p\text{-}MeOC_6H_4\}_2TeI_2]$ molecules associate through two secondary intermolecular Te---I interactions (3.6922(6) – 3.9017(7) Å) to form a centrosymmetric tetramer containing Te_4I_6 open-cubane cores.

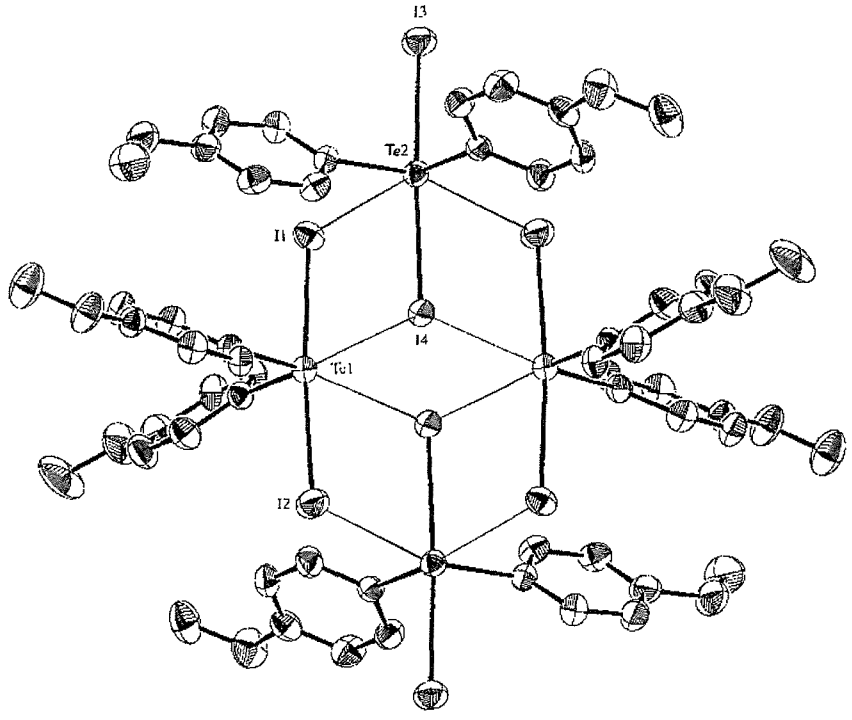

Figure 6.3 View of the open-cubane arrangement of $\{p\text{-}MeOC_6H_4\}_2TeI_2$.[18]

The diiodine adduct of the related ditelluroether $[\{p\text{-}(OMe)C_6H_4Te\}_2CH_2]$ has also been structurally characterised.[19] The crystal structure of this species is similar to that of $\{p\text{-}MeOC_6H_4\}_2TeI_2$, with the tellurium(IV) atom adopting a saw-horse structure, and the two iodine atoms occupying axial positions with angles close to 180 ° (2.809(1) – 3.065(1) Å] (Figure 6.4). Two of the iodine atoms form intermolecular Te---I

contacts with neighbouring tellurium atoms (3.735(1) – 3.879(1) Å) to give an array of rectangular Te_2I_2 bridges, although the extended structure was not discussed in detail.

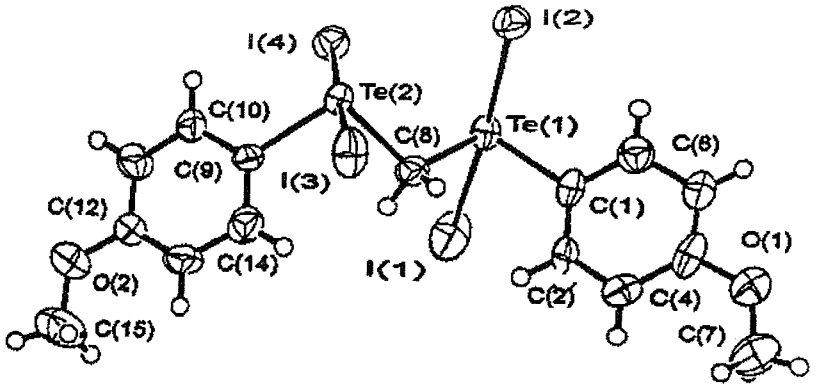

Figure 6.4 View of the $\{p\text{-}(OMe)C_6H_4Te\}_2CH_2$ complex.[19]

A number of other diorganotellurium iodides have been structurally characterised, and all display secondary Te---I interactions.[20, 21] In the majority of cases, these adducts contain a tellurium atom in an irregular octahedral geometry with four primary and two secondary bonds. This bonding pattern is also followed by R_2TeX_2 species when X = F, Cl or Br. For example, the structures of the complete series Ph_2TeX_2 are known and all show similar primary geometry supplemented by secondary Te---X contacts to give a distorted octahedral or square pyramidal geometry at the tellurium atom.[20] The exceptions to this general trend are 4,4-di-iodo-1-thia-4-telluracyclohexane,[22] which contains a tellurium atom in a distorted pentagonal bipyramidal geometry, and one of the two independent molecules in the previously discussed $\beta\text{-}Ph_2TeI_2$.

6.1.2 Main Group Complexes of Telluroethers

The tin(IV) halide complexes $[SnX_4(Me_2Te)]$ and $[SnX_4\{o\text{-}C_6H_4(TeMe)_2\}]$ (X = Cl or Br) are the only structurally characterised examples of p-block adducts of telluroethers currently in the literature, and consist of the ligand chelated to the metal centre to give an octahedral SnX_4Te_2 geometry.[23] These are the only examples of p-block complexes of telluroethers, thus very little is known regarding the ability of these ligands to form coordination complexes with other main group elements.

6.2 Results and Discussion

6.2.1 Organotellurium Iodides

Reaction of the ditelluroether species o-$C_6H_4(CH_2TeMe)_2$[24] with excess MeI in acetone produced the bis(tri-organotelluronium iodide) [o-$C_6H_4(CH_2TeMe_2I)_2$] as a white powder in high yield, which was isolated by filtration and washed with acetone. As for other telluronium salts (and unlike the parent telluroether) the compound is air-stable both as a solid and in solution. The $^{125}Te\{^1H\}$ NMR spectrum of the derivative, obtained in $CDCl_3$ solution, shows a single resonance at 526 ppm. This signal is shifted substantially to high frequency of the parent di-telluroether o-$C_6H_4(CH_2TeMe)_2$ resonance of 264 ppm,[24] indicating conversion of Te(II) to Te(IV) as a result of oxidative addition of MeI to each Te(II) atom. The value is similar to that observed for the $Me(I)Te(CH_2CH_2CH_2Te(I)Me_2)_2$ adduct (522 ppm).[25] Micro-analytical data and ^1H NMR confirm the stoichiomery of the product. In order to establish the structure of the complex in the solid-state, a single crystal X-ray analysis was undertaken. Colourless crystals of [o-$C_6H_4(CH_2TeMe_2I)_2$]. ½ $CHCl_3$ were obtained by slow diffusion of diethyl ether into a $CHCl_3$ solution of the compound.

The [o-$C_6H_4(CH_2TeMe_2I)_2$] species is comprised of a $Me_2Te(\mu^2\text{-}I)_2TeMe_2$ unit bridging the two arms of the o-xylyl fragment. The $Me_2Te(\mu^2\text{-}I)_2TeMe_2$ unit has a similar geometry to the Et_3TeI adduct described previously, although the axial o-xylyl moiety is constrained to *syn* coordination in this example (as opposed to the *anti* disposition of the axial Et fragments in the latter).[7] The most notable aspect of the structure, however, is the formation of a Te_4I_4 pseudo-cubane core, derived from the association of two [o-$C_6H_4(CH_2TeMe_2I)_2$] units through secondary Te---I contacts between alternating tellurium and iodine atoms (Figure 6.5). The o-xylyl units lie diagonally across two opposite faces of the pseudo-cubane core, the Te-C bonds to the benzyl carbon atoms being slightly longer than those to the methyl carbons (2.18(1) *vs.* 2.12(1) Å).

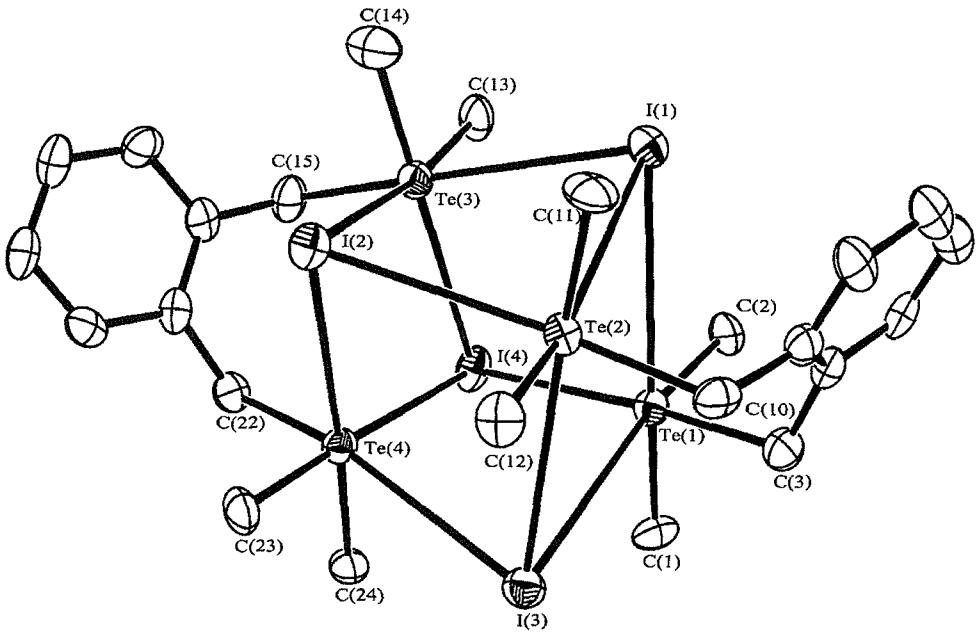

Figure 6.5 View of the [o-$C_6H_4(CH_2TeMe_2I)_2$] complex with the numbering scheme adopted. Ellipsoids shown at 40 % probability, H-atoms omitted for clarity.

The Te---Te separation within the two individual [o-$C_6H_4(CH_2TeMe_2I)_2$] fragments (3.943(3) - 3.995(3) Å for Te(1) – Te(2) and Te(3) – Te(4) respectively) are similar to the corresponding Te-Te distances in the [$MnCl(CO)_3${o-$C_6H_4(CH_2TeMe)_2$}] and [$W(CO)_4${o-$C_6H_4(CH_2TeMe)_2$}] complexes (3.913(2) and 4.039(3) Å respectively), indicating that the o-xylyl moiety acts as a fairly rigid inter-donor linkage.[28] The Te---I contacts linking the two [o-$C_6H_4(CH_2TeMe_2I)_2$] units are *ca.* 0.25 Å shorter than the Te---I distances in the (μ^2-$I)_2$ bridges. Thus, the Te---I distances in the $Me_2Te(\mu^2$-$I)_2TeMe_2$ unit range from 3.647(2) to 3.828(2) Å while the Te---I contacts between these units range from 3.531(2) to 3.595(3) Å. These distances are similar to those in previously discussed R_3TeI and R_2TeX_2 compounds.

The Te-I-Te and I-Te-I bond angles reflect the severe distortion of the Te_4I_4 core. The $Me_2Te(\mu^2$-$I)_2TeMe_2$ dimer units are highly distorted, with values of *ca.* 65° and *ca.* 115° typical for the Te-I-Te and I-Te-I angles (Table 6.1). Such acute Te-I-Te geometry is likely to be a consequence of the rigid o-xylyl linkage between the tellurium atoms. In effect, the organic linking group locks the tellurium atoms in position, enforcing a rhombohedral (rather than rectangular) bridge geometry.

I(1)	Te(1)	3.828(2)	I(1)	Te(2)	3.780(1)
I(1)	Te(3)	3.548(2)	I(2)	Te(2)	3.572(3)
I(2)	Te(3)	3.768(1)	I(2)	Te(4)	3.787(1)
I(3)	Te(1)	3.779(1)	I(3)	Te(2)	3.652(1)
I(3)	Te(4)	3.595(3)	I(4)	Te(1)	3.531(2)
I(4)	Te(3)	3.647(2)	I(4)	Te(4)	3.686(1)
Te(1)	C(1)	2.12(1)	Te(1)	C(3)	2.18(1)

Te(1)	I(1)	Te(2)	62.43(2)	Te(1)	I(1)	Te(3)	80.48(5)
Te(2)	I(1)	Te(3)	80.43(3)	Te(2)	I(2)	Te(3)	80.29(2)
Te(2)	I(2)	Te(4)	75.04(4)	Te(3)	I(2)	Te(4)	76.16(2)
Te(2)	I(3)	Te(4)	76.47(4)	Te(1)	I(4)	Te(3)	83.28(5)
Te(1)	I(4)	Te(4)	78.13(3)	Te(3)	I(4)	Te(4)	66.02(2)
I(1)	Te(1)	I(3)	113.70(2)	I(1)	Te(1)	I(4)	91.07(5)
I(3)	Te(1)	I(4)	97.74(2)	I(1)	Te(2)	I(2)	92.27(3)
I(1)	Te(2)	I(3)	117.95(2)	I(2)	Te(2)	I(3)	99.33(4)
I(1)	Te(3)	I(2)	92.86(2)	I(1)	Te(3)	I(4)	93.86(5)
I(2)	Te(3)	I(4)	114.73(3)	I(2)	Te(4)	I(3)	96.48(4)
I(3)	Te(4)	I(4)	98.13(3)	C(1)	Te(1)	C(2)	94.3(4)
C(1)	Te(1)	C(3)	90.9(4)	C(2)	Te(1)	C(3)	94.7(4)
C(10)	Te(2)	C(11)	94.4(4)	C(10)	Te(2)	C(12)	90.4(4)
C(13)	Te(3)	C(14)	93.8(5)	C(13)	Te(3)	C(15)	91.3(4)
C(22)	Te(4)	C(23)	94.0(4)	C(22)	Te(4)	C(24)	89.8(3)

Table 6.1 Selected bond distances (Å) and angles (°) with e.s.d's for [o-$C_6H_4(CH_2TeMe_2I)_2$].

The intermolecular Te-I-Te and I-Te-I angles are somewhat less distorted and thus, taken with the shorter intermolecular Te---I contact distances, may reveal the approximate location of the tellurium-based lone pair.

It is clear that the lone pair does not point out of the triangular face defined by the three carbon atoms bound to each tellurium atom (e.g. the triangular face formed by C(10), C(11) and C(12)), as judged by the relatively small distortion from regular octahedral geometry in this part of the molecule. This leaves the possibility of the lone pairs being directed either along the vector of the $Te(\mu^2\text{-}I)_2Te$ bridge in the $Me_2Te(\mu^2\text{-}I)_2TeMe_2$ units (i.e. approximately into the centre of the bridge) or into the cavity of the cubane unit (i.e. out of the open triangular face formed by the three iodo-species bound to each tellurium) (Figure 6.6).

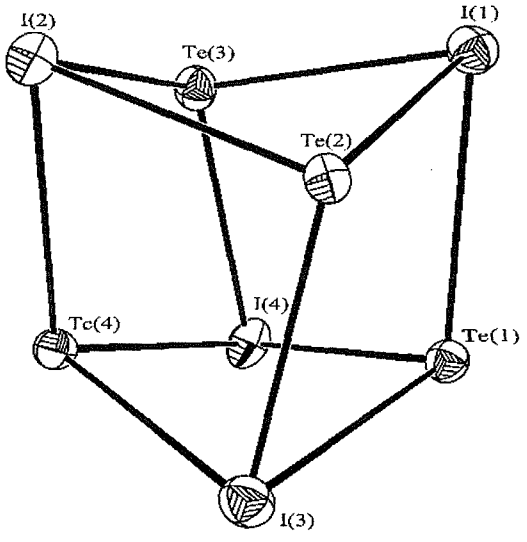

Figure 6.6 View of the Te_4I_4 cubane core with carbon atoms omitted.

In fact, a combination of these two extremes appears to be in operation. The Te---I bond length distribution in the $Te(\mu^2\text{-}I)_2Te$ bridge containing the tellurium atoms Te(3) and Te(4) is quite symmetrical, with the Te---I distances differing by no more than 0.038 Å. In contrast, one side of the bridge containing Te(1) and Te(2) is asymmetric, with the Te---I distances differing by 0.127 Å (I(3)-Te(1) 3.779(1), I(3) – Te(2) 3.652(1)) while the other side is more symmetrical (difference of 0.048 Å). Since each tellurium atom in the $[\underline{o}\text{-}C_6H_4(CH_2TeMe_2I)_2]$ molecule is in an identical coordination environment lone pair effects can be assessed, and the much greater

asymmetry in the side containing Te(1) and Te(2) suggests non-equivalent stereochemical activity of the lone pairs. Although it is difficult to be certain, the bond angle and length distributions suggest that three of the tellurium lone pairs are directed approximately into the cubane cavity, while the lone pair of Te(1) is localised in the region of the Te(μ^2-I)$_2$Te bridge, giving rise to an unsymmetrical unit. However, it is equally likely that the observed distortions are a consequence of the weak, secondary Te---I contacts allowing a degree of flexibility in the cubane unit.

The adoption of a pseudo-cubane arrangement is not unusual for R_3TeX or R_2TeX_2 species. The Et_3TeX species (X = Cl or Br) contain a Te_4X_4 core, however in these examples the cubane units are derived from linkage of four $[Et_3Te]^+$ units by $[X]^-$ ions, with the Te---X distances being shorter in length than in the present compound (3.448(4) and 3.564 Å for X = Cl and Br respectively).[7] The R_2TeX_2 species [{p-$MeOC_6H_4$}$_2TeI_2$] also displays a cubane-like motif, in this case the Te---I interactions (3.6922(6) – 3.9017(7) Å) form a centrosymmetric tetramer containing an open-faced Te_4I_8 cubane core. (Figure 6.3).[19]

In order to determine whether the MeI derivatives of related di- and tri-telluro-ethers adopt similar solid-state structures, and to also gauge the influence of the inter-Te linkage unit in such species, attempts were made to crystallise the MeI derivatives of o-$C_6H_4(TeMe)_2$, $MeTe(CH_2)_3TeMe$ and $MeC(CH_2TeMe)_3$. However, their very low solubility in non-donor solvents frustrated these attempts, and even careful layering of acetone solutions of MeI and the telluro-ether failed to produce crystals of sufficient quality for X-ray diffraction studies.

The reaction of PhTeMe with excess MeI in acetone produced $PhTeMe_2I$ as a white powder in high yield, which was isolated by filtration and washed with acetone.[4] This air-stable species proved soluble enough in $CDCl_3$ to enable collection of the $^{125}Te\{^1H\}$ NMR spectrum, which showed a single resonance at 565 ppm, compared to 329 ppm for the parent PhTeMe.[4] Again, ^{1}H-NMR spectroscopy and micro-analytical data confirmed the identity of the product. Layering of neat MeI onto PhTeMe produced small colourless crystals of $PhTeMe_2I$ suitable for X-ray diffraction studies. The X-ray crystal structure of $PhTeMe_2I$ reveals a centrosymmetric edge-shared dimer (Figure 6.7, Table 6.2), similar to the previously reported Et_3TeI and Ph_3TeCl adducts.[7, 9]

The $PhTeMe_2I$ unit is derived from two $PhTeMe_2^+$ fragments linked through μ^2-iodo bridges (3.6691(7) - 3.7584(8) Å). The tellurium atoms adopt a distorted square pyramidal geometry in the discrete dimer, with the donor set comprised of three organic groups (a phenyl and two methyls) and two iodide anions, with the Te-C bond lengths similar to those reported in the literature (*ca.* 2.13 Å).

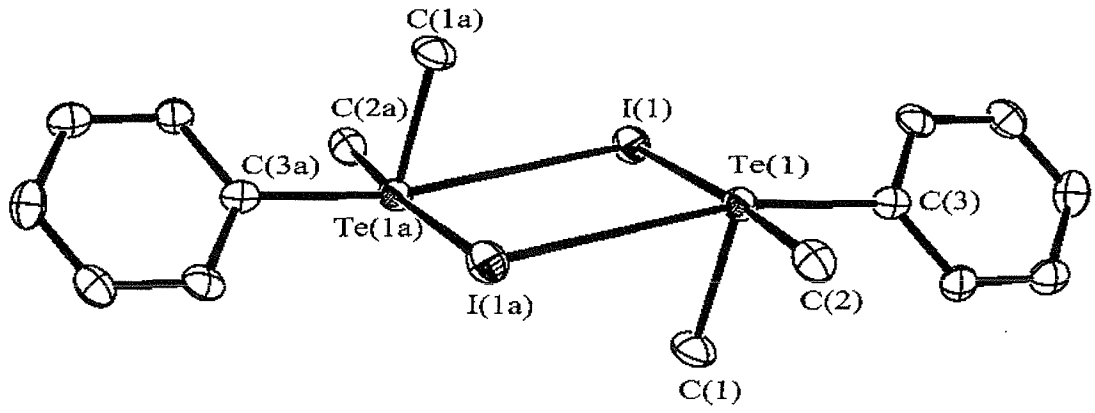

Figure 6.7 View of the $PhMe_2TeI$ dimer with the numbering scheme adopted. Ellipsoids shown at 40 % probability, H-atoms omitted for clarity. Atoms marked (a) are related by the symmetry operation –x, -y, -z.

I(1)	Te(1)		3.6591(7)		I(1a)	Te(1)	3.7584(8)
I(1b)	Te(1)		3.9192(7)		Te(1)	C(1)	2.128(8)
Te(1)	C(2)		2.132(9)		Te(1)	C(3)	2.132(7)
Te(1)	I(1)	Te(1a)	78.68(2)	I(1)	Te(1)	I(1a)	101.32(2)
I(1)	Te(1)	C(1)	79.7(3)	I(1)	Te(1)	C(2)	173.9(3)
I(1)	Te(1)	C(3)	85.2(2)	I(1)	Te(1)	C(1)	77.3(2)
I(1)	Te(1)	C(2)	168.3(2)	C(1)	Te(1)	C(2)	95.4(3)
C(1)	Te(1)	C(3)	94.7(3)	C(2)	Te(1)	C(3)	93.7(3)

Table 6.2 Selected bond distances (Å) and angles (°) with e.s.d's for $[PhTeMe_2I]$.

However, a distorted octahedral coordination environment is completed by a long Te---I interaction (3.9192(7) Å) directed towards the open face of the tellurium atom. This interaction is between tellurium and a μ^2-iodo bridge of an adjacent dimer unit, and each dimer is linked to four other such units *via* bridging iodine atoms, giving rise to an extended sheet network (Figure 6.8). Thus the iodines are μ^3- rather than μ^2-bridging in this species, as observed in the previously discussed [o-$C_6H_4(CH_2TeMe_2I)_2]_2$ molecule (Figure 6.5). All Te---I interactions are *trans* to Te-C bonds.

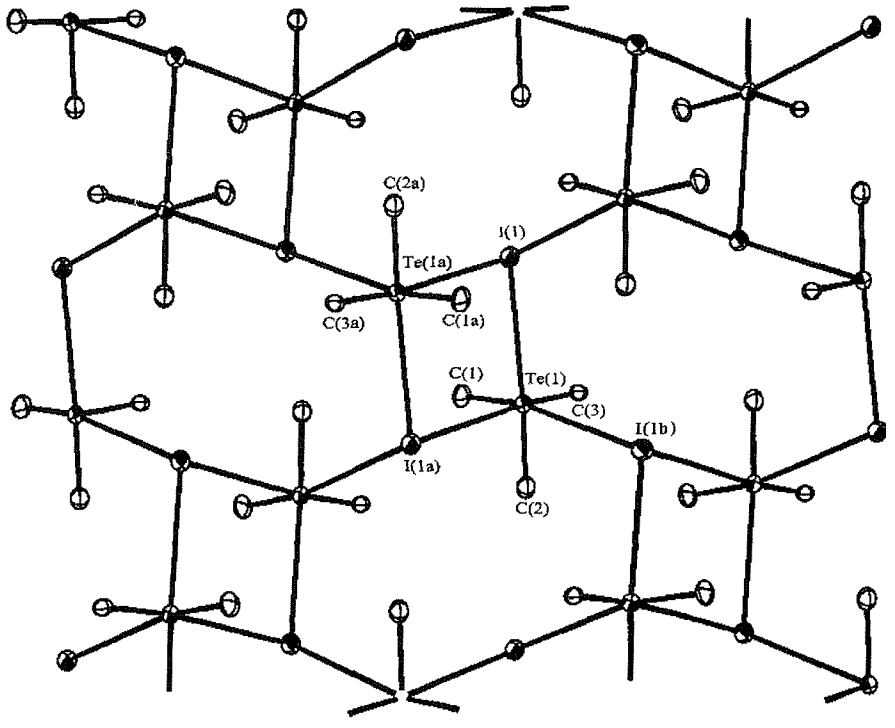

Figure 6.8 View of a portion of the sheet structure of $PhMe_2TeI$ with phenyl groups omitted for clarity.

The Te_2I_2 bridge is slightly asymmetric (Δ = 0.099 Å) but the Te-I-Te angle is not as acute as those in the pseudo-cubane unit discussed above. A similar arrangement was observed in the Ph_3SeI adduct, with two Ph_3Se^+ cations asymmetrically bridged by two μ^3-I species to give a centrosymmetric dimer (4.153(1) – 3.722(1), Δ = 0.431Å).[25] In summary, the adduct can be described as a trigonal pyramidal $PhMe_2Te^+$ cation bridged by I^- anions to give an octahedral tellurium centre within an extended sheet network.

Reaction of the ditelluroether $PhTe(CH_2)_3TePh$ with I_2 in anhydrous THF followed by removal of solvent *in vacuo* produced a red-black powder which was washed with hexane and dried *in vacuo*. The product was sparingly soluble in non-donor solvents, with the $^{125}Te\{^1H\}$-NMR spectrum revealing a weak signal at 651 ppm. This is shifted from the free ligand resonance (466 ppm) and the MeI adduct (609.7, 610.3 ppm).[3] Slow evaporation of a THF solution of the reactants in a 1:1 ratio gave a small amount of dark red crystals suitable for X-ray diffraction studies. Microanalysis consistent with the formula $PhTe(I)_2(CH_2)_3Te(I)_2Ph$ was obtained for both the bulk and crystal samples.

The crystal structure of the discrete $PhTe(I)_2(CH_2)_3Te(I)_2Ph$ unit is similar to that of the related $[\{p\text{-}(OMe)C_6H_4Te\}_2CH_2]$ species, and shows a saw-horse geometry about the tellurium atom with the iodines occupying axial positions and the carbon atoms of the phenyl and propyl groups bound equatorial (Figure 6.8).[23] The phenyl group shows rotational disorder between two perpendicular orientations, and were set as rigid groups for the purposes of data refinement. The Te-I distances (2.883(4) – 2.938(3) Å) are similar to those observed in $\{p\text{-}(OMe)C_6H_4Te(I)_2\}_2CH_2$, and within the literature range for similar bonds in R_2TeX_2 species (*ca.* 2.851(2) – 2.959(1) Å).[26] The coordination geometry about tellurium is close to regular octahedral (Table 6.3).

The description of the $[\{p\text{-}(OMe)C_6H_4Te(I)_2\}_2CH_2]$ structure by Singh alludes to a polymeric array comprised of intermolecular Te---I contacts (3.735(1) – 3.879(1) Å), although no comment was made on the form of this polymer.[23] Examination of the packing of the individual $PhTe(I)_2(CH_2)_3Te(I)_2Ph$ molecules also reveals an extended network. The discrete $PhTe(I)_2(CH_2)_3Te(I)_2Ph$ units are twisted such that each linear I(1)-Te(1)-I(2) moiety is aligned parallel with a I(1)-Te(1)-I(2) moiety from a neighbouring $PhTe(I)_2(CH_2)_3Te(I)_2Ph$ unit, leading to a rectangular, inter-molecular Te_2I_2 arrangement which serves to link the molecules and form a weakly bound chain polymer (Figure 6.9).

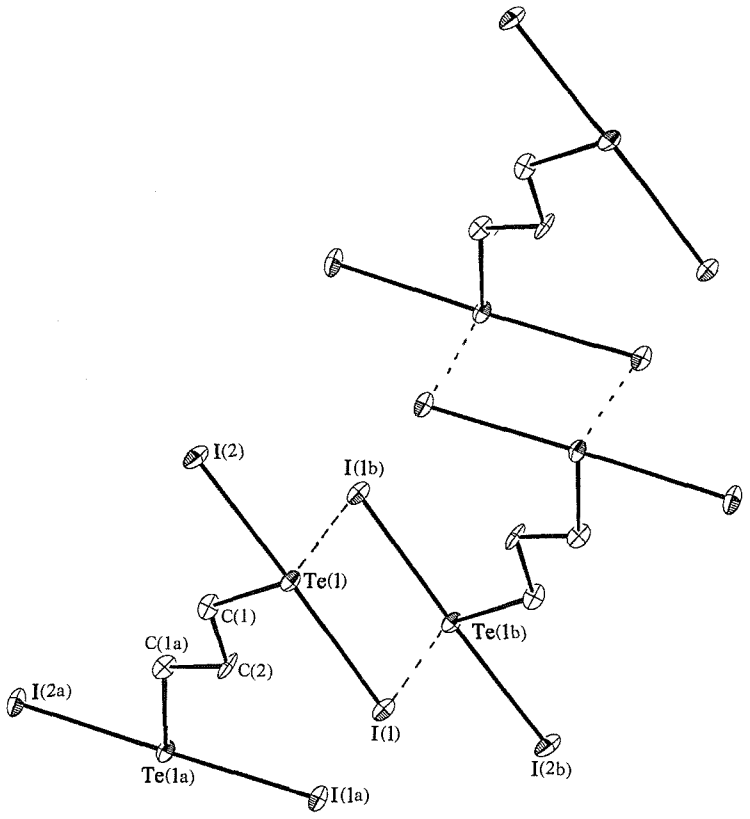

Figure 6.9 View of the Te---I interactions between the $[PhTe(I)_2(CH_2)_3Te(I)_2Ph]$ molecules. Ellipsoids shown at 40 % probability, phenyl groups and H-atoms omitted for clarity.

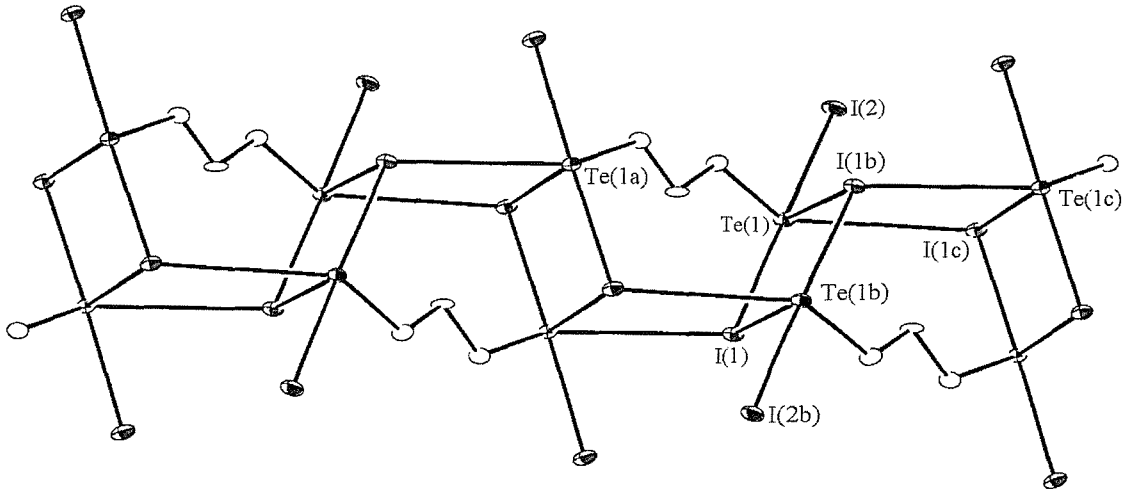

Figure 6.10 View of the fused-cradle arrangement of $[PhTe(I)_2(CH_2)_3Te(I)_2Ph]$

These secondary Te---I interactions (3.702(4) Å) are significantly shorter than those in the related p-$(OMe)C_6H_4Te(I)_2\}_2CH_2$ adduct.[19] In the present species only the I(1) atoms are involved in secondary bonding to tellurium, with the I(2) atoms remaining as terminal ligands. Further examination of this extended chain motif reveals the existence of another, much weaker Te---I interaction (4.069(3) Å). This long-range contact is at the limit of the sum of the van der Waals radii of the atoms (4.04 Å), and exists between a tellurium atom at a corner of a rectangular Te_2I_2 unit and an iodine atom directly opposite, giving rise to a cradle-type motif comprised of three Te_2I_2 units (Figure 6.10). One face of the cradle is shared between two units, leading to an alternating "up-down" chain arrangement with respect to the base of the cradle unit, with the propyl back-bone of the $PhTe(I)_2(CH_2)_3Te(I)_2Ph$ molecule diagonally straddling the top of each cradle. The tellurium(IV) coordination environment may now be described as [5+1] coordinate (i.e. pseudo-six coordinate) however the bond angles involving the long range Te---I contacts are severely distorted from octahedral. The angles subtended at the tellurium(IV) atom indicate a pseudo-octahedral geometry, although two particularly large distortions involving the weakly bound I(1b) and I(1c) (I(1b) Te(1) C(1) 136.24(4), I(1c) Te(1) I(2) 72.63(2) °) indicate that the lone pair may be localised in the triangular face defined by C(1), I(2) and I(1b).

Te(1)	I(1)		2.9384(9)		Te(1)	I(1b)	3.7019(6)
Te(1)	I(2)		2.8830(9)		Te(1)	I(1c)	4.0699(8)
I(1)	Te(1)	I(2)	177.86(3)	I(1)	Te(1)	I(1c)	108.68(2)
I(1)	Te(1)	I(1b)	89.43(2)	I(1)	Te(1)	C(1)	94.94(3)
I(1c)	Te(1)	I(2)	72.63(2)	I(1b)	Te(1)	C(1)	136.24(4)
I(2)	Te(1)	I(1a)	92.62(2)	I(2)	Te(1)	C(2)	85.17(3)
I(2)	Te(1)	I(1b)	92.63(2)	Te(1)	I(1)	Te(1b)	90.53(2)

Table 6.3 Selected bond distances (Å) and angles (°) with e.s.d's for $PhTe(I)_2(CH_2)_3Te(I)_2Ph$

6.2.2 Antimony(III) and Bismuth(III) Halide Complexes of Telluroether Ligands

Reaction of MX_3 (M = Sb or Bi; X = Cl, Br or I) in anhydrous MeCN (X = Cl, Br) or THF (X= I) with an equimolar CH_2Cl_2 solution of L (L = PhTeMe, $MeC(CH_2TeMe)_3$ or $RTe(CH_2)_3TeR$; R = Me or Ph) at room temperature produced, upon concentration of the solution *in vacuo*, a series of orange-brown or dark brown powders which were filtered, washed with CH_2Cl_2 and dried *in vacuo*. Poor solubility in both donor and non-donor solvents prevented NMR measurements for these complexes, however microanalyses show that all the solids are of 1:1 stoichiometry and IR spectra revealed weak features in the region 300 – 200 cm^{-1} due to v(M-Cl). These observations are similar to those made for the $[SbX_3\{MeC(CH_2TeMe)_3\}]$ species (X = Cl, Br or I), which represent the only other reported examples of MX_3-telluroether complexes.[29] Similar reaction of AsX_3 with these ligands produced insoluble black or dark brown solids, which were isolated as above but failed to give reproducible microanalytical data. Slow evaporation of an MeCN solution of $BiBr_3$ layered with an equimolar CH_2Cl_2 solution of PhTeMe produced a very small crop of deep red needle crystals. Similar crystallisation attempts with other MX_3–L combinations produced only powders of 1:1 stoichiomtery.

The structure of the $[BiBr_3(PhTeMe)]$ complex, the first structurally characterized complex containing a bismuth-telluroether bond, consists of a planar, bromide-bridged $Br_2Bi\text{-}(\mu^2\text{-}Br)_2\text{-}BiBr_2$ unit with a PhTeMe ligand bound to each bismuth atom in apical, mutually *anti* positions [Bi-Te 3.0533(7) Å] (Figure 6.12, Table 6.4). This bond is remarkably short, and is approximately equal to the sum of the single bond covalent radii for the elements (2.98 Å). The bromide bridge is asymmetric (2.8286(10) – 3.0806(10), Δ = 0.2520 Å), and the terminal Bi-Br distances differ by 0.208 Å (2.6490(10) – 2.8573(10)). The Te-C distances are similar to those in the species discussed previously (*ca.* 2.11 Å).

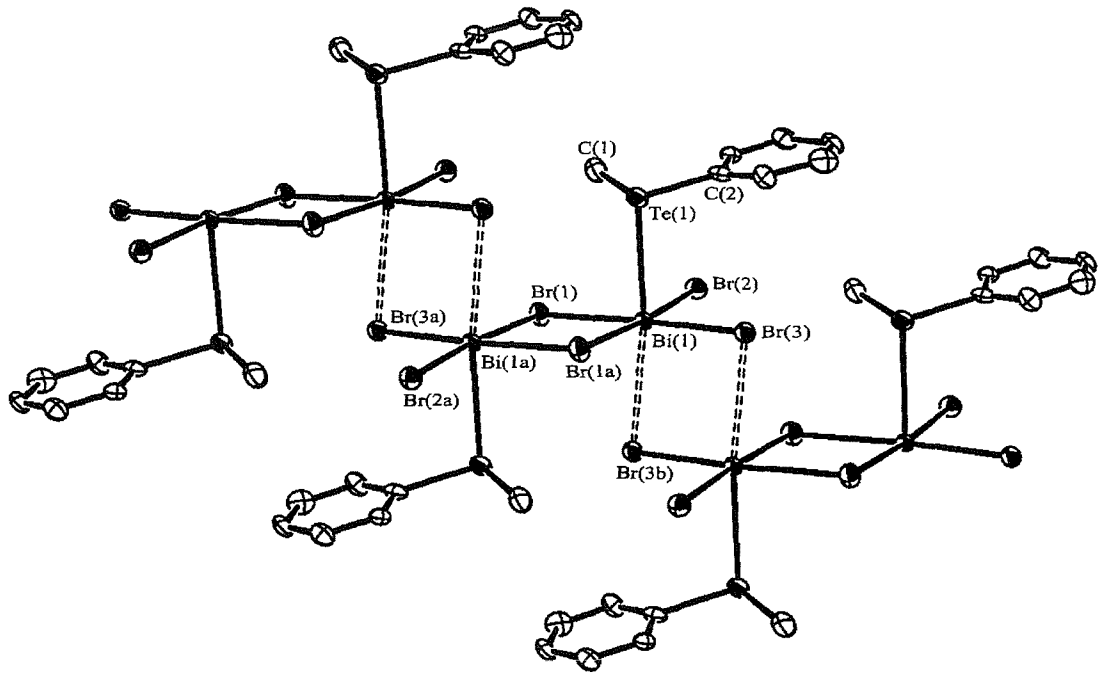

Figure 6.11 View of the extended structure of [$BiBr_3$(PhTeMe)] with the numbering scheme adopted. Ellipsoids shown at 40 % probability, H-atoms omitted for clarity. Atoms marked (a) are related by the symmetry operation 1-x, 1-y, -z.

Bi(1)	Te(1)	3.0533(7)		Bi(1)	Br(3)	2.8573(10)	
Bi(1)	Br(1)	2.8286(10)		Bi(1)	Br(1a)	3.0806(10)	
Bi(1)	Br(2)	2.6490(10)		Bi(1)	Br(3b)	3.1572(10)	
Te(1)	Bi(1)	Br(1)	92.30(3	Br(1)	Bi(1)	Br(3b)	85.10(3)
Te(1)	Bi(1)	Br(2)	90.92(3)	Bi(1)	Br(3)	Bi(1b)	86.65(3)
Te(1)	Bi(1)	Br(3)	87.55(2)	Br(2)	Bi(1)	Br(1a)	175.06(4)
Te(1)	Bi(1)	Br(1a)	84.18(2)	Br(2)	Bi(1)	Br(3)	96.11(3)
Te(1)	Bi(1)	Br(3b)	168.06(3)	Br(2)	Bi(1)	Br(3b)	100.87(2)
Br(1)	Bi(1)	Br(2)	92.45(2)	Bi(1)	Br(1)	Br(1a)	92.17(3)
Br(1)	Bi(1)	Br(3)	171.44(2)	Bi(1)	Br(3)	Bi(1b)	86.65(3)
Br(1)	Bi(1)	Br(1a)	87.83(3)	C(1)	Te(1)	C(2)	96.82(2)

Table 6.4 Selected bond distances (Å) and angles (°) with e.s.d's for [$BiBr_3$(PhTeMe)].

From consideration of the terminal and bridging Bi-Br bonds, the bismuth coordination geometry is most accurately described as irregular octahedral on account of a secondary, inter-dimer Bi---Br contact (3.1572(10) Å) (shown as open, dashed bonods in Figure 6.11). This occurs between the bromine atom Br(3) of one dimer unit and a bismuth atom of another dimer directly above Br(3), and is directed toward the open face of the bismuth atom. Of note is the similarity of the two Bi-Br_{bridge} bond lengths within each dimer (2.8286(10) and 2.8573(10) for Bi(1)-Br(1) and Bi(1)-Br(3) respectively). Thus, the intermolecular Bi---Br contact is *trans* to the Bi-Te bond, and leads to an asymmetric rectangular Bi_2Br_2 unit linking each dimer (2.8573(10) – 3.145 Å, $\Delta = 0.2877$). These contacts give rise to a stacked array of $[BiBr_3(PhTeMe)]$ dimers arranged in a step-wise manner (Figure 6.11). A similar linking unit was observed in the $PhTe(I)_2(CH_2)_3Te(I)_2Ph$ chain (in this case a Te_2I_2 bridge) (Figures 6.9 and 6.10).

The present complex is structurally similar to the discrete $[AsCl_3(PMe_3)]$ molecule described in Chapter 2 (Figure 2.17). However, where each $[AsCl_3(PMe_3)]$ molecule is weakly linked through a single long range, intermolecular As---Cl contact to give a chain of dimer units arranged orthogonally, the $[BiBr_3(PhTeMe)]$ dimers are aligned parallel, giving rise to a stacked array of $[BiBr_3(PhTeMe)]$ dimers arranged in a step-wise manner. The interactions are likely to be due to the combination of a vacant coordination site and the strong acceptor properties of the $BiBr_3$ species. In this regard, the present complex is more akin to the $[SbI_3(PMe_3)]$ species reported by Norman and co-workers (Chapter 2, Figure 2.7).[30]

The adoption of a slightly irregular octahedral geometry about the bismuth(III) atom would indicate that the bismuth-based lone pair does not exert any significant stereochemical activity. However secondary interactions tend to form in the region of the lone pair and so, in view of mild distortions in the Br_2Bi-(μ^2-Br)$_2$-$BiBr_2$ unit, it is arguable that lone pair is directed out of the triangular face defined by Br(1a) – Br(3) – Br(3b).

6.3 Conclusions

The majority of the work described in this chapter has focused upon the solid-state structures adopted by some simple R_3TeX and R_2TeX_2 telluronium compounds obtained from reaction of mono- and bi-dentate telluro-ethers with MeI or I_2. High frequency shifts in the ^{125}Te NMR spectra of the adducts (compared to the parent telluroether) indicate oxidative addition of MeI or I_2 to the tellurium atom. The structures are derived from weak, secondary Te---I interactions between $[R_3Te]^+$ and $[I]^-$ ions, with the tellurium atom adopting a distorted octahedral geometry through three primary Te-C and three weak Te---I interactions, and the iodide ions adopting a μ^3-bridging mode. This bonding arrangement leads to a cubane arrangement in the [o-$C_6H_4(CH_2TeMe_2I)_2$] complex and coordination networks in the $[PhTeMe_2I]$ and $[PhTe(I)_2(CH_2)_3Te(I)_2Ph]$ species, and further illustrates the ability of tellurium to participate in secondary bonding.

Like the structurally characterised MX_3 complexes of thio- and seleno-ether species described in earlier chapters (M = As, Sb or Bi; X = Cl, Br or I). the $[BiBr_3(PhTeMe)]$ complex adopts a coordination polymer structure (in this case an extended chain) derived from secondary, intermolecular Bi---Br contacts (3.0806(10) Å), with the telluroether bound to bismuth through a particularly short secondary bond (3.0533(7) Å). The bismuth(III) atom adopts an octahedral geometry, with little apparent lone-pair distortion. The range of isolated adducts is much more limited than for the MX_3 thio- and seleno-ether complexes discussed in Chapters 3 and 4.

In contrast to the telluronium compounds discussed above, there is no evidence that the tellurium atom in $[BiBr_3(PhTeMe)]$ is involved in secondary bonding interactions to either the bismuth or bromine atoms. However, in view of the established acceptor properties of the group 15 trihalides toward chalcogenoethers, it seems likely that such complexes containing multidentate or macrocyclic telluroethers would display secondary M---Te interactions, giving a range of coordination network motifs similar to those observed in analogous thio- and seleno-ether complexes.

6.4 Experimental

General experimental conditions are given in Appendix 1. Antimony(III) and bismuth(III) halides, MeI and I_2 were obtained commercially (Aldrich and Alfa) and used as received. Telluroether ligands were prepared using literature methods.[3, 24]

[o-$C_6H_4(CH_2TeMe_2I)_2$]. To a degassed acetone solution of o-$C_6H_4(CH_2TeMe)_2$ (0.10g, 0.26 mmol) was added an acetone solution (10 cm^3) containing excess MeI. The mixture was stirred at room temperature for 2 hours, and the resultant white powder filtered and washed with diethyl ether. Yield 0.15g, 88%. Calculated for $C_{12}H_{20}I_2Te_2$: C, 21.4; H, 3.0%. Found: C, 20.9; H, 2.6. ^1H NMR: δ 7.25 (m, 4H), 4.68 (s, 2H), 3.96 (s, 2H), 1.57 (s, 12H) ppm. ^{13}C {^1H} NMR: δ 134.4, 132.2, 129.2, 30.8, 12.8 ppm. ^{125}Te {^1H} NMR: δ 526 (s) ppm.

[$PhTeMe_2I$]. Procedure as above. White powder. Yield 94 %. Calculated for $C_8H_{11}I_1Te_1$. C: 26.6; H, 3.1 %. Found: C, 26.1; H, 3.2 %. IR/cm^{-1}: 537 (Te-C). ^1H NMR: δ 7.29 (m, 5H), 2.24 (s, 6H) ppm. ^{125}Te {^1H} NMR: δ 565 ppm (s).

[$MeC(CH_2TeMe_2I)_3$]. Procedure as above. Pale orange powder. Yield 83%. Calculated for $C_{11}H_{27}I_3Te_3$: C, 14.3; H, 2.9 %. Found: C, 14.9; H, 2.9 %. ^{125}Te {^1H} NMR: δ 464 ppm. IR/cm^{-1} 533 (Te-C).

[$Me_2(I)TeCH_2Te(I)Me_2$]. Procedure as above. Pale orange powder. Yield 88%. Calculated for $C_5H_{14}I_2Te_2$: C, 10.3; H, 2.4 %. Found: C, 10.6; H, 2.4 %. ^{125}Te {^1H} NMR: δ 546 ppm. IR/cm^{-1} 534, 501 (Te-C).

[$PhTe(I)_2(CH_2)_3Te(I)_2Ph$]. To an anhydrous THF solution (10 cm^3) of $PhTe(CH_2)_3TePh$ (0.11 g, 0.12 mmol) was added a THF solution (5 cm^3) of I_2 (0.2 g, excess). The red-black solution was stirred at room temperature for 2 hours and the solvent removed *in vacuo* to give a red-black powder, which was rinsed with hexane and dried *in vacuo*. Yield 46 %. Calculated for $C_{15}H_{16}I_4Te_2$: C, 18.8; H, 1.7. Found: C, 18.5; H, 1.5 %. IR/cm^{-1} 530 (Te-C). ^{125}Te {^1H}-NMR: δ 651 ppm.

[$SbBr_3${$MeTe(CH_2)_3TeMe$}]. To an anhydrous MeCN solution of $SbBr_3$ (0.09 g, 0.25 mmol) was added an equimolar anhydrous MeCN solution of $MeTe(CH_2)_3TeMe$. The resultant orange solution was concentrated *in vacuo* to obtain an orange powder, which was washed with CH_2Cl_2 and dried *in vacuo*. Yield 0.13 g, 74 %. Calculated for $C_5H_{12}Br_3SbTe_2$: C, 8.7; H, 1.7. Found: C, 8.5; H, 1.9 %.

[SbI_3{$MeTe(CH_2)_3TeMe$}]. Procedure as above, using anhydrous THF solutions of SbI_3 and $MeTe(CH_2)_3TeMe$. Yield 82 %. Red powder. Calculated for $C_5H_{12}I_3SbTe_2$: C, 7.2; H, 1.5. Found: C, 7.2; H, 2.1.

[$BiCl_3${$MeTe(CH_2)_3TeMe$}]. Procedure as above, using anhydrous MeCN solutions of $BiCl_3$ and $MeTe(CH_2)_3TeMe$. Brown powder. Yield 44 %. Calculated for $C_5H_{12}Cl_3BiTe_2$: C, 9.3; H, 1.9. Found: C, 9.4; H, 2.1. IR/cm^{-1}: 237, 255 and 261.

[$BiCl_3${$MeC(CH_2TeMe)_3$}]. Procedure as above, using $BiCl_3$ and $MeC(CH_2TeMe)_3$. Orange-brown powder. Calculated for $C_8H_{18}BiCl_3Te_2$: C, 11.8; H, 2.2. Found: C, 11.5; H, 2.0. IR/cm^{-1}: 239, 250 and 260 cm^{-1}.

[$BiBr_3${$MeC(CH_2TeMe)_3$}]. Procedure as above, using $BiBr_3$ and $MeC(CH_2TeMe)_3$. Brown powder. Calculated for $C_8H_{18}BiBr_3Te_2$: C, 10.1; H 1.9. Found: C, 9.8; H, 2.0 %.

[$BiBr_3$(PhTeMe)]. Procedure as above, using $BiBr_3$ and PhTeMe. Red-brown powder. Yield 35 % Calculated for $C_7H_8Bi_1Br_3Te_1$: C, 12.6; H, 1.2 %. Found: C, 12.3; H, 0.9 %.

6.5 X-Ray Crystallography

Details of the crystallographic data collection and refinement parameters are given in Table X. Colourless crystals of [o-$C_6H_4(CH_2TeMe_2I)_2$]. ½ $CHCl_3$ were grown by infusion of diethyl ether into a solution of the compound in $CHCl_3$, while those of [$PhTeMe_2I$] were obtained by drop-wise addition of neat MeI to PhTeMe. Data collection for the former used a Rigaku AFC7S four-circle diffractometer (T = 150 K), while the latter used an Enraf-Nonius Kappa CCD diffractometer (T = 120 K), both with graphite-monochromated Mo-Kα radiation (λ = 0.71073 Å). Although the programme indicated an orthorhombic cell for the [o-$C_6H_4(CH_2TeMe_2I)_2$].½ $CHCl_3$ adduct, the Laue check failed and a precession simulation failed to show the mirror symmetry which would confirm an orthorhombic cell, hence the data were re-collected and the structure solved and refined assuming a monoclinic cell. Otherwise, structure solution and refinement were routine.

	[o-$C_6H_4(CH_2TeMe_2I)_2$].½$CHCl_3$	**[$PhTeMe_2I$]**
Formula	$C_{12.5}H_{15.5}Cl_{1.5}I_2Te_2$	$C_8H_{11}ITe$
Formula Weight	732.99	361.68
Crystal System	Monoclinic	Monoclinic
Space Group	*C*2/*c* (# 15)	$P2_1/n$ (# 14)
a / Å	18.05(2)	8.9319(3)
b / Å	13.34(1)	9.9545(4)
c / Å	33.907(9)	11.7192(4)
α/ °	90	90
β/ °	90.17(4)	104.201(2)
χ/ °	90	90
U / Å ^{3}	8162.5(1)	1010.14(6)
Z	16	4
μ (Mo-K_α)/ cm^{-1}	60.69	59.37
Unique obs. Reflections	7532	2195
Obs. Reflections with [$I > 2\sigma(I)$]	4899	1580
R	0.037	0.040
R_w	0.043	0.044

Table 6.5 Crystallographic data collection and refinement parameters for the [o-$C_6H_4(CH_2TeMe_2I)_2$].½$CHCl_3$ and [$PhTeMe_2I$] complexes.

	[PhTe(I)$_2$(CH$_2$)$_3$Te(I)$_2$Ph]	**[BiBr$_3$(PhTeMe)]**
Formula	$C_{15}H_{16}I_4Te_2$	$C_7H_8BiBr_3Te$
Formula Weight	959.11	668.43
Crystal System	Orthrhombic	Monoclinic
Space Group	*Pbcn (# 60)*	$P2_1/n$ (# 14)
a / Å	23.6450(2)	8.4820(2)
b / Å	9.0897(2)	6.7592(2)
c / Å	10.1816(3)	22.5808(8)
α/ °	90	90
β/ °	90	100.676(1)
χ/ °	90	90
U / Å^3	2188.29(5)	1272.18(6)
Z	4	4
μ (Mo-K$_\alpha$)/ cm^{-1}	83.056	254.863
Unique obs. Reflections	2854	2956
Obs. Reflections with [$I > 2\sigma(I)$]	1747	2144
R	0.052	0.037
R_w	0.071	0.039

Table 6.6 Crystallographic data collection and refinement parameters for the [PhTe(I)$_2$(CH$_2$)$_3$Te(I)$_2$Ph] and [BiBr$_3$(PhTeMe)] complexes.

6.6 References

[1] H. Schumann, A. A. Arif, A. L. Rheingold, C. Janiak, R. Hoffman and N. Kuhn, *Inorg. Chem.*, 1991, **30**, 1618.

[2] W. Levason, S. D. Orchard and G. Reid, *Organometallics*, 1999, **18**, 1275; J. Connolly, A. R. J. Genge, W. Levason, S. D. Orchard, S. J. A. Pope and G. Reid, *J. Chem. Soc., Dalton Trans.*, 1999, 2343.

[3] E. G. Hope, T. Kemmitt and W. Levason, *Organometallics*, 1988, **7**, 78.

[4] T. Kemmitt and W. Levason, *Organometallics*, 1989, **8**, 1303.

[5] N. W. Alcock, *Adv. Inorg. Chem. And Radiochem.*, 1972, **122**, 1.

[6] K. J. Irgolich, *The Organic Chemistry of Tellurium*, Gordon and Breach, New York, 1982; Vol. 2.

[7] R. K. Chadha, J. E. Drake, M. A. Kahn and G. Singh, *J. Organomet. Chem.*, 1984, **260**, 73.

[8] R. K. Chadha and J. E. Drake, *J. Organomet. Chem.*, 1986, **299**, 331.

[9] R. F. Ziolo and M. Extine, *Inorg. Chem.*, 1980, **19**, 2964.

[10] R. F. Ziolo and J. M. Troup, *Inorg. Chem.*, 1979, **18**, 2271.

[11] Z-L. Zhou, Y-Z. Huang, Y. Tang, Z-H. Chen, L-P. Shi, X-L. Jin and Q-C. Yang, *Organometallics*, 1994, **13**, 1575.

[12] M. J. Collins, J. A. Ripmeester and J. F. Sawyer, *J. Am. Chem. Soc.*, 1988, **110**, 8583.

[13] R. H. Vernon, *J. Chem. Soc.*, 1921, 105.

[14] H. D. K. Drew, *J. Chem. Soc.*, 1929, 560.

[15] F. Einstein, J. Trotter and C. Williston, *J. Chem. Soc.*, (A) 1967, 2018.

[16] L. Y. Y. Chan and F. W. B. Einstein, *J. Chem. Soc., Dalton Trans.*, 1972, 317.

[17] N. W. Alcock and W. D. Harrison, *J. Chem. Soc., Dalton Trans.*, 1984, 869.

[18] J. Farren, A. Alvarez-Larena, M. V Capparelli, J. F. Piniella, G. Germain and L. Torres-Castellanos, *Acta Crytsallogr.*, 1998, **C54**, 995.

[19] A. K. Singh, M. Kadarkaraisamy, J. E. Drake and R. J. Butcher, *Inorg. Chim. Acta*, 2000, **304**, 45.

[20] C. Knobler and R. F. Ziolo, *J. Organomet. Chem.*, 1979, 178, 423; J. D. McCullough, *Inorg. Chem.*, 1975, **14**, 1143.

[21] J. D. McCullough, *Inorg. Chem.*, 1973, 12, 2669; *ibid* 2665.

[22] C. Knobler, J. D. McCullough and H. Hope, *Inorg. Chem.*, 1970, **9**, 797.

[23] A. R. J. Genge, W. Levason and G. Reid, *J. Chem. Soc., Dalton Trans.*, 1997, 4549; W. Levason and G. Reid, *J. Chem. Soc., Dalton Trans.*, 2001, 2953.

[24] W. Levason, B. Patel, G. Reid and A. J. Ward, *J. Organomet. Chem.*, 2001, **619**, 218.

[25] H. Fleischer and D. Schollmeyer, *Acta Crystallogr.*, 1999, **C55**, 1572.

[26] J. D. McCullogh, C. Knobler and R. F. Ziolo, *Inorg. Chem.*, 1985, **24**, 1814 and references therein.

[28] A. Bondi, *J. Phys. Chem.*, 1964, **68**, 441.

[29] A. J. Barton, Ph.D Thesis, University of Southampton, 2000.

[30] W. Clegg, M. R. J. Elsegood, V. Graham, N. C. Norman, N. L. Pickett and K. Tavakkoli, J. Chem. Soc., Dalton Trans., 1994, 1743.

[31] G. M. Sheldrick, *SHELXL*-97; University of Göttingen, Germany, 1997.

[32] P. T. Beurskens, G. Admiraal, G. Beurskens, W. P. Bosman, S. Garcia-Granda, R. O Gould, J .M. M. Smits and C. Smykalla, *PATTY, The DIRDIF Program System*; Technical Report of the Crystallography Laboratory, University of Nijmegen, The Netherlands, 1992.

[33] *TeXsan: Crystal Structure Analysis Package*, Molecular Structure Corporation, The Woodlands, TX, 1995.

[34] N. Walker and D. Stuart, *Acta Crystallogr.*, 1983, **A39**, 158.

APPENDIX 1

General Experimental Conditions

Infrared spectra were measured as pressed CsI discs or nujol mulls between CsI plates using a Perkin-Elmer 983G spectrometer over the range 220 - 4000 cm^{-1} and electronic spectra were recorded by diffuse reflectance on a Perkin Elmer Lambda 19 UV/visible spectrometer for samples diluted in a 1:5 ratio with $BaSO_4$. ^{1}H-NMR spectra were obtained in $CDCl_3$ and CD_3NO_2 solutions using a Bruker AC300 spectrometer operating at 300 Hz, while $^{31}P\{^{1}H\}$-, ^{77}Se- and ^{125}Te-NMR were recorded on a Bruker AM360 spectrometer operating at 145.5, 68.7 and 113.6 MHz respectively. Chemical shifts to high frequency of reference compounds ^{1}H ($SiMe_4$), ^{31}P (external 85% H_3PO_4), ^{77}Se (neat Me_2Se) and ^{125}Te (neat Me_2Te) are reported as positive. Samples were prepared in a N_2-purged glove box. Microanalytical data were collected by the University of Strathclyde microanalytical laboratory.

Single crystal X-ray diffraction data were collected on either a Rigaku AFC7S four-circle diffractometer or an Enraf Nonius Kappa CCD diffractometer. Both utilised Mo-K_α X-radiation of wavelength 0.71073 Å. The X-ray source for the former was a sealed X-ray tube, while a Nonius FR591 rotating anode X-ray generator was used for the latter. In all cases, the selected crystal was mounted onto a glass fibre with hydrocarbon grease and immediately cooled (150 K for Rigaku or 120 K for CCD) using an Oxford Systems open-flow cryostat. Residual factors R and R_w are defined thus:

$$R = \Sigma (|F_{obs}| - |F_{calc}|) / \Sigma |F_{obs}|$$

$$R_w = [\Sigma w_i (|F_{obs}^2| - |F_{calc}^2|)^2 / \Sigma w_I |F_{obs}^2|^2]^{1/2}$$

APPENDIX 2

Papers published in primary journals arising from work described in this thesis:

1. **Coordination Networks Derived From Antimony(III) Halide Complexes With Thio- and Seleno-ether Ligation**
   Andrew J. Barton, Nicholas J. Hill, William Levason, Bhavesh Patel and Gillian Reid, *Chem. Commun.*, 2001, 95-96.

2. **Synthesis and Properties of Antimony(III) and Bismuth(III) Halide Complexes of Diphosphines and Diarsines. Crystal structures of $[Bi_2I_6\{o\text{-}C_6H_4(AsMe_2)_2\}_2]$, $[Sb_2Br_6\{o\text{-}C_6H_4(PPh_2)_2\}_2]$, $[Sb_2Cl_6\{o\text{-}C_6H_4(AsMe_2)_2\}_2]$ and $[BiCl_3\{o\text{-}C_6H_4(P(O)Ph_2)\}(thf)]$**
   Anthony R. J. Genge, Nicholas J. Hill, William Levason and Gillian Reid, *J. Chem. Soc., Dalton Trans.*, 2001, 1007-1012.

3. **Synthesis and Structural Studies on Polymeric Assemblies Derived From Antimony(III) Halide Complexes With Bi- and Tri-dentate and Macrocyclic Thio- and Seleno-ether Ligands**
   Andrew J. Barton, Nicholas J. Hill, William Levason and Gillian Reid, *J. Chem. Soc., Dalton Trans.*, 2001, 1621-1626.

4. **1, 2-Bis(diphenylarsino)ethane**
   Nicholas J. Hill, William Levason, Gillian Reid and Michael Webster, *Acta Crystallogr.*, 2001, **E57**, o700-701.

5. **Synthesis and Structural Properties of the First Macrocyclic Selenoether Complex of Arsenic(III) - A Rare Example of Exo and Endo Coordination in a Single Species**
   Andrew J. Barton, Nicholas J. Hill, William Levason and Gillian Reid, *J. Am. Chem. Soc.*, 2001, **123**, 11801-11802.

6. **Synthesis and Molecular Structures of Dimeric Assemblies From Telluronium Salts Derived From o-$C_6H_4(CH_2TeMe)_2$ and PhTeMe**
   Nicholas J. Hill, William Levason, Gillian Reid and Antony J. Ward,
   J. Organomet. Chem., 2002, **642**, 186-190.

7. **Arsenic(III) Halide Complexes With Phosphine and Arsine Co-ligands: Synthesis, Spectroscopic and Structural Properties**
   Nicholas J. Hill, William Levason and Gillian Reid,
   J. Chem. Soc., Dalton Trans, 2002, 1188-1192.

8. **Arsenic(III) Halide Complexes With Acyclic and Macrocyclic Thio- and Seleno-ether Co-ligands: Synthesis, Spectroscopic and Structural Properties**
   Nicholas J. Hill, William Levason and Gillian Reid,
   Inorg. Chem., 2002, **41**, 2070-2076.

9. **Synthesis and Structural Properties of The First Bismuth(III) Telluroether Complex**
   William Levason, Nicholas J. Hill and Gillian Reid,
   J. Chem. Soc., Dalton Trans, 2002, 4316-4317.

10. **Recent Developments in Thio-, Seleno-, and Telluro-ether Ligand Chemistry**
    Andrew J. Barton, Anthony R. J. Genge, Nicholas J. Hill, William Levason, Simon D. Orchard, Bhavesh Patel, Gillian Reid and Antony J. Ward
    Heteroatom Chem., 2002, **13**, 550-560.

11. **Synthesis and Structural Features of The First Thallium(I) Selenoether Derivatives**
    Nicholas J. Hill, William Levason, Mark E. Light and Gillian Reid
    Chem. Commun., 2003, in press.